List of Contributors

D. J. T. Hill and A. K. Whittaker, *Centre for Magnetic Resonance, University of Queensland, Queensland 4072, Australia*

G. E. Martin, *Rapid Structure Characterization Group, Global Corp. Pharmaceutical Development, Pharmacia, 7000 Portage Road, Kalamazoo, Michigan 49001-0199, USA*

T. Asakura and T. Kameda, *Department of Biotechnology, Tokyo University of Agriculture and Technology, Koganei, Tokyo 184, Japan*

D. Jeannerat, *Department of Organic Chemistry, University of Geneva, 30 Quai Ernest Ansermet, 1211 Geneva 4, Switzerland*

Preface

The fecund nature of NMR in many areas of molecular science is evinced by the well-presented contributions in volume 46 of *Annual Reports on NMR Spectroscopy*. It is my great pleasure to introduce the chapters and to simultaneously thank the reporters for their very considerable efforts in providing up-to-date contributions to the present volume.

The first chapter is on NMR Studies of the Radiation Modification of Polymers, by D. J. T. Hill and A. K. Whittaker, following this is a report on Qualitative and Quantitative Exploitation of Heteronuclear Coupling Constants, by G. E. Martin, next comes a review of the Dynamics of Silk Fibroin Studied with NMR Spectroscopy, by T. Kameda and T. Asakura, finally there is an account on Computer Processing Techniques in High-resolution NMR by D. Jeannerat.

My thanks are due to the production staff of Academic Press (London) for their considerable efforts in the reification of this volume of *Annual Reports on NMR*.

Royal Society of Chemistry
Burlington House
London
UK

G. A. WEBB
July 2001

NMR Studies of the Radiation Modification of Polymers

DAVID J. T. HILL and ANDREW K. WHITTAKER

Department of Chemistry, and Centre For Magnetic Resonance, The University of Queensland, Queensland, 4072, Australia

1. Introduction 2
   1.1. Radiation chemistry of polymers 4
   1.2. NMR methods 8
2. Broadline and pulsed NMR of irradiated polymers 8
   2.1. Early broadline NMR and crystal structure 8
   2.2. Pulsed NMR of polymer rubbers and melts 9
3. ^{1}H and ^{13}C solution-state NMR of irradiated polymers 12
   3.1. Solution-state NMR studies of cross-linking 12
   3.2. Solution-state NMR studies of chain scission 14
   3.3. Solution-state NMR studies of racemization 16
   3.4. Solution-state NMR studies of other systems 19
   3.5. Practical limits to solution-state NMR studies 20
4. ^{13}C MAS NMR of irradiated polymers 21
   4.1. High-resolution solid-state NMR methods 21
   4.2. ^{13}C MAS NMR of irradiated poly(olefin)s 22
   4.3. ^{13}C MAS NMR of irradiated poly(diene)s 23
   4.4. ^{13}C MAS NMR studies of crystalline structure in irradiated polymers 25
   4.5. MAS NMR studies of other irradiated polymers 26
5. ^{19}F MAS NMR of irradiated polymers 27
6. NMR studies of oxidative degradation of polymers 28
7. Summary 30
Acknowledgements 31
References 31

This chapter provides a survey of the use of NMR methods to determine structural changes in irradiated polymers. A general survey of other methods is intended to place the NMR measurements in their appropriate context. Generally speaking, two classes of NMR experiment are described, namely the measurement of transverse relaxation times to provide information on the molar mass of the irradiated polymer, and the measurement of chemical structures using

ANNUAL REPORTS ON NMR SPECTROSCOPY
VOLUME 46 ISBN 0-12-505446-7

high-resolution NMR methods. Solid-state NMR methods are of particular use for materials that undergo radiation-induced cross-linking. The spatial distribution of cross-linking reactions may be inferred from a comparison with other measurement methods.

1. INTRODUCTION

The study of the interaction of high-energy radiation with polymeric materials is of importance for a number of reasons. There are a growing number of industrial processes in which polymers are subjected to radiation to modify their properties. For example, poly(olefin)s are irradiated with gamma rays or high-energy electrons to facilitate cross-linking in cable insulation sheathings, hot water pipes, and heat-shrinkable films. Poly(methacrylate)s and poly(sulfone)s are irradiated with electrons to initiate degradation in positive resist films. The more complete discussion given below of the application of radiation in polymer science highlights the increasing importance of this industry.[1]

As will be discussed below, radiation has a profound effect on the physical properties of polymers by virtue of their long chain structure. The net effect of radiation on polymers is to either increase or decrease the average molecular weights through the processes of cross-linking and chain scission, respectively. Whether cross-linking or scission reactions dominate will determine the end use of the material under irradiation. In addition the distribution of radiolytic reactions has been increasingly recognized as an important issue for end product usage. Thus the effective cross-link density will be reduced in materials in which local clusters of cross-links are formed, for example poly(diene)s. In addition the presence of long-lived free radicals trapped in or close to the rigid crystalline materials, for example poly(propylene) or semi-crystalline fluoropolymers, results in long-term instability due to oxidation and subsequently-enhanced probability of chain scission.

The number of industrial applications of irradiation of polymers are myriad. A comprehensive overview of these applications can be gained from a survey of the proceedings of the 11 International Meetings on Radiation Processing, which have been published in *Radiation Physics and Chemistry*.[2–12] The text of Singh and Silverman[1] should also be consulted. To begin with, the use of radiation to effect the polymerization of monomers is of much importance. Typical examples of this technology are radiation curing of coatings, and polymerization of monomers within composites with woods, clays or other naturally-occurring materials. Within this last example, polymerization can be used to improve the stiffness of soft woods, or for valuable archeological materials to improve mechanical integrity and limit the damaging effects of oxygen diffusion.

Also within this category of application is the field of radiation grafting onto pre-existing polymeric substrates. E-beam or gamma sources can be used to initiate grafting onto a range of materials, for example poly(olefin)s, fluoropolymers, and cellulosics. The biocompatibility of poly(olefin)s can be greatly

enhanced by grafting hydrophilic monomers onto their surface, while there has been much progress in the formation of functionalized membranes by grafting for example onto fluoropolymers. Potential uses include ion exchange, ion conducting membranes, gas separation and combinatorial chemistry.

The second class of applications is based on the cross-linking of polymers, usually poly(olefin)s. Included in this class are the industries of cross-linked wire and cable insulation. Cross-linking improves in particular the high temperature resistance to flow of poly(ethylene) in high-voltage cable wires. A large number of gamma facilities worldwide are involved in cross-linking poly(ethylene) pipes to improve high temperature properties. Another familiar example is heat-shrink films, which are cross-linked at ambient temperatures prior to deformation at temperatures above the crystalline melting temperature. After cooling to below the crystallization temperature in the deformed state, the film has the property of being able to return to its initial, undeformed dimensions on reheating, thus forming a barrier around an enclosed object.

Another growing application of radiation cross-linking is the formation of films and devices for slow release of drugs into the body or a wound. These materials are typically hydrogels of poly(amide)s or poly(N-vinyl pyrollidone). An advantage of these methods over chemically-initiated cross-linking reactions is the absence of initiator fragments, and the sterilization of devices during the polymerization process.

The growing concern over the toxicity of residual ethylene oxide after sterilization of polymers for use in the field of medicine has led to the rapid growth of the field of radiation sterilization. The medical industry consumes a massive volume of polymeric material in both equipment and implants. As a consequence there is much interest in the effects of radiation on the physical properties and stability of irradiated polymers. The standard dose for radiation sterilization is 25 kGy, which is sufficient to alter the properties of many polymers, being for example close to or above the gel dose of many elastomers. There is also interest in the reaction of oxygen with long-lived radical species formed during irradiation. A common polymer used in medical equipment, poly(propylene) is susceptible to oxidative degradation, and must be blended with appropriate stabilizers before radiation sterilization.

Polymers which undergo radiation degradation on exposure to radiation are also important commercially. The best-known example is the group of polymers used as positive resist materials in electron beam microlithography. These include aliphatic poly(sulfone)s and poly(methacrylate)s. Finally, an understanding of the radiation chemistry of polymers is essential for their application in environments where they are exposed to high doses of ionizing radiation, for example in the nuclear and space industries.

It is clear from this brief introduction that the field of radiation chemistry of polymers is of major, and growing importance commercially. An understanding of the mechanisms of the radiation-induced reactions is crucial for process design

and improvement. The aim of this review is to demonstrate the role NMR spectroscopy has played in building this understanding.

1.1. Radiation chemistry of polymers

1.1.1. Primary events

The focus of this review will be the effects of so-called ionizing radiation, namely gamma and electron-beam irradiation, on polymers. We will not consider, for example, the effects of UV radiation on materials, although this is an important method in the field of radiation grafting.[13]

The initial result of the interaction of a gamma photon or an electron with a material is the formation of ionized and excited species via Compton scattering and the photo-electron effect.[14,15] For each initial 1 MeV electron or photon entering a material there may be around 10^5 particles formed, distributed in the main track of the particle, branch tracks formed by the passage of Compton electrons, and blobs of particles formed as the electron energy drops towards thermal levels. It is the reaction of these particles which leads to dramatic changes in the material properties of polymers.

A large number of reactive pathways have been envisaged for the ionic, radical and excited species formed at short times. These include homolytic cleavage of bonds, combination reactions, disproportionation and hydrogen-atom abstraction reactions.[14] The two most important classes of reaction in polymers are cross-linking and main-chain scission. These result in respective increases and decreases in average molecular weights of the polymers. A number of other reactions, for example formation or reaction of double bonds, cyclization of short chain segments, loss of side-chains also may occur, however, these tend to have a less pronounced effect on polymer properties than cross-linking and scission.

1.1.2. Cross-linking versus scission

Basic relationship between structure and relative yields

A very large body of literature enables one to make predictions about the radiation sensitivity of particular polymers.[1–12,15–22] In particular it is possible to estimate the relative propensity of the polymer to undergo cross-linking or main-chain scission, and thus predict the final properties of the irradiated polymer. For linear addition polymers, those with quaternary main-chain carbons are likely to undergo main-chain scission. The classic example of this is poly(methyl methacrylate) (PMMA). Polymers having tertiary carbon atoms in the main chain, for example poly(propylene) (PP) will generally undergo a combination of chain scission and cross-linking (with cross-linking dominating), while for largely unbranched materials, e.g. poly(ethylene) (PE), cross-linking tends to dominate over scission.

It is well known that the presence of aromatic groups in irradiated systems reduces both the yield of primary fragments and the final yield of products. Thus, while poly(styrene) (PSTY) and poly(propylene) both undergo cross-linking on irradiation in vacuum, the yield of cross-links in PSTY is several orders of magnitude smaller than in PP.[23,24] In addition the incorporation of aromatic groups into an aliphatic polymer, through copolymerization or blending, often reduces dramatically the radiation sensitivity of the aliphatic component. This is due to a combination of energy or charge transfer to the aromatic groups, and scavenging of intermediates in systems with sufficient molecular mobility.[25,26]

A number of other chemical groups have been demonstrated to have enhanced sensitivity to ionizing radiation. These include sulfone and ester groups. Thus in the series of aromatic polymers, the aromatic sulfones have enhanced radiation sensitivity compared with aromatic poly(ether)s or poly(ketone)s.[27] The aliphatic poly(sulfone)s are particularly susceptible to radiation degradation,[28] and have become useful as positive resists in microlithography.[29] The presence of chlorine or bromine groups has been shown to enhance the radiation sensitivity of a number of materials, including fluoropolymers.[30,31] Finally the high propensity of double bonds to undergo addition by free radicals leads to their sensitivity to radiation, either as end groups in cross-linked poly(ethylene),[32] as cross-link promoters in EPDM terpolymers,[33] or finally in poly(diene)s.[34]

1.1.3. Other methods for studying radiation chemistry

The characterization of radiation-induced reactions has been a major goal of instrumental scientists over the past 50 years. The advent of high-resolution NMR spectroscopy has led to many advances in the analysis of radiation effects in polymers. However, for a complete description of the mechanisms of radiation-induced structural changes, the NMR methods described in this review should be used in concert with other analytical methods, briefly reviewed here with a few examples from the literature. For example, the free radical intermediates formed during the early stages of the reactions can be usefully observed using electron spin resonance spectroscopy.[35] Generally materials are irradiated at liquid nitrogen temperatures to permit observation of species which are short-lived at ambient temperatures. While it is true that the ESR spectra of complex mixtures of organic radicals are often difficult to assign conclusively, the use of slow warming of the sample and observation of changes in the spectral shape and intensity often permits identification of the radical species. Differences in the rates of power saturation of radical species has often also been used to separate components in the spectra. In addition the use of photobleaching to identify the contribution of radical ions to the spectrum should be noted.

1.1.4. FTIR

The other methods used in the study of the radiation chemistry of polymers have aimed to identify the final products of irradiation. The important method

of infra-red spectroscopy has been applied in detail to many systems. The high sensitivity of FTIR compared with many other spectroscopic techniques has led to a number of studies of low concentrations of reacting groups. For example, FTIR has been demonstrated to be useful in the study of the formation and decay of trans-vinylidene groups in irradiated poly(ethylene).[36,37] This work has led to the suggestion of the use of such measurements to determine applied radiation doses. An interesting recent application of FTIR has been the spatial mapping of degradation products using micro-FTIR.[38]

1.1.5. Volatile products analysis

As mentioned above, the interaction of ionizing radiation with polymers generally results in the evolution of low molecular weight volatile products. The evolved gases are conveniently identified and quantified using methods such as mass spectrometry and gas chromatography. In most polymer systems the principal gaseous product is molecular hydrogen, formed either by combination of hydrogen radicals, or abstraction of hydrogen by highly-reactive H$^{\bullet}$ radicals. Irradiation of polymers containing side groups often results in the observation of the products of cleavage of these groups. For example, a number of papers has reported the observation of low molecular weight alkanes formed by cleavage of side-chains in branched poly(olefin)s.[39,40] It has even been suggested that the measurement of the yields of evolved gases could be used to quantify the branching type and content in the original polymer.[41] In other polymers containing highly-reactive groups, the distribution of volatile products reflects the presence of these groups. For example irradiation of aliphatic poly(peptide)s results in the formation of large quantities of carbon monoxide and dioxide through degradation of the ester linkages.[42] In another example irradiation of aliphatic poly(sulfone)s results in the formation of sulfur dioxide and the corresponding alkene.[43] The yields of these products are greatly enhanced when irradiation is carried out above the ceiling temperature of the polymers.[44]

1.1.6. Measurements of molecular weights

The most important events occurring during radiolysis of polymers are cross-linking and chain scission. Thus measurement of changes in molecular weights as a function of radiation dose is a convenient means of obtaining effective yields of cross-linking and scission. Moad and Winzor[45] have reviewed in detail the effects of these reactions on polymer molecular weight distributions and some of the common methods for measuring molar masses. They have, however, only considered the effects of H-type cross-linking reactions; for a discussion of the changes in average molar masses during Y-type cross-linking the reader is referred to the paper of Lewis *et al.*[46]

1.1.7. Measurement of soluble fractions

In systems where cross-linking predominates, irradiation to sufficiently high doses results in the formation of a partially-insoluble network. In these cases the measurement of the gel fraction, after extraction of the soluble fraction by boiling in a suitable solvent, can lead to the yields of cross-linking and chain scission. The relationships between soluble fraction and yields of reactions were originally derived by Saito[47] and Charlesby and Pinner,[48] and have been used by many workers.

1.1.8. Mechanical properties

Finally, it is clear that radiation has a profound effect on the mechanical properties of polymers. The changes are most pronounced when main-chain scission predominates over cross-linking, as is the case for irradiation of most polymers in air. The effects of cross-linking on mechanical properties of polymers is, however, more difficult to predict, being very dependent on the initial form of the polymer, i.e. whether elastomeric, semi-crystalline or glassy. Destruction of crystalline material can also lead to changes in mechanical properties. Examples of measurements of mechanical properties of irradiated polymers are given in the texts of Charlesby[16] and Chapiro,[17] as well as in the papers of Williams *et al*.,[49] and El-Naggar *et al*.[50]

1.1.9. Radiation chemistry reviews

A number of reviews of the effects of radiation chemistry on polymer systems have been published. The classic texts are those of Charlesby,[16] Chapiro[17] and Dole.[18,19] Since then a number of extensive reviews of the effects of radiation have been published. For example, the *Polymer Handbook* has previously tabulated lists of the radiochemical yields reported elsewhere.[20] The ACS has published a number of collections of papers presented at radiation chemistry meetings,[21,22] and the two journals *Radiation Physics and Chemistry* and *Polymer Degradation and Stability* are of much interest. As mentioned above the proceedings of major meetings on radiation processing,[2–12] and the text by Singh and Silverman[1] provide an excellent overview of the field.

1.1.10. Aims of this review

As discussed by Singh and Silverman,[1] the dramatic increase in the importance of the radiation processing industry has resulted from a number of factors, not least of which is the increased understanding of the mechanisms of reaction of polymer on exposure to ionizing radiation. The aim of this review is to highlight the contributions NMR methods have made in this field. The review necessarily focuses on studies of radiation chemistry in vacuum, however in a later section

we discuss the smaller number of papers concerned with studies of oxidative degradation.

It is particularly hoped to highlight the areas where NMR will make increasing contributions to the field of radiation chemistry. The use of NMR to help unravel *mechanisms of reaction* is well established. Furthermore, NMR has enabled qualitative assessment of the *distribution of these reaction sites* throughout homogeneous and heterogeneous polymers. It is envisaged that NMR will continue to shed light on this issue, through, for example, use of spin diffusion measurements in cross-linked and glassy materials. The use of microimaging NMR experiments to determine the macroscopic dose distributions in electron-beam irradiated materials is also predicted.

1.1.11. A note on units

The unit of radiation dose used in this review is the Gray (Gy), which corresponds to an energy absorption of one joule per kilogram of material. Typical applied doses are in the range of tens of kGy, however, in some cases irradiation up to 10 MGy has been required to induce sufficiently large changes in molecular structure. The yield of radiochemical events is expressed as the G-value (written for example G(X) for the G-value of cross-linking). The G-value is defined as the yield of products for each 16 aJ (100 eV) of absorbed energy. Thus, 1 kGy of radiation will produce $G \times 1.036 \times 10^{-7}$ mole per gram of irradiated polymer.[14] The SI unit for radiation yield is the $\mu molJ^{-1}$ which is the equivalent of 10 G.[51]

1.2. NMR methods

The two main classes of NMR experiment applied to the study of the radiation chemistry of polymers are concerned with measurement of either the *chemical* structure of the polymer after irradiation, or the changes in the *physical* properties brought about by cross-linking or scission. In Sections 3–5 of this review the use of NMR to identify changes in chemical structure is discussed. The changes in the NMR line shape and relaxation times induced by radiation, and the use of these methods to determine radiochemical yields, are discussed in Section 2.

2. BROADLINE AND PULSED NMR OF IRRADIATED POLYMERS

2.1. Early broadline NMR and crystal structure

The earliest studies of the changes to the NMR spectrum of irradiated polymers were reported by Sohma *et al.*[52] and Tutiya and Yamamoto.[53–56] Of particular interest are the studies of Tutiya of the irradiation of poly(tetrafluoroethylene) (PTFE) at a range of temperatures.[55,56] The ^{19}F NMR spectrum of unirradiated

PTFE consists of two superimposed signals, a broad signal due to the crystalline material, and a narrow signal due to the chains in the amorphous phase above the glass transition temperature. The materials were irradiated to doses of 8.9 MGy at temperatures ranging from 25–340°C. After irradiation at room temperature an additional narrow signal was observed in the ^{19}F NMR spectrum recorded at 90°C. This was assigned to low molecular weight materials formed by degradation of the PTFE. It is well known that PTFE undergoes extensive radiation degradation on irradiation at normal temperatures.[57,58] On heating this material to near its melting temperature and recooling, the narrow signal disappeared, due to reorganization of the crystalline structure and removal of low molecular weight products. In their later paper[56] the authors reported on the behaviour of PTFE irradiated at just above its crystalline melting point. A pronounced decrease in the crystalline content, determined from the NMR spectrum, after irradiation in a small band of temperatures was ascribed to the formation of cross-links between the PTFE chains. This early NMR study thus predates the work of Sun[59] and Oshima *et al.*[60] on cross-linked PTFE by some years. Details of the chemical processes occurring are discussed in Section 5 of this review.

The effect of radiation on the crystalline phase of non-fluorinated polymers has been the subject of intense investigation using a number of techniques including NMR spectroscopy.[61–65] The focus of this interest is the determination of the location of radiation-induced products after irradiation. There is evidence that in fully-saturated amorphous materials, radiation events occur randomly throughout the material,[66] while in diene rubbers the distribution of reactions is highly heterogeneous.[67,68] Similarly, there is much evidence that radiation events are concentrated in the amorphous phase of semi-crystalline polymers,[69–72] and possibly more specifically at the interface between the crystalline and amorphous phases. None-the-less radiation does have profound affects on the crystallinity of semi-crystalline materials. Irradiation of poly(ethylene), for example, results in a progressive decrease in crystallinity above a dose of approximately 2 MGy, while at lower doses there have been reports of both increases and decreases in crystallinity.[63,73,74] Ahmad and Charlesby[61] used broadline ^{1}H NMR to study these changes in poly(ethylene). A progressive decrease in width of the broad signal due to the protons within the crystalline phase was taken as evidence of the formation of defects and hence increased mobility within the crystals. The width of the narrow component increased with cross-linking. Related ^{13}C MAS NMR measurements are discussed in Section 4.4 of this review.

2.2. Pulsed NMR of polymer rubbers and melts

It is well known that the spin–spin relaxation times of protons in condensed polymers are determined by the strength of the homonuclear dipolar coupling between the protons, and are therefore strongly influenced by the presence of chain entanglements involving more than one polymer chain. These chain entanglements may

be physical in nature, or chemical, that is cross-links formed during irradiation of many systems. On the other hand, the entanglement density will decrease in materials which undergo main-chain scission. In practice the decay of transverse magnetization can be decomposed into usually two or in the case of cross-linked poly(ethylene) three exponential decay functions. The most rapid decay process is assigned to relaxation of protons in chain segments close to cross-links, while the slower decays to protons in segments well removed from the cross-links. Therefore the decay of magnetization is described by $M(t) = \Sigma M_i(0) \exp(-t/T_2^i)$, where M_i and T_2^i are the amplitude and time constant of the ith decay process, respectively, and i can take the values 1, 2 and in some cases 3. It is important to note that M_1, i.e. the amplitude of the fastest decay, does not give a direct measure of the number of cross-links, but rather the number of protons having short relaxation times due to the proximity of the cross-links. Furthermore the form of the fastest decay is often noted to deviate from exponential and rather has the form of a Gaussian decay. The majority of the workers in the field of radiation chemistry of polymers have been more concerned with the relative amplitudes, M_i, of the decay functions rather than the precise forms of the decay functions. The interested reader is referred to the work of Gotlib[75] and Fry and Lind[76] for early descriptions of the analysis of the rapid transverse relaxation function.

Charlesby's group has introduced many new concepts to the field of radiation chemistry of polymers. They introduced and explored in some detail the use of the measurement of spin–spin relaxation times to determine cross-link density in polymers. Poly(dimethyl siloxane) (PDMS) undergoes cross-linking on exposure to ionizing radiation. Folland and Charlesby[77] reported the changes in T_2 relaxation times in PDMS using the Hahn echo sequence, followed as a function of radiation dose and initial molecular weight. The initial molecular weights of all polymers investigated were above the critical molecular weight for entanglement, and therefore in the unirradiated material the T_2 decay was bi-exponential in nature. The proportion of protons having a long T_2 relaxation time was labelled f by Charlesby. The change in this fraction with dose was modelled by considering that unirradiated polymer had received a 'virtual radiation dose' producing chain entanglements or cross-links proportional to this dose. The applied radiation dose was corrected for the virtual radiation dose, to allow analysis of the radiation chemical processes. Figure 1 shows the plot of the fraction f of the slowly relaxing protons, plotted as a function of 'corrected' radiation dose divided by the gel dose, for all four polymers analysed. The solid line on the figure is the result of fitting the data to the Charlesby–Pinner equation.[48] The agreement between experimental and theory is excellent, and yields a G-value for cross-linking of G(X) = 2.8 (G(S) = 0.0), in agreement with results obtained with more traditional methods. The figure also demonstrates that the yield of cross-links is independent of molecular weight, as expected for high molecular weight polymers. Most importantly the method demonstrates that NMR can provide a direct measure of soluble fraction rapidly and without the use of extensive extraction methods used traditionally.

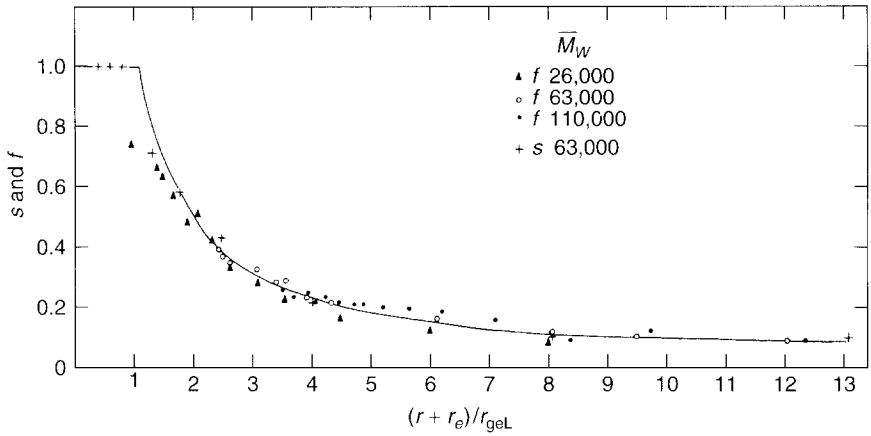

Fig. 1. The fraction, f, of protons having long T_2 relaxation times, and soluble fractions, s, in irradiated PDMS as a function of corrected radiation dose. The gel doses, r_g, were determined experimentally, while the effective radiation dose, r_e, was 60 kGy and 0 kGy for NMR and soluble fraction measurements, respectively. Reproduced from ref. 77 with permission. Copyright 1977 Elsevier Science.

In similar work,[78] the effect of gamma irradiation on the ^{1}H transverse relaxation decay of cis-poly(isoprene) was studied, and the G(X) value of 0.81–0.88 obtained from NMR was in good agreement with the value of G(X) = 0.8 previously reported. In addition the magnitude of the virtual dose, described above, allowed an estimate of the initial molecular weight between entanglements of 40 000 at 423 K. This was compared with the estimate of $M_c = 30\,000$ also obtained by measurement of T_2 relaxation times of unirradiated polymers.[79] Later Charlesby and Bridges[80] explored in some detail the relationship between molecular weight and the time constant of the slower relaxation decay in cis-poly(isoprene) below M_c.

Charlesby and coworkers[81] have also measured the changes in T_2 relaxation times at 150°C of high molecular weight PE irradiated to a range of doses. For ease of description the decay curves were fitted to two exponential decay processes, despite the fit being less adequate than that obtained assuming three processes. The two processes could not be assigned to protons in entangled and unentangled chains in the manner described above. This was ascribed to either non-random cross-linking, or the possibility that the short T_2 decay does not arise solely from protons associated with radiation-induced cross-links. The possibility that the results are dominated by effects of the very broad molecular weight distribution commercial PE samples, or that the morphology of the polymer is retained to some extent at these elevated temperatures was discussed.

More recently Whittaker[82] re-examined the spin–spin relaxation behaviour of irradiated PE. The decay curves, obtained using the CPMG sequence at 430 K, were fitted to the sum of three exponential processes. The most rapid decay

was ascribed to residual order in the molten phase, as suggested for unirradiated poly(ethylene) by previous workers.[83–85] The two longer decay processes were assigned to chains in a transition zone, and chains distant from both regions of order and cross-links, in order of increasing T_2. The change in the amplitude of the shortest T_2 process with dose was closely mirrored by the changes in the heat of fusion, and hence crystallinity, of the polymer. This similarity suggests that at low radiation doses the crystalline regions of poly(ethylene) are especially sensitive to radiation degradation, and that cross-linking occurs within or at the surface of the crystalline regions.

Finally, Charlesby and Steven[86] have shown that T_2 relaxation times can provide a measure of the changes in molecular mass of a degrading polymer, namely poly(isobutylene), after irradiation. The authors used an empirical relationship between the longest T_2 relaxation time and the number average molecular weight to establish that the yield of scission reactions could be calculated given knowledge of the initial number-average molecular weight.

3. ^{1}H AND ^{13}C SOLUTION-STATE NMR OF IRRADIATED POLYMERS

3.1. Solution-state NMR studies of cross-linking

The methods described in the previous section are sensitive to changes in the physical state of the irradiated polymer, whether that be crystalline perfection, or chemical and physical entanglements. It is not possible from these measurements to make direct conclusions about the mechanisms of cross-linking reactions, and so it was apparent at an early stage that high-resolution ^{13}C solution-state NMR methods are required to complement these early studies. The chemical shift dispersion in ^{1}H NMR is insufficiently small compared with the large linewidths in spectra of polymers to make this method feasible for detecting very small concentrations of new structures. However, ^{13}C solution-state NMR has been used with success to help identify the mechanisms of cross-linking in a number of polymers. An early aim was to determine the relative proportion of H- and Y-type cross-links (Fig. 2) formed in irradiated poly(olefin)s. The earliest high-resolution NMR study of the radiation-induced formation of cross-links was of irradiated liquid model compounds of poly(ethylene), n-hexadecane and n-eicosane.[87] These authors reported the formation of so-called H-link structures apparently via recombination of two secondary main-chain alkyl radicals. Not long after this Bovey *et al.*[88] reported the identification of both H- and Y-type links in n-$C_{44}H_{90}$ irradiated in the melt using ^{13}C solution-state NMR. Irradiation in the crystalline state produced only linear dimers, apparently through end-linking of molecules at the crystal surfaces.

A fundamental impediment to the use of solution-state NMR in the analysis of cross-linked materials is the tendency of the polymers to become partially insoluble at the gel dose. As will be discussed below the rapid increase in strength

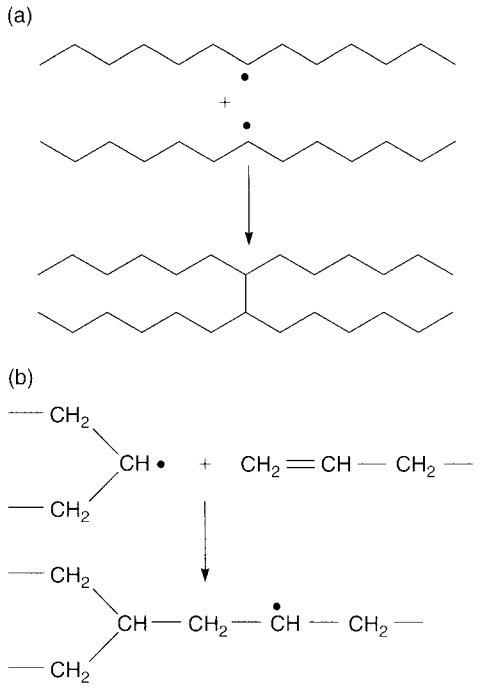

Fig. 2. Proposed mechanisms of (a) H- and (b) Y-linking of poly(olefin)s.[87 89] The secondary radicals formed in (b) will terminate by abstraction of, or combination with, a hydrogen atom.

of the dipole–dipole coupling at the gel dose precludes standard solution-state methods and in particular standard scalar decoupling of the protons. Therefore examination of irradiated polymers by solution-state NMR is limited to samples irradiated to below the gel dose. The gel dose for polymers which undergo predominately cross-linking is the dose at which there has been formed on average one cross-link per weight-average polymer chain, and is therefore related to the inverse of the initial molar mass. Thus low molecular weight model compounds remain fully soluble up to relatively high radiation doses, and therefore, at the gel dose, the total number of cross-links formed per unit mass of material is high. On the other hand, the number of cross-links formed at the gel dose on irradiation of a typical high polymer may be of the order of one or less per thousand main-chain carbon atoms. These concentrations are at the limit of sensitivity of standard solution-state NMR techniques.

None-the-less, a number of thorough studies of cross-linking in high poly(olefin)s have been reported.[89–92] In early work, Randall *et al.*[89,90] studied irradiated high-density poly(ethylene)s (HDPE) using ^{13}C NMR, and identified a number of new structures, including internal double bonds and Y-type cross-links. The materials under consideration contained initially a high concentration of vinyl end

groups, which react readily with secondary alkyl radicals (Fig. 2) to form Y-links. The authors were unable to identify H-links in their irradiated HDPE samples, and suggested that for these materials irradiated to low doses, the H-linking mechanism is relatively unimportant.

In a more recent study, Horii and coworkers[91,92] studied changes in the ^{13}C solution-state NMR spectra of relatively-low molecular weight PE samples irradiated under a range of experimental conditions. The lower molecular weight resulted in lower viscosity and hence smaller line widths and thus the authors claimed they were able to observe resonances in the spectra due to H-type cross-links in all samples. Figure 3 shows the ^{13}C solution-state NMR spectra of irradiated HDPE. The yields of H-links and Y-links were measured as a function of temperature,[92] and it was found that H-links were the dominant product when PE was irradiated in the molten state, while Y-links were more commonly formed on irradiation at ambient temperatures. It was suggested that at higher temperatures the probability of reaction of the primary radicals (II) in Fig. 2 above with $H^{\bullet}$ is higher in the molten state, and thus recombination of the longer-lived secondary radicals (I) dominates. The formation of internal double bonds and methyl side-chains is also reported, and mechanisms discussed. The conclusions of this work are supported by the study of O'Donnell and Whittaker[93] in which the formation of H-type cross-links in fully-saturated ethylene propylene rubber (EPR) irradiated well above T_g was confirmed.

3.2. Solution-state NMR studies of chain scission

As discussed below solution-state NMR methods cannot be successfully applied to materials irradiated to above their gelation dose. This situation naturally does not arise for polymers for which chain scission is the dominant reaction on irradiation. The two systems of this type which have been most extensively studied are the poly(methacrylate)s and poly(isobutylene).

Hill and O'Donnell's group[94,95] has examined the radiation chemistry of a number of poly(methacrylate)s having different length side-chains using a number of methods including high-resolution solution-state NMR. As mentioned in the introduction, poly(methacrylate)s undergo predominantly main-chain scission, however in this work, the authors found, from GPC measurement, that cross-linking became significant with increasing length of the side-chain. Thus for poly(methacrylate)s with side-chains of length $n = 1, 2$ and 3, there was no evidence of cross-linking reactions, however for polymers with $n > 3$ cross-linking became increasingly important until for poly(2-methylheptyl methacrylate) the yield of cross-linking was sufficient compared to chain scission for the molecular weight of the polymer to increase on irradiation. Cross-linking proceeds through linking of side-chain groups in the higher analogues. The suggested mechanism for main-chain scission in methacrylates involves cleavage of the ester side chain, and subsequent beta scission of the main chain.[96] This was

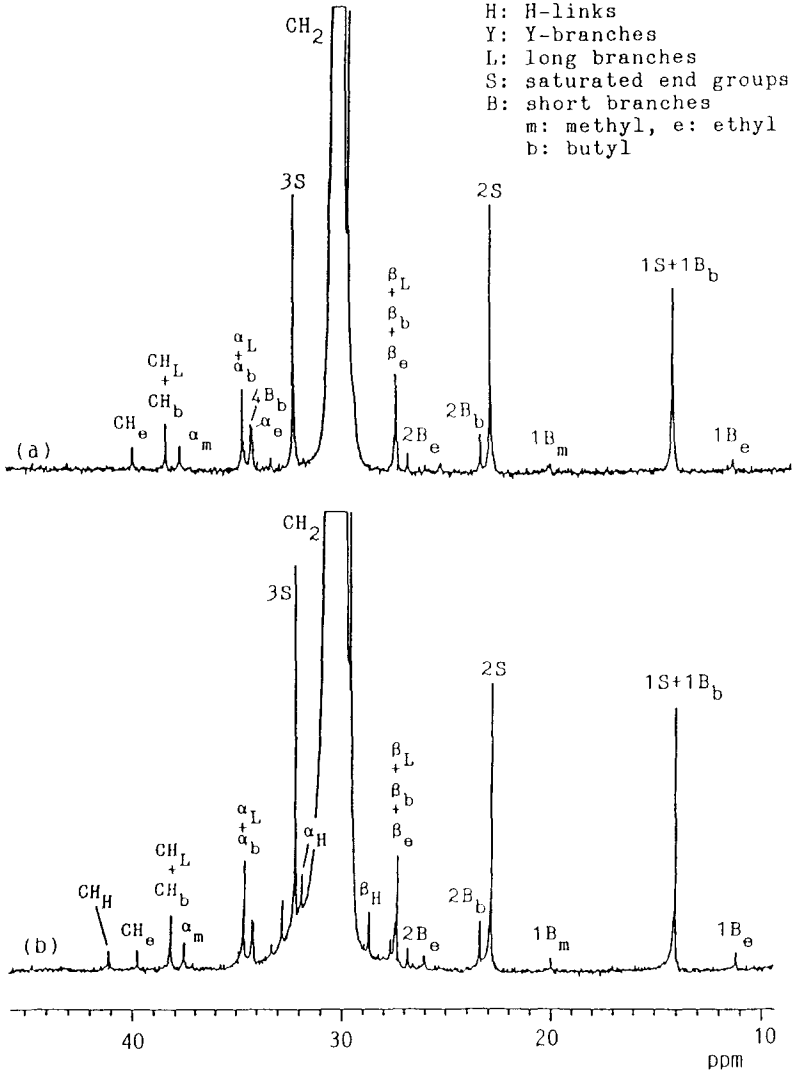

Fig. 3. ^{13}C solution-state NMR spectra of a low molecular weight (Mw = 1.45×10^4, Mn = 1.07×10^4) poly(ethylene) fraction (a) unirradiated and (b) irradiated to 300 kGy at 423 K in vacuum. Reproduced from ref. 92 with permission. Copyright 1992 John Wiley & Sons.

confirmed by ^1H and ^{13}C solution-state NMR observation of esters as low molecular weight products. The role of alkyl radicals initially formed on the side-chain in poly(2-methylheptyl methacrylate) was underlined by the observation of unsaturated groups on the side chains. Irradiation of benzyl methacrylate led to the formation of toluene and 1,2-diphenyl ethane through initial side-chain cleavage

and decarboxylation reactions. The use of spin-echo modified multidimensional ^{1}H NMR methods was highlighted in these papers.

The same group has reported on the use of ^{13}C solution-state NMR to study changes in the structure of poly(isobutylene) (PIB) on irradiation.[97,98] This material undergoes chain scission, by virtue of the presence of quaternary carbon atoms on the main chain (see Section 1.1). The mechanism of chain scission was determined through these studies. The changes in the ^{13}C NMR spectra on irradiation are large as can be seen from Fig. 4, and have been assigned to contributions from five different chain end structures. Terminal vinyl groups were found to undergo secondary reactions at higher radiation doses. In addition loss of methyl groups from the main chain resulted in formation of vinylidene groups well removed from the chain end. These studies resulted in the confirmation of three major pathways to degradation, namely (1) initial cleavage of the polymer main chain, and (2) and (3) beta-scission after loss of protons from the methyl or methylene groups. Two other previously suggested mechanisms of degradation were not supported by the NMR evidence.

Butyl rubber is a copolymer of isobutylene and 1–2% isoprene. As a result the polymer chains contain internal double bonds which are expected to participate in cross-linking reactions. However, the overall molecular mass is expected to fall on irradiation due to the predominance of main-chain scission through the isobutylene units. Thus the radiation chemistry of the isoprene units within butyl rubber is accessible to study via solution NMR. In a comprehensive study Hill *et al.*[99] identified the primary free radical species by electron spin resonance spectroscopy at low temperatures, and the products of their subsequent reaction by ^{13}C solution-state NMR. A number of new cross-link structures were identified and the mechanisms of cross-linking determined. Initial reaction involves addition of radicals either directly to the isoprene double bonds or to allyl radicals. Further addition of hydrogen atoms results in a mixture of fully-saturated and unsaturated cross-link structures. Cross-links of both H- and Y-type were identified and the yields of products agreed closely with the yields determined from measurement of changes in molecular weight on irradiation.

3.3. Solution-state NMR studies of racemization

The NMR study of irradiated polymers of high stereoregularity has resulted in a number of interesting observations and conclusions concerning the mechanism of energy deposition and energy transfer in condensed systems. It was noted as early as 1965 that stereoregular poly(methyl methacrylate) (PMMA) undergoes a racemization reaction on exposure to ionizing radiation.[100] In addition it has been observed that the yields of racemization reactions are much higher than the yields of any other radiochemical reaction not involving a chain reaction thus far identified. The overall mechanism of racemization is summarized in Fig. 5; it involves the formation of a transition state, in which the sp^3 hybridization of the main-chain carbon can adopt for some (unspecified) time sp^2 character,

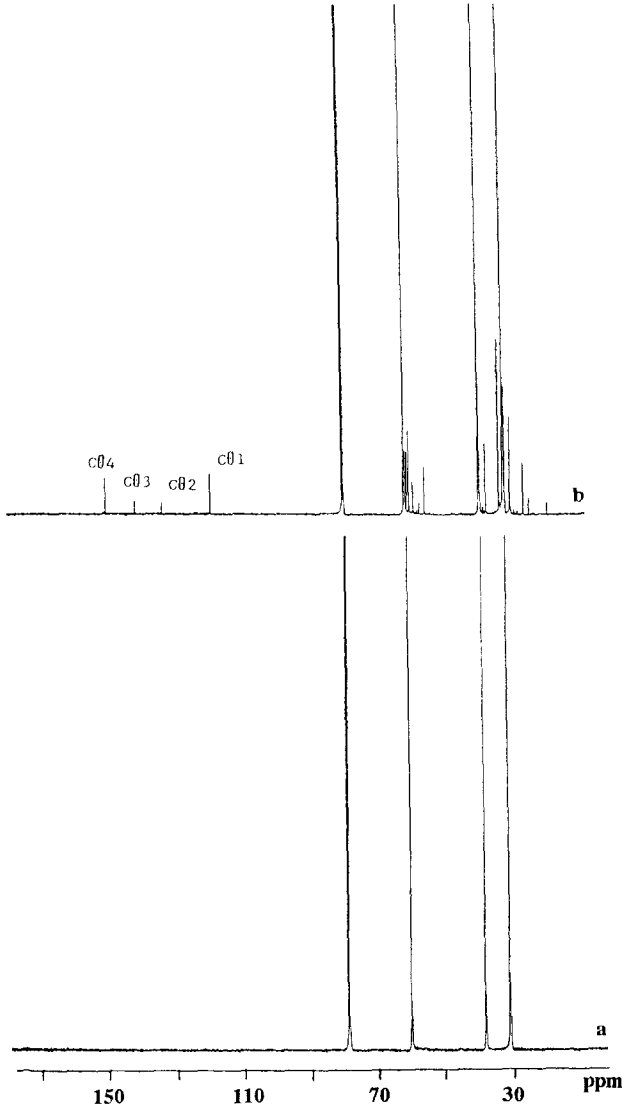

Fig. 4. ^{13}C solution-state NMR spectra of PIB, (a) unirradiated and (b) after irradiation with a dose of 9 MGy in vacuum at 303 K. Reproduced from ref. 97 with permission. Copyright 2000 American Chemical Society.

and hence undergo isomerization to its complementary configuration followed by stabilization. The intermediate species may have free radical or ionic character, or may be an excited state species. The NMR experiment detects a change in stereoregularity resulting from the intermediate species adopting a different configuration prior to stabilization.

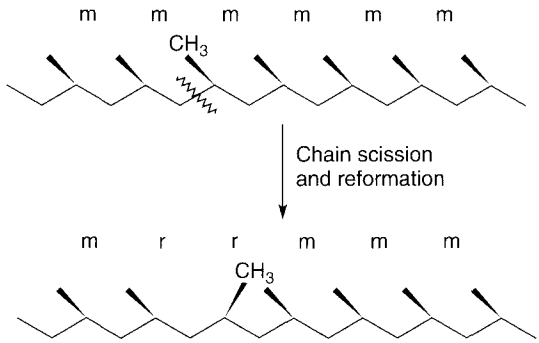

Fig. 5. Schematic representation of the process of racemization. In this example bond scission occurs in the main chain, however, scission might similarly occur at the side chain. The scission is followed by rotation about the main chain and reformation of the initially-broken bond. There is a resultant formation of two racemic diads and destruction of two meso diads.

The ^{13}C and ^{1}H solution-state NMR spectra of PMMA show tacticity splittings generally to pentad levels. In addition the polymer remains soluble to high doses after irradiation. Thus it has been possible to measure changes in chain stereoregularity after irradiation.[100–102] In a recent study by Dong *et al.*[101] the changes in tacticity of both highly isotactic and syndiotactic PMMA irradiated in vacuum up to 1.6 MGy were reported. Figure 6 shows the changes in the carbonyl region of the ^{13}C spectrum of isotactic PMMA irradiated at 80°C. A clear increase in the intensity of the peaks assigned to racemic diads can be observed after irradiation. Such changes were observed only in materials irradiated at temperatures above the glass transition temperature ($T_g = 38$°C). It was suggested that the racemization process involved rotation of the bulky ester side chain and that below T_g there is insufficient free volume for this to occur. The authors simulated the changes in tacticity on irradiation using a Monte Carlo approach with varying probability of reaction and stabilization in the meso configuration. It was found that the probability of stabilization in the meso arrangement was close to that observed during free radical polymerization at these temperatures, thus suggesting that the racemization reaction involves the formation of short-lived radicals similar to the PMMA propagating radicals. The yield of racemization reactions was thus used to calculate a yield of chain scission reactions of G(temporary chain scission) = 18.6 at 80°C. This compares with a yield of permanent chain-scission reactions of G(S) ~2. If the most probable reaction on irradiation of PMMA is initial cleavage of the side-chain ester linkage, it must be concluded that only 10% of these reactions result in permanent scission and that the remaining 90% lead to recombination reactions. Finally it was noted that a much less significant change in the NMR spectrum of syndiotactic PMMA was observed since the probability of formation of meso units compared with racemic units is relatively small.

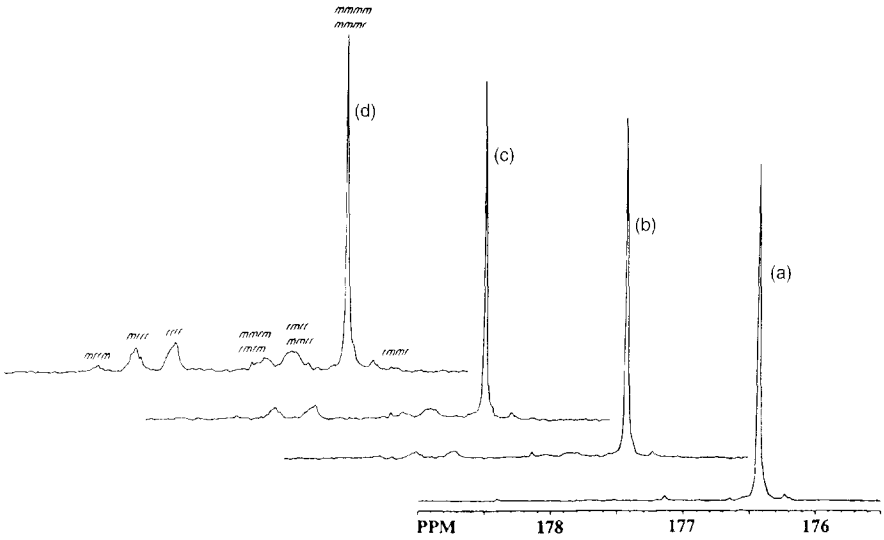

Fig. 6. Expansion of the carbonyl region of the ^{13}C solution-state NMR spectrum of isotactic PMMA irradiated at 80°C by doses of (a) 0, (b) 165, (c) 200 and (d) 500 kGy. Reproduced from ref. 101 with permission. Copyright 2000 American Chemical Society.

In the studies described above the stereochemistry of the irradiated PMMA was described well using a simple model assuming that the racemization reactions consisted of isolated reaction events. Studies of irradiated isotactic poly(propylene) (PP)[102-107] have on the other hand provided evidence that the racemization reactions are not in this case isolated, but rather that they may occur in clusters. The methyl region of the solution-state ^{13}C NMR spectrum of PP can be resolved to the pentad level. The changes in the pentad distribution on irradiation are not consistent with random reactions occurring along the polymer backbone;[103-106] a number of schemes have been suggested involving, for example, an increased probability of reaction after initial reaction, but all schemes have in common the observation that the proportion of syndiotactic sequences formed on irradiation is high and the rate of equilibration of these sequences is low. It should also be noted that electron-beam irradiation at high doses was much more effective in promoting changes in tacticity than gamma irradiation to comparable doses.[104]

3.4. Solution-state NMR studies of other systems

^{13}C solution-state NMR has provided useful information on the radiation chemistry of a number of other polymers.[108-114] For example, a Y-linking mechanism in poly(aryl sulfone), previously suggested from ESR and molecular weight

studies, was confirmed by high resolution ^{13}C NMR.[108] Similarly, the structure of new chain ends in irradiated bisphenol-A poly(carbonate) was confirmed by this method.[109] This material undergoes predominately chain-scission reactions and so remains in solution at all doses. Other reports have been made of the NMR spectra of irradiated Nylon-6,[110] poly(arylene ether ketone)s,[111] poly(arylene ether phosphine oxide)s,[112] poly(lactic acid) and poly(glycolic acid)[113] and poly(hydroxybutyrate-co-hydroxyvalerate).[114]

3.5. Practical limits to solution-state NMR studies

The preceding section has been concerned with the observation of changes in the NMR spectra of polymers which undergo predominantly chain scission and hence remain soluble at all doses, or cross-linking polymers irradiated to below their gel doses. For this latter class of polymers it is well known that the total NMR signal intensity in spectra collected using standard solution-state techniques, will decrease with irradiation doses above the gel dose. Figure 7 shows that both the soluble fraction and NMR signal intensity decrease in a similar manner for irradiated EPR.[93] Ford and coworkers reported similar observations for chemically-cross-linked polymers.[115–118] It is thus concluded that the chain segments both involved in, and adjacent to the cross-link units do not contribute to the NMR spectrum. This is due largely to the dramatic increase in the strength of the $^{1}H-^{13}C$ heteronuclear dipole–dipole couplings at these sites as the molecular motion becomes slower and more anisotropic. Standard solution-state decoupling

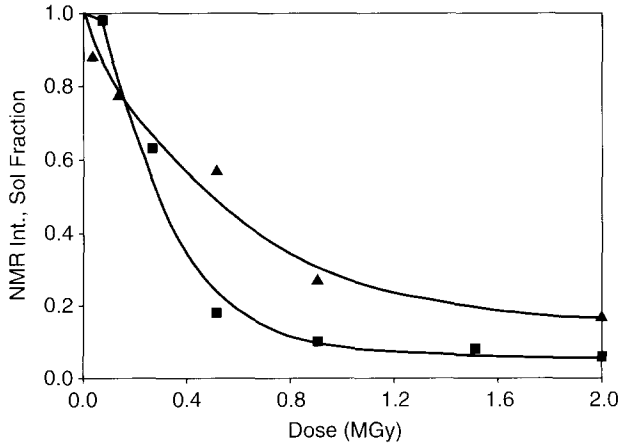

Fig. 7. Dependence of soluble polymer fraction (■) and intensity of ^{13}C NMR signal collected under standard high-resolution conditions (▲) of EPR containing 36% propylene, irradiated in vacuum by doses up to 2 MGy. The solid lines are drawn as a guide to the eye. Adapted from ref. 93 with permission. Copyright 1992 Elsevier Science.

methods are incapable of averaging these strong couplings and the effective T_2 relaxation times of the ^{13}C nuclei become very short. Such observations mirror those seen in the measurements of ^{1}H T_2 relaxation times discussed in Section 2.2 of this review. It is clear that other methods are required to examine polymers irradiated to above the gel dose. These might include swelling of the cross-linked polymer and hence increasing the available free volume for chain motion, or artificially averaging the dipole–dipole couplings with magic-angle spinning. In practice the former method does not result in appreciable averaging of the dipolar couplings, so that solid-state NMR methods must be employed.

4. ^{13}C MAS NMR OF IRRADIATED POLYMERS

As discussed in the previous section, on irradiation polymers often become insoluble in their normal solvents. Hence, resort must be made to solid-state NMR techniques. In general the resolution in solid-state spectra is significantly inferior to that achievable in solution-state NMR of polymers, due to a number of factors including most importantly increased chemical shift dispersion from frozen-in conformations, and incomplete decoupling or line narrowing by magic-angle spinning (MAS) arising from interference from molecular motion with the decoupling or spinning.[119-121] Therefore, it is often difficult to identify new peaks having low intensity in spectra of irradiated materials. None-the-less, important information has arisen from solid-state NMR spectra of irradiated polymers.

4.1. High-resolution solid-state NMR methods

The technique of magic-angle spinning (MAS) was introduced by Andrew and coworkers[122] and Lowe[123] in 1959. The aim of the experiment at that time was to partially average homonuclear dipole–dipole couplings in ^{1}H-rich materials. It was not until more than a decade later that MAS was first used in ^{13}C NMR spectroscopy. By this time Pines, Gibbey and Waugh[124] had introduced the experiment now known as cross-polarization (CP). The combination of the two techniques, as well as the use of high-power ^{1}H decoupling was first applied to solid polymers by Schaefer and Stejskal in 1976,[125] and opened up the field of NMR analysis of insoluble materials, including irradiated polymers.

In the absence of isotropic motion, the ^{13}C NMR lineshape is dominated by strong dipole–dipole couplings to neighbouring protons, and the relatively large anisotropy of the chemical shift tensor. The technique of MAS deals effectively with the latter of these effects, since rapid rotation of the sample around the magic angle leaves only the trace of the tensor, i.e. the isotropic chemical shift, observable. Rotation at intermediate spinning speeds results in a series of rotational echoes in the FID, which on Fourier transformation results in the familiar spinning sidebands.[126] Magic-angle spinning also partially averages the heteronuclear dipole–dipole couplings, however, high-power proton decoupling during

acquisition is required to fully remove this contribution to the ^{13}C NMR lineshape. The combination of MAS and high-power ^{1}H decoupling is sufficient to achieve high-resolution ^{13}C NMR spectra of solid polymers.

The sensitivity of the ^{13}C NMR experiment is limited by the often very long spin-lattice relaxation times of the ^{13}C nuclei. Values of ^{13}C T_1 of over 1000 s have been measured in solid poly(ethylene).[127] It is likely that ^{13}C nuclei involved in rigid cross-link structures also possess very long ^{13}C T_1 relaxation times. As a result pulse repetition times, and hence total scan times are often prohibitively long, especially when the aim is to observe peaks due to low concentrations of products of irradiation. The technique of cross-polarization reduces this problem since the spin temperature of the protons and not the ^{13}C nuclei has to re-equilibrate before pulse repetition. The ^{1}H T_1 in proton-rich condensed systems is usually much shorter than ^{13}C T_1. In addition the signal-to-noise in the CPMAS spectrum is increased by a factor of up to four compared with spectra obtained by direct excitation of the ^{13}C spins, due to the larger Boltzmann population of the proton nuclei.

Despite these apparent insurmountable advantages care must be taken when using CPMAS to acquire spectra of irradiated polymers. The possible heterogeneity of reactions or morphology throughout the bulk polymer often means that parts of the polymer are very rigid, i.e. the cross-linked groups or crystalline regions, and other parts are highly mobile, i.e. the uncrosslinked amorphous regions above the glass transition temperature. The rate of cross-polarization depends strongly on the strength of the dipolar couplings of near-neighbour ^{1}H nuclei with the respective ^{13}C nuclei and hence ^{13}C nuclei in cross-linked parts of the polymer undergo cross-polarization more effectively than in uncross-linked parts. Thus much care must be taken in the quantitative analysis of CPMAS spectra of irradiated polymers.

4.2. ^{13}C MAS NMR of irradiated poly(olefin)s

Sohma and coworkers reported the first solid-state NMR spectrum of an irradiated poly(olefin).[128] The ^{13}C CPMAS spectrum of irradiated ethylene-propylene rubber showed an increase in intensity in the spectrum at 37 ppm on cross-linking, due to the methine groups of cross-links, as well as a new peak at 24 ppm due to the products of main-chain scission. The peak at 37 ppm was poorly resolved, and the low signal-to-noise level made definite assignment difficult. O'Donnell and Whittaker[66] applied the same technique to ethylene-propylene rubbers irradiated to a radiation dose of 10 MGy, and were able to estimate yields for cross-linking and scission which were in excellent agreement with values obtained from measurement of the soluble fractions and from solution-state NMR.[93] The authors concluded that the assumption of random cross-linking, implicit in the Charlesby–Pinner analysis[48] of the soluble fractions, was valid in the case of this amorphous polymer.

The solution-state ^{13}C NMR spectrum of poly(ethylene) is composed of a single large peak at close to 30 ppm with respect to tetramethylsilane, and a number of much smaller peaks to higher and lower chemical shifts due to structures associated with branch points (e.g. ref. 129). A single peak for the dominant methylene sequences is observed at a chemical shift reflecting the relative populations of gauche and trans isomers rapidly exchanging with each other in solution. In the solid state this exchange is hindered by the presence of crystalline material. The solid-state ^{13}C NMR spectrum of poly(ethylene) consists largely of two peaks, one at 32.5 ppm due to methylene units in chain segments adopting the all-trans configuration, and another broad peak centred around 29.0 ppm due to chains with a high proportion of gauche configurations.[130,131] The broad shoulder of the peak at 32.5 ppm, and the appearance of a peak at 34.0 ppm due to all-trans chains in monoclinic unit cells[132] makes observation of a new peak due to the methine group of the cross-link (expected at 35–45 ppm) problematic. Cholli and coworkers[133] were the first to convincingly demonstrate the direct observation of cross-links in poly(ethylene) by solid-state NMR. ^{13}C CPMAS NMR spectra of high-density poly(ethylene) irradiated to 6 MGy showed two small new peaks at 43 ppm and 39.7 ppm, assigned to methine carbons in Y- and H-links, respectively. The formation of Y-links or branches was confirmed by the appearance of new peaks at 30.0, 7.8 and 15.4 ppm due to branch structures. O'Donnell and Whittaker[63] also reported the appearance of an additional peak in the ^{13}C CPMAS spectrum of irradiated PE at 39.5 ppm, also assigned to methine carbons in H-cross-links. It was found that the carbon nuclei giving rise to this peak is associated with protons having a very long ^{1}H $T_{1\rho}$, and therefore the peak became more prominent at longer CP contact times. The long value of ^{1}H $T_{1\rho}$ is consistent with these carbons being situated in very rigid structures.

Pérez and VanderHart[134] have also used ^{13}C CPMAS to study irradiated poly(ethylene), however they were unable to observe peaks due to carbons in cross-link structures in samples irradiated up to 2 MGy. New peaks in the spectra were observed due to methyl chain ends (15 ppm) and internal double bonds (130 ppm). The authors applied a methodology previously developed by them[135] to determine the extent of partitioning of side groups between the crystalline and amorphous phases in semi-crystalline PE. This involved recording three spectra with different preparation of ^{1}H magnetization prior to cross-polarization to the ^{13}C spins. Linear combinations of these spectra were used to obtain spectra of 'pure crystalline' and 'pure non-crystalline' phases of the material. Peaks due to both the methyl end groups and the internal vinyl groups were observed in both spectra, however the concentration of methyl end groups in the amorphous phase exceeded that in the crystalline phase.

4.3. ^{13}C MAS NMR of irradiated poly(diene)s

A number of careful studies have shown that the radiation-cross-linking of cis-1,4-poly(butadiene) (cis-PBD) proceeds via a chain-reaction mechanism involving

consumption of a number of double bonds for each effective cross-link.[67,68,136,137] ESR spectroscopy was used to identify the primary radical species as the allyl radical formed through a H-atom abstraction reaction. Figure 8 shows the changes in the ^{13}C CPMAS spectra of samples irradiated to various doses up to 10 MGy. The peak at 130.5 ppm due to double bonds decreases in intensity on irradiation, while a new, broad peak at 45.8 ppm assigned to methine carbons in cross-link structures appears. A peak at 30.5 ppm due to methine groups adjacent to cross-links was revealed through the simulation of the aliphatic region of the spectrum. The NMR spectra were recorded as a function of cross-polarization contact time, and from this information quantitative intensities for each carbon type were calculated. The yield of cross-links G(X) was of the order of 28,[68] indicating a chain reaction was involved in the cross-linking. The clustering of cross-links implied by this mechanism explains the relatively low G-values for cross-linking (G(X) = 3–6) determined from gel contents and swelling measurements. It was also found that double bonds undergo a cis–trans isomerization reaction during irradiation through formation of allyl radicals, isomerization and subsequent H-atom abstraction of these radicals.

The effect of chemical composition, and dose on a range of different poly(butadiene) samples was also examined by these authors.[68] Similar results were obtained for cis- and trans-1,4-poly(butadiene), however, even larger G-values were measured for 1,2-poly(butadiene), presumably because of the higher reactivity of pendant vinyl groups compared with internal double bonds and the close proximity of side-chains allowing a zipping chain reaction. Among

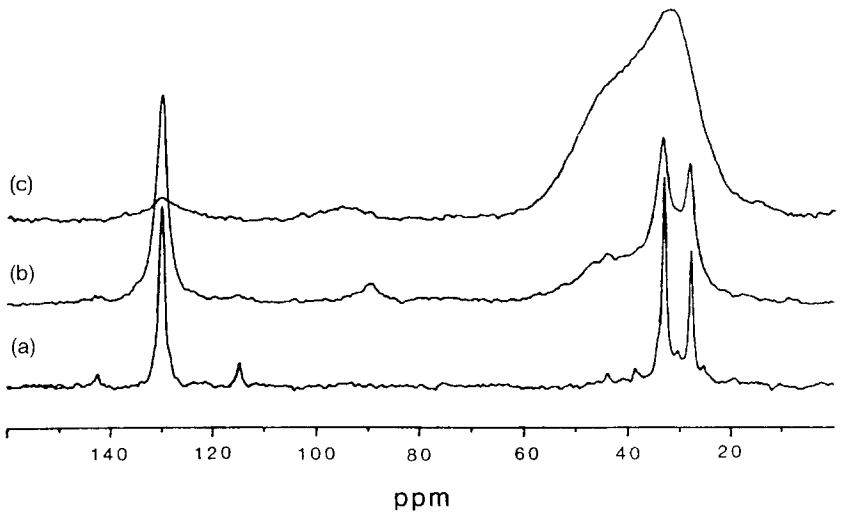

Fig. 8. ^{13}C CPMAS spectra of cis-PBD irradiated in vacuum by (a) 0.44 MGy, (b) 3 MGy and (c) 10 MGy. Reproduced from ref. 68 with permission. Copyright 1992 John Wiley & Sons.

other systems investigated by this group are butyl rubber,[138] natural rubber sensitized with acrylates,[139] chloroprene,[140] chlorobutyl rubber[141] and nitrile rubber.[142] More recently, Perera has examined the relationship between chemical changes in radiation-grafted natural rubber, determined using ^{13}C MAS NMR, and mechanical properties measured using dynamic mechanical analysis.[143,144]

Koenig and coworkers have reported a very large number of studies of the chemical structure of cross-linked rubbers using solid-state ^{13}C NMR.[145,146] In these papers they explore the factors affecting the observed ^{13}C NMR signal intensities, and methods for assigning the spectra. Most of their work has concentrated on chemically-cross-linked rubbers, however, they have examined the radiation cross-linking of natural rubber, cis-poly(isoprene), using solid-state ^{13}C NMR.[145] A highly heterogeneous structure was evidenced by differences in the spectra obtained by direct excitation of the ^{13}C nuclei, and those obtained using cross-polarization. CPMAS spectra showed resonances due to cross-links, and new chain ends formed by degradation processes. The isomerization of cis-double bonds to the trans configuration was also followed. A lower yield of isomerization of double bonds was measured compared with a peroxide-cured sample.

4.4. ^{13}C MAS NMR studies of crystalline structure in irradiated polymers

As discussed in Section 2.1 NMR can provide a sensitive measure of the changes in the morphology of semi-crystalline polymers on irradiation. Recent studies by Okazaki and Toriyama[147] have supported the findings of Ahmad and Charlesby[61] discussed above. The authors observed an additional set of peaks in the ^{13}C MAS spectra of irradiated long chain n-alkanes, considered models for the crystalline material in poly(ethylene). The chemical shifts of the new peaks correspond to those of the n-alkane in solution, and thus it was concluded that they are due to n-alkanes in a glassy, disorder state. The mobility of the ordered chains was affected by the proximity to these defect regions. The effects of irradiation on the crystalline structure of poly(ethylene) was studied by O'Donnell and Whittaker[63] and Zhu *et al.*[64] O'Donnell and Whittaker[63] reported a gradual decrease in average lamellar thickness on irradiation through measurement of the ^{13}C-detected ^{1}H $T_{1\rho}$ relaxation times. Zhu *et al.*[64] reported a decrease in the ^{13}C T_1 of the peak due to chains in the all-trans configuration, also consistent with a decrease in lamellar thickness on irradiation. In addition the value of T_{2C} for the carbon nuclei located in the amorphous and interphase regions decrease on irradiation due to cross-linking. Finally they report the appearance of a peak due to monoclinic crystals, indicating distortion of the crystalline lattice. Spevacek and coworkers also reported the destruction of the crystalline phase in irradiated cellulose.[65]

Schilling and coworkers[148] have studied the effects of γ-irradiation on the ^{13}C NMR spectra of poly(ethylene oxide). The ^{13}C MAS spectrum of the unirradiated material consists of two superimposed peaks at approximately 72.2 and 73.2 ppm.

These peaks are due to chains in the amorphous and crystalline phases, respectively. In the CPMAS spectrum collected using a short cross-polarization time, the broad peak due to the crystalline regions is only weakly visible, since the ^{1}H $T_{1\rho}$ relaxation time of the crystalline protons is very short at ambient temperatures. This is due to the close proximity of the measurement temperature to the temperature of the minimum in ^{1}H $T_{1\rho}$. On irradiation, the intensity of the broad peak in the ^{13}C CPMAS spectrum increases markedly, resulting from a change in the proton spin dynamics in the mid-kHz frequency range on cross-linking. The width of this broad peak decreases on irradiation, also consistent with a decrease in the spectral density of motions in the mid-kHz frequency range. On the other hand, measurement of ^{13}C T_1 relaxation times showed that the motion of the crystalline carbons in the MHz frequency range was not affected by irradiation. The pronounced effect of cross-linking on the motion of the crystalline chains suggested that cross-linking at the interphase region was relatively important.

Another example of the effect of cross-linking on chain motion is the report of Schmidt-Rohr and Spiess[149] of the suppression of translational motion of polymer chains between crystalline and amorphous regions in irradiated poly(ethylene). The authors demonstrated, using a ^{13}C 2D exchange experiment, that in unirradiated poly(ethylene) polymer chains within the crystalline regions undergo a slow exchange with chains in the amorphous phase. To demonstrate that the exchange peaks in the 2D spectrum were due to molecular exchange and not ^{13}C–^{13}C spin diffusion, they showed that the peaks were not present in the spectrum of the radiation-cross-linked polymer. This result suggests that cross-linking occurs close to the surface of the crystalline lamellae.

4.5. MAS NMR studies of other irradiated polymers

Poly(dimethyl siloxane) has long been recognized as a polymer which predominantly undergoes cross-linking on exposure to radiation. A large number of studies have been concerned with identifying the reactions leading to cross-linking, using methods such as measurement of volatile products, gel fractions, swelling ratios, and formation of new structures using infra-red spectroscopy. Recently we have studied the radiation chemistry of irradiated PDMS using ^{13}C and ^{29}Si MAS NMR.[150] Differences in the signal intensities in the CPMAS and Bloch decay experiments were used to identify cross-linked or chain-end structures. The major new cross-link structure detected was a Y-type cross-link formed by combination of –O–Si– chain ends with main-chain radicals formed through loss of methyl groups. H-type cross-links in which the main chains are linked via methylene bridges were also identified. A significant yield of new chain ends formed via scission of the main chain was also measured. In an accompanying paper[151] the yields of new structures were used to analyse the changes in molecular weight below the gel dose measured by gel permeation chromatography.

5. ^{19}F MAS NMR OF IRRADIATED POLYMERS

The field of ^{19}F NMR of intractable polymers has received an enormous boost in the past few years following the introduction of commercial high-spinning-speed ^{19}F MAS probes.[152–163] This has led to a number of studies of the effects of radiation on fluoropolymers.[152,153,157,159–163] The most important commercial material, i.e. poly(tetrafluoroethylene) (PTFE) has attracted the most interest. As mentioned above, from an early time it was noted that PTFE undergoes degradation on exposure to ionizing radiation. Following quite small radiation doses, there is a drama deterioration in mechanical properties of PTFE, making the material unusable for structural applications. The observed decrease in molecular mass and particle size of PTFE following irradiation has led to the industrial production of additives for coatings, inks, etc.

In recent years it has been found that irradiation at temperatures just superior to the melting temperature leads to the formation of a cross-linked network.[56,59,60] The change in behaviour at higher temperatures is believed to be due to the increased mobility of radical species permitting secondary radical reactions. At lower temperatures the long-lived radicals react and form scission products, or undergo depropagation reactions. Furthermore, these radicals are highly susceptible to addition by oxygen, and hence can initiate further degradation. The phenomenon of high-temperature cross-linking of PTFE has created a great deal of interest,[60,164–166] including several studies of structures formed by ^{19}F solid-state NMR.[159,160]

The ^{19}F solid-state NMR spectrum of PTFE irradiated at 365°C to a dose of 3 MGy is shown in Fig. 9.[160] The spectrum of the original material consists of a single peak at −122 ppm with respect to $CFCl_3$, due to isolated methylene units, since the degree of polymerization of commercial PTFE samples is of the order of 10^6. The assignments to peaks from new structures are shown on the spectrum. The major new structures identified by ^{19}F NMR are methyl side chains, long-chain branches and H-type cross-links. A number of small peaks appear at higher chemical shifts (> −60 ppm) that are not conclusively assigned. The NMR spectrum of the material irradiated at room temperature showed only new CF_3-chain ends, and no evidence of cross-linking or long-chain branching. The authors have measured the yields of new structures from the spectra, and calculated average molecular weights for materials irradiated to a range of doses.

In other studies the mechanism of cross-linking in irradiated copolymers of tetrafluoroethylene and perfluoromethylvinylether has been studied by Forsythe *et al.*[153] This material is rubbery at room temperature, and hence sufficient molecular mobility is available to permit radical–radical recombination reactions. Thus the material undergoes both chain scission and cross-linking. The authors were able to quantify the yields of new products using ^{19}F MAS NMR at moderate spinning speeds, since the chemical shift anisotropy and homonuclear dipole–dipole couplings of the fluorine nuclei are partially averaged by rapid molecular motion in the rubbery state.

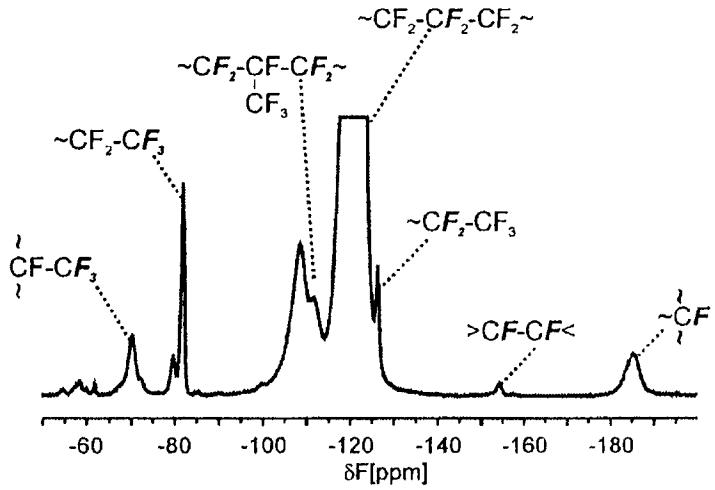

Fig. 9. ^{19}F solid-state MAS NMR spectrum of PTFE irradiated at 365°C by a dose of 3 MGy. Reproduced from ref. 160 with permission. Copyright 2000 American Chemical Society.

More recently, this group has also reported the identification of new structures formed by radiolysis of fluorinated ethylene–propylene copolymers (FEP).[161,162] The changes to the spectra are similar to those reported for irradiated PTFE by Fuchs and Scheler, and thus the radiation chemistry of these two polymers is similar. Irradiation at low temperatures resulted in the formation of new $-CF_3$ chain ends, while irradiation in the melt (523 K) resulted in the formation of long-chain branches. However, it was clear that chain-scission reactions were still dominant at these higher temperatures.

6. NMR STUDIES OF OXIDATIVE DEGRADATION OF POLYMERS

The above survey of the literature has largely dealt with the analysis of the changes in molecular structure in polymers irradiated in the absence of air. The vast majority of the literature has been concerned with irradiation in non-oxidative conditions due to the desire to identify the fundamental processes occurring on radiolysis. However, the influence of oxygen on the radiation chemistry of polymers is profound and must not be ignored. To this end a number of papers have been concerned with the measurement of changes in the NMR spectra of polymers irradiated in oxygen.[167–169]

A number of papers have reported the use of ^{13}C solution-state NMR to measure new products formed by oxidative thermal degradation of polymers, however only a single NMR study has appeared concerned with the radiation-induced oxidative degradation. Arakawa *et al.*[167] report the G-values for

formation of carboxylic acid groups in a number of ethylene homo- and co-polymers irradiated in air. Unfortunately the authors did not include examples of the NMR spectra of the oxidized materials. Sohma *et al.*[168] have used solid-state ^{13}C NMR to observe peaks due to carbonyl carbons methyl chain ends in HDPE irradiated in air. Most recently, Assink *et al.*[169] have measured changes in the ^{13}C spectrum of ^{13}C-enriched PE irradiated in air at several temperatures. The use of enriched materials resulted in excellent signal-to-noise ratios, and as a result they were able to identify peaks due to ketones, acids and esters, hydroperoxides and alcohols in the spectra. The rates of reaction of the hydroperoxides were measured from the rates of disappearance of the corresponding peaks in the spectra on annealing at elevated temperatures.

Very recently the group at Sandia National Laboratories have reported the use of ^{17}O NMR to detect oxygen-containing species formed during thermal and radiation oxidation of polymers in the presence of $^{17}O_2$.[170–172] The advantage of this technique is the complete absence of peaks in the NMR spectrum of the polymer prior to irradiation. Thus the issue of peaks due to structures formed during radiolysis being obscured by peaks due to the unaltered polymer does not arise. In addition the chemical shift dispersion of ^{17}O is large compared with the linewidths, with peaks resolved over a range of approximately 650 ppm.

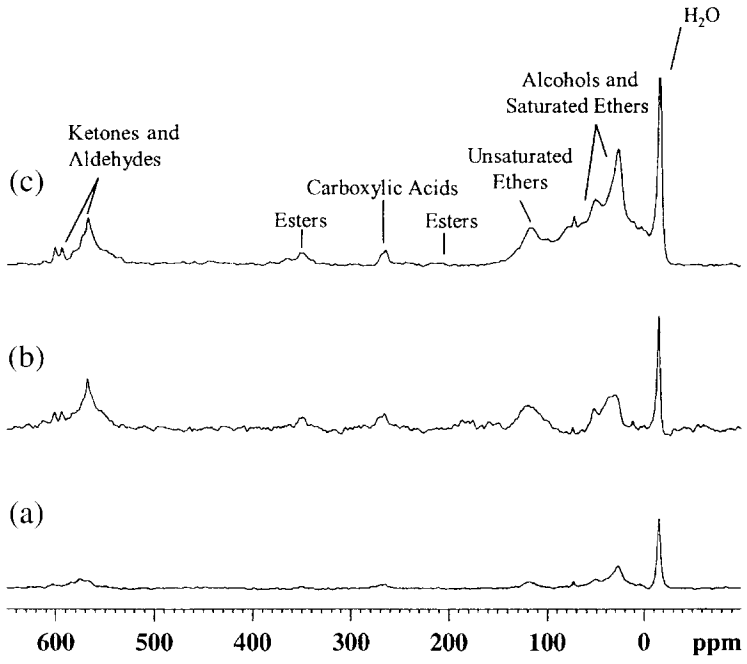

Fig. 10. ^{17}O solution-state NMR spectrum of poly(isoprene) irradiated at 300 K in $^{17}O_2$; (a) 98 kGy, (b) 172 kGy and (c) 244 kGy. Reproduced from ref. 172 with permission. Copyright 2001 Elsevier Science.

Figure 10 shows the ^{17}O NMR spectra of poly(isoprene) gamma irradiated in the presence of ^{17}O-enriched oxygen.[172] The authors have identified classes of peaks through comparison with model compounds; it is conceivable that in future a database of ^{17}O chemical shifts will aid researchers in this area. The authors were able to show that irradiation of poly(isoprene) in oxygen results in the formation largely of alcohols and ethers from hydrogen abstraction and termination reactions, respectively, of alkoxy radicals. These radicals are products of homolysis of hydroperoxy radicals.

7. SUMMARY

NMR spectroscopy has made a significant contribution to the understanding of radiation effects in polymeric systems. The use of high-resolution NMR methods, either in the solution or solid state, has permitted the identification of the products of radiolysis in a large number of systems. Careful measurements have in many cases enabled the yields of products to be determined. Such measurements of *chemical* structure have helped in the development of mechanisms of radiation-induced reactions. Measurements of *physical* properties have also been invaluable. Changes in the transverse relaxation times, due to the changes in the entanglement or cross-link density on radiolysis can be directly related to the yield of cross-links (or chain cleavages) by analogy with the classical relationships between molar masses or gel contents and radiochemical yields. It is possible to envisage such simple and rapid measurements providing the basis of measurement of cross-link densities in industrial facilities; Cohen-Addad has made such a suggestion for chemically-cross-linked poly(ethylene) materials.[173]

An important field of nuclear magnetic resonance, namely NMR imaging has not yet been applied to the study of radiation modified polymers. This is a result of the relatively low resolution of NMR imaging compared with say micro-FTIR and more traditional methods of microscopy. In many other fields this lower resolution has been offset by the other powers of NMR, namely the sensitivity of the NMR signal to molecular motion in the material of interest. It is suggested, therefore, that a number of important questions may be resolved through the use of NMR microimaging. For example, the distribution of chain-scission reactions occurring during oxidative degradation will in many cases be non-uniform due to the depletion of oxygen and the finite diffusion times of oxygen through large sections. Smith and Koenig[174] have shown that the inhomogeneous distribution of reactions in sulfur-cured poly(butadiene) swollen with a deuterated solvent can be mapped by NMR imaging.

Much information on the distribution of radiolytic reactions has been obtained from NMR studies of irradiated polymers. For example, the measurement of very high G-values for racemization in stereoregular polymers, and the apparent non-uniform distribution of reactions along the polymer chain, provides a unique picture of the mechanism deposition of energy within the polymer. In addition,

comparison of yields of reactions measured by NMR and other methods have provided a measure of the effective cross-link structure, and hence the extent of clustering of cross-linking reactions. As indicated above, it is suggested that in the future measurements of spin diffusion in cross-linked materials close to or below their glass transition temperatures, will provide information on the spatial distribution of cross-links.

ACKNOWLEDGEMENTS

The authors would like to acknowledge the pioneering contributions of the late Professor James H. O'Donnell to many aspects of the study of the radiation chemistry of polymers. Financial support from NASA, the Australian Research Council and from the Australian Nuclear Science and Technology Organization is also gratefully acknowledged.

REFERENCES

1. A. Singh and J. Silverman (eds), *Radiation Processing of Polymers*, Prog. Polym. Proc., Hanser, Munich, 1992.
2. Proceedings of the 1st International Meeting on Radiation Processing, *Radiat. Phys. Chem.*, 1977, **7**, 1.
3. Proceedings of the 2nd International Meeting on Radiation Processing, *Radiat. Phys. Chem.*, 1979, **14**, 1.
4. Proceedings of the 3rd International Meeting on Radiation Processing, *Radiat. Phys. Chem.*, 1981, **18**, 1.
5. Proceedings of the 4th International Meeting on Radiation Processing, *Radiat. Phys. Chem.*, 1983, **22**, 1.
6. Proceedings of the 5th International Meeting on Radiation Processing, *Radiat. Phys. Chem.*, 1985, **25**, 1.
7. Proceedings of the 6th International Meeting on Radiation Processing, *Radiat. Phys. Chem.*, 1988, **31**, 1.
8. Proceedings of the 7th International Meeting on Radiation Processing, *Radiat. Phys. Chem.*, 1990, **35**, 1.
9. Proceedings of the 8th International Meeting on Radiation Processing, *Radiat. Phys. Chem.*, 1993, **42**, 1.
10. Proceedings of the 9th International Meeting on Radiation Processing, *Radiat. Phys. Chem.*, 1995, **46**, 399.
11. Proceedings of the 10th International Meeting on Radiation Processing, *Radiat. Phys. Chem.*, 1998, **52**, 1.
12. Proceedings of the 11th International Meeting on Radiation Processing, *Radiat. Phys. Chem.*, 2000, **57**, 203.
13. J. P. Fouassier and J. F. Rabek (eds), *Radiation Curing in Polymer Science and Technology*, Elsevier Applied Science Publishers, London, 1993.
14. J. H. O'Donnell and D. F. Sangster, *Principles of Radiation Chemistry*, Arnold, London, 1970.
15. Farhataziz and M. A. J. Rodgers (eds), *Radiation Chemistry: Principles and Applications*, VCH Publishers, New York, 1987.
16. A. Charlesby, *Atomic Radiation and Polymers*, Pergamon Press, Oxford, 1960.
17. A. Chapiro, *Radiation Chemistry of Polymeric Systems*, Interscience, New York, 1962.

18. M. Dole (ed.), *The Radiation Chemistry of Macromolecules*, Vol. 1, Academic Press, New York, 1972.
19. M. Dole (ed.), *The Radiation Chemistry of Macromolecules*, Vol. 2. Academic Press, New York, 1972.
20. J. Brandrup, E. H. Immergut and E. A. Grulke (eds), *Polymer Handbook*, 4th edn, Wiley, New York, 1999.
21. R. L. Clough and S. W. Shalaby (eds), *Radiation Effects on Polymers*, ACS Symp. Ser. 475, American Chemical Society, Washington, DC, 1991.
22. R. L. Clough and S. W. Shalaby (eds), *Irradiation of Polymers: Fundamentals and Technological Applications*, ACS Symp. Ser. 620, American Chemical Society, Washington, DC, 1996.
23. B. J. Lyons and M. Dole, *J. Phys. Chem.*, 1964, **68**, 526.
24. J. H. O'Donnell and P. J. Pomery, *J. Polym. Sci., Polym. Symp.*, 1976, **55**, 269.
25. J. P. Manion and M. Burton, *J. Phys. Chem.*, 1952, **56**, 560.
26. J. Kroh and S. Karolczak, *Radiat. Res. Rev.*, 1969, **1**, 411.
27. K. Heiland, D. J. T. Hill, J. L. Hopewell, D. A. Lewis, J. H. O'Donnell, P. J. Pomery and A. K. Whittaker, *Adv. Chem. Ser.*, 1996, **249**, 637.
28. J. Brown and J. H. O'Donnell, *Macromolecules*, 1970, **3**, 265.
29. M. J. Bowden, in L. F. Thompson, C. G. Willson and J. M. J. Frechet (eds), *Materials for Microlithography. Radiation Sensitive Polymers*, ACS Symp. Ser 266, American Chemical Society, p. 39.
30. M. A. Hartney, *J. Appl. Polym. Sci.*, 1989, **37**, 695.
31. J. S. Forsythe, D. J. T. Hill, A. L. Logothetis, P. J. Pomery and A. K. Whittaker, *J. Appl. Polym. Sci.*, 2000, **75**, 1447.
32. B. J. Lyons and A. S. Fox, *J. Polym. Sci., Polym. Symp.*, 1968, **21**, 159.
33. R. J. Eldred, *Rubber Chem. Technol.*, 1974, **47**, 924.
34. B. Jankowski and J. Kroh, *J. Appl. Polym. Sci.*, 1965, **9**, 1363.
35. B. Ranby and J. F. Rabek, *ESR Spectroscopy in Polymer Research*, Springer-Verlag, Berlin, 1977.
36. W. C. Johnson and B. J. Lyons, *Radiat. Phys. Chem.*, 1995, **46**, 829.
37. B. J. Lyons and W. C. Johnson, *ACS Symp. Ser.*, 1993, **527**, 62.
38. Y. Hama, K. Hamanaka, H. Matsumoto, H. Kudoh, T. Sasuga and T. Seguchi, *Radiat. Phys. Chem.*, 1995, **46**, 819.
39. T. N. Bowmer and J. H. O'Donnell, *Polymer*, 1977, **18**, 1032.
40. T. N. Bowmer, S. Y. Ho and J. H. O'Donnell, *Polym. Deg. Stab.*, 1983, **5**, 449.
41. D. A. Doyle, W. Simpson and J. D. Waldron, *Polymer*, 1961, **2**, 323.
42. D. J. T. Hill, R. W. Garrett, S. Y. Ho, J. H. O'Donnell and P. W. O'Sullivan, *Radiat. Phys. Chem.*, 1981, **17**, 163.
43. J. R. Brown, and J. H. O'Donnell, *Macromolecules*, 1970, **3**, 265.
44. T. N. Bowmer and J. H. O'Donnell, *J. Macromol. Sci.- Chem.*, 1982, **A17**, 243.
45. C. L. Moad and D. J. Winzor, *Prog. Polym. Sci.*, 1998, **23**, 759–813.
46. D. J. T. Hill, D. A. Lewis, J. H. O'Donnell, P. J. Pomery, J. L. Hedrick and J. E. McGrath, *Polym. Adv. Technol.*, 1991, **2**, 15.
47. O. Saito, *J. Phys. Soc. Japan*, 1958, **13**, 4327.
48. A. Charlesby and S. H. Pinner, *Proc. Roy. Soc. (London)*, 1959, **A249**, 367.
49. J. L. Williams, T. S. Dunn, H. Sugg and V. T. Stannett, *Adv. Chem. Ser.*, 1978, **169**, 142.
50. A. M. El-Naggar, L. C. Lopez and G. L. Wilkes, *J. Appl. Polym. Sci.*, 1990, **39**, 427.
51. J. H. O'Donnell, in *Radiation Effects on Polymers*, R. L. Clough and S. W. Shalaby (eds), ACS Symp. Ser. 475, American Chemical Society, Washington, DC, 1991, Chapter 24.
52. J. Sohma, *Radiat. Phys. Chem.*, 1992, **40**, 121.
53. M. Tutiya and K. Yamamoto, *J. Phys. Soc. Japan*, 1968, **25**, 1518.
54. M. Tutiya and K. Yamamoto, *Jpn. J. Appl. Phys.*, 1968, **7**, 440.
55. M. Tutiya, *Jpn. J. Appl. Phys.*, 1970, **9**, 1204.

56. M. Tutiya, *Jpn. J. Appl. Phys.*, 1972, **11**, 1542.
57. B. J. Lyons, *Radiat. Phys. Chem.*, 1995, **45**, 159.
58. D. J. T. Hill and J. S. Forsythe, *Prog. Polym. Sci.*, 2000, **25**, 101.
59. J. Sun, Y. Zhang, X. Zhong and X. Zhu, *Radiat. Phys. Chem.*, 1994, **44**, 655.
60. A. Oshima, Y. Tabata, H. Kudoh and T. Seguchi, *Radiat. Phys. Chem.*, 1995, **45**, 269.
61. S. R. Ahmad and A. Charlesby, *Int. J. Radiat. Phys. Chem.*, 1976, **8**, 497.
62. M. Okazaki and K. Toriyama, *Chem. Phys. Lett.*, 1989, **160**, 21.
63. J. H. O'Donnell and A. K. Whittaker, *Radiat. Phys. Chem.*, 1992, **39**, 209.
64. Q. R. Zhu, P. S. He, F. Horii and R. Kitamaru, *J. Mater. Sci.*, 1996, **31**, 3129.
65. J. Spevacek, J. Straka and B. Schneider, *J. Appl. Polym. Sci., Appl. Polym. Symp.*, 1991, **48**, 371.
66. J. H. O'Donnell and A. K. Whittaker, *Br. Polym. J.*, 1985, **17**, 51.
67. P. F. Barron, J. H. O'Donnell and A. K. Whittaker, *Polym. Bull.*, 1985, **14**, 339.
68. J. H. O'Donnell and A. K. Whittaker, *J. Polym. Sci., Polym. Chem. Ed.*, 1992, **30**, 185.
69. M. Dole, *Polym.-Plast. Technol. Eng.*, 1979, **13**, 41.
70. N. Gvozdic and M. Dole, *Radiat. Phys. Chem.*, 1980, **15**, 435.
71. G. N. Patel and A. Keller, *J. Polym. Sci., Polym. Phys. Ed.*, 1975, **13**, 303.
72. J. H. O'Donnell and A. K. Whittaker, *J. Macromol. Sci., Pure Appl. Chem.*, 1991, **A29**, 1.
73. S. R. Ahmad and A. Charlesby, *Int. J. Radiat. Phys. Chem.*, 1976, **8**, 585.
74. A. M. Rijke and L. Mandelkern, *J. Polym. Sci., Polym. Lett. Ed.*, 1969, **7**, 651.
75. Yu. Ya. Gotlib, M. I. Lifshits, V. A. Shevelev, I. S. Lishanskii and I. V. Balanina, *J. Polym. Sci. USSR*, 1976, **18**, 2630.
76. C. G. Fry and A. C. Lind, *Macromolecules*, 1988, **21**, 1292.
77. R. Folland and A. Charlesby, *Radiat. Phys. Chem.*, 1977, **10**, 61.
78. R. Folland and A. Charlesby, *Polymer*, 1979, **20**, 211.
79. R. Folland and A. Charlesby, *Polymer*, 1979, **20**, 207.
80. A. Charlesby, P. Käfer and R. Folland, *Radiat. Phys. Chem.*, 1978, **11**, 83.
81. A. Charlesby and B. J. Bridges, *Eur. Polym. J.*, 1981, **17**, 645.
82. A. K. Whittaker, *Radiat. Phys. Chem.* 1996, **48**, 601.
83. I. Kamel and A. Charlesby, *J. Polym. Sci., Polym. Phys. Ed.*, 1981, **19**, 803.
84. W. L. Gölz and H. G. Zachmann, *Makromol. Chem.*, 1975, **176**, 2721.
85. T. Bremner and A. Rudin, *J. Polym. Sci., Polym. Phys. Ed.*, 1992, **30**, 1247.
86. A. Charlesby and J. Steven, *Int. J. Radiat. Phys. Chem.*, 1976, **8**, 719.
87. R. L. Bennett, A. Keller, J. Stejny and M. Murray, *J. Polym. Sci., Polym. Chem. Ed.*, 1976, **14**, 3027.
88. F. A. Bovey, F. C. Schilling and H. N. Cheng, *ACS Symposium Series*, 1978, **169**, 133.
89. J. C. Randall, F. J. Zoepfl and J. Silverman, *Makromol. Chem., Rapid Commun.*, 1983, **4**, 149.
90. J. C. Randall, F. J. Zoepfl and J. Silverman, *ACS Symposium Series*, 1984, **247**, 245.
91. F. Horii, Q. Zhu, R. Kitamaru and H. Yamaoka, *Macromolecules*, 1990, **23**, 977.
92. Q. Zhu, F. Horii, R. Kitamaru and H. Yamaoka, *J. Polym. Sci., Polym. Chem. Ed.*, 1990, **28**, 2741.
93. J. H. O'Donnell and A. K. Whittaker, *Polymer*, 1992, **33**, 62.
94. L. Dong, D. J. T. Hill, J. H. O'Donnell, P. J. Pomery and I. M. Brereton, *Macromol. Chem. Phys.*, 1995, **196**, 3379.
95. L. Dong, D. J. T. Hill, J. H. O'Donnell, P. J. Pomery and K. Hatada, *J. Appl. Polym. Sci.*, 1996, **59**, 589.
96. K. Hatada, T. Kitayama, N. Fujimoto and T. Nishiura, *J. Macromol. Sci., Pure Appl. Chem.*, 1993, **A30**, 645.
97. D. J. T. Hill, J. H. O'Donnell, M. C. S. Perera and P. J. Pomery, *ACS Symp. Ser.*, 1996, **620**, 139.
98. T. Bremner, D. J. T. Hill, J. H. O'Donnell, M. C. S. Perera and P. J. Pomery, *J. Polym. Sci., Polym. Chem. Ed.*, 1996, **34**, 971.
99. D. J. T. Hill, J. H. O'Donnell, M. C. S. Perera and P. J. Pomery, *Radiat. Phys. Chem.*, 1992, **40**, 127.

100. E. V. Thompson, *J. Polym. Sci., Polym. Lett. Ed.*, 1965, **3**, 675.
101. L. Dong, D. J. T. Hill, J. H. O'Donnell, T. G. Carswell-Pomerantz, P. J. Pomery and A. K. Whittaker, *Macromolecules*, 1995, **28**, 3681.
102. Y. Luo, H. Yang, B. Yin, M. Ding and B. Jiang, *Radiat. Phys. Chem.*, 1993, **42**, 233.
103. W. K. Busfield, J. V. Hanna, J. H. O'Donnell and A. K. Whittaker, *Brit. Polym. J.*, 1987, **7**, 223.
104. P. F. Barron, W. K. Busfield and J. V. Hanna, *Polym. Commun.*, 1988, **29**, 70.
105. P. F. Barron, W. K. Busfield and J. V. Hanna, *J. Polym. Sci., Polym. Lett. Ed.*, 1988, **26**, 225.
106. W. K. Busfield and J. V. Hanna, *Polym. J.*, 1991, **23**, 1253.
107. T. Asanuma, T. Shiomura, Y. Hirase, T. Matsuyama, H. Yamaoka, A. Tsuchida, M. Ohoka and M. Yamamoto, *Polym. Bull.*, 1992, **29**, 79.
108. D. J. T. Hill, D. A. Lewis, J. H. O'Donnell and A. K. Whittaker, *Polym. Adv. Technol.*, 1998, **9**, 45.
109. A. Babanalbandi, D. J. T. Hill and A. K. Whittaker, *Polym. Adv. Technol.*, 1998, **9**, 62.
110. M. C. Gupta and R. R. Pandey, *J. Polym. Sci., Polym. Chem. Ed.*, 1988, **26**, 491.
111. K. B. Kingsbury, D. S. Hawkins, R. A. Orwoll, R. L. Kiefer, S. A. T. Long and G. F. Sykes, *Macromolecules*, 1989, **22**, 3486.
112. J. L. Hopewell, D. J. T. Hill, J. H. O'Donnell, P. J. Pomery, J. E. McGrath, D. B. Priddy and C. D. Smith, *Polym. Deg. Stab.*, 1994, **45**, 293.
113. A. Babanalbandi, D. J. T. Hill and A. K. Whittaker, *Polym. Deg. Stab.*, 1997, **58**, 203.
114. S. Luo and A. N. Netravali, *J. Appl. Polym. Sci.*, 1999, **73,** 1059.
115. W. T. Ford and T. Balakrishnan, *Macromolecules*, 1981, **14**, 284.
116. W. T. Ford, M. Periyasamy and H. O. Spivey, *Macromolecules*, 1984, **17**, 2881.
117. S. Mohanraj and W. T. Ford, *Macromolecules*, 1985, **18**, 351.
118. W. T. Ford, M. Periyasamy, H. O. Spivey and J. P. Chandler, *J. Magn. Reson.*, 1985, **63**, 298.
119. D. L. VanderHart, W. L. Earl and A. H. Garroway, *J. Magn. Reson.*, 1981, **44**, 361.
120. W. P. Rothwell and J. S. Waugh, *J. Chem. Phys.*, 1981, **74**, 2721.
121. K. Takagoshi and K. Hikichi, *J. Chem. Phys.*, 1991, **94**, 3200.
122. E. R. Andrew, A. Bradbury and R. G. Eades, *Nature*, 1959, **183**, 1802.
123. I. J. Lowe, *Phys. Rev. Lett.*, 1959, **2**, 285.
124. A. Pines, M. G. Gibby and J. S. Waugh, *J. Chem. Phys.*, 1973, **59**, 569.
125. J. Schaefer and E. O. Stejskal, *J. Am. Chem. Soc.*, 1976, **98**, 1031.
126. J. Herzfeld and A. Berger, *J. Chem. Phys.*, 1979, **73**, 6021.
127. D. E. Axelson, L. Mandelkern, R. Popli and P. Mathieu, *J. Polym. Sci., Polym. Phys. Ed.*, 1983, **21**, 2319.
128. J. Sohma, M. Shiotani, S. Murakami and T. Yoshida, *Radiat. Phys. Chem.*, 1983, **21**, 413.
129. J. C. Randall, *J. Polym. Sci., Polym. Phys. Ed.*, 1973, **11**, 275.
130. C. A. Fyfe, J. R. Lyerla, W. Volksen and C. S. Yannoni, *Macromolecules*, 1979, **19**, 757.
131. W. L. Earl and D. L. VanderHart, *Macromolecules*, 1979, **19**, 763.
132. D. L. VanderHart and F. Khoury, *Polymer*, 1984, **25**, 1589.
133. A. L. Cholli, W. M. Ritchey and J. L. Koenig, *Appl. Spectrosc.*, 1987, **41**, 1418.
134. E. Pérez and D. L. VanderHart, *J. Polym. Sci., Polym. Phys. Ed.*, 1988, **26**, 1979.
135. E. Pérez and D. L. VanderHart, *Macromolecules*, 1986, **19**, 1902.
136. D. J. T. Hill, J. H. O'Donnell, M. C. S. Perera, P. J. Pomery and A. K. Whittaker, *Macromol. Symp.*, 1995, **98**, 689.
137. D. J. T. Hill, J. H. O'Donnell, M. C. S. Perera, P. J. Pomery and A. K. Whittaker, *J. Macromol. Sci. - Pure Appl. Chem.*, 1993, **A30**, 633.
138. D. J. T. Hill, J. H. O'Donnell, M. C. S. Perera and P. J. Pomery, *Radiat. Phys. Chem.*, 1992, **40**, 127.
139. D. J. T. Hill, J. H. O'Donnell, M. C. S. Perera, P. J. Pomery and P. Smetsers, *J. Appl. Polym. Sci.*, 1995, **57**, 1155.
140. D. J. T. Hill, J. H. O'Donnell, M. C. S. Perera and P. J. Pomery, *ACS Symp. Ser.*, 1993, **527**, 74.

141. D. J. T. Hill, J. H. O'Donnell, M. C. S. Perera and P. J. Pomery, *Polymer*, 1995, **36**, 4185.
142. D. J. T. Hill, J. H. O'Donnell, M. C. S. Perera and P. J. Pomery, *J. Polym. Sci., Polym. Chem. Ed.*, 1996, **34**, 2439.
143. M. C. S. Perera, *J. Polym. Sci., Polym. Phys. Ed.*, 1999, **37**, 1141.
144. M. C. S. Perera and C. C. Rowen, *Polymer*, 2000, **41**, 323.
145. D. J. Patterson and J. L. Koenig, *Appl. Spectrosc.*, 1987, **41**, 441.
146. M. Mori and J. L. Koenig, *Ann. Rep. NMR Spectr.*, 1997, **34**, 231.
147. M. Okazaki and K. Toriyama, *Chem. Phys. Lett.*, 1989, **160**, 21.
148. F. C. Schilling, A. E. Tonelli and A. L. Cholli, *J. Polym. Sci., Polym. Phys. Ed.*, 1992, **30**, 91.
149. K. Schmidt-Rohr and H. W. Spiess, *Macromolecules*, 1991, **24**, 5288.
150. D. J. T. Hill, C. M. L. Preston and A. K. Whittaker, *Polymer*, submitted 2001.
151. D. J. T. Hill, C. M. L. Preston, A. K. Whittaker and S. M. Hunt, *Macromol. Symp.*, 2000, **156**, 95.
152. E. Katoh, H. Sugimoto, Y. Kita and I. Ando, *J. Mol. Struct.*, 1995, **355**, 21.
153. J. S. Forsythe, D. J. T. Hill, A. L. Logothetis, T. Seguchi and A. K. Whittaker, *Macromolecules*, 1997, **30**, 8101.
154. K. S. Lau and K. K. Gleason, *J. Phys. Chem. B*, 1997, **101**, 6839.
155. K. S. Lau and K. K. Gleason, *J. Phys. Chem. B*, 1998, **102**, 5977.
156. G. Legey, A. Coudreuse, J.-M. Legeais, L. Werner, A. Bulou, J.-Y. Buzare, J. Emery and G. Silly, *Eur. Polym. J.*, 1998, **34**, 1457.
157. U. Scheler, *Solid State Nucl. Magn. Reson.*, 1998, **12**, 9.
158. U. Scheler, *Bull. Magn. Reson.*, 1999, **19**, 52.
159. E. Katoh, H. Sugisawa, A. Oshima, Akihiro, Y. Tabata, T. Seguchi, T. Yamazaki, *Radiat. Phys. Chem.*, 1999, **54**, 165.
160. B. Fuchs and U. Scheler, *Macromolecules*, 2000, **33**, 120.
161. J. S. Forsythe, D. J. T. Hill, S. Mohajerani and A. K. Whittaker, *Radiat. Phys. Chem.*, 2001, **60**, 439.
162. K. K. Gleason, D. J. T. Hill, K. K. S. Lau, S. Mohajerani and A. K. Whittaker, *Nucl. Instr. Meth.*, 2001, in press.
163. J. S. Forsythe, D. J. T. Hill and A. K. Whittaker, *Radiat. Phys. Chem.*, 2001, **60**, 609.
164. Y. Tabata, A. Oshima, K. Takashika and T. Seguchi, *Radiat. Phys. Chem.*, 1996, **48**, 563.
165. A. Oshima, S. Ikeda, T. Seguchi and Y. Tabata, *Radiat. Phys. Chem.*, 1997, **49**, 279.
166. A. Oshima, T. Seguchi and Y. Tabata, *Radiat. Phys. Chem.*, 1997, **50**, 601.
167. K. Arakawa, T. Seguchi, Y. Watanabe and N. Hayakawa, *J. Polym. Sci., Polym. Chem. Ed.*, 1982, **20**, 2681.
168. J. Sohma, M. Shiotani, S. Murakami, K. Deguchi and K. Eguchi, *Polym. Deg. Stab.*, 1984, **9**, 51.
169. R. A. Assink, M. Celina, T. D. Dunbar, T. M. Alam, R. L. Clough and K. T. Gillen, *Macromolecules*, 2000, **33**, 4023.
170. T. M. Alam, M. Celina, D. R. Wheeler, R. A. Assink, R. L. Clough and K. T. Gillen, *Polym. News*, 1999, **24**, 186.
171. T. M. Alam, M. Celina, R. A. Assink, R. L. Clough, K. T. Gillen and D. R. Wheeler, *Macromolecules*, 2000, **33**, 1181.
172. T. M. Alam, M. Celina, R. A. Assink, R. L. Clough and K. T. Gillen, *Radiat. Phys. Chem.*, 2000, **60**, 121.
173. J. P. Cohen-Addad, C. Schmitt, Y. Boscher, J. C. Roussel and J. Jarrin, European Patent Application, 1989, EP 313435.
174. S. R. Smith and J. L. Koenig, *Macromolecules*, 1991, **24**, 3496.

Qualitative and Quantitative Exploitation of Heteronuclear Coupling Constants

GARY E. MARTIN

Rapid Structure Characterization Group, Global Pharmaceutical Sciences, Pharmacia Corporation, Kalamazoo, Michigan 49009-0199, USA

1. Introduction 37
2. Direct heteronuclear shift correlation methods 39
   2.1. Accordion-optimized direct heteronuclear shift correlation methods 40
3. Long-range heteronuclear shift correlation methods 45
   3.1. Important considerations from heteronucleus-detected long-range correlation experiments 46
   3.2. HMBC/GHMBC 47
   3.3. New long-range heteronuclear shift correlation experiments 48
   3.4. Simultaneous direct and long-range heteronuclear shift correlation 83
4. Quantitative measurement and use of long-range heteronuclear couplings 85
   4.1. Methods for the determination of long-range heteronuclear couplings 85
   4.2. Applications of quantitatively determined long-range heteronuclear couplings to chemical structure problems 87
5. Conclusions 96
References 96

1. INTRODUCTION

Coupling constants have been around nearly as long as NMR. Following the first observation of differences in the chemical shift of the three types of protons in ethanol in a 30 MHz NMR spectrum, which was seen as a nuisance by physicists but seized upon by enterprising chemists because of the chemical structure significance,[1] it was not long before coupling constants were discovered and appropriated by chemists for their utility as reporters of structural chemistry information. For decades thereafter, chemists using NMR spectroscopy in numerous subdisciplines have gone about tabulating coupling constants. At first, only couplings between high natural abundance nuclides such as homonuclear

ANNUAL REPORTS ON NMR SPECTROSCOPY
VOLUME 46 ISBN 0-12-505446-7

$^{1}H-^{1}H$ or heteronuclear couplings such as $^{1}H-^{19}F$ or $^{1}H-^{31}P$ were readily observable. Following the description of pulsed Fourier transform NMR[2] and the subsequent commercial availability of Fourier transform NMR methods in the early 1970s, the acquisition of ^{13}C spectra became a facile undertaking. It then became feasible to begin to explore the utility of heteronuclear couplings involving heteronuclide pairs such as $^{1}H-^{13}C$, $^{19}F-^{13}C$, and $^{31}P-^{13}C$. To this point in time, heteronuclear coupling constants were usually measured and tabulated somewhere. For the most part, the information wasn't used a great deal.

Two-dimensional NMR methods were anticipated in a visionary presentation by Jeener in 1971.[3] The first reports of the experimental demonstration of 2D NMR methods to appear in the literature were reported by Ernst and co-workers in 1976.[4] Again, things began with homonuclear two-dimensional methods such as COSY and homonuclear J-resolved experiments. Beginning in 1977, interest was directed toward the development of two-dimensional heteronuclear shift correlation experiments.[5–9] These experiments utilized the fundamentals of the spin population transfer experiments;[10,11] the timing of events was a function of the heteronuclear coupling constants involved. Through a number of iterations, the ^{13}C-detected heteronuclear shift correlation experiment evolved, culminating in the useful, quadrature-detected heteronuclear shift correlation pulse sequence described by Bax and Morris in 1981.[12] At this point, the compilations of heteronuclear spin coupling data began to serve a useful purpose. An investigator had to have at least a general idea of the size of the heteronuclear coupling through which magnetization would be transferred to appropriately optimize the duration of the delays in the experiment being performed. The exploitation of heteronuclear spin coupling constants had now truly begun!

In addition to direct heteronuclear shift correlation experiments, interest in correlating heteronuclide pairs across several bonds through long-range heteronuclear coupling constants, which are much smaller than the one-bond couplings used in direct heteronuclear shift correlation experiments, was expressed early in the history of 2D heteronuclear shift correlation spectroscopy. Hallenga and van Binst[13] were the first to suggest the possibility of long-range heteronuclear shift correlation experiments although they were unable to experimentally demonstrate the concept. The first report of successful long-range heteronuclear shift correlation experimental results was the seminal contribution of Reynolds and co-workers in 1984.[14] Intense research activity in the area of heteronucleus-detected long-range heteronuclear shift correlation experiments ensued over a span of several years before these experiments were supplanted by the advent of proton- or 'inverse'-detected direct and long-range heteronuclear shift correlation methods. After a span of over a decade, there has again recently been a resurgence of interest in the development of new long-range heteronuclear shift correlation methods, and techniques to facilitate the measurement, from 2D NMR spectra, of long-range heteronuclear coupling constants.

Following a very brief review of heteronuclide-detected methods, the discussion of new proton-detected direct and long-range shift correlation experiments

will constitute the balance of this chapter. While we might traditionally think in terms of $^{1}H-^{13}C$ correlation experiments, over approximately the last 5 years there has been tremendous interest in long-range $^{1}H-^{15}N$ heteronuclear shift correlation methods at natural abundance, which were the subject of a recent review.[15]

2. DIRECT HETERONUCLEAR SHIFT CORRELATION METHODS

Stemming from the work of research groups led by Ernst and Freeman and their co-workers,[5–11] Bax and Morris reported the first truly usable, quadrature-detected heteronuclear shift correlation method in 1981,[12] actually a year after the suggestion of long-range heteronuclear chemical shift correlation by Hallenga and van Binst.[13] Paradoxically, the first suggestion of proton-detected methods *via* the then foreign concept of heteronuclear multiple quantum coherence appeared in a 1979 report by Müller,[16] followed shortly thereafter by the report of the development of the proton-detected heteronuclear single quantum correlation (HSQC) by Bodenhausen and Ruben.[17]

During the early 1980s the development of an assortment of heteronucleus-detected direct heteronuclear shift correlation methods with various modifications and improvements was reported. The reader interested in the development and application of the various of heteronucleus-detected direct correlation experiments is referred to any of the excellent monographs on 2D NMR methods that are now widely available. Long-range heteronucleus-detected heteronuclear shift correlation methods have been reviewed by Martin and Zektzer.[18] The extensive development of heteronucleus-detected methods took place largely because commercially available instruments were not generally well suited to the acquisition of proton-detected heteronuclear shift correlation data in the early 1980s. While heteronucleus-detected direct heteronuclear shift correlation methods have become much less frequently used in recent years, it should still be recalled that these methods, when an investigator is not restricted by sample size, still afford the most efficient means of obtaining spectra with high digital resolution in the heteronuclear frequency domain. An excellent example is found in the work of Reynolds and co-workers.[19] When heteronucleus detection is employed in conjunction with small volume NMR probes, e.g. 3 mm microprobes,[20,21] small samples can be readily investigated.[22]

Beginning with the report of the HMQC experiment in 1986 by Bax and Subramanian[23] the utilization of proton- or inverse-detected heteronuclear shift correlation experiment was essentially ushered in. Despite reports that have demonstrated the superior resolution of single quantum-based heteronuclear shift correlation methods,[24–26] the HMQC experiment still remains the most widely employed, proton-detected heteronuclear shift correlation method. Gradients were incorporated into the HMQC experiment in 1991 by Hurd and John[27] and are discussed in the excellent contribution of Ruiz-Cabello and co-workers[28] and

the more recent work of Leibfritz and co-workers[29] and the recent review of Parella.[30]

2.1. Accordion-optimized direct heteronuclear shift correlation methods

Irrespective of which heteronuclear shift correlation method is to be used, the duration of various delays in the experiment must be optimized as a function of the one-bond heteronuclear coupling constant. Aliphatic one-bond coupling constants generally are in the range from about 125 Hz for a pure aliphatic compound to about 145 Hz for protonated carbons bearing heteroatoms such as oxygen or nitrogen. Exceptions can include species such as epoxides, in which the one-bond heteronuclear coupling constant of protonated resonances can range as large as 180 Hz, and highly strained systems such as [1.1.0]bicyclobutane with a 222 Hz one-bond coupling. Most aromatic and simple heteroaromatic ring systems have one-bond heteronuclear coupling constants in the range of 160–180 Hz. When dealing with aralkyl species, direct heteronuclear shift correlation experiments are generally optimized for an assumed average one-bond heteronuclear coupling of about 140 Hz. Under most circumstances, this compromise value works reasonably well and usable response intensity is observed for all of the protonated carbon resonances in the structure.

In the case of some heteroaromatic systems such as furan, pyrimidine, and others, the one-bond heteronuclear coupling constants can exceed 200 Hz. For example, the $^{1}J_{CH}$ coupling of the 2-position of furan is ~210 Hz; the 2-position of pyrimidine is also about ~208 Hz. When molecules containing such structural moieties are studied by direct heteronuclear shift correlation methods using the normal ~140 Hz compromise optimization, responses for positions in the molecule such as the 2-position of a furanyl substituent may be either very weak or even completely absent.

2.1.1. Accordion Direct Single Quantum Correlation – ADSQC

Drawing on the growing body of literature that deals with accordion-optimized long-range heteronuclear shift correlation experiments that are discussed below, Hadden and Angwin[31] recently reported a new, accordion-optimized direct heteronuclear shift correlation experiment that was given the acronym ADSQC (accordion-optimized direct single quantum correlation). The pulse sequence for this experiment is shown in Fig. 1. The experiment is derived, simply, from the familiar gradient HSQC experiment. The authors used static optimization of the delays in the forward INEPT step of the ADSQC pulse sequence in the usual fashion. Rather than using static optimization of the delays in the reverse INEPT portion of the experiment, accordion optimization was instead employed.

In this implementation, the optimization range, e.g. 120 (T_{max}) to 210 Hz (T_{min}), is divided into a number of steps corresponding to the number of increments of

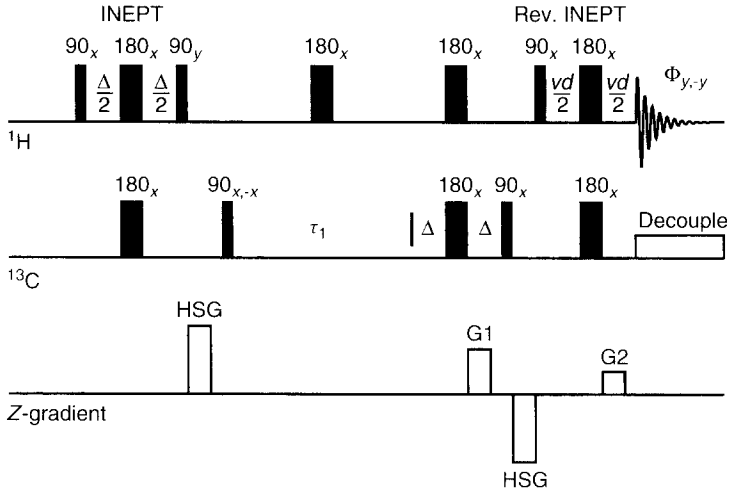

Fig. 1. ADSQC direct heteronuclear shift correlation pulse sequence (**A**ccordion-optimized **D**irect **S**ingle **Q**uantum **C**orrelation) developed by Hadden and Angwin.[31] The experiment is designed using the template of the familiar HSQC (**H**eteronuclear **S**ingle **Q**uantum **C**orrelation) experiment developed by Bodenhausen and Reuben.[17] The ADSQC experiment, however, differs in that it is intended to provide usable response intensity across a broad range of potential $^{1}J_{CH}$ heteronuclear couplings to ensure that protonated carbons in various heterocyclic systems, which have unusually large one-bond coupling constants will give a correlation response in survey spectra. The experiment uses a fixed duration delay in the forward INEPT step and accordion-optimized delays ($vd/2$) in the reverse INEPT portion of the pulse sequence. The latter allows the sampling of a broad range of one-bond couplings, e.g. 120–210 Hz as shown for the example of the antibiotic ceftiofur (**1**) shown in Fig. 2. The use of accordion-optimized delays in only one of the two INEPT steps helps to suppress artifacts (see Fig. 3).

the evolution time used in digitizing the indirectly detected time domain, t_1. The variable delay is decremented from T_{max} (120 Hz) to T_{min} (210 Hz) in ni steps, where the decrement is defined by

$$(T_{max} - T_{min})/ni \tag{1}$$

The authors note that decrementation in this fashion results in a non-linear sampling across the optimization range used and suggest that linear sampling is preferred using

$$\tfrac{1}{2}[T_{max} - T_{min}]/ni \tag{2}$$

to define the decrement value.

The authors used the cephalosporin antibiotic ceftiofur (**1**), which contains a furanyl substituent in its structure, as a test case. Coupling constants in the structure of ceftiofur range from 130 Hz to 208 Hz for the 2-furanyl site (C29). Three spectra are compared in Fig. 2. Using the conventional gradient HSQC

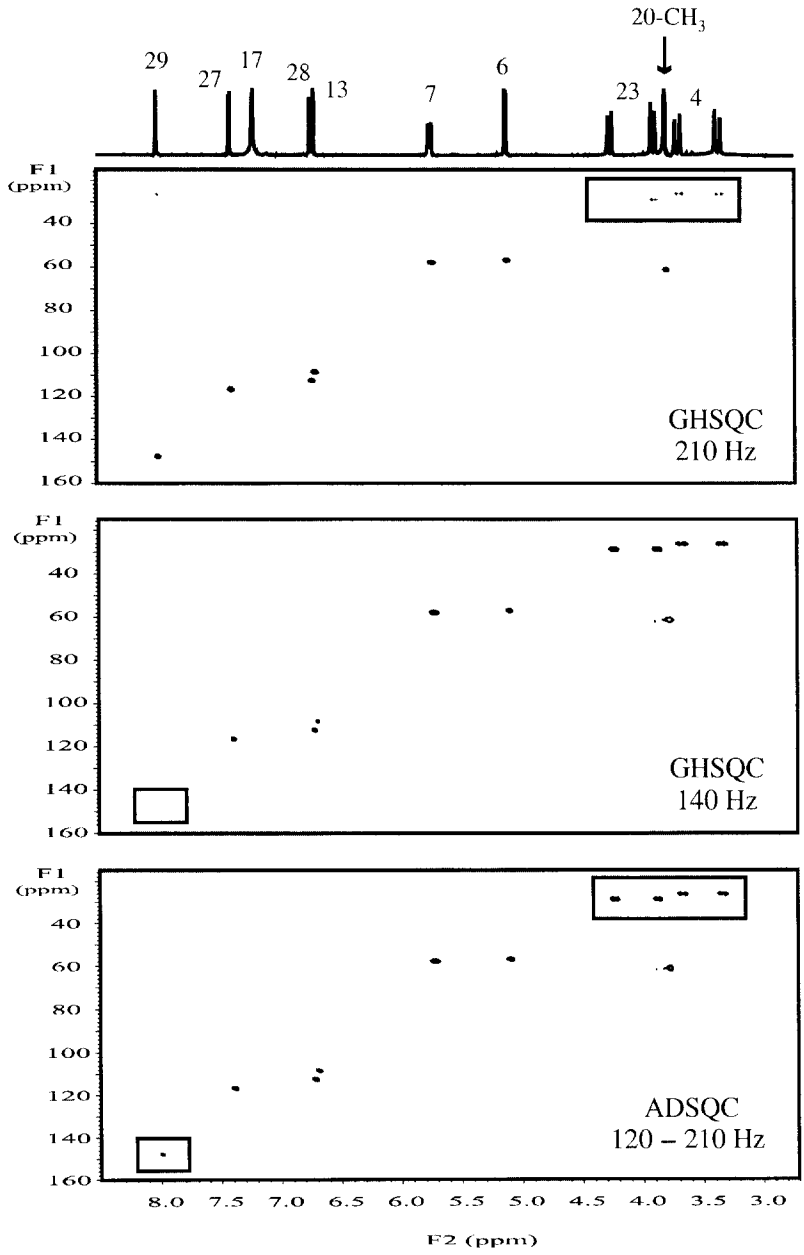
20-CH3
29
27
17
28
13
7
6
23
4
F1 (ppm)
40
60
80
100
120
140
160
GHSQC
210 Hz
GHSQC
140 Hz
ADSQC
120 – 210 Hz
8.0
7.5
7.0
6.5
6.0
5.5
5.0
4.5
4.0
3.5
3.0
F2 (ppm)

experiment (GHSQC), spectra were acquired with the fixed delays optimized for 140 and 210 Hz (bottom and center panels, respectively). When the experiment was optimized for 140 Hz, good signal intensity was seen for the C4 and C23 methylene carbons ($^1J_{CH}$ = 130 and 144 Hz, respectively) while there was no trace of the C29 carbon at the 2-position of the furanyl substituent. Conversely, when optimized for 210 Hz, there was excellent response intensity for the C29 furanyl carbon while the C4 and C23 aliphatic carbon responses were weak and barely visible. Because of the broad range of one-bond heteronuclear couplings, compromise optimization of the delays in the experiment is not a good choice. In contrast, when the ADSQC pulse sequence was employed, the range of the variable delay optimized from 120–210 Hz, very usable response intensity was seen for all of the responses in the spectrum, as shown in the top panel of Fig. 2.

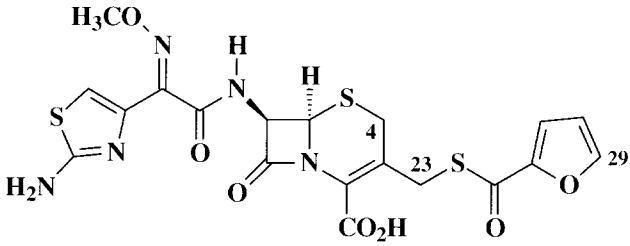

1

2.1.2. Random Direct Single Quantum Correlation – RDSQC

While good results were obtained with the ADSQC technique, the authors note that artefacts of a 'triplet' nature were observed in F_1, as suggested by the analysis of Zangger and Armitage in their report of the accordion-HMQC experiment (see p. 44).[32] To address this potential deficiency, Hadden *et al.*[33] utilized randomization of the variable delay table to provide essentially complete suppression of the artefacts observed in the ADSQC. The modified experiment has been given

Fig. 2. Panels showing the results from two gradient HSQC experiments optimized for 140 (bottom panel) and 210 Hz (center panel) performed on the cephalosporin antibiotic ceftiofur (**1**). The responses for the C4 and C23 methylene carbons (boxed responses in the aliphatic region) show good response intensity in the 140 Hz experiment, as expected, since these methylene carbons have one-bond couplings of 133 and 144 Hz, respectively. Note that there is no response for the C29 furanyl methine carbon, which has a 208 Hz one-bond coupling in the 140 Hz optimized spectrum. In contrast, in the 210 Hz optimized HSQC spectrum shown in the center panel the C29 correlation exhibits a strong response but does so at the expense of response intensity for the C4 and C23 methylene resonances. When compared to the results from the 120–210 Hz optimized ADSQC spectrum shown in the top panel, excellent and relatively uniform response intensity is observed for all of the direct correlation responses in the spectrum. Multiplicity-editing, as shown, is also possible using this experiment. (C. E. Hadden and D. T. Angwin, *Magn. Reson. Chem.*, 2001, © John Wiley & Sons, Ltd. Reproduced with permission.)

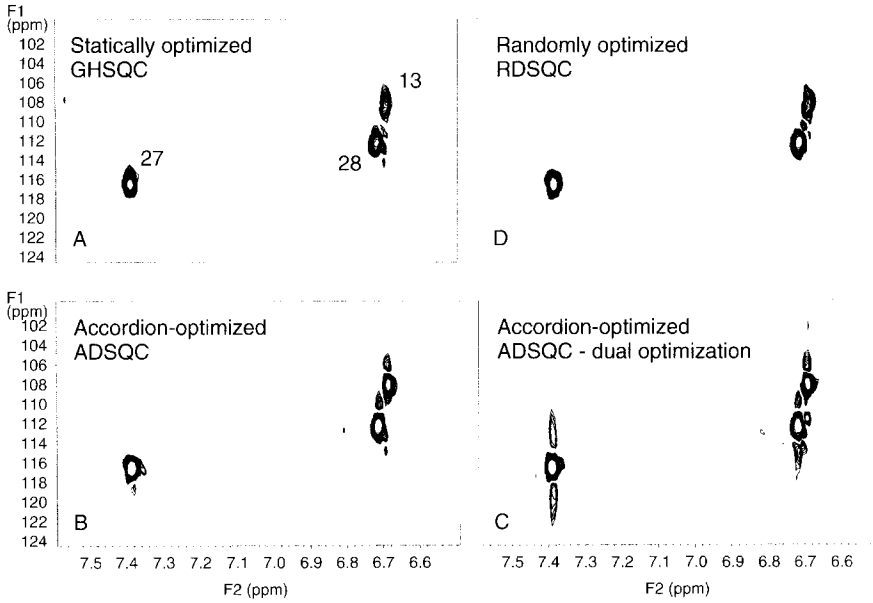

Fig. 3. The RDSQC (**R**andom **D**irect **S**ingle **Q**uantum **C**orrelation) experiment developed by Hadden *et al.*[33] employs a randomized table of delays to sample the range of potential couplings specified by the accordion-optimization range of the experiment. As shown in the four comparison panels, the ADSQC experiment has artefact responses when only the reverse INEPT portion of the experiment is accordion-optimized which worsen when both INEPT steps are accordion-optimized. In contrast, the RDSQC experiment optimized for the same range of potential one-bond couplings affords data that are comparable to HSQC data and free of artefacts. (Reproduced with permission, © Hetero Corp. 2001.)

the acronym RDSQC. Segments comparing the results from several experimental variants are shown in Fig. 3.

2.1.3. Accordion HMQC

As noted above, Zangger and Armitage[32] have developed another accordion-optimized experimental variant to which they've given the acronym accordion-HMQC for use in the study of metallothioneins; the pulse sequence is shown in Fig. 4. Generally, such proteins are made amenable to NMR study by substituting cadmium as an isomorphic replacement for the zinc atoms typically bound to metallothioneins isolated from natural sources. The range of Cd-H coupling constants in metallothioneins are typically between ~10 and ~50 Hz. Results comparing HMQC spectra optimized at 20 and 40 Hz and an accordion-HMQC experiment optimized for the range from 10 to 40 Hz were shown in the report. As might be expected, some of the responses that were clearly visible in the accordion-HMQC spectrum were either weak or absent from the conventional HMQC spectra. Finally, the authors reported that a least-squares, non-linear

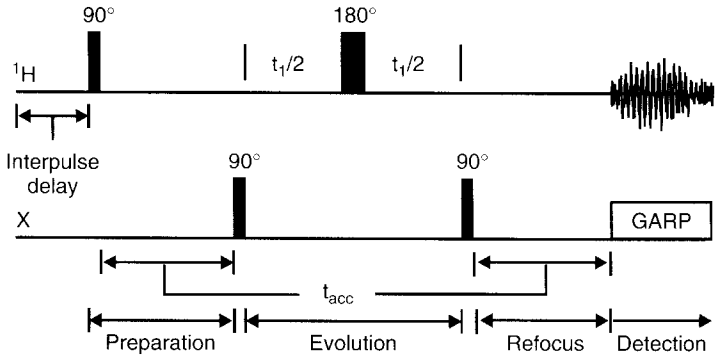

Fig. 4. Accordion HMQC pulse sequence developed by Zangger and Armitage.[32] This experiment was developed to facilitate the study of metallothioneins in which cadmium has been inserted as an isomorphic replacement for the zinc atoms normally bound to metallothioneins. By using the accordion HMQC experiment, Zangger and Armitage were able to observe correlation responses to the seven cadmium atoms in a single experiment rather than having to perform several conventional experiments with varied optimization.

multi-parameter analysis of the data to extract the ^{113}Cd–^{1}H couplings gave results that compared favorably with couplings measured by direct detection.

2.1.4. Summary

With the development of the ADSQC, RDSQC, and accordion-HMQC experiments described above, it is likely that there will be more variants to follow. Although the variability of one-bond heteronuclear couplings is a minor problem in ^{1}H–^{13}C direct heteronuclear shift correlation experiments, the large degree of variability in the coupling of other heteronuclide pairs makes the use of accordion delays potentially attractive in the design of new pulse sequences.

3. LONG-RANGE HETERONUCLEAR SHIFT CORRELATION METHODS

Variability in the size of long-range heteronuclear coupling constants is a well-recognized concern in the acquisition of ^{1}H–^{13}C long-range correlation spectra of natural products and other classes of molecules. Many investigators report the acquisition of HMBC spectra with two or even three different optimizations in an effort to insure that they will observe all possible long-range correlation responses. The problem of coupling constant variability for ^{1}H–^{15}N long-range correlation experiments at natural abundance is even larger as noted in the recent review of Martin and Hadden.[15] Although there are no examples in the literature yet, the problem of coupling constant variability with ^{19}F–^{15}N is still worse. The $^2J_{NF}$ coupling of 2-fluoropyridine is ~52 Hz while the $^3J_{NF}$ coupling of 3-fluoropyridine is ~4 Hz.[34] This range of long-range couplings would mandate

either the acquisition of multiple, conventional long-range correlation spectra or the utilization of accordion methods to sample the broad range of couplings.

3.1. Important considerations from heteronucleus-detected long-range correlation experiments

A period of intense research effort devoted to the development of new long-range heteronucleus-detected heteronuclear shift correlation experiments followed Reynolds'[14] first demonstration of the feasibility of performing long-range heteronuclear shift correlation experiments. These methods have been reviewed[18] and only a couple of salient points will be discussed here.

First, as noted by Bauer *et al.*[35] response intensity in heteronucleus detected long-range correlation experiments can be modulated by the large one-bond heteronuclear coupling. Methods to suppress these modulations were the subject of reports from the author's laboratory,[36–40] as well as the laboratories of Reynolds,[41] and Batta.[42] The important point of these studies is not the actual experiments which they described but rather that they focused on the selective manipulation of a specific component of magnetization operating in an adverse manner in the context of the experiment. Pulse operators were introduced in the experiments that allowed the one-bond modulation of long-range correlation responses to be suppressed. In this fashion, investigators were less likely to miss a long-range response due to modulation effects arising from the inopportune optimization of a long-range delay.

A second concept that has direct bearing on the development of contemporary long-range heteronuclear shift correlation experiments were the constant evolution time experiments developed by the research groups of Freeman,[35] Kessler,[43,44] and by Krishnamurthy and Casida.[45] Again, it is not these old experiments that are germane to this chapter but rather the idea of using constant evolution times to suppress the evolution of components of magnetization in the experiment.

A final example worth revisiting is the XCORFE experiment developed by Reynolds and co-workers.[46] XCORFE is a constant evolution time experiment that employed a BIRD pulse midway through the final refocusing period to suppress one-bond modulations of the long-range correlation responses. The pulse sequence employed a second BIRD pulse in a very creative fashion during the evolution period. The successively relocated BIRD pulse in the evolution period provides variable refocusing of some components of magnetization while leaving others unaffected to evolve in constant time. Reynolds' creative and discrete exploitation of selected components of magnetization during the XCORFE experiment provided the basis for the differentiation of $^{2}J_{XH}$ and $^{3}J_{XH}$ correlation responses. Two-bond long-range correlation responses are 'skewed' or 'tilted' in F_1 while three-bond correlation responses are not, thereby allowing them to be differentiated from one another.

3.2. HMBC/GHMBC

The first proton-detected long-range heteronuclear shift correlation experiment to be developed was the HMBC experiment reported in 1986 by Bax and Summers.[47] The pulse sequence for the experiment is shown in Fig. 5. The experiment is quite simple in constitution, utilizing only a total of five pulses. Following the first proton pulse, a fixed delay, Δ, is inserted, optimized as a function of $\frac{1}{2}({}^{1}J_{CH})$. The phase of the following 90° ^{13}C or X-pulse is alternated 0202 while the receiver phase is alternated 0022. This pulse operator is referred

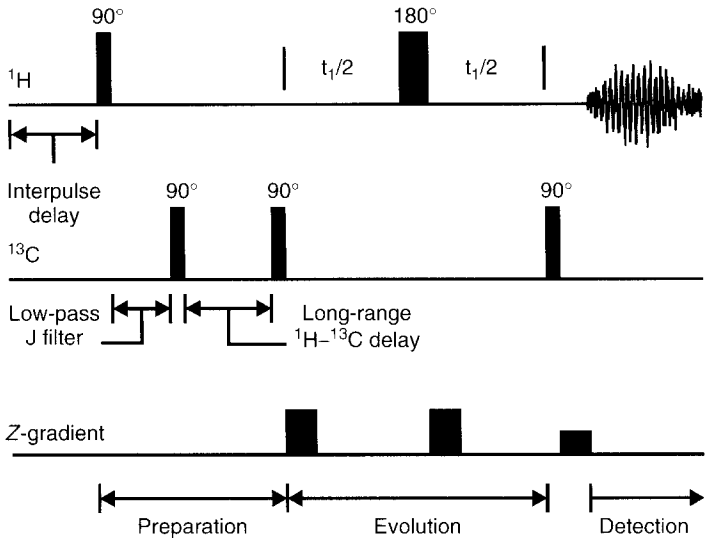

Fig. 5. HMBC pulse sequence developed by Bax and Summers.[47] The experiment, as initially reported, did not use gradients and employed a single-stage low-pass J-filter (first 90° ^{13}C pulse)[48] to destructively eliminate unwanted direct correlation responses. The gradient version of the experiment is shown.[29,49] Coherence selection gradients, as shown, may be applied using a variety of ratios determined by the gyromagnetic ratios of the heteronuclide pair being investigated. Ratios of 2 : 2 : 1 and 5 : 3 : 4 are probably the most commonly employed for ^{1}H–^{13}C correlation experiments. For ^{1}H–^{15}N, gradient ratios of 5 : 5 : 1 may be employed. The long-range delay follows, optimized as a function of $1/2({}^{n}J_{CH})$, where $n = 2$–4. Values frequently reported in the primary literature have generally been in the range of from 6 to 10 Hz, although some studies have reported optimization for still smaller coupling constants in an effort to observe long-range couplings across four or more bonds.[53] The second 90° ^{13}C pulse creates heteronuclear multiple quantum coherence (zero and double), which evolves during the first half of the evolution period ($t_1/2$). The 180° ^{1}H pulse midway through the evolution period 'decouples' proton chemical shift evolution and interchanges zero and double quantum coherence terms, which then continue to evolve through the second half of the evolution period. The final 90° ^{13}C pulse recovers antiphase proton single quantum coherence, at which point detection is initiated.

to as a low-pass J-filter.[48] Using this approach, magnetization associated with the directly coupled protons is alternately added and subtracted in memory due to the manipulation of the receiver phase, while the low-frequency, long-range coupling component of magnetization 'passes' the filter. After the first 90° X-pulse, a delay, δ, optimized as a function of $\frac{1}{2}({}^{n}J_{CH}$, where $n = 2-4$) follows to allow long-range components of heteronuclear magnetization to evolve for sampling. Long-range components of magnetization are sampled by the 90° X-pulse following this delay. That pulse creates heteronuclear multiple quantum coherence; zero and double quantum coherences are created and begin to evolve during the first half of the evolution period, $t_1/2$. The 180° proton refocusing pulse midway through the evolution period interchanges zero and double quantum coherence terms in addition to refocusing evolving proton magnetization during the t_1 interval (in the second frequency domain, F_1, after data processing). Proton evolution is 'decoupled' after the second half of evolution. The final 90° X-pulse in the sequence converts the multiple quantum coherence back into observed, antiphase proton magnetization that has been labeled with the ^{13}C chemical shift frequency or frequencies of the carbons long-range coupled to the proton in question.

Gradient versions of the HMBC, now generally referred to using the acronyms gHMBC or GHMBC, were developed in the early 1990s.[29,49] Other modifications that have been incorporated include dual stage gradient low-pass J-filters,[50] selective excitation and refocusing schemes,[51] and double pulsed field gradient spin echoes (DPGSE).[52] Regardless of the variant of the HMBC used by an investigator, the impact of this experiment on the structure elucidation process has been monumental. Any comprehensive discussion of the diverse range of applications is beyond the scope of this or any other review at this point. It is interesting to note that the description of the HMBC experiment by Bax and Summers[47] is one of the most frequently cited NMR papers of all time – a recent Science Citation Index search found >2100 references to this report in the published literature. There are, however, a few reviews in the literature that touch various aspects. Applications of inverse-detected heteronuclear shift correlation methods in the area of alkaloid structure elucidation have been reviewed by this author.[24] More recently, Araya-Maturana and co-workers[53] reviewed applications of the HMBC experiment as well as some of the newer accordion-optimized long-range experiments. This review is interesting in that it tabulates work in the literature in terms of the number of intervening bonds between the proton in question and the heteroatom. While new methods are being developed and evaluated, it is quite certain that extensive utilization of the HMBC experiment or one of its variants will continue to be widely used for structure elucidation studies.

3.3. New long-range heteronuclear shift correlation experiments

Following the development of the HMBC experiment described by Bax and Summers in 1986,[47] aside from the incorporation of pulse field gradients[29,49]

into the HMBC experiment along with other minor modifications, nearly a decade passed before reports began to appear of new, proton-detected, long-range heteronuclear shift correlation experiments. These experiments are described in this section and range from relatively simple modifications to the development of a series of accordion-optimized long-range heteronuclear shift correlation experiments.

3.3.1. Decoupled HMBC or D-HMBC

The HMBC experiment, as originally described, makes no effort to refocus newly recreated antiphase magnetization following the evolution time because of the variability in the size of the long-range couplings. Rather, immediately after the last 90° X-pulse in the conventional pulse sequence, or following a gradient and a gradient stabilization delay in the gradient-selected version of the experiment, acquisition is initiated. No broadband heteronuclear decoupling is employed as this would lead to losses of signal intensity to varying degrees as a function of the size of the individual long-range coupling constants. The idea of a refocusing delay to allow broadband heteronuclear decoupling during acquisition was first introduced by Bermel, Wagner, and Griesinger in 1989.[51] Evidently unaware that this modification had already been reported in the literature, in a 1995 report Furihata and Seto[54] described essentially the same experiment, giving it the acronym D-HMBC.

The decoupled- or D-HMBC experiment introduces a refocusing delay following the end of the evolution period equal in duration to the delay used for sampling long-range components of magnetization. The pulse sequence is shown in Fig. 6. The long-range delay values most commonly employed seem to range from about 6 to 10 Hz (83 to 50 ms), with some authors reporting optimization in the range of 3.5 or 4 Hz in an effort to observe small couplings. It is also noteworthy that there is a larger difference between strong and weak long-range correlation responses in the D-HMBC experiment than in the conventional HMBC experiment. Long-range components of magnetization evolve as a function of a sine squared function in the D-HMBC experiment rather than as a simple sine function as in the HMBC experiment. Broadband heteronuclear decoupling can be applied during acquisition in this experiment as magnetization has been refocused.

There have been a number of applications of this version of the HMBC experiment that have been reported in the literature that are discussed in the following sections. The majority of the applications that have appeared employ the experiment for the observation of small long-range $^{1}H-^{13}C$ couplings that were not observable in conventionally optimized HMBC experiments. There have been a few long-range $^{1}H-^{15}N$ 2D applications at natural abundance.

Long-range $^{1}H-^{13}C$ applications of the D-HMBC experiment

The first application of the D-HMBC experiment to appear in the literature of which we are aware was a 1995 report of the elucidation of the structure of

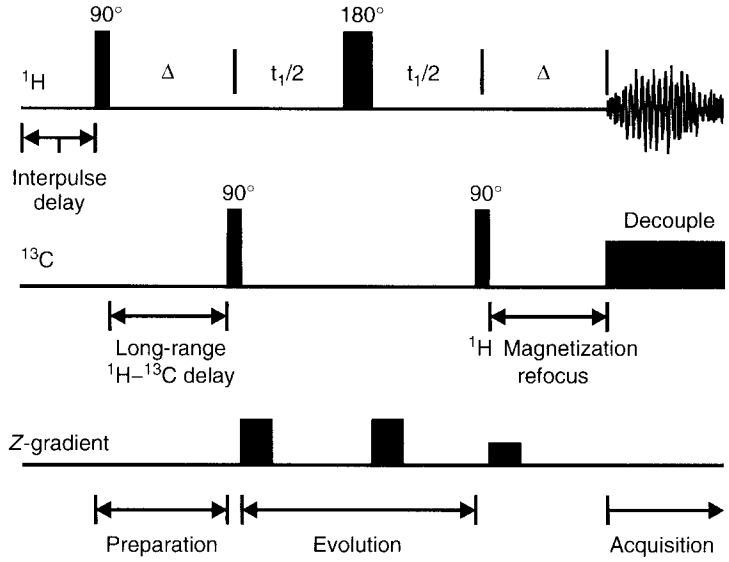

Fig. 6. Pulse sequence for the refocused- or D-HMBC experiment. The idea of refocusing anti-phase proton single quantum coherence prior to acquisition to allow broadband heteronuclear decoupling during acquisition was first reported by Bermel *et al.*[51] in 1989. Evidently unaware of the initial report, Furihata and Seto[54] again described this experiment in a 1995 communication, giving it the acronym D-HMBC. There have been a number of applications of this experiment for the acquisition of both ^{1}H–^{13}C and ^{1}H–^{15}N long-range heteronuclear shift correlation data (see p. 49 and p. 55, respectively).

a naphthoquinone antibiotic, griseusin-B (**2**) reported by Igarashi *et al.*[55] The authors reported using the D-HMBC experiment to observe a ^{2}J correlation from the 3′ oxymethine proton to the spiro 2/2′ carbon resonating at 99.2 ppm as well as a ^{4}J correlation from the 3′ oxymethine proton to the C8a quaternary carbon

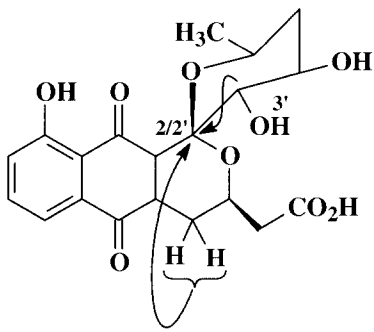

2

resonating at 139.4 ppm. In addition, ^{4}J correlations were observed from both of the 9-methylene protons to the spiro 2/2′ center. The authors did not discuss the optimization used in the acquisition of the D-HMBC data.

In a 1996 report, Kim *et al.*[56] described the structure of an anthraquinone antibiotic, espicufolin (**3**). D-HMBC was used in lieu of the HMBC experiment to determine the structure.

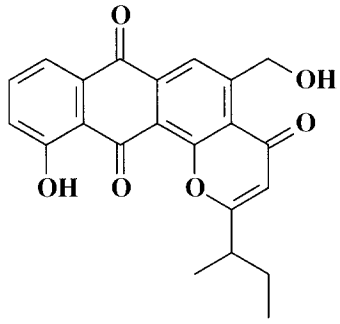

3

The elucidation of the structure of a much more complicated molecule, naphthomycinol (**4**), was reported by the same research group in late 1996.[57] The D-HMBC experiment was again used in conjunction with the conventional HMBC experiment. Correlations specifically noted in the report that were observed using the D-HMBC experiment correlated the 38-methyl resonance in the naphthoquinone portion of the molecule to the C25, C26, and C7 aromatic carbons via two- or three-bonds and via a ^{5}J correlation to the carbonyl at C23 in the ansa bridge resonating at 202.3 ppm.

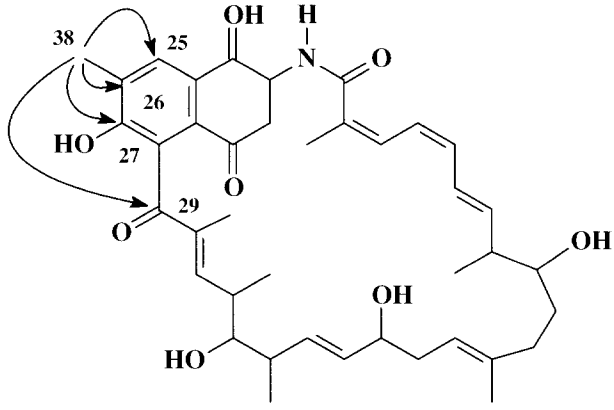

4

Kobayashi and co-workers[58] reported using the D-HMBC experiment in the structural characterization of the cytotoxic oxazole-containing halishigamides A-D from an Okinawan sponge. Specifically, D-HMBC was used to link the 8-methyl to the amide carbonyl as well as the ester carbonyl to the 12-O-methyl and H-14 oxazole protons as shown by **5**.

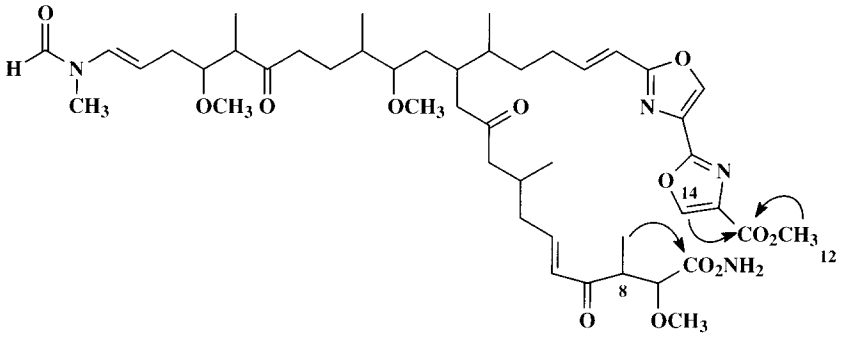

5

Kim and co-workers[59] in another 1997 report described the characterization of mescengricin, **6**, a novel neuronal cell protecting substance produced by *Streptomyces griseoflavus*. A combination of HMBC and D-HMBC experiments were used in the structure elucidation process. Correlations were observed in the D-HMBC spectrum to link the H-3 resonance to the C-10 quaternary carbon via three-bonds and to the C-11 and C-14 quaternary carbons via four-bonds in the δ-lactone portion of the molecule. The H-3 resonance was also linked via four-bonds to the C9a quaternary carbon. The indole NH proton at the 9-position of the α-carboline nucleus was linked in the D-HMBC to the C4b, C8a, and C9a quaternary carbons the last of these correlations across four-bonds; the H-5 resonance was correlated to the C4a quaternary carbon via four-bonds. These authors also used the D-HMBC experiment to establish the long-range $^{1}H-^{15}N$ correlations in the molecule (see following subsection).

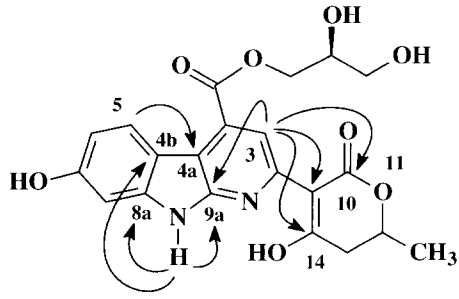

6

A novel acetylene-containing natural product, taurospongin A, consisting of a taurine and two fatty acid residues from an Okinawan marine sponge was characterized by Ishiyama and co-workers.[60] The authors mention using a combination of HMBC and D-HMBC experiments but do not elaborate further on the correlations observed in one experiment versus the other. A number of four-bond long-range correlations were reported in the manuscript, hence it might be assumed that these were observed using the D-HMBC experiment.

D-HMBC data optimized for 4 Hz were used in the structural characterization of several antifungal metabolites from the fungus *Cerdcophora sordariodes*.[61] Correlations were observed from both of the C1 methylene proton resonances to a carbonyl resonating at 185.6 ppm. Arguing that correlations via three-bonds were more likely to be observed than four-bond correlations, the O-methyl group of cedarin (**7**) was located at the 3-position of the molecular framework.

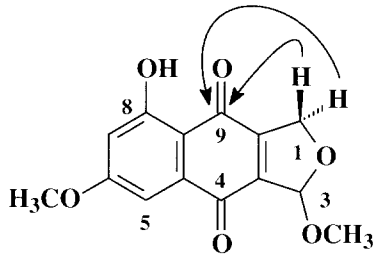

7

Taxezopidine A, **8**, a novel taxoid from a Japanese yew, was characterized using the D-HMBC experiment by Wang *et al*.[62] The authors made use of the D-HMBC experiment in the process of characterizing the oxabicyclo[2.2.2]octene moiety contained in the structure, although there is no specific mention made

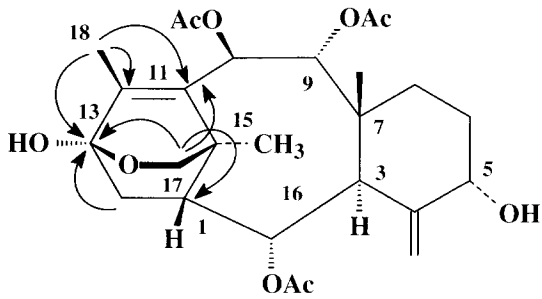

8

by them why they resorted to the D-HMBC experiment for this portion of the structure elucidation. The authors also note using the HMBC experiment although they do not mention the optimization of either of the experiments.

In another 1997 report, Kobayashi *et al.*[63] reported the characterization of two new bromo-containing alkaloids with tyrosine kinase inhibitory activity using the D-HMBC experiment. Although numerous two- and three-bond correlations were reported, there is no obvious reason for using the D-HMBC experiment in lieu of the more conventional HMBC experiment. Kobayashi and coworkers[64] also described the structure of nakadomarin A (**9**), a novel hexacyclic, 8/5/5/5/15/6 manzamine-related alkaloid. A combination of a 10 Hz optimized HMBC experiment and an ~6 Hz (80 ms) optimized D-HMBC experiment were used in elucidating the structure. Numerous two- and four-bond long-range correlations were observed using the D-HMBC data. Notable correlations are shown on the structure.

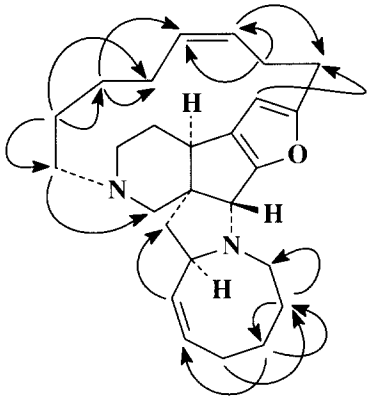

9

Nothramycin, **10**, an anthracycline antibiotic from *Nocardia sp.*, was characterized using a combination of HMBC and D-HMBC experiments by Momose *et al.*[65] The H-2 and H-3 protons were correlated via four-bonds in the D-HMBC experiment to the C12 and C13 carbonyl resonances, respectively. Unfortunately, the optimization of the experiments used was not reported.

In an interesting departure from the otherwise exclusive applications of the D-HMBC experiment in natural product structure elucidation that have been cited above, Carbajo *et al.*[66] used the D-HMBC experiment in a ^{183}W study of alkenylcarbyne- and alkenylvinylidene-tungsten complexes. Using both ^{1}H–^{183}W and ^{31}P–^{183}W inverse detection methods, the authors demonstrated an approximately $\sqrt{2}$ improvement in experimental performance with ^{183}W during acquisition. Interestingly, the authors note the observation of long-range correlations through ^{5}J(^{183}W,^{1}H), although there was no mention made of how this observation compared with other studies of organo-metallic systems.

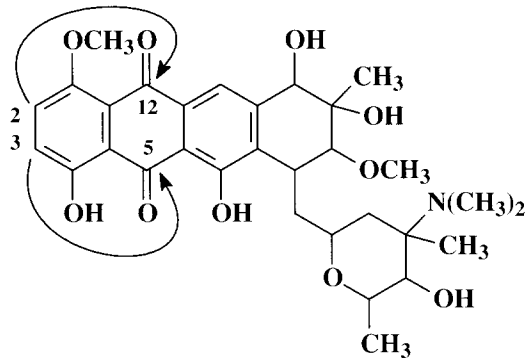

10

In 1999, Seto[67] reported examples of applications of the 3D-HMBC and CT-HMBC experiments (see Sections 3.3.2 and 3.3.4) in addition to an interesting example of the D-HMBC experiment in a published plenary lecture. In his comments on the D-HMBC experiment, Seto noted that the use of a low-pass J-filter is essentially an option. He also makes the useful point that broadband X-decoupling during acquisition places higher decoupler duty cycle demands on the spectrometer than would a direct heteronuclear shift correlation experiment on the basis of the spectral window that must frequently be decoupled with the D-HMBC experiment. In contrast to an F_1 window of perhaps no more than 160 ppm when one acquires direct heteronuclear shift correlation data, in comparison, the D-HMBC experiment for some molecules may require decoupling of F_1 spectral windows as wide as 230 ppm. In addition to discussing the application of the D-HMBC experiment to monazomycin, the compound used in the original report describing the D-HMBC experiment, Seto also showed some very long-range correlations for the thiopeptide antibiotic promothiocin B (**11**). Correlations across four- and five-bonds were observed by optimizing the D-HMBC experiment for 120 and 500 ms. These correlations were not observable in conventional HMBC spectra according to Seto.

In a relatively recent report, Coxon *et al.*[68] reported utilizing the D-HMBC and gradient-enhanced D-HMBC experiments in the structural characterization of an O-specific octasaccharide of *Shigella dysenteriae*. Unfortunately no details of the specific application of the experiments were presented in the report.

Long-range $^1H-^{15}N$ applications of the D-HMBC experiment

To date, there are three applications of the D-HMBC experiment reported in the literature for the observation of long-range $^1H-^{15}N$ couplings at natural abundance of which the author is aware.[15] In the earliest of these reports, Kawamura *et al.*,[69] reported using the D-HMBC experiment in the characterization of the antibiotic pyralomycin 1a (**12**). The authors note the effectiveness of the D-HMBC experiment for the observation of several two- and three-bond

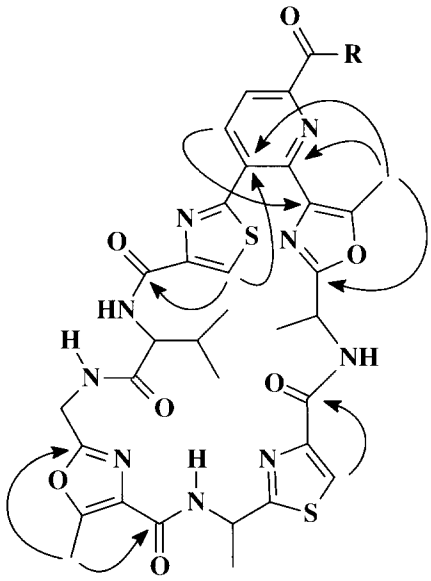

11

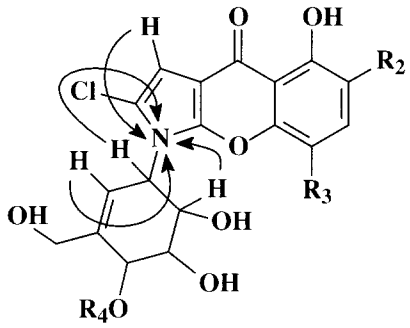

12

long-range correlations to the pyrrole nitrogen in the structure. Since all but one of the correlations observed were from protons in the sugar moiety attached to the pyrrole nitrogen, it is likely that these correlations would not have been observed in a conventional gradient HMBC experiment. Unfortunately, the authors did not report the optimization of the experiment employed in the study.

The next application of the D-HMBC experiment for the observation of long-range $^{1}H-^{15}N$ correlations at natural abundance was in the characterization of the neuronal cell-protecting substance mescengricin, as noted above.[59] A three-bond long-range coupling was observed from the α-carboline H8 resonance to the N9 resonance, which, based on the experience of the author,[15] is not a readily

observed response. A three-bond long-range correlation was also observed from the H-3 resonance to the N1 resonance. These correlations are shown by **13**.

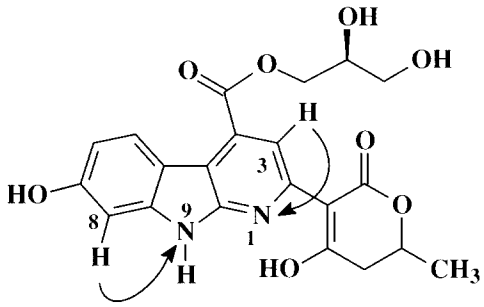

13

The final application was in a $^{1}H-^{15}N$ long-range 2D NMR study of the thiopeptide antibiotic sulfomycin-I, by Martin *et al.*[70] On comparison of the results obtained with this relatively complex molecule, which contains 16 nitrogens in its structure, the authors noted no advantage in using the D-HMBC experiment relative to a conventional gradient HMBC experiment. At this time, it is quite probable that a better choice for the routine observation of long-range $^{1}H-^{15}N$ 2D data at natural abundance is the use of the IMPEACH-MBC experiment that was developed in 1999 by the author and co-workers.[15,71,72]

3.3.2. 3D-HMBC

Furihata and Seto next reported the development of the 3D-HMBC experiment in a 1996 communication.[73] The 3D-HMBC experiment, in a sense, was a forerunner of the accordion-optimized experiments that have been developed more recently. A new variable delay, t_1, is introduced following the low-pass J-filter delay, Δ_1, as shown in the pulses sequence in Fig. 7. The delay t_1 should not be confused with the evolution delays, which are normally given the same label. In the 3D-HMBC experiment, the delays during the normal evolution period are labeled t_2, with the acquisition period now relabeled as t_3. The t_1 delay is optimized as a function of a series of values for the long-range coupling constant. In the application of the experiment to monazomycin reported by Furihata and Seto, the duration of t_1 was optimized in 4 ms steps beginning with an initial value of 20 ms (25 Hz). A total of 16 experiments were performed, each containing the equivalent of an HMBC experiment in a separate plane of the 3D experiment. The experiment sampled across the range from 25 to 6.25 Hz. Conceptually, this experiment differs from the accordion-optimized experiment described below in that each optimization of the long-range delay is a separate 2D spectrum in a plane of the 3D data matrix while the accordion experiments, in contrast, compress all of the data into a single experiment.

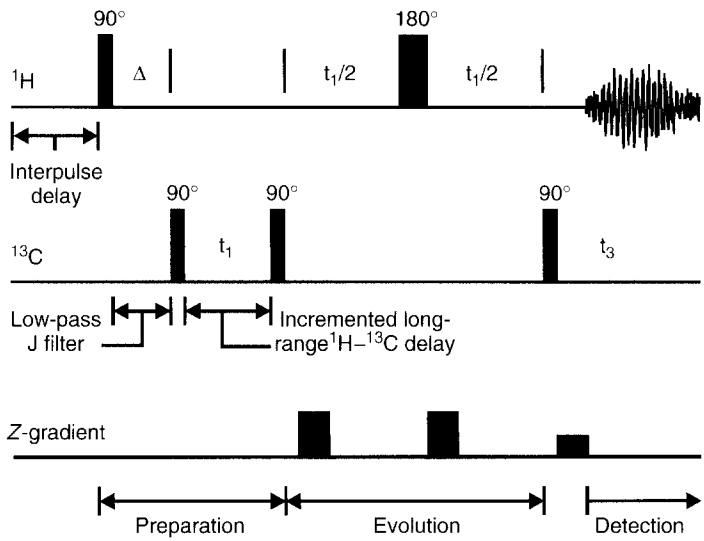

Fig. 7. Pulse sequence for the 3D-HMBC experiment developed by Furihata and Seto.[73] Recognizing that responses are observed in the HMBC experiment as a function of the congruence between the optimization of the long-range delay and the actual long-range coupling constant among other things, Furihata and Seto developed a pseudo-3D experiment in which individual planes of the experiment are each optimized for a different long-range heteronuclear coupling constant as a function of the value of t_1. By performing a series of such experiments, with the optimization range for the long-range coupling varied across the range from 6.25 to 25 Hz, more uniform extraction of all of the potential long-range correlation responses was achieved. This experiment is the forerunner of the accordion-optimized experiments later pioneered by Wagner and Berger.[89] The 3D-HMBC experiment has a considerable sensitivity drawback in the opinion of the author since it is a composite of a number of individual 2D HMBC experiments (each plane represents a separate 2D HMBC spectrum). Hence, 3D-HMBC is likely to be of limited utility unless one has relatively generous samples for study.

Furihata and Seto contend the 3D-HMBC experiment to be the 'method of choice for observing ^{1}H–^{13}C long-range couplings...'. However, when one considers that for smaller samples it is frequently necessary to acquire data for a single experiment overnight, the utility of the 3D-HMBC experiment becomes, in the opinion of this author, somewhat questionable. To date, there have been no reported applications of the 3D-HMBC experiment, although one group has reported the use of a phase-sensitive 3D J-resolved HMBC experiment.[74]

3.3.3. Gradient-enhanced HSQC – the GSQMBC experiment

In 1997 Sklenář and co-workers[75] reported the development of a single quantum based long-range experiment to which they gave the acronym GSQMBC. Recognizing that the magnitude-mode presentation format normally applied with

HMBC data precluded the measurement of small couplings, a long-range version of the phase-sensitive HSQC experiment was developed. The pulse sequence is shown in Fig. 8. In the original communication, application of the experiment to the measurement of $^{1}H-^{13}C$, $^{1}H-^{15}N$ and $^{1}H-^{77}Se$ two- and three-bond long-range couplings was reported. While the results of the experiment when the proton in question is a simple doublet are certainly useful, the authors have not demonstrated the utility of the experiment to protons that appear as complex multiplets, in which case the utility of the experiment is expected to degrade.

Since the original report of the GSQMBC experiment in 1997, there have been a number of applications of the technique to the solution of structural problems, most emanating from the laboratories of the originators. The first such application was a report on the alkaloid armepavine.[76] Although the authors

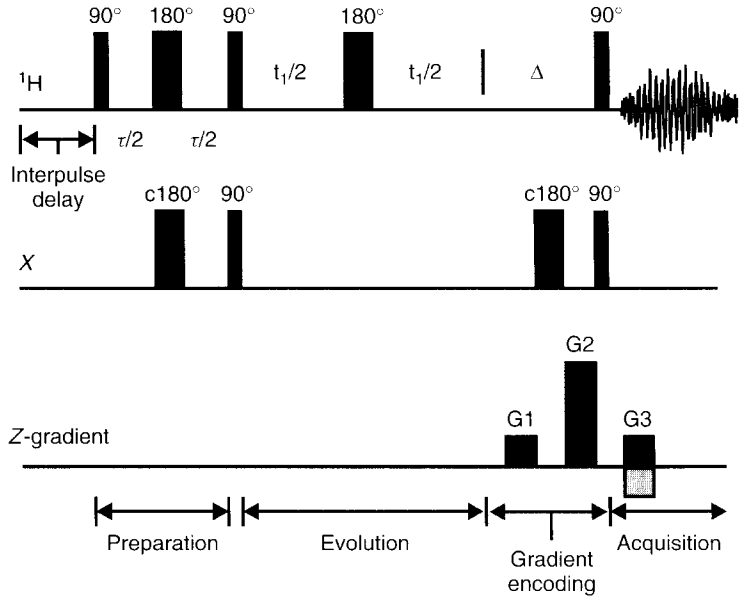

Fig. 8. Pulse sequence for the GSQMBC experiment devised by Sklenář and co-workers[75] in 1997. The experiment is phase-sensitive rather than employing a magnitude mode presentation as does the HMBC experiment. The experiment is also single quantum-based, derived from the HSQC direct correlation experiment. The experiment begins with an INEPT step where the delay, τ, is set as a function of $\frac{1}{2}(^{n}J_{XH})$. At the end of the INEPT step, only heteronuclear, long-range single quantum magnetization is generated, which then evolves during t_1. Two phase encoding gradients, G1 and G2, flank the composite 180° X pulse to suppress X nucleus chemical shift evolution during gradient dephasing. The receiver is enabled immediately following the last 90° pulse sandwich and the final gradient is applied during the acquisition period, t_2. The GSQMBC experiment has been used by the authors responsible for its development in a number of applications and for the extraction of relatively small long-range heteronuclear coupling constants.

note using both the GHMBC and GSQMBC experiments in observing the long-range heteronuclear couplings of the molecule, no specific mention is made of couplings that were observed in one experiment versus the other. Later in 1997, Marek[77] reported the results of a study of 2,2-dimethylpenta-3,4-dienal derivatives in which the GSQMBC experiment was used to measure the long-range $^{1}H-^{15}N$ coupling constants of the molecules studied. In a related study, Marek and co-workers[78] reported the preparation of a series of new 2,2-dimethylpenta-3,4-dienal azines via a Claisen–Cope rearrangement in which the GSQMBC experiment was used in the structural characterization.

In a study of the structure and transformations of the alkaloid sanguilutine, Dostal *et al.*[79] utilized the GSQMBC experiment in conjunction with GHMBC to establish the dimeric structure of the alkaloid. The authors report optimizing the experiments used for 11, 7, and 4 Hz, but again don't comment on specifics of the data from the two experiments. In a non-polar environment, 6-hydroxy-5,6-dihydrosanguilutine was reported to spontaneously transform to bis[6′(5,6-dihydrosanguilutinyl)] ether; in the presence of aqueous ammonia, the corresponding bis amine was also formed.

Kilian and co-workers[80,81] reported using the GSQMBC pulse sequence in the characterization of new P-S-N-containing heterocyclic ring systems. The authors used a $^{1}H-^{31}P$ GSQMBC experiment to establish long-range $^{1}H-^{31}P$ correlations and a conventional GHMBC experiment in the first study to determine the $^{1}H-^{13}C$ long-range couplings with ^{31}P decoupling during acquisition to simplify the spectra. In the second study, $^{1}H-^{15}N$ GSQMBC data were used in establishing the structure as were $^{31}P-^{15}N$ GHMQC data.

In a pair of papers, Dostal *et al.*[82,83] reported utilizing the GSQMBC experiment in studies of chelirubine and chelilutine free bases and sanguinarine pseudobase, respectively. The GSQMBC experiment was used to establish both $^{1}H-^{13}C$ as well as $^{1}H-^{15}N$ long-range correlations. A comprehensive study of the ^{15}N-NMR of 40 tertiary and quaternary isoquinoline alkaloids of six different constitutional types was also reported by Marek *et al.*,[84] in which the GSQMBC and GHMBC experiment were used to observe the $^{1}H-^{15}N$ long-range correlations. Marek and co-workers[85] also reported using the GSQMBC experiment in a ^{1}H and ^{13}C NMR study of quaternary benzo[c]phenanthridine alkaloids in 1999. In this study, the GSQMBC experiment was used to measure the long-range $^{1}H-^{13}C$ heteronuclear coupling constants.

Finally, in a report dealing with the regio-selective preparation of N^{7} and N^{9}-alkyl derivatives of N^{6}-[(dimethylamino)methylene]adenine, Hocková *et al.*[86] used the GSQMBC experiment to determine the long-range $^{1}H-^{15}N$ correlation responses and the respective long-range $^{1}H-^{15}N$ coupling constants.

3.3.4. Constant Time HMBC – CT-HMBC

Utilizing the concept of the constant time experiment noted in the introduction to this section (see Section 3.1) Furihata and Seto next reported the development of two constant time HMBC variants, to which they gave the acronyms

CT-HMBC-1 and CT-HMBC-2.[87] The pulse sequences for CT-HMBC-1 and CT-HMBC-2 are shown in Figs. 9(a) and 9(b), respectively. The idea behind the development of these pulse sequences was a desire to suppress the characteristic 'skew' that responses in HMBC/GHMBC experiments exhibit at high F_1 digital resolution that arises due to J-modulation from proton–proton homonuclear coupling. Although the 180° proton pulse midway through the evolution period, t_1, refocuses proton chemical shift evolution, the variable duration of the evolution period from one increment of the evolution period to the next is responsible for the observed 'skew'. Homonuclear proton–proton couplings evolve in non-constant time from one increment of the evolution time to the next.

The approach of Furihata and Seto[87] was to introduce a constant time evolution period in the CT-HMBC-1 pulse sequence shown in Fig. 9(a). Thus, rather than a sequence in which evolution is represented by

$$t_1/2 - 180^\circ\ ^1\mathrm{H} - t_1/2 \tag{3}$$

as in the conventional HMBC/GHMBC pulse sequences, the CT-HMBC-1 experiment instead has an evolution period consisting of

$$(\Delta_3 - t_1/2) - t_1/2 - 180^\circ\ ^1\mathrm{H} - t_1/2 - (\Delta_3 - t_1/2) \tag{4}$$

As the evolution time t_1 is incremented, the delay Δ_3 is correspondingly decremented, thereby keeping the overall evolution time constant. In this process, J-modulation is suppressed, correspondingly improving F_1 resolution.

The CT-HMBC-2 pulse sequence utilizes a decremented delay prior to the evolution period, with a 180° proton pulse midway through it of the type

$$(\Delta_3 - t_1/2) - 180^\circ\ ^1\mathrm{H} - (\Delta_3 - t_1/2) - 90^\circ\ \mathrm{X} - t_1/2 - 180^\circ\ ^1\mathrm{H} - t_1/2 - 90^\circ\mathrm{X} \tag{5}$$

Again, the $(\Delta_3 - t_1/2)$ terms are decremented as the evolution periods $t_1/2$ are correspondingly incremented, keeping the overall evolution time in the experiment constant. The authors note that this modification not only suppresses J-modulation due to homonuclear coupling, but also heteronuclear coupling as well, thereby improving resolution further relative to the CT-HMBC-1 experiment.

The concepts of the CT-HMBC experiments are fundamentally quite important, and have been exploited in the development of some of the accordion-optimized experiments described below (see Section 3.3.5). To date there have not been any reported applications of either of the experiments described in this section.

3.3.5. Accordion-optimized long-range heteronuclear shift correlation experiments

A useful starting point for this discussion is the definition of an accordion delay. The concept of accordion optimization of a delay is first found in the report of Bodenhausen and Ernst in 1982.[88] Quite simply, the selected delay in the pulse

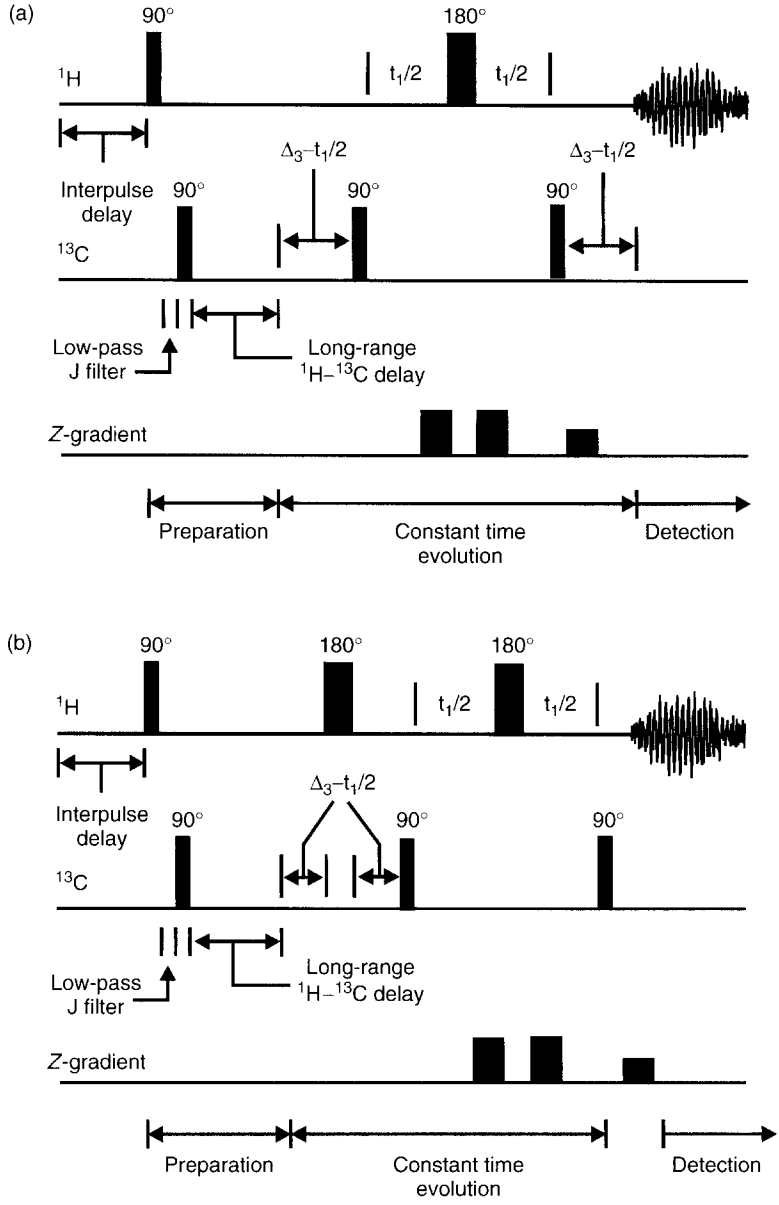
(a)
90°
180°
^{1}H
$t_1/2$
$t_1/2$
$\Delta_3-t_1/2$
$\Delta_3-t_1/2$
Interpulse delay
90°
90°
90°
^{13}C
Low-pass J filter
Long-range ^{1}H–^{13}C delay
Z-gradient
Preparation
Constant time evolution
Detection
(b)
90°
180°
180°
^{1}H
$t_1/2$
$t_1/2$
$\Delta_3-t_1/2$
Interpulse delay
90°
90°
90°
^{13}C
Low-pass J filter
Long-range ^{1}H–^{13}C delay
Z-gradient
Preparation
Constant time evolution
Detection

sequence is successively re-optimized from one increment of the evolution time to the next across a predefined range of values selected before the initiation of the experiment. Although there have been other applications of accordion optimization, the first application of this concept to long-range heteronuclear shift correlation experiments was in the ACCORD-HMBC experiment developed in 1998 by Wagner and Berger[89] (see following subsection). IMPEACH-MBC was a modification of the ACCORD-HMBC experiment to control F_1 'skew' reported in 1999 by the author and co-workers[71] (see IMPEACH-MBC subsection, p. 68). User controlled F_1 skew, to allow the use of this feature of the experiment for the authentication of weak correlations was introduced in the CIGAR-HMBC experiment (p. 70). An accordion experiment offering the means of unequivocally differentiating ^2J from ^3J long-range correlations to protonated ^{13}C or ^{15}N resonances was introduced with the $^2J,^3J$-HMBC experiment (p. 74). Other accordion-based experiments have also been described for the determination of long-range heteronuclear coupling constants, and are discussed in Section 3.4.

ACCORD-HMBC

The first reported application of accordion-optimized delays in a long-range heteronuclear shift correlation experiment is found in the description of the ACCORD-HMBC experiment by Wagner and Berger.[89] The pulse sequence for the experiment is presented in Fig. 10. The experiment begins with a dual-stage, gradient, low-pass J-filter.[90,91] The three gradients applied during the dual-stage, gradient, low-filter must sum to zero. The variable delay, *vd*, follows. The delay begins with a duration of T_{max} ($\frac{1}{2}J_{min}$) and is decremented to T_{min} ($\frac{1}{2}J_{max}$) in *ni* steps, where *ni* is the number of increments used to digitize the indirectly detected frequency domain. The decrementation value is defined by $t_1\,\mathrm{max}/ni$. The variable delay, *vd*, is decremented rather than being incremented to keep the overall duration of the experiment shorter than if *vd* were incremented in concert with the incrementation of the evolution time, t_1. The evolution time is

Fig. 9. Pulse sequence for the constant time CT-HMBC experiments devised by Furihata and Seto.[87] The authors reported two variants of the experiment, the CT-HMBC-1 pulse sequence shown in Panel (a) and the more complex CT-HMBC-2 pulse sequence shown in Panel (b). (a) The CT-HMBC-1 sequence utilizes a pair of decremented delays ($\Delta_3 - t_1/2$) flanking the incremented duration of the evolution period. As the delays used for the evolution period (t_1) are incremented from zero to $t_1{}^{max}$, the delay intervals $\Delta_3 - t_1/2$ are correspondingly decremented from $\Delta_3 = t_1{}^{max}$ to zero, thereby keeping the overall duration of the CT-HMBC-1 pulse sequence constant. This approach has the beneficial effect of suppressing J-modulation due to homonuclear couplings, thereby improving resolution in the indirectly detected frequency domain. (b) The CT-HMBC-2 pulse sequence utilizes a decremented delay with a 180° ^1H pulse midway through it prior to the evolution period of the type $(\Delta_3 - t_1/2) - 180°\ ^1H - (\Delta_3 - t_1/2)$. The authors note that this modification, in addition to suppressing J-modulation due to homonuclear coupling also suppresses heteronuclear couplings to provide a further improvement in resolution relative to the CT-HMBC-1 pulse sequence.

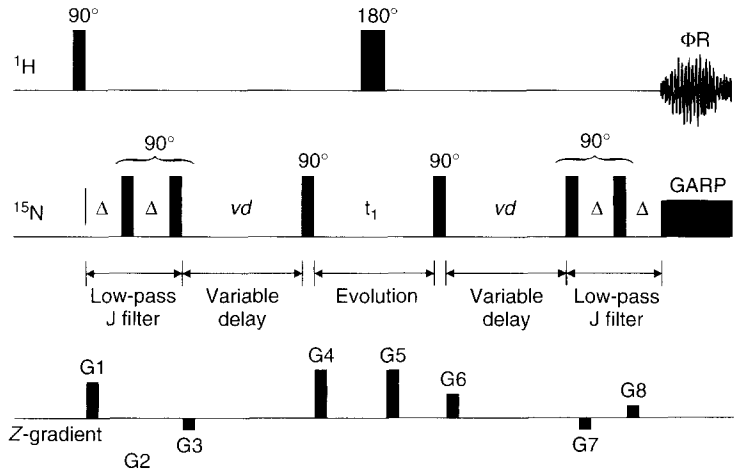

Fig. 10. Pulse sequence for the innovative ACCORD-HMBC experiment developed by Wagner and Berger.[89] The experiment begins with a dual-stage gradient low-pass J-filter[90,91] followed by the variable delay, *vd*. The ACCORD-HMBC experiment utilizes the so-called 'accordion principle' first described in 1982 by Bodenhausen and Ernst.[88] The experiment samples a broad range of potential long-range heteronuclear couplings by adjusting the duration of the variable delay, *vd*, beginning from T_{max} (which corresponds to the minimum J-value selected, as a function of $\frac{1}{2}({}^{n}J_{min})$) which is decremented in *ni* equivalent steps where *ni* is the number of increments of the evolution time, t_1, to T_{min} (which is a function of the maximum J-value as a function of $\frac{1}{2}({}^{n}J_{max})$). The evolution period, t_1, is incremented in the usual manner from zero to $t_1{}^{max}$. Wagner and Berger kept the original version of the pulse sequence symmetric about the evolution period to allow broadband heteronuclear decoupling to be performed during acquisition. In the experience of the author, however, any benefits of being able to apply broadband heteronuclear decoupling during acquisition are offset by losses in response intensity due to the long duration of the variable delays. The experiment uses a total of eight gradient pulses. Gradients labeled G1–G3 applied in the gradient dual-stage low-pass J-filter must sum to zero. Gradients G4–G6 are the coherence selection gradients and are optimized as in the GHMBC experiment using a ratio such as 2 : 2 : 1 for ^{1}H–^{13}C long-range correlation experiments. The final bipolar gradients, G7 and G8, again must sum to zero for the experiment to work properly.

incremented in the usual fashion, from zero to $t_1$max; gradients applied during the evolution phase of the experiment are applied in the usual ratios, 2 : 2 : 1 for ^{1}H–^{13}C or 5 : 5 : 1 for ^{1}H–^{15}N or a comparable ratio.

To keep the pulse sequence symmetric to allow broadband heteronuclear decoupling during acquisition, a second variable delay, *vd*, follows the recreation of antiphase single quantum proton magnetization. A 'reverse' low-pass J follows to make ACCORD-HMBC sequence completely symmetric, followed by acquisition with broadband heteronuclear decoupling.

The benefit that obtains from the use of an accordion-optimized long-range experiment is illustrated with strychnine (**14**) and the aliphatic spectral panels shown in Fig. 11(a) and 11(b).[92] A conventional 6 Hz GHMBC spectrum, which

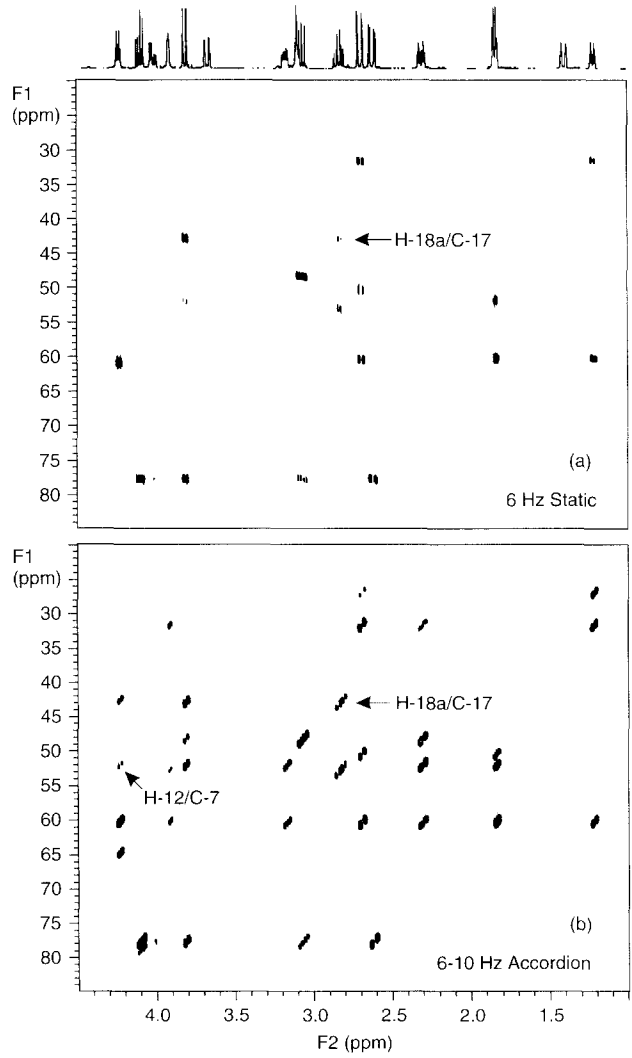

Fig. 11. Comparison of a 6 Hz, statically-optimized GHMBC spectrum of strychnine (**14**) shown in Panel (a) with a 6 to 10 Hz optimized ACCORD-HMBC spectrum shown in Panel (b). Beginning with a comparison of the responses for the H12 resonance, which is observed furthest down field at 4.27 ppm, only a single long-range correlation is observed in the 6 Hz GHMBC spectrum. In contrast, four long-range correlations are observed from the H12 resonance in the 6–10 Hz optimized ACCORD-HMBC spectrum. If the weak H18a/C17 long-range correlation in the 6 Hz GHMBC spectrum (denoted by arrow) is compared with the same response in the 6–10 Hz optimized ACCORD-HMBC spectrum (denoted by arrow) it will be observed that the response is considerably more intense in the latter spectrum as a result of sampling a broader range of potential long-range couplings through the use of the accordion-optimized variable delay, *vd*. It should also be noted that responses in the ACCORD-HMBC spectrum are 'skewed' in F_1 as a consequence of the evolution of homonuclear magnetization, for which the variable delay serves as an evolution period in much the same sense that the t_1 interval serves as an evolution period. This behavior has been analyzed in detail by Martin and co-workers.[92] (G. E. Martin *et al.*, *Magn. Reson. Chem.*, 1999 © John Wiley & Sons, Ltd. Reproduced with permission.)

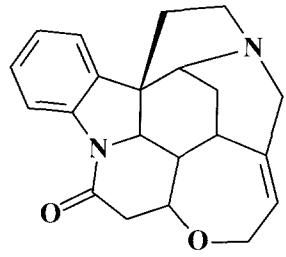

14

is referred to as 'statically' optimized, is shown in Fig. 11(a). These data are compared to the 6–10 Hz accordion-optimized ACCORD-HMBC spectrum. Several interesting observations can be drawn. Examining the GHMBC spectrum in Fig. 11(a), only a single response is observed for the H12 resonance at 4.27 ppm. The weak H18a/C17 long-range correlation denoted by the arrow in the GHMBC spectrum could easily be questioned as to its authenticity. In contrast, in the 6–10 Hz optimized ACCORD-HMBC shown in Fig. 11(b), four responses are observed from the H12 resonance. Of these responses, the obvious F_1 skew of the H12/C7 correlation denoted by the arrow, serves to authenticate this response since noise spikes are not subject to being skewed. There are considerably more responses observed in the ACCORD-HMBC spectrum and those which were weak in the 6 Hz GHMBC spectrum, e.g. H18a/C17, are now considerably stronger.

Aside from the advantage of the ACCORD-HMBC spectrum shown by Fig. 11, Martin and co-workers[92] examined various aspects of the accordion-optimization process on the character of the spectrum. Modulation in the ACCORD-HMBC experiment is affected by both the optimization range selected and the number of increments of the evolution time (ni) used to digitize the indirectly detected time domain, t_1. F_1 skew is governed by a scaling factor, N, which is defined by

$$N = 2\tau/\Delta F_1 \tag{6}$$

where

$$\tau = (T_{max} - T_{min})/ni \tag{7}$$

This facet of the experiment is similar to the EXSIDE experiment developed by Krishnamurthy.[93] Modulation is illustrated by the nature of the responses in the four panels presented in Fig. 12. Segments are shown from four ACCORD-HMBC spectra, each acquired with $ni = 128$. Panels (a)–(d) were acquired with optimization ranges of 6–10, 4–12, 2–16, and 2–25 Hz, respectively. In Panel (a), no response is observed for the H-11α proton resonating at ~3.05 ppm. The response correlating H-11α/C12 is observed in the 4–12 Hz data shown in Panel (b). Note that in the 3–16 and 2–25 Hz data shown in Panels (c) and

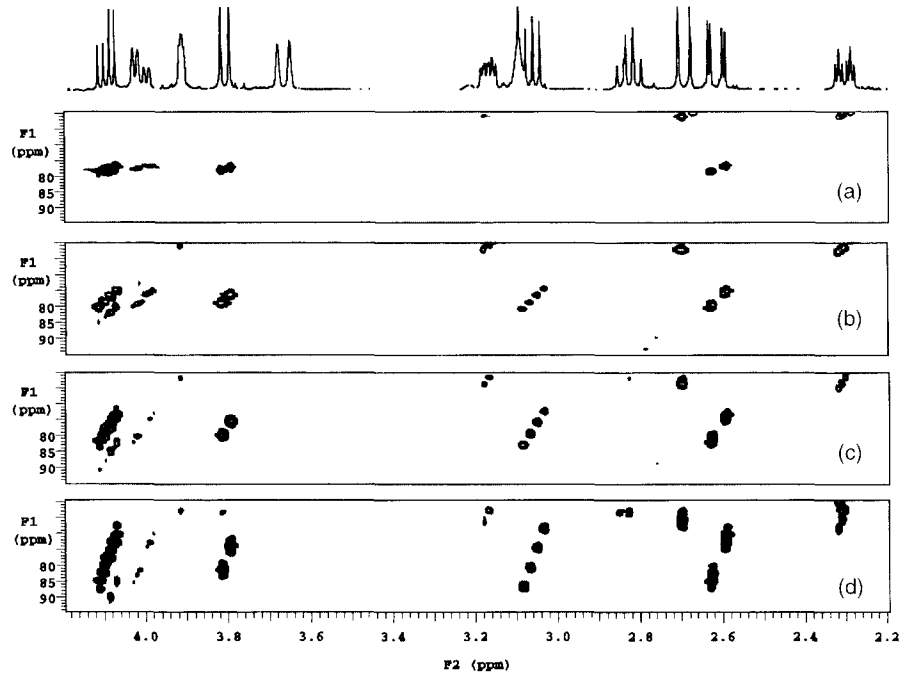

Fig. 12. Segments from four ACCORD-HMBC spectra, each digitized with 128 increments of the evolution time, t_1. In Panel (a), recorded with an accordion-optimization range of 6–10 Hz, no response is observed for the proton resonating at ~3.05 ppm. In the 4–12 Hz optimized spectrum shown in Panel (b), a response is observed at ~3.05 ppm correlating this proton with the C12 resonance. The intensity of the response increases in the 3–16 and 2–25 Hz optimized spectra shown in Panels (c) and (d), respectively. In addition, note that the degree of skew associated with the response in F_1 also increases as a function of broadening the accordion-optimization range. (G. E. Martin *et al.*, *Magn. Reson. Chem.*, 1999 © John Wiley & Sons, Ltd. Reproduced with permission.)

(d), respectively, that the degree of skew increases as the optimization range is broadened, as expected from Eq. (6).

Data shown in Fig. 13 illustrate the effect of changing the number of increments of the evolution time when the optimization range is held constant at 2–25 Hz. There is very significant F_1 skew when coarse digitization of the second time domain (e.g. $ni = 64$), with the degree of skew progressively minimized as digitization is increased to a maximum of $ni = 512$.

Both of the features just described must be taken into account when setting up an ACCORD-HMBC experiment. The utilization of an aggressive optimization range in an effort to observe large numbers of weak couplings, i.e. $^2J_{XH}$ and $^3J_{XH}$ correlations, can lead to severe long-range response overlap in congested regions of the 2D NMR spectrum. This behavior was illustrated by Martin *et al.*[92] in the

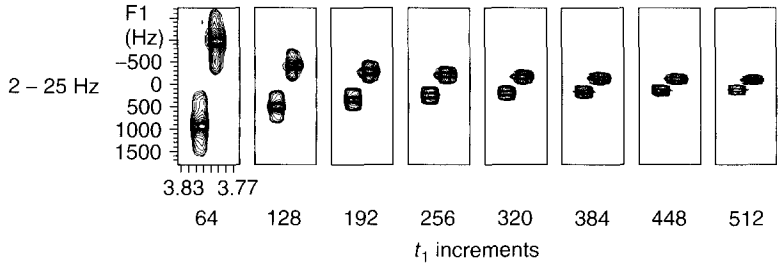

Fig. 13. Panels taken from a series of 2–25 Hz optimized ACCORD-HMBC spectra in which the number of increments of the evolution time, t_1, was varied from 64 to 512. The response shown is the $^3J_{CH}$ correlation of the H12 resonance to the C23 methylene carbon across the ether linkage of the seven-membered oxepin ring of strychnine (**14**).

case of strychnine (**14**), which was used as an example in that report. Despite the parameterization problems of the experiment, using a 2–25 Hz optimization in conjunction with $ni = 512$ allowed the observation of 18 $^4J_{CH}$ long-range correlations in the ACCORD-HMBC spectrum of strychnine in comparison to only four very weak $^4J_{CH}$ long-range correlations in a 10 Hz optimized GHMBC spectrum.

In addition to the importance of parameter selection on F_1 skew, the ACCORD-HMBC experiment has also been shown to exhibit strong coupling artifact responses similar to those observed in heteronuclear 2D J-resolved spectra.[92,94,95] Finally, the 'triplet' character of responses in the second frequency domain superimposed over the F_1 skew was mathematically accounted for by Zangger and Armitage in their development of the ACCORD-HMQC experiment.[32]

There have been no applications of the ACCORD-HMBC experiment reported in the literature to date.

IMPEACH-MBC – IMproved PErformance ACcordion-optimized Heteronuclear multiple bond correlation

In an effort to address the essentially uncontrolled F_1 skew inherent to the ACCORD-HMBC, the author and co-workers[71] next reported the development of the IMPEACH-MBC experiment, the pulse sequence for which is shown in Fig. 14. Recognizing that F_1 skew arises due to homonuclear scalar coupling modulation for which the variable duration accordion-optimized delay serves as an evolution time, the variable delay, *vd*, was modified in the IMPEACH-MBC experiment. The variable delay can be made into a constant time delay for homonuclear components of magnetization by adding a new segment to the overall delay centered about a 180° X pulse to refocus heteronuclear magnetization. The thus modified 'constant time' variable delay is given by

$$D/2 - 180^\circ\ \mathrm{X} - D/2 - vd \qquad (8)$$

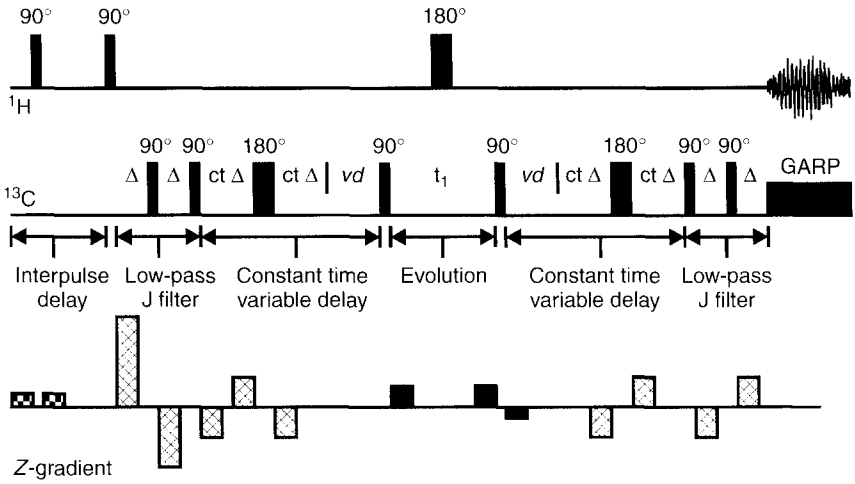

Fig. 14. IMPEACH-MBC (**IM**proved **PE**rformance **AC**cordion-optimized **H**eteronuclear multiple bond correlation) pulse sequence developed by Martin and co-workers.[71] The experiment is a further modification of the ACCORD-HMBC experiment that utilizes a constant time variable delay in lieu of a simple variable delay. The constant time variable delay introduces the interval, $D/2 - 180° \ ^{13}C - D/2$, which precedes the variable delay interval, *vd*. As the evolution time t_1 is incremented, the interval *vd* is decremented in the usual fashion. However, at the same time, the $D/2$ (ct Δ) intervals are incremented in a manner to keep the overall duration of the period $D + vd$ a constant time interval. Hence, homonuclear modulation, which plagues ACCORD-HMBC experiments, is suppressed by the constant time of the interval $D + vd$. In contrast, evolving heteronuclear couplings are refocused at time D by the 180° ^{13}C pulse located at $D/2$. These couplings then evolve during the variable interval *vd* to be sampled in the usual, accordion manner. By using this approach, the constant time variable delay pulse sequence element is of constant duration for homonuclear components of magnetization while serving as a variable delay for heteronuclear components.

As the interval *vd* is decremented from T_{max} to T_{min} in steps of $(T_{max} - T_{min})/ni$, the delay D, is correspondingly incremented from zero, thereby keeping the overall duration of $D + vd$ constant. Modulation due to homonuclear scalar coupling is suppressed since it 'evolves' in what is now a constant time delay. Heteronuclear components of magnetization are refocused at D by the 180° X pulse applied at $D/2$, after which they evolve in 'variable' time during *vd*. In this fashion, the constant time variable delay suppresses F_1 skew while at the same time allowing accordion sampling of the desired range of long-range heteronuclear couplings.

In the initial form of the IMPEACH-MBC pulse sequence shown in Fig. 14, the experiment was designed symmetrically to allow broadband X-decoupling during acquisition. Sensitivity, however, is improved by forgoing X-decoupling and initiating data acquisition following the coherence selection gradient and its associated delay. The modified version of the experiment is currently in use in the author's

laboratory. A useful illustration of the utility of the experiment is found in the report by Martin and Hadden[72] that deals with the application of accordion excitation in the acquisition of 2D $^{1}H-^{15}N$ long-range heteronuclear shift correlation data at natural abundance. Because of the high degree of variability of long-range $^{1}H-^{15}N$ couplings[15] acquiring these data using accordion-optimized experiments should be beneficial. Moreover, using IMPEACH-MBC rather than ACCORD-HMBC will also suppress the F_1 skew inherent to the latter data. The three panels shown in Fig. 15 compare an 8 Hz optimized $^{1}H-^{15}N$ GHMBC experiment (Panel (a)) with 3–16 Hz optimized ACCORD-HMBC (Panel (b)) and 3–16 Hz optimized IMPEACH-MBC (Panel (c)) spectra. First, as expected, the F_1 skew inherent to the ACCORD-HMBC data is suppressed in the IMPEACH-MBC spectrum. Additionally, both of the accordion-optimized spectra exhibit nominally better overall signal-to-noise than the statically optimized GHMBC spectrum. Comparison traces from the GHMBC and IMPEACH-MBC experiment taken at the N9 amide carbon chemical shift are compared in Fig. 16. The overall s/n ratio of the IMPEACH-MBC spectrum is somewhat lower (36 : 1) than that of the GHMBC spectrum (42 : 1). In contrast, the H8/N9 and H13/N9 response intensity is vastly superior in the trace from the IMPEACH-MBC experiment while the H11α/N9 response intensity in the IMPEACH-MBC data is only slightly lower than the GHMBC response. In general, the author's laboratory has found IMPEACH-MBC to be the experiment of choice for the acquisition of long-range $^{1}H-^{15}N$ 2D NMR data at natural abundance.

CIGAR-HMBC – Constant time Inverse-detected Gradient Accordion Rescaled Heteronuclear Multiple Bond Correlation

Retrospectively, after demonstrating in the implementation of the IMPEACH-MBC experiment that it is possible to suppress F_1 skew, it was evident that the skew of responses in F_1, while a nuisance if uncontrolled, could serve as a useful means of response authentication if F_1 skew was under user control. The CIGAR-HMBC experiment accomplishes this task.[96] While the constant time variable delay of the IMPEACH-MBC experiment (see Eq. (8)) renders the duration of the variable delay constant, the CIGAR-HMBC pulse sequence modifies the variable delay interval of the experiment still further, as shown below; the complete pulse sequence is shown in Fig. 17.

$$(D/2 + \Delta 2/2) - 180^{\circ}\ \mathrm{X} - (D/2 + \Delta 2/2) - vd \tag{9}$$

Rather than incrementing the $D/2$ intervals flanking the 180° X pulse as in the IMPEACH-MBC experiment, D is instead incremented by

$$(\tau_{max} - \tau_{min})/ni + \Delta 2 \tag{10}$$

where $\Delta 2$ is defined as

$$\Delta 2 = (J_{scale} - 1)t_1/2 \tag{11}$$

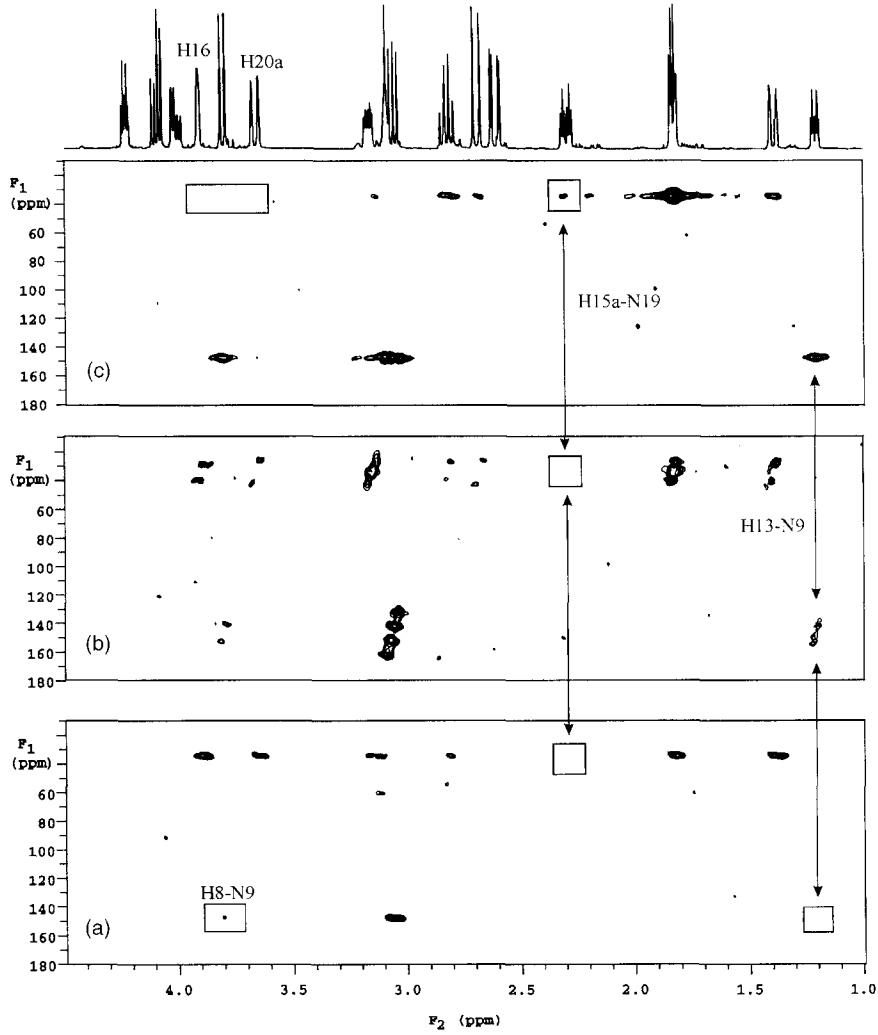

Fig. 15. Comparison of long-range $^{1}H-^{15}N$ GHMBC (Panel (a)), ACCORD-HMBC (Panel (b)), and IMPEACH-MBC (Panel (c)) spectra of the aliphatic region of strychnine (**14**) at natural abundance.[72] All three of the experiments were digitized using 128 increments of the evolution time, t_1. The GHMBC spectrum shown in Panel (a) was optimized for an assumed 8 Hz long-range $^{n}J_{NH}$ coupling. The ACCORD-HMBC and IMPEACH-MBC spectra shown in Panels (b) and (c), respectively, were optimized from 3 to 16 Hz. As expected, the F_1 skew inherent to the ACCORD-HMBC spectrum shown in Panel (b) is suppressed in the IMPEACH-MBC data shown in Panel (c). In addition, both of the accordion-optimized spectra exhibit nominally better response intensity than the corresponding GHMBC traces. (G. E. Martin and C. E. Hadden, *Magn. Reson. Chem.* 2000 © John Wiley & Sons, Ltd. Reproduced with permission.)

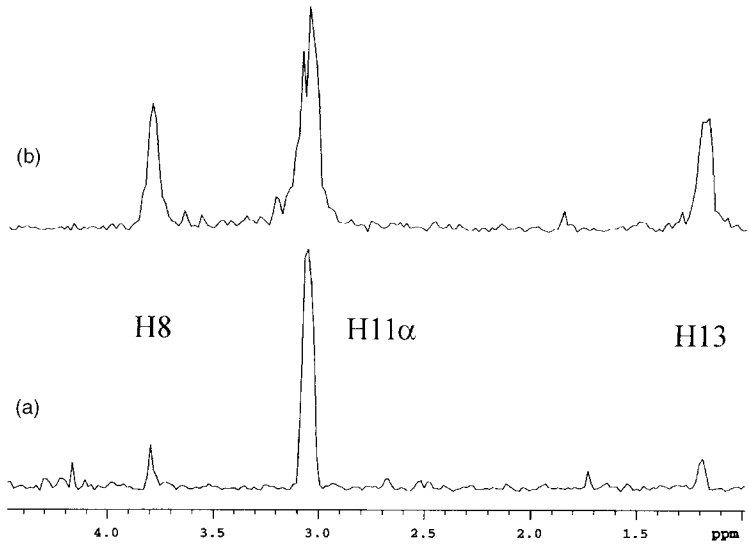

Fig. 16. Comparison N9 amide resonance traces from the 8 Hz optimized GHMBC and 3–16 Hz optimized IMPEACH-MBC spectra shown in Fig. 15 Panels (a) and (c), respectively. The overall signal-to-noise (s/n) ratios of the two spectra are 42 : 1 and 36 : 1, respectively. Despite the higher overall s/n associated with the GHMBC spectrum, the IMPEACH-MBC experiment clearly affords superior response intensity for the H8 and H13 long-range correlations to the N9 amide resonance, circumventing the difficulties inherent to optimizing GHMBC spectra for long-range $^{1}H-^{15}N$ studies at natural abundance.[15] (G. E. Martin and C. E. Hadden, *Magn. Reson. Chem.* © John Wiley & Sons, Ltd. Reproduced with permission.)

where t_1 is the increment of the evolution period. In this fashion, limited F_1 modulation or 'skew' can be introduced into the spectrum independently of the digitization used in the second frequency domain unlike the ACCORD-HMBC in which F_1 modulation is directly proportional to the degree of F_1 digitization and the accordion-optimization range (see ACCORD-HMBC subsection, p. 63).

Three choices are possible for the new parameter J_{scale} introduced in the CIGAR-HMBC pulse sequence. When $J_{scale} = 0$, the term $\Delta 2 = (J_{scale} - 1)t_1/2$, is obviously negative. With this parameter choice, the overall duration of the variable delay is successively decremented from one increment of the evolution time t_1 to the next. In this fashion, the overall duration of the experiment $(vd + t_1)$ is truly constant. All modulation in F_1 is suppressed giving maximum F_1 resolution. This version of the CIGAR-HMBC experiment is hence analogous to the CT-HMBC experiments described by Furihata and Seto[87] (see Section 3.3.4). The second choice available to the investigator is $J_{scale} = 1$. This choice gives behavior of the variable delay that is identical to the IMPEACH-MBC experiment (described earlier). Finally, the investigator may also choose $J_{scale} > 1$, which introduces user-determined F_1 modulation as a function of the degree of prolongation of the $(D/2 + \Delta 2/2)$ intervals of the pulse sequence. As the value

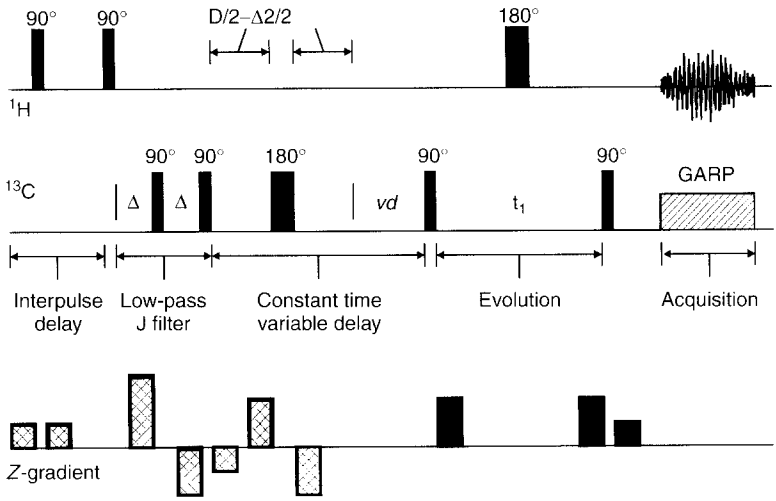

Fig. 17. CIGAR-HMBC (**C**onstant time **I**nverse-detected **G**radient **A**ccordion **R**escaled-**H**eteronuclear **M**ultiple **B**ond **C**orrelation) pulse sequence developed by Hadden and co-workers.[96] The experiment is a further modification of the IMPEACH-MBC pulse sequence shown in Fig. 14. Recognizing that F_1 skew can provide a valuable means of authenticating weak, long-range correlations if it is user controllable, the constant time variable delay was further modified to introduce a delay controlled by a parameter called J_{scale}. Rather than employing a constant time interval $(D + vd)$ as in the IMPEACH-MBC experiment, a new, incremented component to the delay, $\Delta 2$, is introduced in the form $(D/2 + \Delta 2/2) - 180^\circ\ ^{13}C - (D/2 + \Delta 2/2) - vd$. The segments of the interval represented by D and vd are incremented and decremented, respectively, in a fashion analogous to the IMPEACH-MBC experiment. The interval $\Delta 2$ is defined as $\Delta 2 = (J_{scale} - 1)t_1/2$. In this fashion, a user-controlled amount of skew can be introduced in F_1 by the selection of appropriate values for the parameter J_{scale}. When $J_{scale} = 0$, the value for $\Delta 2$ becomes negative and the sum of the intervals $D + vd$ is decremented during the course of the experiment by t_1^{max} making the entire experiment constant time and thereby offering the maximum possible resolution in F_1. When $J_{scale} = 1$, the results of the experiment are identical to an IMPEACH-MBC experiment. Finally, when $J_{scale} > 1$, F_1 skew is introduced to a progressively larger degree as the value of J_{scale} is increased.

of J_{scale} gets progressively larger, a greater degree of F_1 skew is introduced into the responses in F_1. However, unlike the ACCORD-HMBC experiment, the degree of F_1 skew is independent of ni and the accordion-optimization range and depends solely on the value selected for J_{scale}.

To illustrate the role of the parameter J_{scale} on introducing F_1 skew for response authentication, consider the multiplet shown in Fig. 18. Three panels are shown, in which J_{scale} is varied from 0 to 6 and then 24. As expected, in the case of $J_{scale} = 0$, there is no homonuclear modulation in F_1. As J_{scale} is increased to 6 and then 24, the degree of F_1 skew correspondingly increases. In practice, J_{scale} settings of approximately 15 have been found to work well with the CIGAR-HMBC experiment.

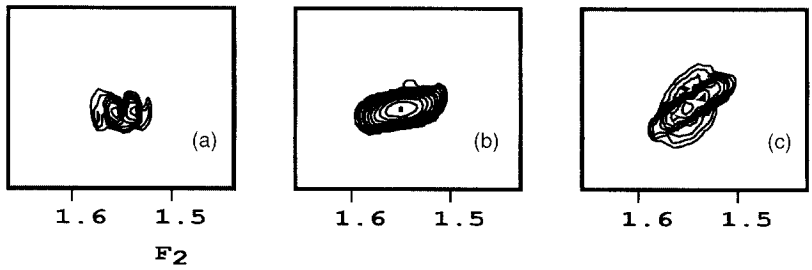

Fig. 18. H4/C3 $^{2}J_{CH}$ response in three CIGAR-HMBC spectra of 2-pentanone showing the effect of varying the parameter J_{scale}. The response shown in Panel (a) was acquired with $J_{scale} = 0$. As expected, no skew is observed in F_1. When J_{scale} is increased to 6, a modest degree of skew is introduced as shown in Panel (b). Finally, when $J_{scale} = 24$, a considerable degree of F_1 skew is introduced. In practice, we have found it useful in the author's laboratory to use $J_{scale} = 15$ to afford an adequate degree of F_1 skew for long-range response authentication.

At present, other than the initial report of the CIGAR-HMBC experiment by the author, the only other application reported in the literature is in the review of Reynolds and Enriquez.[97] These authors reported use of the CIGAR-HMBC experiment with $J_{scale} = 0$ to provide significantly improved resolution in heavily congested regions of the long-range correlation spectrum of kauradienoic acid relative to a conventional GHMBC experiment.

^{2}J,^{3}J-HMBC – a proton-detected 2D NMR method to differentiate ^{2}J from ^{3}J long-range correlations to protonated carbon or nitrogen

One of the inherent difficulties of interpreting and utilizing long-range heteronuclear shift correlation data, regardless of which experiment is used to acquire the data, is determining whether a particular correlation response is across two- or three-bonds. To a lesser extent, four-bond correlations are also possible, but these will generally only be observed with accordion-optimized long-range experiments when t_{max} is <4 Hz. Reynolds and co-workers[46] very creatively addressed this problem in their report on the development of the XCORFE pulse sequence, using a BIRD pulse to selectively manipulate specific components of magnetization while leaving others to evolve unaffected. This same principle is used in the ^{2}J,^{3}J-HMBC experiment developed by Krishnamurthy *et al.*[98]

In the original version of the ^{2}J,^{3}J-HMBC pulse sequence, which is shown in Fig. 19, the constant time variable delay was again extensively modified. Before considering the modification, which afforded a pulse sequence operator given the acronym STAR (Selectively Tailored Accordion F_1 Refocusing), it is appropriate to first consider a hypothetical chemical structure fragment, **15**, and the various long-range heteronuclear and homonuclear coupling constants which can operate in such a fragment. Active heteronuclear couplings include the $^{1}J_{CH}$ coupling to $^{13}C_1$; as well as $^{2}J_{CH}$ and $^{3}J_{CH}$ long-range couplings from the protons attached to $^{12}C_2$ and $^{12}C_3$, respectively to $^{13}C_1$. Homonuclear couplings in the hypothetical

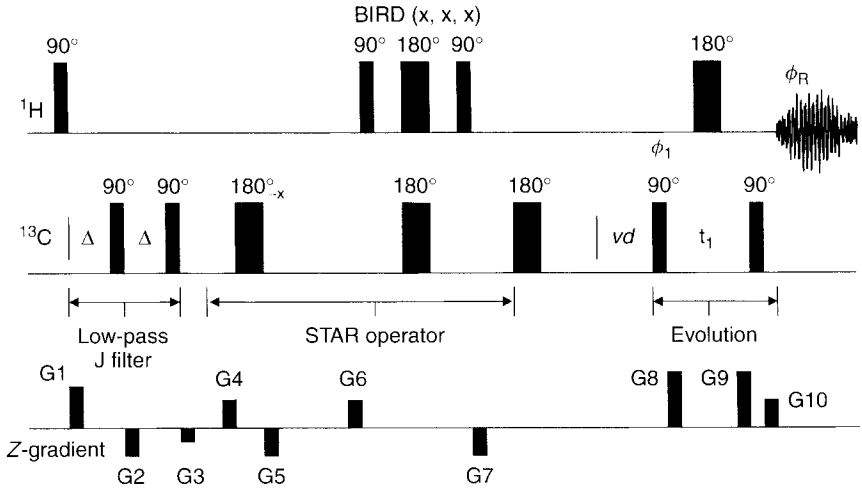

Fig. 19. Pulse sequence for the ^{2}J, ^{3}J-HMBC experiment described by Krishnamurthy *et al.*[98] This experiment represents the most refined version of the accordion-optimized experiments to be developed thus far and allows the differentiation of $^2J_{XH}$ from $^3J_{XH}$ long-range correlations to protonated heteroatoms (^{13}C and ^{15}N). The experiment further modifies the concept of the constant time variable delay used in the IMPEACH-MBC[71] and CIGAR-HMBC[96] experiments to even more selectively manipulate various components of magnetization. This is done using the pulse sequence operator given the acronym STAR (**S**electively **T**ailored **A**ccordion F_1 **R**efocusing) (see also Fig. 20). Differentiation of various components of heteronuclear long-range magnetization is accomplished within the STAR operator, with the balance of the pulse sequence similar to that of the IMPEACH-MBC and CIGAR-HMBC experiments.

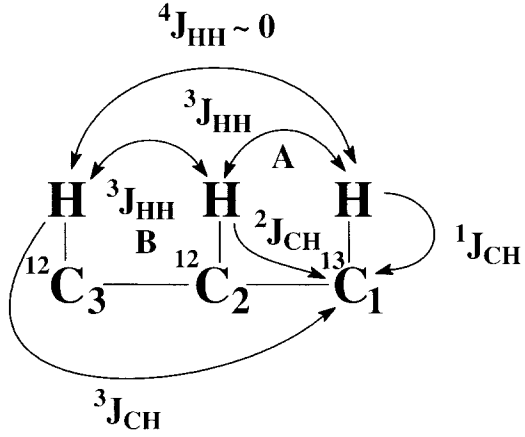

structure fragment include a pair of $^3J_{HH}$ couplings, labeled A and B, and a $^4J_{HH}$ coupling, which can be ignored since this coupling will likely be close to zero.

The STAR operator used in the $^2J,^3J$-HMBC sequence is shown in Fig. 20. The STAR operator utilizes four variable delays, D, which are incremented from zero in concert with the decrementation of vd, $\Delta 1$ and $\Delta 2$, the sum of which is held constant, and vd, which is decremented as a function of the accordion-optimization range selected in the usual fashion from T_{max} to T_{min}. Hence, the overall duration of the variable delay interval is constant. Within the STAR operator, the first variable delay, $\Delta 1$, is incremented from zero to $J_{scale} \times t_{1max}$ in steps of $J_{scale} \times t_1$, while conversely $\Delta 2$ is decremented from a starting value of $J_{scale} \times t_{1max}$ to zero in steps of $J_{scale} \times t_1$. Thus, while the sum of $\Delta 1 + \Delta 2$ is constant, each of the delays are variable and a function of the evolution time, t_1.

Referring to **15**, we next must consider the role of the pulses and delays within the STAR operator. Three scenarios are possible for individual components of magnetization passing through the STAR operator: (i) any coupling that evolves during one of the two delays, $\Delta 1$ or $\Delta 2$, but is refocused during the other will modulate the F_1 response by a factor of $J_{scale} \times J$; (ii) any coupling that evolves during both $\Delta 1$ and $\Delta 2$ will not have any effect on the F_1 response; (iii) any coupling that is refocused during both $\Delta 1$ and $\Delta 2$ will not have an affect on the F_1 response. The 180° X pulse located midway through the $\Delta 1$ delay refocuses all components of heteronuclear magnetization ($^nJ_{XH}$) but allows

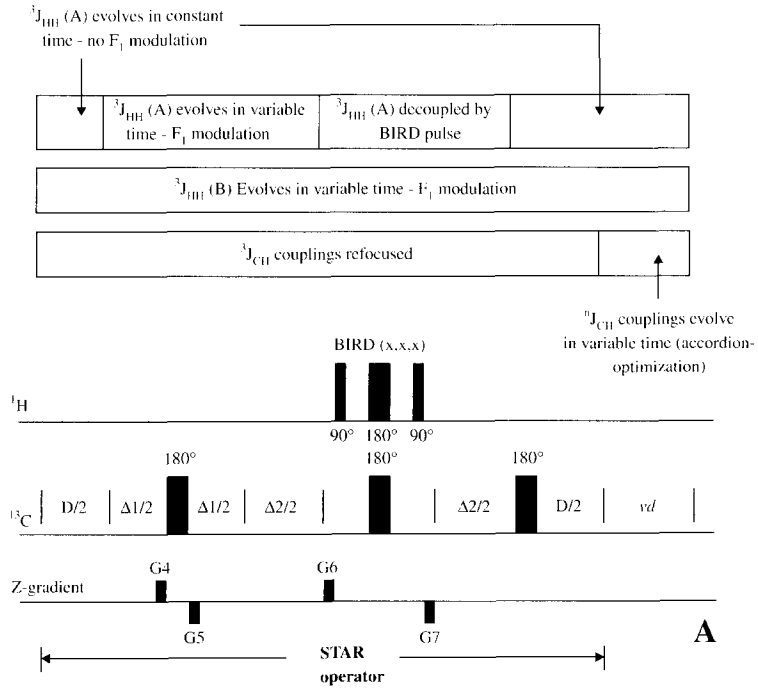

all homonuclear components of magnetization to continue to evolve ($^nJ_{HH}$). The BIRD pulse midway through the $\Delta 2$ interval behaves as a 180° pulse for X and the proton(s) directly attached to it (H–$^{13}C_1$), but as a 0° pulse for all other protons, including the '*active*' proton of a long-range XH spin pair. Hence, the BIRD pulse in the STAR operator is similar in function to the BIRD pulse located midway through $\Delta 2$ in the XCORFE pulse sequence developed by Reynolds and co-workers.[46] As a consequence of the action of the BIRD pulse, the $^1J_{C1H1}$ coupling is refocused during the $\Delta 2$. As a consequence of the action of the BIRD pulse, the $^3J_{HH}$ coupling labeled '*A*' in **15** evolves during $\Delta 1$ and is refocused during $\Delta 2$. This meets the condition (i) above, resulting in a modulation in F_1 of the $^2J_{C1H2}$ coupling by $J_{scale} \times J$. In contrast, since $^4J_{HH} \sim 0$ Hz, there is no net effect on the $^3J_{C1H3}$ long range coupling; this component of magnetization evolves through both the $\Delta 1$ and $\Delta 2$ intervals of the STAR operator.

Fig. 20. Schematic representation of the STAR operator as originally incorporated in the ^{2}J, ^{3}J-HMBC experiment.[98] Referring to the hypothetical structure fragment, **15**, the various components of the operator act on specific components of magnetization. There are four variable duration delays in the STAR operator. The first of these encountered during the execution of the pulse sequence operator is *D*. As in the IMPEACH-MBC and CIGAR-HMBC experiments, this delay is halved (*D*/2) with a 180° ^{13}C pulse centered in it. In the specific case of the STAR operator, however, the 180° ^{13}C pulse and the second half of the delay, *D*/2, immediately precede the final variable delay, *vd*, rather than following directly as in previous versions of the experiment. As the variable delay, *vd*, is decremented from T_{max} to T_{min} in steps of $t_1{}^{max}/ni$, which are the maximum duration of the evolution time and the number of increments of the evolution time, respectively, the *D*/2 intervals are incremented accordingly, keeping the sum $D + vd$ constant, again precluding homonuclear modulation during these intervals. The other two variable delay intervals, $\Delta 1$ and $\Delta 2$, provide differentiation of two-bond from three-bond long-range heteronuclear couplings to proton-bearing ^{13}C or ^{15}N resonances. To preclude homonuclear modulation during the STAR operator, the sum of the intervals $\Delta 1 + \Delta 2$ is constant; both delays are variable delays and have durations which are a function of the evolution time, t_1. Any heteronuclear coupling that: (i) evolves during $\Delta 1$ or $\Delta 2$ but is refocused during the other will modulate the F_1 response frequency by a factor of $J_{scale} \times {}^nJ_{XH}$; (ii) any heteronuclear coupling that evolves during both $\Delta 1$ and $\Delta 2$ will not have any effect on the F_1 response; (iii) any heteronuclear coupling that is refocused during both $\Delta 1$ and $\Delta 2$ will not have an effect on the F_1 response. The 180° X pulse located at $\Delta 1/2$ refocuses all components of heteronuclear magnetization ($^nJ_{XH}$, where $n = 1$ to 4) but allows all homonuclear magnetization components ($^nJ_{HH}$) to continue to evolve. The BIRD pulse midway through $\Delta 2$ behaves as a 180° pulse for X and the proton(s) directly attached to it (e.g. H–$^{13}C_1$ of **15**), but as a 0° pulse for all other protons, including the '*active*' proton of a long-range XH spin pair. Hence, the BIRD pulse in the STAR operator is similar in function to the BIRD pulse located midway through the $\Delta 2$ delay in the XCORFE pulse sequence developed by Reynolds and co-workers.[46] As a consequence of the action of the BIRD pulse, the $^3J_{HH}$ coupling labeled '*A*' in **15** evolves during $\Delta 1$ and is refocused during $\Delta 2$. This meets condition (i) described above, resulting in modulation of the F_1 response of the $^2J_{C1H2}$ as a function of $J_{scale} \times {}^nJ_{XH}$. In contrast, since $^4J_{HH} \approx 0$ Hz, there is no net effect on the $^3J_{C1H3}$ long-range coupling response; instead, this component of magnetization evolves through both $\Delta 1$ and $\Delta 2$.

The F_1 modulation of $^2J_{C1H2}$ by the STAR operator is manifest as shown schematically in Fig. 21. The extent of F_1 modulation is a function of the value of J_{scale} selected in performing the experiment. The $^3J_{C1H3}$ long-range correlation, in contrast, exhibits only the modulation or 'skew' in F_1 that is normally associated with the incrementation of the evolution period, t_1.

Using strychnine (**14**) as a model compound to demonstrate the concept of the $^2J,^3J$-HMBC experiment, Krishnamurthy and co-workers[98] published the spectrum shown in Fig. 22. These data were acquired using a 6 to 10 Hz accordion-optimization range and a $J_{scale} = 16$ setting. Responses in the aliphatic region of the spectrum enclosed in boxes are $^2J_{CH}$ correlation responses. The expansion shows the long-range correlations of the H11α resonance. The $^2J_{C12H11\alpha}$ response exhibits F_1 modulation analogous to that expected for the $^2J_{CH}$ correlation shown in Fig. 21. The $^3J_{C13H11\alpha}$, in contrast, exhibits only the expected modulation due to the incrementation of the evolution time, t_1.

To illustrate the choice of J_{scale} on the degree of F_1 modulation ($J_{scale} \times J$) observed in the $^2J,^3J$-HMBC spectrum, Krishnamurthy and co-workers[98] utilized 2-pentanone (Figure 23) the same model compound used by Reynolds and co-workers[46] in the 1985 report on the XCORFE experiment. The effect of varying the value of J_{scale} is shown in Fig. 23. The two $^3J_{CH}$ long-range correlations from the 1-methyl and 5-methyl groups to C3 are unaffected by varying J_{scale}. In contrast, as J_{scale} is varied from 0, where there is no F_1 modulation of the $^2J_{C3H4}$ correlation to successively larger values (6, 12, 18, and 24) the degree of F_1 modulation of the $^2J_{C3H4}$ progressively increases. In general, we have found that usable results are obtained with settings of J_{scale} at about 15.

There have been no reported applications of the $^2J,^3J$-HMBC experiment published to date. There has, however, been one report of a COSY-type artefact observed in $^2J,^3J$-HMBC spectra of a cyclopentafurnanone.[99] The COSY-type responses observed are displaced in F_1 as a function of the choice of J_{scale}. Removing the bipolar gradients flanking the BIRD pulse in the $\Delta 2$ interval of the STAR operator and superimposing a CYCLOPS phase cycle on the BIRD pulse completely suppresses the COSY-type response artefacts associated with the $^2J,^3J$-HMBC experiment.[100]

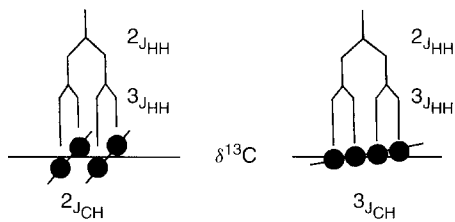

Fig. 21. Schematic representation of the differentiation of $^2J_{CH}$ from $^3J_{CH}$ long-range correlation responses in the $^2J,^3J$-HMBC experiment as a function of the operation of the STAR operator shown in Fig. 20.

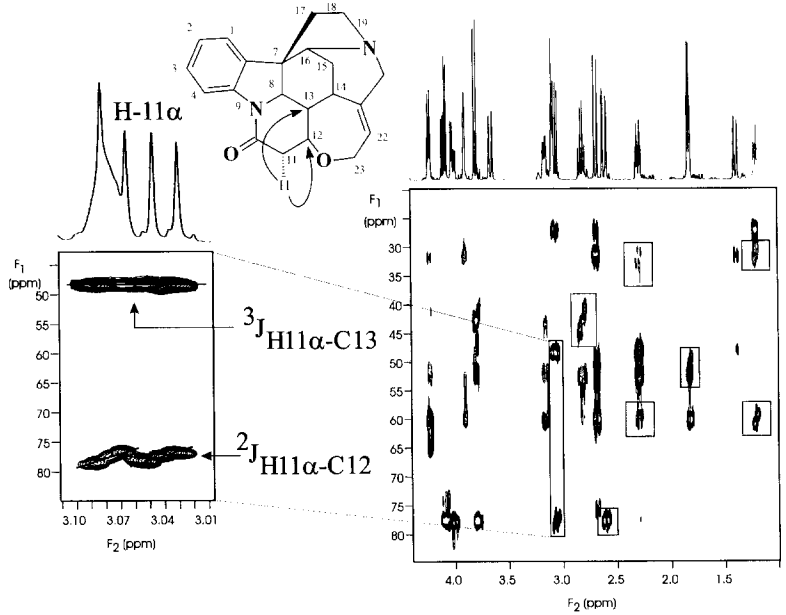

Fig. 22. Aliphatic region of the 6 to 10 Hz optimized ^{2}J, ^{3}J-HMBC spectrum of strychnine, **14**, with $J_{scale} = 16$. Responses in the aliphatic region enclosed in boxes are $^2J_{CH}$ long-range correlation responses. The two- and three-bond long-range correlations of the H11α resonance to C12 and C13 via two- and three-bonds, respectively, is shown in the expansion to the left. As expected, the $^2J_{CH}$ correlation to C12 is modulated in F_1 as a function of the STAR operator, while the $^3J_{CH}$ correlation to the C13 is unaffected by the operation of the STAR operator.

3.3.6. BIRD-HMBC

Another new entry into the repertoire of long-range heteronuclear shift correlation experiments is the BIRD-HMBC experiment recently described by Berger *et al.*[101] Noting the inherent drawbacks of refocused variants of the long-range heteronuclear shift correlation experiments, specifically the degree of $^1J_{CH}$ residual response suppression when a dual-stage gradient low-pass J-filter is employed, the authors set about the development of a variant that could provide improved suppression of direct correlation responses. The BIRD-HMBC pulse sequence shown in Fig. 24 replaces the traditionally employed low-pass J-filter by a BIRDy pulse. Both the direct ($^1J_{CH}$) and long-range ($^nJ_{CH}$) components of magnetization pass through the BIRDy pulse and are recorded. The former are subtracted on successive scans; the desired long-range correlations are additive on all scans. The authors compared the BIRD-HMBC experiment with pulse sequences employing single and two-step low-pass J-filters as both non-refocused (those not allowing decoupling) and refocused variants of

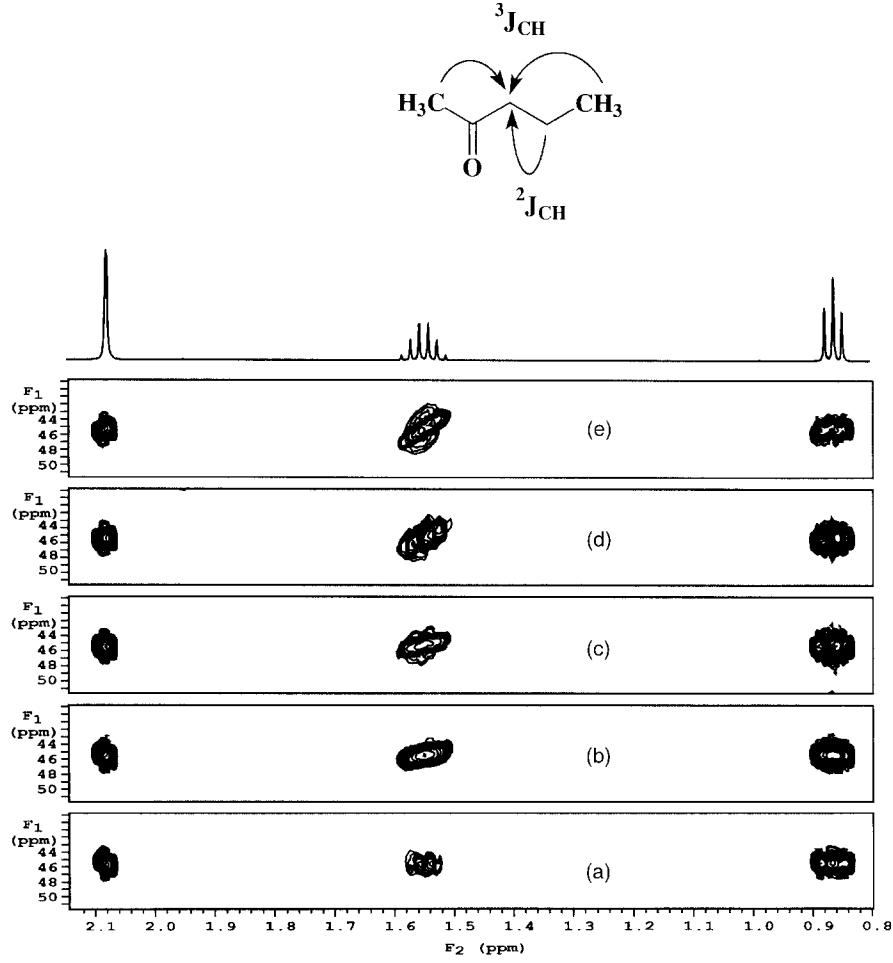

Fig. 23. Panels from a series of ^{2}J, ^{3}J-HMBC spectra in which the parameter J_{scale} was varied using 2-pentanone as a model compound, which Reynolds and co-workers[46] used in their original report of the XCORFE experiment. As the value of J_{scale} is varied from 0 in Panel (a) to successively larger values of 6, 12, 18, and 24, in Panels (b) through (e), respectively, the F_1 skew of the $^2J_{C3H4}$ correlation progressively increases while the $^3J_{CH}$ correlations from the 1- and 5-methyl proton resonances are unaffected.

the conventional HMBC and ACCORD-HMBC experiments. Using the BIRD-HMBC experiment the authors were able to demonstrate response intensity and lineshape comparable to HMBC data without refocusing, and lineshape and response intensities that were superior to those that could be recorded using the ACCORD-HMBC experiment. When the BIRD-HMBC experiment was performed in a refocused format using single- and two-stage low-pass J-filters, the lineshape was maintained but with a 15–20% reduction of signal intensity

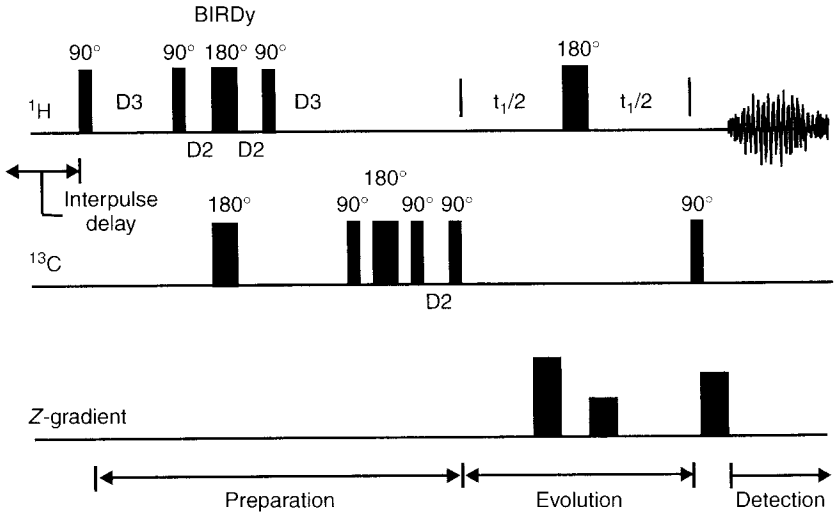

Fig. 24. Pulse sequence for the BIRD-HMBC experiment recently reported by Berger *et al.*[101] The experiment is intended to provide an improvement in the suppression of the unwanted direct ($^1J_{CH}$) correlation responses relative to what can be obtained by the conventional HMBC/GHMBC experiments using a low-pass J-filter or the gradient, dual-stage low-pass J-filter employed in the accordion-optimized long-range experiments. Both the direct ($^1J_{CH}$) and long-range ($^nJ_{CH}$) components of magnetization pass through the BIRDy pulse but are phase manipulated in the process. The former are subtracted on successive scans while the latter are coherently added. The authors demonstrated lineshape and response intensities comparable to those of the GHMBC experiment using strychnine, **14**, as a model system while the results from an ACCORD-HMBC experiment afforded poorer lineshape and sensitivity in both non-refocused and refocused experiments, the latter with broadband heteronuclear decoupling during acquisition.

relative to the non-refocused variants of the experiment. The authors concluded their report by suggesting that incorporation of variable (accordion) delays into the BIRD-HMBC sequence should be possible but they did not show examples of the results from this type of experiment. To date there have been no reported applications of the BIRD-HMBC experiment in the literature.

3.3.7. Broadband HMBC

Nearly simultaneously with the report of the BIRD-HMBC experiment, Meissner and Sørensen[102] described another modification of the basic long-range heteronuclear shift correlation experiment that they refer to as 'broadband' HMBC. The authors employ the gradient dual-stage low-pass J-filter used in the accordion-optimized experiments described above (Section 3.3.5) followed by a delay, Δ, which replaces the accordion-optimized delay or a 'normal' fixed delay for the evolution of long-range heteronuclear components of magnetization. Instead, Meissner and Sørensen acquire a series of several experiments with different

optima for Δ. Broadband 'excitation' is obtained by co-adding the data from the series of experiments performed. The authors recommend a starting delay Δ^{max} where

$$\Delta^{max} = [1/\pi^{n}J_{CH}]\tan^{-1}[J_{CH}/\Delta\upsilon_{1/2}] \quad (12)$$

where $\upsilon_{1/2}$ is the proton linewidth at half-height, followed by values that '...step downwards to about half this value...' Following completion of the evolution period, t_1, the authors insert a 180° X pulse flanked by gradients in the ratio +5, −3 or −3, +5, with appropriate gradient recovery delays as shown in Fig. 25.

The authors compared data from a 65 ms HMBC experiment with a broadband HMBC experiment performed by co-adding four Δ values of 440.7, 343.4, 290.3, and 242.2 ms. The authors state that when combined, these four Δ values provide uniform excitation of long-range couplings up to ~20 Hz, which is achieved by larger couplings being in-phase when magnetization is converted back to observable single quantum coherence following the various long delays. The authors also comment that in practical application, the broadband HMBC experiment

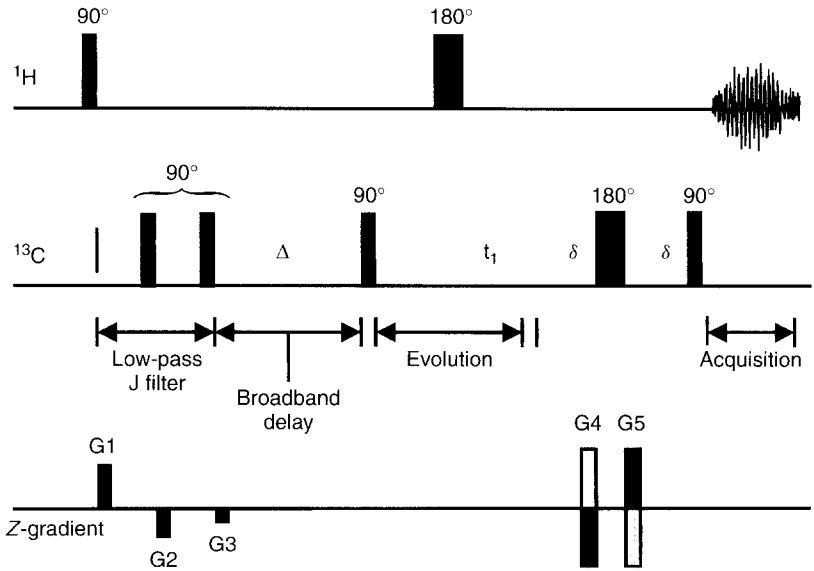

Fig. 25. Pulse sequence for the broadband HMBC experiment proposed by Meissner and Sørensen.[102] A series of experiments are acquired in which the delay, Δ, is varied and used in lieu of an accordion-optimized delay. This series of experiments is in some senses analogous to the processed result of the 3D-HMBC experiment proposed by Furihata and Seto.[73] The authors used a series of four Δ values of 440.7, 343.4, 290.3, and 242.2 ms and claim uniform excitation to ~20 Hz. The authors also comment that the application of broadband HMBC requires higher numbers of transients/t_1 increment than conventional HMBC or accordion-optimized experiments, which is not surprising given the likelihood of considerable losses of magnetization due to relaxation processes during the very long Δ delays that are employed to achieve 'broadband' excitation in this approach.

requires a higher number of acquisitions/t_1 increment than conventional HMBC or accordion-optimized long-range experiments. In the opinion of this author, the long Δ delays in the range of 242 to 440 ms will have associated with them considerable losses of signal intensity due to relaxation processes. Indeed, in the experience of the author, optimization of accordion-optimized delays for long-range couplings smaller than 4 Hz (125 ms) has associated with it a significant penalty in the form of losses of sensitivity. Again, to date, there have been no applications of the broadband HMBC experiment reported in the literature.

3.4. Simultaneous direct and long-range heteronuclear shift correlation

Since the introduction of the HMBC experiment by Bax and Summers in 1986,[47] spectroscopists have generally been 'programmed' to think of these experiments in the sense of the residual direct correlation responses being an undesired and complicating nuisance to the interpretation of the desired long-range correlation responses. To this end, ever more sophisticated filters have been designed for the elimination of direct correlation responses. Recently, however, several groups have addressed the issue of direct correlation responses in long-range heteronuclear shift correlation spectra from the opposite standpoint. That is, they have explored the question of recording both direct ($^1J_{CH}$) and long-range ($^nJ_{CH}$) correlation responses in such a way as to allow them to be separated during data processing. This has led to the description of first the MBOB (Multiple Bond–One Bond, see Section 3.4.1) experiment by Meissner and Sørensen[102] in the same report as the broadband HMBC technique. More recently, Berger *et al.*[103] have described an experiment to which they've given the acronym HMSC (Heteronuclear Multiple-bond and Single-bond Coupling connectivities, see Section 3.4.2). The extent to which these experiments will enjoy application remains to be determined, but the idea is, none-the-less, an interesting potential way to economize on spectrometer time.

3.4.1. MBOB – Multiple-Bond One-Bond heteronuclear shift correlation

The HMBC experiment, in principle, uses a series of phase shifts to alternately add and subtract the signals for the direct correlation responses from the data matrix. If, instead of adding and subtracting in memory, two separate data sets are stored, they can be added or subtracted during processing. It was in this fashion that Meissner and Sørensen[102] developed the approach of the MBOB (Multiple-Bond One-Bond) simultaneous direct and long-range heteronuclear shift correlation experiments. By adding the two data sets, Meissner and Sørensen took advantage of the low-pass J-filter function typically employed in HMBC experiments, obtaining a long-range correlation spectrum in the usual fashion. By subtracting the two data sets, the direct correlation experiment was obtained, the individual correlation responses appearing as multiplets in F_2 since no broadband heteronuclear decoupling was applied during the acquisition period, t_2.

As noted by the authors in their discussion of this approach, there exists the possibility of accidental cancellation of long-range correlation responses under some conditions when the long-range response and the ^{13}C coupled direct correlation response multiplet overlap in F_2. The authors go on to note, however, that by using the broadband excitation approach (see Section 3.3.6) that this problem can be circumvented. Again, there hasn't been any reported application of this technique in the literature.

3.4.2. HMSC – Heteronuclear Multiple-bond and Single-bond Coupling connectivities

In a report that appeared in 2001, Berger *et al.*[103] described an experiment to which they gave the acronym HMSC (Heteronuclear Multiple-bond and Single-bond Coupling connectivities), commenting in the introduction to their report that they were unaware of any report of an experiment for the simultaneous detection of direct and long-range heteronuclear shift correlation data, probably due to the publication of the report of Meissner and Sørensen only approximately a month prior to that of the HMSC experiment.

The HMSC pulse sequence bears considerable resemblance to the BIRD-HMBC experiment (see Section 3.3.6). The HMSC pulse sequence begins with a 90°_x proton pulse followed by a delay, D3, and then a BIRDy pulse in which the 180° ^{13}C pulse is replaced by a $90^\circ_x - 180^\circ_y - 90^\circ_x$ composite pulse. The BIRDy pulse is centered in at the midpoint of the long-range delay, where D3 is optimized as a function of $\frac{1}{4}(^nJ_{CH})$. The coherence of the $^nJ_{CH}$ coupled protons is labeled selectively with a ^{13}C pulse adjusted to either 180° or 0° using x,y,x or $x,-x,x$ composite 180° pulses, respectively. In contrast, in-phase $^1J_{CH}$ coherence evolves under the influence of the direct or one-bond coupling and proton chemical shift into antiphase coherence in the subsequent D2 delay, where $D2 = \frac{1}{2}(^1J_{CH})$. There is essentially no further evolution of $^nJ_{CH}$ coherence during D2 because of its short duration, which is optimized as a function of the large, one-bond heteronuclear coupling constant. The next 90° ^{13}C pulse transforms $^nJ_{CH}$ and $^1J_{CH}$ antiphase components into multiple quantum coherence that evolves in the usual fashion during the evolution time, t_1, followed by reconversion to the corresponding single quantum coherences.

To exploit the acquisition of both $^1J_{CH}$ and $^nJ_{CH}$ coherences, for each increment of the evolution time, t_1, two FIDs with phase φ_2 (y or $-x$, respectively) are acquired and stored in separate locations. In the first phase of data processing, each separately stored set of t_1 data is processed separately. To disentangle the $^1J_{CH}$ and $^nJ_{CH}$ responses, the individually processed data are added and subtracted from each other to recover the individual spectra. Obviously, since broadband decoupling is not applied during the pulse sequence, the $^1J_{CH}$ spectrum will be fully coupled as was the data from the MBOB experiment (see Section 3.4.1). If X-decoupled direct correlation data are desired, the authors[103] note that a refocused variant of the experiment can be employed

as in the case of the D-HMBC (see Section 3.3.1) or accordion-optimized (see Section 3.3.5) experiments. However, as would be expected with refocused experiments, there will be signal losses due to relaxation during the second potentially long refocusing delay.

Bigler and co-workers[103] illustrated the application of the HMSC experiment using strychnine (**14**) as a model compound. Excellent discrimination in the processed data was obtained between the direct and long-range correlation responses. Results obtained with the HMSC experiment were compared to conventional HMBC and statically-optimized ACCORD-HMBC data. The sensitivity and lineshape were comparable to the HMBC data and superior to the statically-optimized ACCORD-HMBC data due to the evolution of antiphase coherence into in-phase coherence prior to detection, resulting in FIDs that are not optimal for magnitude calculated presentation. This observation is analogous to that made with the BIRD-HMBC data above (see Section 3.3.6).

4. QUANTITATIVE MEASUREMENT AND USE OF LONG-RANGE HETERONUCLEAR COUPLINGS

Long-range heteronuclear couplings, $^{n}J_{XH}$ where $n = 2$, 3 and X is typically ^{13}C or ^{15}N, can be used to establish molecular conformation in much the same manner as $^{3}J_{HH}$ homonuclear couplings. Unfortunately, long-range heteronuclear couplings are experimentally much less accessible than their homonuclear counterparts. Despite the inherent difficulties in measuring long-range heteronuclear couplings, (i) due to the low natural abundance of the heteronuclides of interest, typically ^{13}C and ^{15}N, which have relative abundance of 1.1 and 0.37%, respectively, and (ii) due to the fact that $^{n}J_{XH}$ are comparable in magnitude to $^{3}J_{HH}$ couplings, there has still been considerable interest in the development of new experiments to facilitate their measurement. The key experiments used for the measurement are very briefly surveyed in this section; a more extensive survey is the excellent recent comparative review of Márquez *et al.*[104] Their review is especially valuable in that it compares the results that can be obtained with the various experiments now available using a sample of strychnine, **14**, as a model compound.

4.1. Methods for the determination of long-range heteronuclear couplings

One of the earliest efforts to measure and utilize long-range heteronuclear coupling constants is found in the work of Bermel *et al.*[51] The first example of an experiment specifically designed for the measurement of long-range heteronuclear couplings is found in the description of the development of the hetero (ω_1) half-filtered HETLOC experiment by Kessler and co-workers.[105] An updated version of the ω_1 half-filtered HETLOC experiment has been developed by Kövér

et al.[106,107] A quantitative heteronuclear J-correlation method was also described during 1994 by Zhu *et al.*[108] that employs the estimation of heteronuclear coupling constants from the normal, magnitude-mode processed HMBC data. This method has been further refined by Murata and co-workers.[109] One-dimensional inverse-[110] and selective inverse-detected long-range J-resolved[111] methods were reported in 1994 and 1995, respectively. Willker and Leibritz[112] also reported a variant of the standard HMBC experiment in 1995 that has had several applications. Rather than a simple long-range delay, their J-HMBC experiment instead uses a pulse sequence element identical to the components of the constant time variable delay (8) employed by the author and coworkers[96] in the IMPEACH-MBC experiment (see p. 68). More detail on this experiment is presented in Section 4.2.2. below.

Koźmiński and Nanz[113] reported the development of the HECADE experiment that allowed the determination of heteronuclear coupling constants from E-COSY-type crosspeaks. A sensitivity improved HSQC-HECADE pulse sequence has since been developed by the same authors.[114] The HSQC-based GSQMBC experiment reported in 1997 by Sklenář and coworkers,[115] and discussed in Section 3.3.3, has also been used for the measurement of small, long-range heteronuclear coupling constants.

In 1999, Furihata and Seto[115] described a pair of J-resolved HMBC pulse sequences given the acronyms J-resolved HMBC-1 and J-resolved HMBC-2. There have been a number of applications of the latter which are briefly surveyed in the following section. These methods circumvent the need to extract the size of the long-range heteronuclear coupling constant by mathematical analysis. Instead, the size of the coupling constant is scaled to allow convenient, direct measurement in F_1. Later in 1999, Koźmiński[116] described a simple, multiplet pattern HSQC-TOCSY experiment for the measurement of long-range heteronuclear coupling constants.

Further increases in research effort in this area of NMR was also seen during 2000. Williamson and co-workers[117] reported the development of gradient-selected one- and two-dimensional HSQMBC experiments that have been applied by the same group of authors in the characterization of several complex marine natural products. Additional applications of the HSQMBC experiment have also begun to appear. These applications are also briefly surveyed in the following section. Ding[118] reported the direct measurement of long-range heteronuclear coupling constants from phase-sensitive HMBC data. Previous reports of the measurement of long-range $^{1}H-^{15}N$ coupling constants from phase-sensitive HMBC data have appeared[119,120] as well as the psHMBC method proposed by Sheng and van Halbeek[121] which has not been applied to structural problems since the initial report. Gotfredsen and co-workers[122] reported the development of an accordion-based method for the measurement of long-range $^{1}H-^{31}P$ heteronuclear couplings in nucleic acids. Seki and co-workers[123] described a modified version of the HMBC experiment designed to suppress proton homonuclear J-modulation in both selective 1D and non-selective 2D pulse sequences. Their modification

uses a constant time approach and a successively relocated 180° X pulse in a constant time delay that is very similar to the J-HMBC method of Willker and Leibfritz[112] and the IMPEACH-MBC experiment (see p. 68) described by the author and colleagues.[71] Finally, Xia *et al.*[124] described the J-multiplied HMQC (MJ-HMQC) experiment for the measurement of $^{3}J_{NHH\alpha}$ coupling constants in ^{15}N-labeled proteins. While this method has yet to be applied, it does have the potential for application to small molecules as well.

In 2001, Meissner and Sørensen[126] described methods for the measurement of J_{HH} and $^{n}J_{CH}$ couplings employing the broadband excitation approach (see Section 3.3.7) with the report of the broadband XLOC and broadband J-HMBC experiments, respectively. In a further extension of the idea of accordion optimization, Williamson *et al.*[127] reported the development of the J-IMPEACH-MBC pulse sequence. This approach is similar to the EXSIDE experiment previously described by Krishnamurthy[93] and the J-resolved HMBC experiments of Furihata and Seto[115] in its use of J-scaling to render small, long-range heteronuclear couplings conveniently measurable. Finally, Williamson *et al.*[104] also described a new method, G-BIRD$_R$-HSQMBC, that was reported in their survey of the available methods.

4.2. Applications of quantitatively determined long-range heteronuclear couplings to chemical structure problems

As noted in the introduction to this section, Márquez *et al.*[104] have recently published a comprehensive, comparative review of the methods now available for the measurement of long-range heteronuclear couplings as well as a comparative evaluation of the various methods. Their review compliments the earlier review by Tvaroska and Taravel[128] on the use of carbon–proton coupling constants in the conformational analysis of carbohydrates. Consequently, no effort will be made here to exhaustively review this area of the literature. It is sufficiently noteworthy, however, to provide the interested reader with a brief survey of some of the pertinent applications of these methods, which are attracting increasing attention.

Matsumori *et al.*[129] described what they referred to as a 'J-based conformation analysis method' of establishing relative stereochemistry using a combination of $^{3}J_{HH}$ and $^{n}J_{CH}$ coupling constants. This approach has essentially been utilized in a number of following applications.

4.2.1. Conformational analysis using HETLOC and phase-sensitive HMBC

Early reports of NMR-based configuration analysis relied on a combination of the HETLOC[105–107] and phase-sensitive HMBC[108] methods that were then available in conjunction with $^{3}J_{HH}$ homonuclear coupling constant data. Quite simply, HETLOC can be employed to establish the relative stereochemistry of

two chiral centers when they are separated by contiguous chiral methine or resolvable diastereotopic methylenes. Whenever there is an intervening heteroatom or quaternary carbon center, the relative value of the $^{n}J_{CH}$ coupling can be calculated on the basis of the intensity of the cross-peak in a phase-sensitive HMBC spectrum.[108]

When an alpha carbon bears an electronegative substituent such as an oxygen or halogen atom (e.g., $^{1}H-^{12}C-^{13}C-X$, where X = O, Cl, etc.), there is a clear relationship of the size of the $^{2}J_{CH}$ coupling and the dihedral angle between the proton and the heteroatom. Recognizing this, Matsumori *et al.*[130] applied a combination of HETLOC and phase-sensitive HMBC methods to establish the structure of acyclic portions of the marine toxin okadaic acid (**16**).

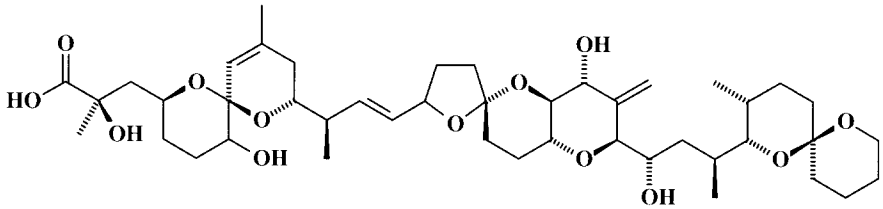

16

At the time Murata's study was reported, the solution structure of acyclic portions of the okadaic acid structure were not known despite extensive NOE measurements coupled with distance geometry calculations.[131] Using $^{3}J_{HH}$ coupling constants measured from E. COSY data and $^{n}J_{CH}$ ($n = 2, 3$), determined predominantly from HETLOC spectra for the contiguous protonated carbon portions of the molecule and phase-sensitive HMBC data for segments containing quaternary carbons, Murata and co-workers[130] were able to successfully establish the solution structure of okadaic acid.

Maitotoxin, one of the toxins responsible for ciguatera poisoning, is the largest known non-biopolymer (MW 3422). Elucidating the structure of this complex molecule has attracted very considerable attention from natural products chemists and synthetic chemists alike. Following the establishment of the 'planar' structure of this unique toxin,[132,133] in a series of communications Murata and co-workers[134,135] were able to establish the configuration of the C1–C14 and C135–C142 side-chains of the molecule. A combination of $^{n}J_{CH}$ couplings measured using HETLOC,[105–107] phase-sensitive HMBC,[108] and $^{3}J_{HH}$ coupling constants were used in the configuration analysis. While such problems have occasionally been approached by synthetic trial and error methods for simpler compounds, the importance of the availability of methods based on long-range heteronuclear coupling constants becomes glaringly apparent with a problem such as that presented by the C1–C14 side-chain of maitotoxin. There are seven asymmetric centers in this 14 carbon segment, and hence the number of possible stereoisomers is 128 making any consideration of a synthetic approach impossible until the configuration has been defined by either NMR or X-ray methods.

The structure determination of the neuroexcitotoxin dysiherbaine (**17**)[137] is another example of the usage of HETLOC[105–107] data to establish molecular configuration. The authors used $^{3}J_{HH}$ coupling data and NOE measurements to establish the relative stereochemistry within the tetrahydropyran ring. Extending these data, the configuration at the 4-position was next assigned. Finally $^{n}J_{CH}$ coupling constants using HETLOC data allowed the relative stereochemistry at C2 to be established via conformation analysis at the C3–C4 and C2–C3 bonds.

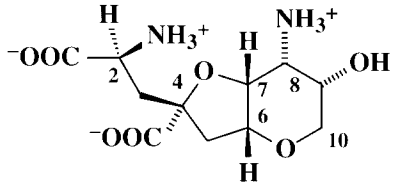

17

Following their report describing in detail the J-based configuration analysis method,[129] Murata and co-workers[138] next applied the method to the completely flexible molecule amphidinol 3 (**3**). Once again, $^{3}J_{HH}$ couplings were measured from E. COSY data, $^{n}J_{CH}$ long-range couplings in the contiguous protonated regions of the molecule were determined from HETLOC[105–107] experiments and phase-sensitive HMBC data[108] were used where there were intervening quaternary carbons.

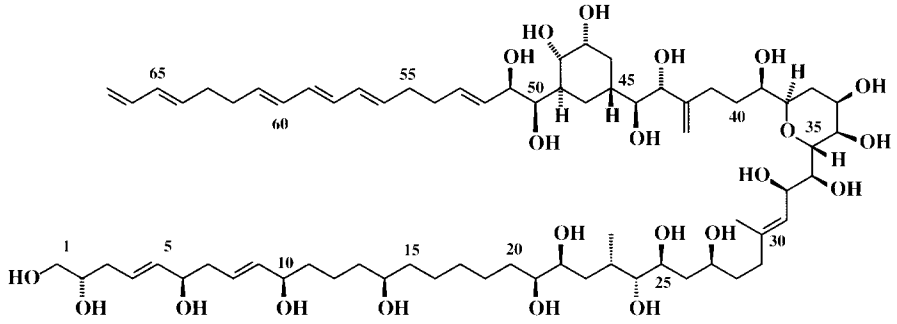

18

Continuing from their 1997 work on the glycoside strictosidine (**19**), which used slices from a phase-sensitive HSQC experiment as a source of long-range heteronuclear coupling constants,[139] Szabó and co-workers[140] reported using an improved version of the HETLOC experiment to measure long-range heteronuclear couplings in another study of strictosidine and other vincoside derivatives.

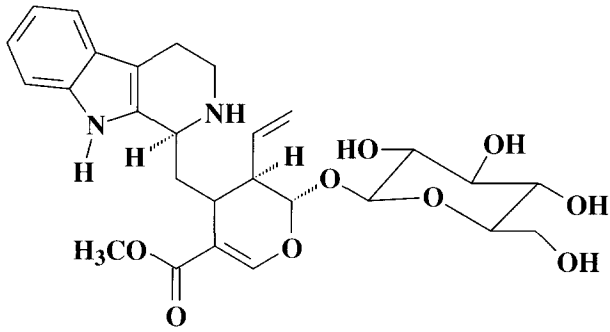

19

4.2.2. Measurement of long-range heteronuclear coupling constants using J-HMBC

As noted in the introduction to the previous section, phase-sensitive HMBC data can be used to measure long-range heteronuclear coupling constants.[108,141] There have been several recent reports that have employed the rather time-consuming J-HMBC process rather than using one of the more efficient experiments which employs J-scaling that are described below. As noted above, the J-HMBC experiment uses a long-range sampling delay containing components identical to those used in the IMPEACH-MBC[71] experiment as shown by (8) (see also p. 68). Rather than decrementing the variable delay interval, *vd*, in a single experiment, the J-HMBC experiment instead requires the acquisition of a series of experiments, typically ten or more, in which the total time for sampling long-range heteronuclear couplings is held constant to prevent proton modulations. The duration of the D/2-180° ^{13}C-D/2 interval is incremented or decremented in concert with the decrementation or incrementation, respectively, of the variable delay period. Long-range heteronuclear couplings are then determined by fitting peak intensity to an amplitude curve modulated by the relationship $\sin(\pi^{n}J_{XH})$.

Takayama *et al.*[142] utilized J-HMBC data in the determination of the conformation of several pyrrolidine alkaloids, pandamarilactonine-A and -B (**20A** and **B**, respectively). Specifically, long-range heteronuclear coupling constants were used in conjunction with NOE measurements to assign the stereochemistry and conformation of the pyrrolidine-γ-lactone linkage. The authors performed a total of 15 experiments varying the evolution time from 10 to 290 ms in 20 ms steps. Response amplitudes were fitted using a least squares analysis to extract the long-range heteronuclear coupling constants.

Nagatsu and co-workers[143] reported using a J-HMBC experiment in the determination of the long-range heteronuclear coupling constants for monensin sodium (**21**). A series of 10 experiments were performed, varying the optimization of the long-range delay from 20 to 200 ms in 20 ms steps. Again, peak intensities

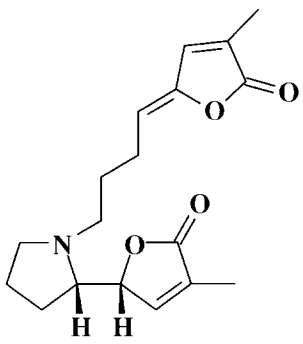

20A

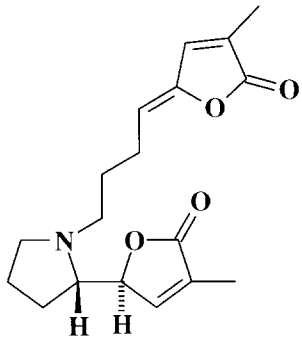

20B

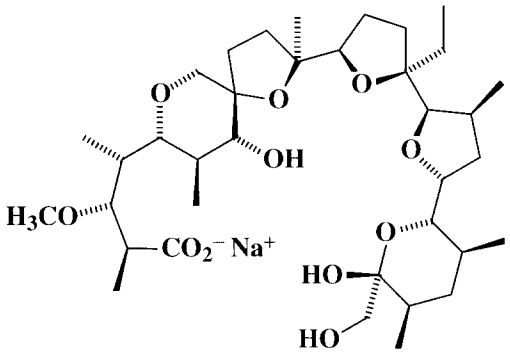

21

were fitted using a least squares analysis to extract the size of the long-range heteronuclear couplings.

Tokunaga, and co-workers[125] reported using the J-HMBC experiment to measure the long-range two- and three-bond $^{1}H-^{15}N$ couplings in a series of substituted pyridines. Seki *et al.*[123] subsequently reported using selective one- and two-dimensional versions of the J-HMBC pulse sequence to measure the long-range $^{1}H-^{13}C$ and $^{1}H-^{15}N$ heteronuclear couplings of the simple β-carboline alkaloid harman (**22**).

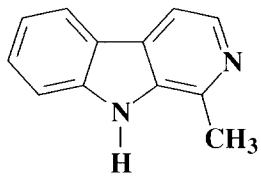

22

4.2.3. Conformational analysis using EXSIDE

The EXSIDE experiment developed by Krishnamurthy[93] uses the idea of J-scaling to 'scale-up' small long-range couplings in the second frequency domain to render them more readily measured without the imposition of high digital resolution requirements in F_1. As noted in the introduction, long-range heteronuclear coupling constants have seen frequent usage in the conformational analysis of oligosaccharides.[128] Rundlöf and co-workers[144] reported using the EXSIDE experiment to determine $^{n}J_{CH}$ couplings in a series of oligosaccharides.

4.2.4. Measurement of $^{n}J_{CH}$ couplings using a 3D J-resolved HMBC experiment

Using the fundamental concept of the 3D-HMBC experiment proposed in 1996 by Furihata and Seto,[73] Martins *et al.*[145] reported a study of the conformation of erythromycin A (**23**) in benzene in 1999. The experiment was employed in the measurement of 26 $^{3}J_{CH}$ correlations needed for the conformational analysis of the molecule in solution. To obtain the data necessary for the determination of the long-range coupling constants, the authors reported acquiring a total of 16 experiments in which the duration of the long-range coupling delay was varied from 0 to 500 ms in successive planes of the data matrix. A three-dimensional Fourier transform of the data matrix was not performed. Coupling constants were determined using an analysis similar to that employed with the J-resolved HMBC experiment (see Section 4.2.5 for further discussion).

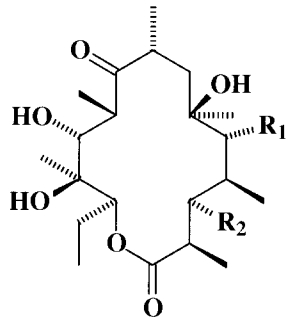

23

R_1 = desosamine

R_2 = cladinose

4.2.5. Measurement of small $^{n}J_{XH}$ couplings using GSQMBC

The GSQMBC experiment developed in 1997 by Sklenář and co-workers[75] (see Section 3.3.3) has also been used for the measurement of small coupling constants from the anti-phase component of the multiplet structure. These applications

are discussed above in conjunction with the discussion of the experiment itself. Unfortunately, however, there is a problem with dispersive lineshape components which precludes the application of this experiment in the extraction of small long-range heteronuclear coupling constants from complex multiplets.

4.2.6. Conformational analysis using J-resolved HMBC

Furihata and Seto[115] reported the development of the J-resolved HMBC-1 and -2 experiments in 1999. These experiments also use the idea of J-scaling, employing either a 180° pulse 'sandwich' alone, flanked by $nt_1/2$ delays where n is a scaling factor typically set in the range of 20 or 30, or in conjunction with a $\Delta_2 - mt_1/2180° \ ^1H - \Delta_2 - mt_1/2$ operator to 'decouple' proton J-modulation by allowing proton magnetization to evolve in constant time.

The solution conformation of two new clerodane-type diterpenes, dytesinin A and B (**24**) was reported by Shimbo *et al.*[146] Long-range heteronuclear couplings were determined using the J-resolved HMBC-2 experiment[115] following structural characterization using conventional 2D NMR methods. The J-scaling factors n and m (see Section 4.2.5) were set to 30 and 31, respectively. The nt_1^{max} delay was 333 ms; the acquisition of the data required over-weekend accumulation for a samples 5.5 mg sample of dytesinin A. Long-range couplings from the H6α proton to C8, C10, and C18 were used in establishing the relative stereochemistry of dytesinin A.

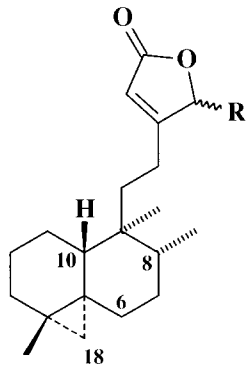

24

A R = OH
B R = H

4.2.7. Applications of the HSQMBC experiment

Since being reported in 2000, the HSQMBC experiment has been applied to a number of complex structural analyses.[117] The authors initial demonstration of the technique employed sucrose, strychnine (**14**) and the complex marine natural

product phormidolide. The HSQMBC experiment is based on the evolution of heteronuclear single quantum coherence as in the HSQC[17] and GSQMBC[75] experiments. HSQMBC was also designed to facilitate the direct extraction of the desired long-range heteronuclear coupling constants without the necessity of curve fitting routines or the acquisition of reference spectra.

Later in 2000, Williamson and co-workers reported the use of the HSQMBC experiment to determine long-range heteronuclear coupling constants that were used in the structural characterization of two new malyngamides.[147] Long-range heteronuclear couplings shown on the structure were used to assign the *Z* stereochemistry of the chlorinated double bond of malyngamide R (**25**), which differs from that of other known members of this class of compounds such as malyngamide F (**26**) and malyngamide I (**27**).

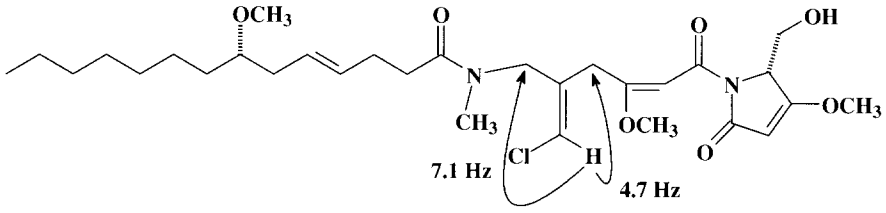

25

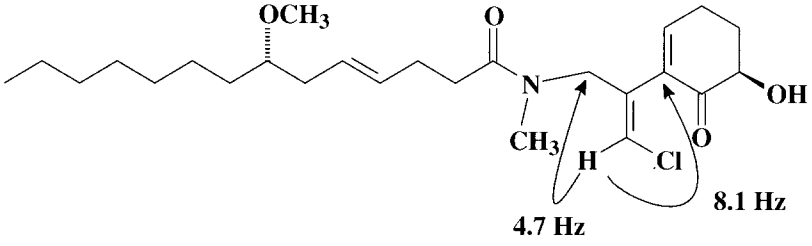

26

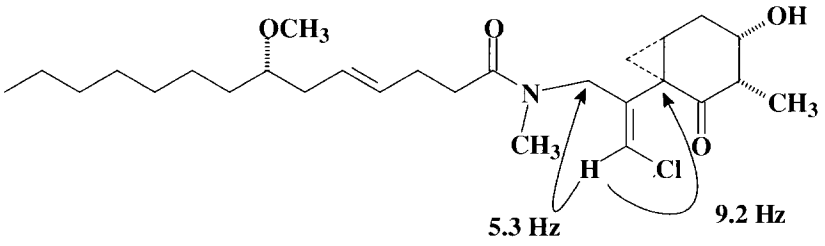

27

Long-range heteronuclear coupling constants determined from HSQMBC spectra were also used in the J-based conformational analysis[129] of the aliphatic stereocenters at C7 through C10 of the neurotoxin kalkitoxin (**28**) from the marine cyanobacterium *Lyungba majuscula*.[148]

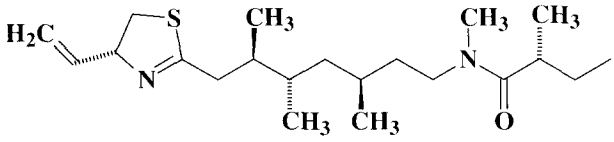

28

Phormidolide (**29**) the complex marine cyanobacterial metabolite used as one of the examples in the initial report describing the HSQMBC experiment,[117] is the subject of a recent report.[149] It is noteworthy that during the J-based conformational analysis[129] of phormidolide that the authors had an unprecedented five conformational restraints (homo- and heteronuclear couplings, NOE, and ROE) per stereocenter.

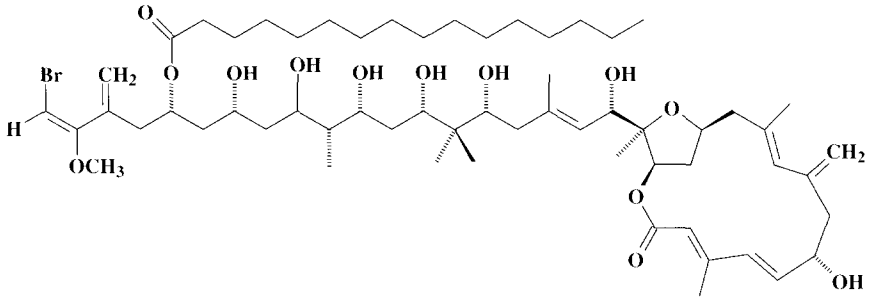

29

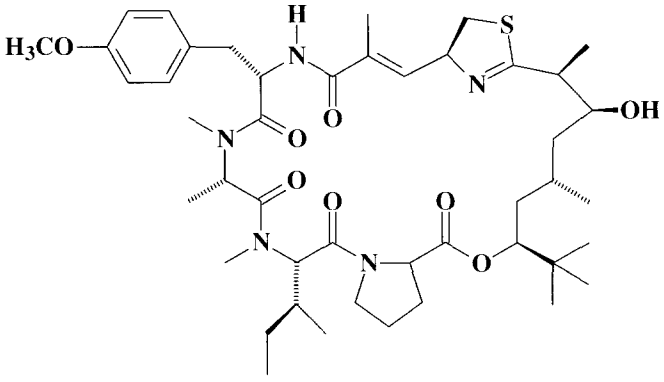

30

Finally, Moore and co-workers[150] reported using a combination of HETLOC and HSQMBC experiments to measure the long-range heteronuclear coupling constants of apratoxin A (**30**), a cytotoxin from the marine cyanobacterium *Lyngba majuscula*.

5. CONCLUSIONS

Following the seminal suggestion of long-range heteronuclear shift correlation by Hallenga and van Binst[13] in 1980, it was not until the 1984 report by Reynolds and co-workers[14] that this powerful structure elucidation technique was experimentally realized. There followed an intense period of activity focused on the development of new long-range heteronuclear shift correlation experiments that was reviewed by Martin and Zektzer in 1988.[18] The heteronucleus-detected experiments were supplanted by the 1986 development of the HMBC experiment reported by Bax and Summers,[23] and the subsequent development of gradient-enhanced variants of the heteronuclear shift correlation experiments.[27–30] There followed a period nearly a decade long during which the HMBC/GHMBC experiments were the 'cornerstone' of contemporary structure elucidation experimental protocols. While the idea of a refocused HMBC experiment to allow broadband heteronuclear decoupling during acquisition was first described in 1989 by Bermel, Wagner, and Griesinger[51] it was not until the 1995 report of Furihata and Seto[54] 'reinventing' what they referred to as the D-HMBC experiment that the development of modifications of the proton-detected long-range heteronuclear shift correlation experiment began to appear on a regular basis. The series of long-range experiments reported since 1995 are surveyed in this chapter and include GSQMBC,[75] constant time variants (CT-HMBC-1 and CT-HMBC-2);[87] three-dimensional experiments (3D-HMBC);[73] a series of accordion-optimized experiments (ACCORD-HMBC,[89,92] IMPEACH-MBC,[71,72] CIGAR-HMBC,[96] and ^{2}J, ^{3}J-HMBC);[98] and most recently the BIRD-HMBC[101] and broadband HMBC[102] experiments. It is uncertain at the time of writing (mid-2001) what impact the growing series of new long-range heteronuclear shift correlation experiments will have on the manner in which chemical structure elucidation is undertaken. It is certain, however, that long-range heteronuclear shift correlation experiments have, in general, had a profound effect on the conduct of structure elucidation efforts in laboratories world-wide and have spurred much of the recent interest in the development of more versatile, new long-range correlation experiments.

REFERENCES

1. J. T. Arnold, S. S. Dharmatti and M. E. Packard, *J. Chem. Phys.*, 1951, **19**, 507.
2. R. R. Ernst and W. A. Anderson, *Rev. Sci. Instr.*, 1966, **37**, 93.
3. J. Jeener, Ampere International Summer School, Basko Polje, Jugoslavia, 1971.
4. W. P. Aue, E. Barthold and R. R. Ernst, *J. Chem. Phys.*, 1976, **64**, 2229.

5. A. A. Maudsley and R. R. Ernst, *Chem. Phys. Lett.*, 1977, **50**, 368.
6. A. A. Maudsley, L. Müller and R. R. Ernst, *J. Magn. Reson.*, 1977, **28**, 463.
7. G. Bodenhausen and R. Freeman, *J. Magn. Reson.*, 1977, **28**, 471.
8. G. Bodenhausen and R. Freeman, *J. Am. Chem. Soc.*, 1978, **100**, 320.
9. R. Freeman and G. A. Morris, *J. Chem. Soc., Chem. Commun.*, 1978, 684.
10. K. G. R. Pachler and P. L. Wessels, *J. Magn. Reson.*, 1973, **12**, 337.
11. S. Sørensen, R. S. Hansen and H. J. Jakobsen, *J. Magn. Reson.*, 1974, **14**, 243.
12. A. Bax and G. A. Morris, *J. Magn. Reson.*, 1981, **42**, 501.
13. K. Hallenga and G. van Binst, *Bull. Magn. Reson.*, 1980, **2**, 343.
14. W. F. Reynolds, R. G. Enriquez, L. I. Escobar and X. Lozoya, *Can. J. Chem.*, 1984, **62**, 2421.
15. G. E. Martin and C. E. Hadden, *J. Nat. Prod.*, 2000, **63**, 543.
16. L. Müller, *J. Am. Chem. Soc.*, 1979, **101**, 4481.
17. G. Bodenhausen and D. J. Ruben, *Chem. Phys. Lett.*, 1980, **69**, 185.
18. G. E. Martin and A. S. Zektzer, *Magn. Reson. Chem.*, 1988, **26**, 631.
19. W. F. Reynolds, S. McLean, H. Jacobs and W. W. Harding, *Can. J. Chem.*, 1999, **77**, 1922.
20. R. C. Crouch and G. E. Martin, *J. Nat. Prod.*, 1992, **55**, 1343.
21. R. C. Crouch and G. E. Martin, *Magn. Reson. Chem.*, 1992, **30**, S66.
22. W. F. Reynolds, M. Yu and R. G. Enriquez, *Magn. Reson. Chem.*, 1997, **35**, 614.
23. A. Bax and S. Subramanian, *J. Magn. Reson.*, 1986, **67**, 565.
24. G. E. Martin and R. C. Crouch, Inverse-detected 2D NMR applications in alkaloid chemistry, in *Modern Methods of Plant Analysis*, vol. 15, H. F. Linskens and J. F. Jackson, eds, Springer-Verlag, Berlin, 1994, pp. 25–89.
25. W. F. Reynolds, S. McLean, L. L. Tay, R. G. Enriquez, D. M. Eastwick and K. O. Pascoe, *Magn. Reson. Chem.*, 1997, **35**, 455.
26. T. D. W. Claridge, *High-Resolution NMR Techniques in Organic Chemistry*, Pergammon, Amsterdam, 1999, pp. 229.
27. R. E. Hurd and B. K. John, *J. Magn. Reson.*, 1991, **91**, 648.
28. J. Ruiz-Cabello, G. W. Vuister, C. T. W. Moonen, P. Van Geldern, J. S. Cohen and P. C. M. Van Zilj, *J. Magn. Reson.*, 1992, **100**, 282.
29. W. Willker, D. Leibfritz, R. Kerssebaum and W. Bermel, *Magn. Reson. Chem.*, 1993, **31**, 287.
30. T. Parella, *Magn. Reson. Chem.*, 1998, **36**, 467.
31. C. E. Hadden and D. T. Angwin, *Magn. Reson. Chem.*, 2001, **39**, 1.
32. K. Zangger and I. M. Armitage, *Magn. Reson. Chem.*, 2000, **38**, 452.
33. C. E. Hadden, J. B. Moon and D. T. A. Hadden, *J. Heterocyclic Chem.*, 2001, **38**, 843.
34. G. C. Levy and R. L. Lichter, *Nitrogen-15 Nuclear Magnetic Resonance Spectroscopy*, Wiley-Interscience, New York, 1979, p. 134.
35. C. Bauer, R. Freeman and S. Wimperis, *J. Magn. Reson.*, 1984, **58**, 526.
36. M. J. Quast, A. S. Zektzer, G. E. Martin and R. N. Castle, *J. Magn. Reson.*, 1987, **71**, 554.
37. A. S. Zektzer, B. K. John, R. N. Castle and G. E. Martin, *J. Magn. Reson.*, 1987, **72**, 556.
38. A. S. Zektzer, B. K. John and G. E. Martin, *Magn. Reson. Chem.*, 1987, **25**, 752.
39. M. Salazar, A. S. Zektzer and G. E. Martin, *Magn. Reson. Chem.*, 1988, **26**, 24.
40. M. Salazar, A. S. Zektzer and G. E. Martin, *Magn. Reson. Chem.*, 1988, **26**, 28.
41. M. Perpick-Dumont, R. G. Enriquez, S. McLean, F. V. Puzzuoli and W. F. Reynolds, *J. Magn. Reson.*, 1987, **75**, 416.
42. G. Batta and K. E. Köver, *Magn. Reson. Chem.*, 1987, **25**, 125.
43. H. Kessler, C. Griesinger, J. Zarbock and H. R. Loosli, *J. Magn. Reson.*, 1984, **57**, 331.
44. H. Kessler, C. Griesinger and J. Lautz, *Angew. Chem. Int. Ed., Engl.*, 1984, **23**, 444.
45. V. V. Krishnamurthy and J. E. Casida, *Magn. Reson. Chem.*, 1987, **25**, 837.
46. W. F. Reynolds, D. W. Hughes, M. Perpick-Dumont and R. G. Enriquez, *J. Magn. Reson.*, 1985, **63**, 413.
47. A. Bax and M. F. Summers, *J. Am. Chem. Soc.*, 1986, **108**, 2093–2094.
48. H. Kogler, O. W. Sørensen, G. Bodenhausen and R. R. Ernst, *J. Magn. Reson.*, 1983, **55**, 157.
49. P. L. Rinaldi and P. A. Keifer, *J. Magn. Reson.*, 1994, **108A**, 259.

50. A. Meissner, D. Moskau, N. C. Nielsen and O. W. Sørensen, *J. Magn. Reson.*, 1997, **124**, 245.
51. W. Bermel, G. Wagner and C. Griesinger, *J. Magn. Reson.*, 1989, **83**, 223–232.
52. K. Stott, J. Stonehouse, J. Keeler, T. L. Hwang and A. J. Shaka, *J. Am. Chem. Soc.*, 1995, **117**, 4199.
53. R. Araya-Maturana, T. Delgado-Castro, W. Cardona and B. E. Weiss-López, *Curr. Org. Chem.*, 2001, **5**, 253.
54. K. Furihata and H. Seto, *Tetrahedron Lett.*, 1995, **36**, 2817.
55. M. Igarashi, W. Chen, T. Tsuchida, M Umekita, T. Sawa, H. Naganawa, M. Hamada and T. Takeuchi, *J. Antibiotics*, 1995, **48**, 1502.
56. J. S. Kim, K. Shin Ya, J. Eishima, K. Furihata and H. Seto, *J. Antibiotics*, 1996, **49**, 947.
57. J. S. Kim, K. Sinya, J. Eishima, K. Furihata and H. Seto, *J. Antibiotics*, 1996, **49**, 1172.
58. J. Kobayashi, M. Tsuda, H. Fuse, T. Sasaki and Y. Mikami, *J. Nat. Prod.*, 1997, **60**, 150.
59. J. S. Kim, K. Shin Ya, K. Furihata, Y. Hayakawa and H. Seto, *Tetrahedron Lett.*, 1997, **38**, 3431.
60. H. Ishiyama, M. Ishibashi, A. Ogawa, S. Yoshida and J. Kobayashi, *J. Org. Chem.*, 1997, **62**, 3831.
61. A. C. Whyte, K. B. Gloer, J. B. Gloer, B. Koster and D. Malloch, *Can. J. Chem.*, 1997, **75**, 768.
62. X. X. Wang, H. Shigemori and J. Kobayashi, *Tetrahedron Lett.*, 1997, **38**, 7587.
63. J. Kobayashi, K. Inaba and M. Tsuda, *Tetrahedron*, 1997, **53**, 16679.
64. J. Kobayashi, D. Watanabe, N. Kawasaki and M. Tsuda, *J. Org. Chem.*, 1997, **62**, 9236.
65. I. Momose, N. Kinoshita, R. Sawa, H. Naganawa, H. Iinuma, M. Hamada and T. Takeuchi, *J. Antibiotics*, 1998, **51**, 130.
66. R. J. Carbajo, L. Zhang and F. Lopez-Ortiz, *Magn. Reson. Chem.*, 1998, **36**, 807.
67. H. Seto, *Pure Appl. Chem.*, 1999, **71**, 1133.
68. B. Coxon, N. Sari, G. Batta and V. Pozsgay, *Carbohydrate Res.*, 2000, **324**, 53.
69. N. Kawamura, R. Sawa, Y. Takahashi, K. Isshiki, T. Sawa, H. Naganawa and T. Takeuchi, *J. Antibiotics*, 1996, **49**, 651.
70. G. E. Martin, F. W. Crow, B. D. Kaluzny, J. G. Marr, G. D. Fate and T. J. Gilbertson, *Magn. Reson. Chem.*, 1998, **36**, 635.
71. C. E. Hadden, G. E. Martin and V. V. Krishnamurthy, *J. Magn. Reson.*, 1999, **140**, 274.
72. G. E. Martin and C. E. Hadden, *Magn. Reson. Chem.*, 2000, **38**, 251.
73. K. Furihata and H. Seto, *Tetrahedron Lett.*, 1996, **37**, 8901.
74. K. H Sze, X. Z. Yan, X. M. Kong, C. T. Che and G. Zhu, *Tetrahedron Lett.*, 1999, **40**, 5587.
75. R. Marek, L. Králík and V. Sklenář, *Tetrahedron Lett.*, 1997, **38**, 665.
76. R. Marek, J. Marek, J. Dostál and J. Slavík, *Collec. Czech. Chem. Commun.*, 1997, **62**, 1623.
77. R. Marek, *Collec. Czech. Chem. Commun.*, 1997, **62**, 1747.
78. R. Marek, I. St'astna-Sedlackova, J. Marek and M. Potacek, *Bull. Soc. Chim. Belg.*, 1997, **106**, 645.
79. J. Dostál, J. Slavík, M. Potacek, R. Marek, V. Sklenář, E. de Hoffman, R. Rozenbert, B. Tinant and J. P. Declerq, *Phytochem.*, 1998, **47**, 879.
80. P. Kilian, J. Marek, R. Marek, J. Tou-in, O. Humpa, J. Novosad and J. D. Woolins, *J. Chem. Soc., Dalton Trans.*, 1998, 1175.
81. P. Kilian, J. Marek, R. Marek, J. Toušek, O. Humpa, A. M. Z. Slawin, J. Touzin, J. Novosad and J. D. Woolins, *J. Chem. Soc., Dalton Trans.*, 1999, 2231.
82. J. Dostál, J. Slavík, M. Potacek, R. Marek, O. Humpa, V. Sklenář, J. Toušek, E. de Hoffman and R. Rozenberg, *Collec. Czech. Chem. Commun.*, 1998, **63**, 1045.
83. J. Dostál, R. Marek, J. Slavík, E. Taborska, M. Potacek and V. Sklenář, *Magn. Reson. Chem.*, 1998, **36**, 869.
84. R. Marek, O. Humpa, J. Dostál, J. Slavík and V. Sklenář, *Magn. Reson. Chem.*, 1999, **37**, 195.
85. R. Marek, J. Toušek, J. Dostál, J. Slavík, R. Dommisse and V. Sklenář, *Magn. Reson. Chem.*, 1999, **37**, 781.
86. D. Hocková, M. Budešínsky, R. Marek, J. Marek and A. Holý, *Eur. J. Org. Chem.*, 1999, 2675.

87. K. Furihata and H. Seto, *Tetrahedron Lett.*, 1998, **39**, 7337.
88. G. Bodenhausen and R. R. Ernst, *J. Am. Chem. Soc.*, 1982, **104**, 1304.
89. R. Wagner and S. Berger, *Magn. Reson. Chem.*, 1998, **36**, S44.
90. O. W. Sørensen, N. C. Nielsen, H. Bildso and H. J. Jakobsen, *J. Magn. Reson.*, 1982, **70**, 54.
91. A. Meissner, D. Moskau, N. C. Nielsen and O. W. Sørensen, *J. Magn. Reson.*, 1997, **124**, 245.
92. G. E. Martin, C. E. Hadden, R. C. Crouch and V. V. Krishnamurthy, *Magn. Reson. Chem.*, 1999, **37**, 517.
93. V. V. Krishnamurthy, *J. Magn. Reson., Ser. A*, 1996, **121**, 33.
94. A. Kumar, *J. Magn. Reson.*, 1978, **30**, 227.
95. G. Bodenhausen, R. Freeman, G. A. Morris and D. L. Turner, *J. Magn. Reson.*, 1978, **31**, 75.
96. C. E. Hadden, G. E. Martin and V. V. Krishnamurthy, *Magn. Reson. Chem.*, 2000, **38**, 143.
97. W. F. Reynolds and R. G. Enriquez, *J. Nat. Prod.*, 2001, **64**, in press.
98. V. V. Krishnamurthy, D. J. Russell, C. E. Hadden and G. E. Martin, *J. Magn. Reson.*, 2000, **146**, 232.
99. D. J. Russell, C. E. Hadden, G. E. Martin and V. V. Krishamurthy, 'Accordion-optimized direct correlation experiments', *SMASH 2000 – Small Molecule NMR Conference*, Argonne, IL, Aug 13–15, poster #34.
100. D. J. Russell, C. E. Hadden, G. E. Martin and K. Krishnamurthy, *Magn. Reson. Chem.*, 2001, **39**, in press.
101. R. Berger, C. Schorn and P. Bigler, *Magn. Reson. Chem.*, 2000, **38**, 963.
102. A. Meissner and O. W. Sørensen, *Magn. Reson. Chem.*, 2000, **38**, 981.
103. R. Berger, C. Schorn and P. Bigler, *J. Magn. Reson.*, 2001, **148**, 88.
104. B. L. Márquez, W. H. Gerwick and R. T. Williamson, *Magn. Reson. Chem.*, 2001, **39**, 499.
105. M. Kurz, P. Schmieder and H. Kessler, *Angew. Chem. Int. Ed. Engl.*, 1991, **30**, 1329.
106. D. Uhrín, G. Batta, V. J. Hruby, P. N. Barlow and K. E. Kövér, *J. Magn. Reson.*, 1994, **108**, 160.
107. D. Uhrín, G. Batta, V. J. Hruby, P. N. Barlow and K. E. Kövér, *J. Magn. Reson.*, 1998, **130**, 155.
108. G. Zhu, A. Renwick and A. Bax, *J. Magn. Reson.*, 1994, **110**, 257.
109. N. Matsumori, M. Murata and K. Tachibana, *Tetrahedron*, 1995, **51**, 12 229.
110. D. Uhrín, A. Mele, K. E. Kövér, J. Boyd and R. A. Dwek, *J. Magn. Reson.*, 1994, **108A**, 160.
111. M. Liu, R. D. Farrant, J. M. Gillam, J. K. Nicholson and J. C. Lindon, *J. Magn. Reson.*, 1995, **109B**, 275.
112. W. Willker and D. Leibfritz, *Magn. Reson. Chem.*, 1995, **33**, 632.
113. W. Koźmiński and D. Nanz, *J. Magn. Reson.*, 1997, **124**, 383.
114. W. Koźmiński and D. Nanz, *J. Magn. Reson.*, 2000, **142**, 294.
115. K. Furihata and H. Seto, *Tetrahedron Lett.*, 1999, **40**, 6271.
116. W. Koźmiński, *J. Magn. Reson.*, 1999, **137**, 408.
117. R. T. Williamson, B. M. Márquez, W. H. Gerwick and K. E. Kövér, *Magn. Reson. Chem.*, 2000, **38**, 265.
118. K. Ding, *Magn. Reson. Chem.*, 2000, **38**, 321.
119. G. E. Martin and R. C. Crouch, *J. Heterocyclic Chem.*, 1995, **32**, 1665.
120. G. E. Martin and R. C. Crouch, *J. Heterocyclic Chem.*, 1995, **32**, 1759.
121. S. Sheng and H. van Halbeek, *J. Magn. Reson.*, 1998, **130A**, 296.
122. C. H. Gotfredsen, A. Meissner, J. Ø. Duus and O. W. Sørensen, *Magn. Reson. Chem.*, 2000, **38**, 692.
123. H. Seki, T. Tokunaga, H. Utsumi and K. Yamaguchi, *Tetrahedron*, 2000, **56**, 2935.
124. Y. Xia, X. Kong, N. Ip and G. Zhu, *J. Magn. Reson.*, 2000, **146**, 228.
125. T. Tokunaga, H. Seki, H. Utsumi, M. Nakakoshi and K. Yamaguchi, *Analytical Sciences*, 1999, **15**, 1157.
126. A. Meissner and O. W. Sørensen, *Magn. Reson. Chem.*, 2001, **39**, 49.
127. R. T. Williamson, B. L. Márquez, W. H. Gerwick, G. E. Martin and V. V. Krishnamurthy, *Magn. Reson. Chem.*, 2001, **39**, 127.

128. I. Tvaroska and F. R. Taravel, *Adv. Carbohydrate Chem. Biochem.*, 1995, **51**, 15.
129. M. Matsumori, D. Kaneno, M. Murata, H. Nakamura and K. Tachibana, *J. Org. Chem.*, 1999, **64**, 866.
130. N. Matsumori, M. Murata and K. Tachibana, *Tetrahedron*, 1995, **51**, 12 229.
131. M. Kuramoto, T. Ishida, N. Yamada, A. Yamada, D. Uemura, T. Aino, K. Yamada, Y. Ijuin and K. Fujita, *Symposium Papers, 35th Symposium on the Chemistry of Natural Products*, pp. 693–700, 1993.
132. A. Yokoyama, M. Murata, Y. Ohshima, T. Iwashita and T. Yasumoto, *J. Biochem.*, 1988, **104**, 184.
133. M. Murta, H. Naoki, S. Matsunaga, M. Satake and T. Yasumoto, *J. Am. Chem. Soc.*, 1994, **116**, 7098.
134. N. Matsumori, T. Nonomura, M. Sasaki, M. Murata, K. Tachibana, M. Satake and T. Yasumoto, *Tetrahedron Lett.*, 1996, **37**, 1269.
135. M. Sasaki, N. Matsumori, T. Maruyama, T. Nonomura, M. Murata, K. Tachibana and T. Yasumoto, *Angew. Chem. Int. Ed., Engl.*, 1996, **35**, 1672.
136. T. Nonomura, M. Sasaki, N. Matsumori, M. Murata, K. Tachibana and T. Yasumoto, *Angew. Chem. Int. Ed., Engl.*, 1996, **35**, 1675.
137. R. Sakai, H. Mamiya, M. Murata and K. Shimamoto, *J. Am. Chem. Soc.*, 1997, **119**, 4112.
138. M. Murata, S. Matsuoka, N. Matsumori, G. K. Paul and K. Tachibana, *J. Am. Chem. Soc.*, 1999, **121**, 870.
139. Á. Patthy-Lukáts, L. Károlyházy, L. F. Szabó and B. Podányi, *J. Nat. Prod.*, 1997, **60**, 69.
140. Á. Patthy-Lukáts, Á. Kocsis, L. F. Szabó and B. Podányi, *J. Nat. Prod.*, 1999, **62**, 1492.
141. W. Willker and D. Leibfritz, *Magn. Reson. Chem.*, 1995, **33**, 632.
142. H. Takayama, T. Ichikawa, T. Kuwajim, M. Kitajima, H. Seki, N. Aimi and M. G. Nonato, *J. Am. Chem. Soc.*, 2000, **122**, 8635.
143. A. Nagatsu, R. Tanaka, H. Mizukami, Y. Ogihara and J. Sakakibara, *Terahedron*, 2001, **57**, 3369.
144. T. Rundlöf, A. Kjellberg, C. Damberg, T. Nishida and G. Widmalm, *Magn. Reson. Chem.*, 1998, **36**, 839.
145. J. C. Martins, R. Willem and M. Biesemans, *J. Chem. Soc., Perkin Trans. 2*, 1999, 1513.
146. K. Shimbo, M. Tsuda, E Fukushi, J. Kawabata and J. Kobayashi, *Tetrahedron*, 2000, **56**, 7923.
147. K. E. Milligan, B. Márquez, R. T. Williamson, M. Davies-Coleman and W. H. Gerwick, *J. Nat. Prod.*, 2000, **63**, 965.
148. M. Wu, O. Tatsufumi, L. M. Nogle, B. L. Marquez, R. T. Williamson, N. Sittachitta, F. W Berman, T. F. Murray, K. McGough, R. Jacobs, K. Colsen, T. Asano, F. Yokokawa, T. Shiori and W. H. Gerwick, *J. Am. Chem. Soc.* 2000, **122**, 12 041.
149. R. T. Williamson, A. Boulanger, A. Vulpanovici, M. A. Roberts and W. H. Gerwick, *J. Org. Chem.*, submitted.
150. H. Luesch, W. Y. Yoshida, R. E. Moore, V. J. Paul and T. H. Corbett, *J. Am. Chem. Soc.*, 2001, **123**, 5418.

Dynamics of Silk Fibroin Studied with NMR Spectroscopy

TSUNENORI KAMEDA and TETSUO ASAKURA

Department of Biotechnology, Tokyo University of Agriculture and Technology, Koganei, Tokyo 184, Japan

1. Introduction 102
2. The amino acid composition and primary structure of *B. mori* and *S.c. ricini* silk fibroin 104
3. ^{13}C NMR spectra of silk fibroin in solution and in the solid state 106
4. Motion of amino acid residues of silk fibroin in aqueous solution and in living silkworms 109
5. Motion of Gly and Ala residues in silk fibroins in the solid state 113
6. Motion of Ser residue in silk fibroins in the solid state 117
7. Motion of Tyr residue in silk fibroins in the solid state 123
8. Structural transition of *S.c. ricini* silk fibroin 127
9. Dynamics of water molecules in *B. mori* silk fibroin film 135
10. Dynamics of *B. mori* silk fibroin in swollen silk fibroin membrane 139
11. Dynamics of small organic molecules in swollen silk fibroin gel 143
Acknowledgement 147
References 147

Dynamic NMR studies of the silk fibroin from silkworms have been reviewed. The chain dynamics of *B. mori* and *S.c. ricini* silk fibroins in aqueous solution were studied to determine the relaxation parameters spin-lattice relaxation time, nuclear Overhauser enhancement and line width. ^{13}C NMR observations were also made to study the chain dynamics of silk fibroin stored in the silk gland of living silkworms. The chain dynamics of the *B. mori* and *S.c. ricini* silk fibroin fiber were studied with ^{2}H and ^{13}C solid-state NMR. The solid-state NMR spectra of *S.c. ricini* silk fibroins showed a gradual and monotonic slowdown of the overall molecular motions leading to molecular aggregation. The chain dynamics of silk fibroin absorbed solvent were detected by ^{1}H and ^{13}C solid-state NMR methods, and also using an NMR imaging method. ESR approaches were applied to the dynamic studies of Tyr side-chain in the silk fibroin.

ANNUAL REPORTS ON NMR SPECTROSCOPY
VOLUME 46 ISBN 0-12-505446-7

1. INTRODUCTION

Investigations of the molecular dynamics of polymers in both solid and solution states are of significant practical importance and much interest being focused on the relationships between structure and molecular motions, and the mechanical performance of these materials.[1] Techniques used to characterize molecular dynamics include variable temperature and/or frequency dielectric measurement and mechanical spectroscopy, electron spin resonance (ESR), fluorescence spectroscopy, and nuclear magnetic resonance (NMR).[2] The magnetic resonance methods, NMR and ESR, have the advantage of being more structurally specific than other methods. NMR, in particular, can probe a wide range of frequencies for molecular motions, which are reflected differently in the various NMR parameters.

NMR observations are basically of spin relaxation processes which are associated with molecular motions of different specific frequencies in a given system. When interest is focused on molecular motions, spin relaxation parameters such as spin–lattice relaxation time (T_1), spin–spin relaxation time (T_2), and nuclear Overhauser enhancement (NOE), are directly measured as a function of temperature or field frequency by using appropriate pulse sequences. Such temperature or frequency dependencies of the spin relaxation parameters are analyzed using appropriate models to obtain detailed information on molecular motions with frequencies 10^6–10^{12} Hz in the system. The T_1 relaxation times can be correlated with segmental motion on, and local environments of, the polymer backbone, while T_2 relaxation data are more closely related to rotational and librational behavior. Silk fibroin, a fibrous protein, as described below is expected to exhibit dynamic characteristics similar to those of polymers in which the molecular weight-independent segmental motion of the chain can contribute significantly to the T_1 and NOE values.[3] The choice of nuclei which can be observed for NMR gives the advantage of observing specific atoms of a repeat unit or segment. The ^{13}C nuclei are studied for dynamics because interpretation of the relaxation parameters is generally not complicated by intermolecular relaxation processes, unlike the situation for ^1H and ^{19}F nuclei.[4] For protonated ^{13}C nuclei in particular, relaxation is generally dominated by a single mechanism: the intermolecular ^{13}C–^1H dipolar with directly bonded protons.[5] Moreover, the large chemical shift range of the ^{13}C nucleus makes it possible to resolve most individual carbons and thus multiple sites are often available at which to probe a molecule's motional features.

In addition to spin relaxation, there are the methods that measure molecular motion. The spectra reflecting the ^2H quadrupolar interaction are sensitive to the mid-range of frequencies. Therefore, ^2H NMR spectroscopy is a powerful tool to examine the molecular motion of polymers in the solid state.[6–8,9] Different types of motion can be discriminated on the basis of their time scale and their exchange geometry. The one-dimensional quadrupole echo lineshape of ^2H NMR is sensitive to dynamics in the range $10^{-8}\,s < \tau_c < 10^{-3}\,s$, where τ_c is the

motional correlation time.[1,10] Within these limits, the ^2H NMR lineshape can be analyzed comprehensively in terms of well-known models to yield the geometry and rate of segmental motion.

NMR imaging is a modification of NMR spectroscopic techniques that uses linear magnetic field gradients to spatially encode the spins according to frequency and phase and has been widely and successfully employed in medical science.[11] NMR imaging has the advantage that it does not disturb the diffusion process, unlike most other techniques which require stopping the diffusion process and destroying the sample.[12–16] Relaxation contrasts are intrinsic in all imaging experiments and provide information on motions with a time scale on the order of the rotational correlation times of the observed spins. T_1, T_2 and $T_{1\rho}$ probe different motional time scales and thus, by appropriate choice of contrast method, images can be made to reflect particular motions.[17]

The spectroscopy of electron spin resonance (ESR) is a means of detecting direct transitions between electron Zeeman levels. The phenomenon of electron spin resonance is observed only in atomic or molecular systems having net electron spin angular momentum, that is, materials containing one or more unpaired electrons. One of the most useful parameters that can be extracted from ESR spectra is the spectral linewidth; this parameter provides information on rotating correlation time (τ_c).[18]

There is considerable interest in the study of silk fibers as a guide to the commercial production of protein-based structural polymers through genetic engineering. Silk fibers combine strength and toughness. For example, silkworm silk exhibits up to 35% elongation,[19] with tensile strengths approaching those of high strength synthetic fibers. The tensile strength of silkworm silks is approximately $6 \times 10^8\,N\,m^{-2}$, the modulus is approximately $5 \times 10^9\,N\,m^{-2}$, and the energy to break is approximately $7 \times 10^4\,J\,kg^{-1}$. This is particularly impressive when considering that natural silk fibers undergo minimal draw to enhance molecular orientation, which improves mechanical properties. Unlike most fibers, increased rates of loading of silk fibers result in increased strength and modulus as well as elongation; this increases the amount of work to rupture. The structures of *Bombyx mori* (*B. mori*), wild silkworm (*Antheraea yamamai, A. pernyi, A. mylitta,* and *Samia cynthia ricini*), and spider dragline silks have been studied in order to clarify the origin of the excellent mechanical properties.

Studies of structure–property relationships are very active. It is well known that such dynamics as the several orders of the scale of the motions significantly influence the properties of polymers including silk fibroins. However, previous study of silk fibroin from the viewpoint of dynamics is limited and therefore, in this review, we describe mainly our work on the study of the dynamics of silk fibroins from *B. mori* and *Samia cynthia ricini* (*S.c. ricini*). The latter silkworm is a wild one and the NMR study was performed as a comparison with *B. mori* silk because of the amino acid composition changes.

2. THE AMINO ACID COMPOSITION AND PRIMARY STRUCTURE OF *B. mori* AND *S.c. ricini* SILK FIBROIN

Silks are generally defined as spun fibrous protein polymer secretions produced by biological systems[19] and are synthesized by a variety of organisms including silkworms (and most other Lepidoptera larvae), spiders, scorpions, mites and flies. The structure and function of silk fibers depend on the organism producing the silk. Figure 1 shows, as an example, anterior, middle and posterior silkglands in a fifth larval stage *B. mori* silkworm.

After the fourth larval molt or ecdysis, the silk glands of these silkworms develop rapidly for active fibroin production and in the fifth instar larva it is the second largest organ following the alimentary canal. Fibroin, the main component of silk proteins, is exclusively synthesized in the posterior region of the silk gland and is transferred by peristalsis into the middle region of the gland in which it is stored as a very viscous aqueous solution until required for spinning. In the walls of the middle region of the gland, another silk protein, sericin, is produced which coats the silk fibroin, acting as an adhesive. The two glands join together immediately before the spinneret through the anterior region and the silk fiber is spun into the air.

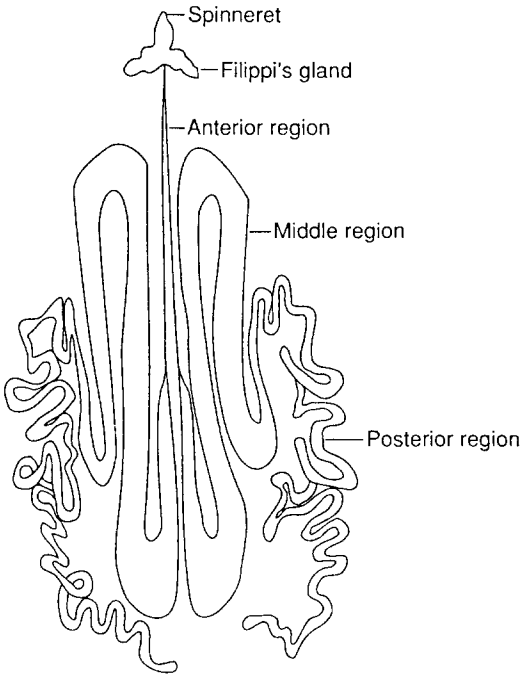

Fig. 1. Silk glands of *B. mori* larva.

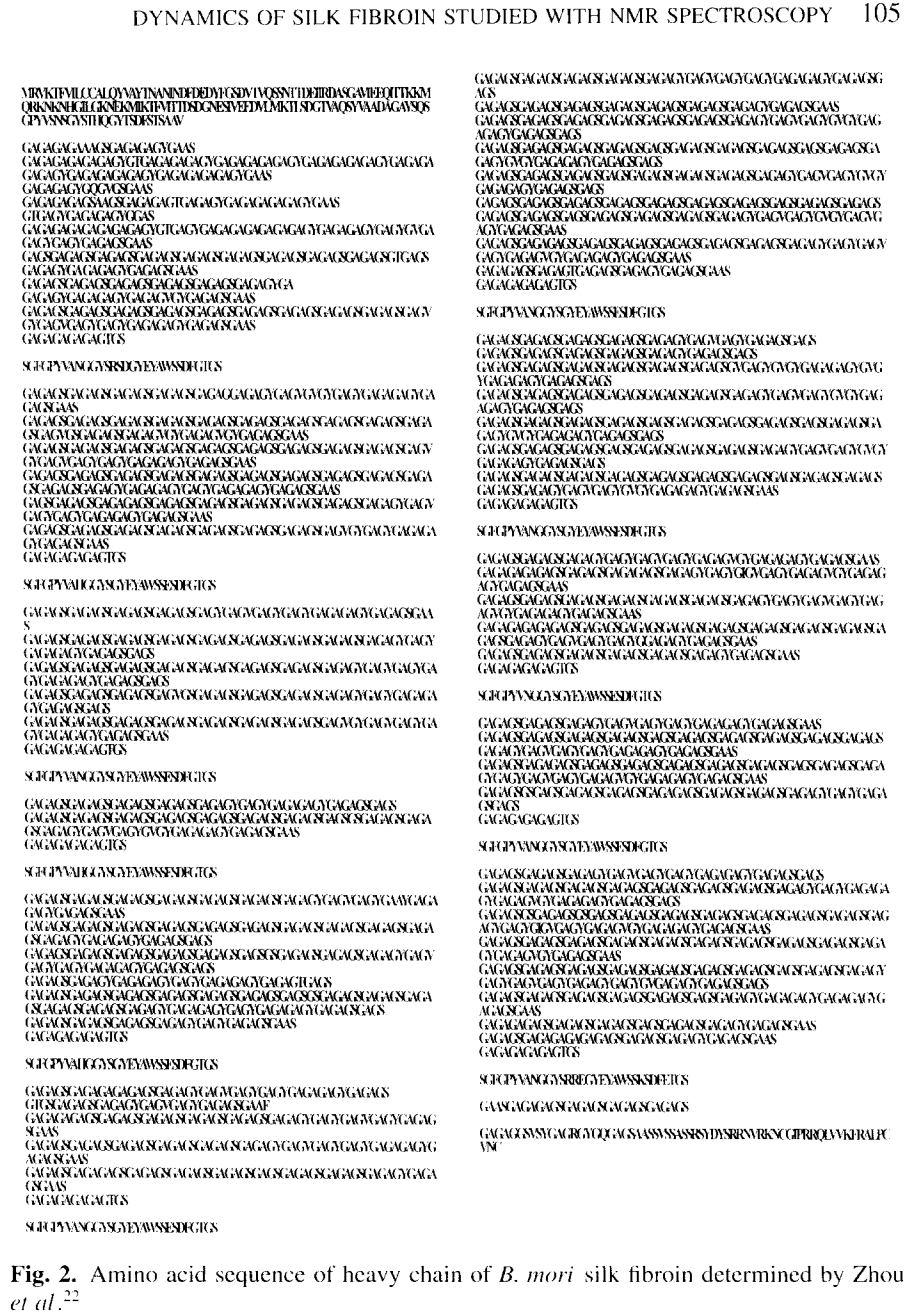

Fig. 2. Amino acid sequence of heavy chain of *B. mori* silk fibroin determined by Zhou *et al.*[22]

The amino acid composition of the silk fibroins from *B. mori* and *S.c. ricini* (in mole percent) is listed in Table 1.[20]

For both *B. mori* and *S.c. ricini* silk fibroins, the major amino acid residues are Ala and Gly. The sum of Gly and Ala residues for *B. mori* silk fibroin is

Table 1. Amino acid composition of silk fibroins from *B. mori* and *S.c. ricini* (mol %)

Amino acid	*B. mori*	*S.c. ricini*	Amino acid	*B. mori*	*S.c. ricini*
Ala	30.0	48.4	Val	2.5	0.4
Gly	42.9	33.2	Leu	0.6	0.3
Ser	12.2	5.5	Ile	0.6	0.4
Tyr	4.8	4.5	Phe	0.7	0.2
Asp	1.9	2.7	Pro	0.5	0.4
Arg	0.5	1.7	Thr	0.9	0.5
His	0.2	1.0	Met	0.1	0.01
Glu	1.4	0.7	Cys	0.03	0.01
Lys	0.4	0.2	Trp		0.3

73%, which is basically the same as that of *S.c. ricini* silk fibroin (82%), but the relative composition of Ala and Gly is reversed.[21] As a result, the striking conformational difference of *S.c. ricini* silk fibroin is the presence of α-helical portions which are composed of Ala residues $(Ala)_n$.

Silks are encoded by highly repetitive structural genes that are under tight regulatory control in the cell. The repetitive domains influence the higher-order conformation and result in fibers with unusual functional properties. Information on the sequences of several kinds of spider silks have been rapidly accumulated: recently, the complete sequence has been reported for silk fibroin from *B. mori* silk fibroin heavy chain.[22]

In the repetitive domain there are two types of repeat units (Fig. 2). One unit is characterized by GlyAlaGlyAlaGlySer: the other unit is the peptides of GlyAla repeats followed by GlyTyr.

The primary structure of the silk fibroin from *S.c. ricini* has recently been determined by Yukihiro *et al.* (personal communication). The silk mainly consists of about 100 repeated similar sequences where there are alternative appearances of a polyalanine region and a glycine-rich region as in spider (major ampullate) silk. As a result, the most striking conformational characteristic of these silk fibroins in the silk gland or in aqueous solution is the presence of α-helical domains consisting of Ala residues.

3. ^{13}C NMR SPECTRA OF SILK FIBROIN IN SOLUTION AND IN THE SOLID STATE

Typical ^{13}C NMR spectra of the aqueous solution of the regenerated silk fibroin prepared from *B. mori* cocoon are shown in Fig. 3.[4]

The preparation of *B. mori* fibroin solution is summarized as follows. The cocoon was degummed twice with 0.5% Marseilles soap solution at 100°C for 0.5 h and then washed with distilled water. The degummed *B. mori* silk fibroin was dissolved in 9 M MLiBr at 40°C. After dialysis against distilled water for 4 days, the solution was clarified by spinning in a centrifuge at 10 000 rpm for

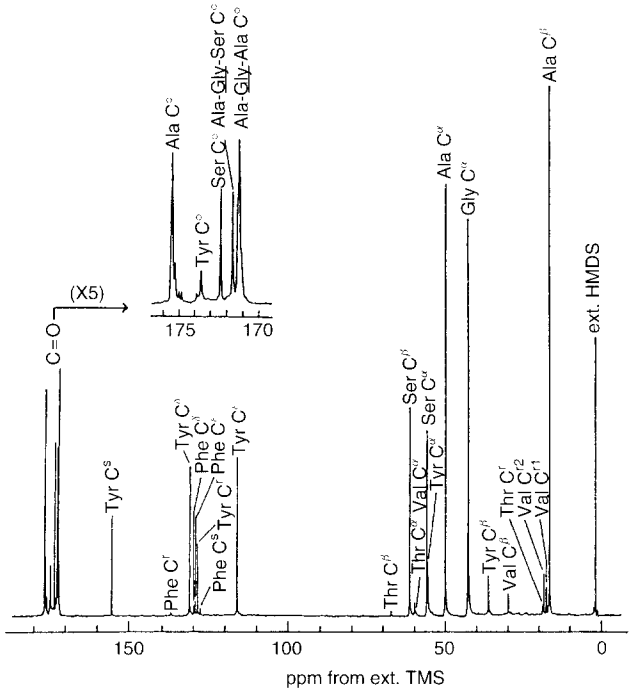

Fig. 3. Proton-noise-decoupled ^{13}C NMR spectrum of *B. mori* silk fibroin in aqueous solution (8.7 w/v%). The carbonyl resonance region was expanded and inserted in the figure.

20–30 min. The supernatant was collected and concentrated using an electric fan. Assignment was readily performed by reference to the chemical shifts of Ac-X-NHMe (where X = Gly, Ala, Ser, Tyr, or Val) and of the small peptides reported elsewhere.[23] The Gly, Ala, Ser, Tyr, and Val residues, of which silk fibroin has relatively large amounts, give well-resolved spectra. There are small but explicit peaks which are assigned to the L-Phe and L-Thr residues.

Figure 4 shows the ^{13}C NMR spectrum of the liquid silk from *S.c. ricini* mature larva.[24] The spectrum of *S.c. ricini* liquid silk is sharp, indicating very rapid segmental motion of the main chain characterized by a very small correlation time on the order of 10^{-10} s at room temperature (as in the case of *B. mori* silk fibroin). Assignment was performed by reference to chemical shift data of the pentapeptides, Gly-Gly-X-Gly-Gly, where X equals the specified residue,[25–27] and the amino acid composition. Solution ^{13}C and ^{15}N NMR studies of *S.c. ricini* silk fibroin in aqueous solution indicate that about 70% of Ala residues form α-helices while, the conformation of the other Ala residues is random coil.[20,24,28]

Figure 5 illustrates typical solid-state ^{13}C NMR (CP/MAS) spectra of the *B. mori* (a) and *S.c. ricini* (b) silk fibroin.

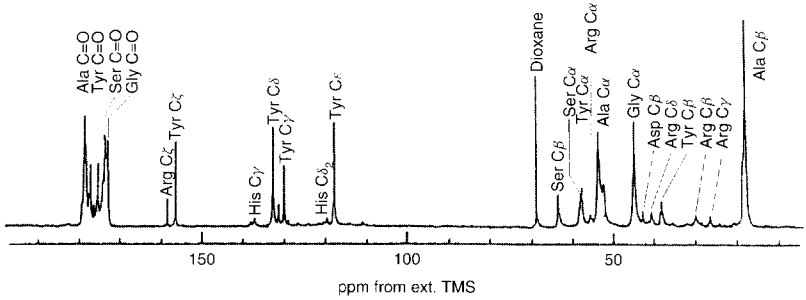

Fig. 4. Proton-noise-decoupled ^{13}C NMR spectrum of *S.c. ricini* liquid silks (sample concentration 18.0% (w/v)) at 25°C.

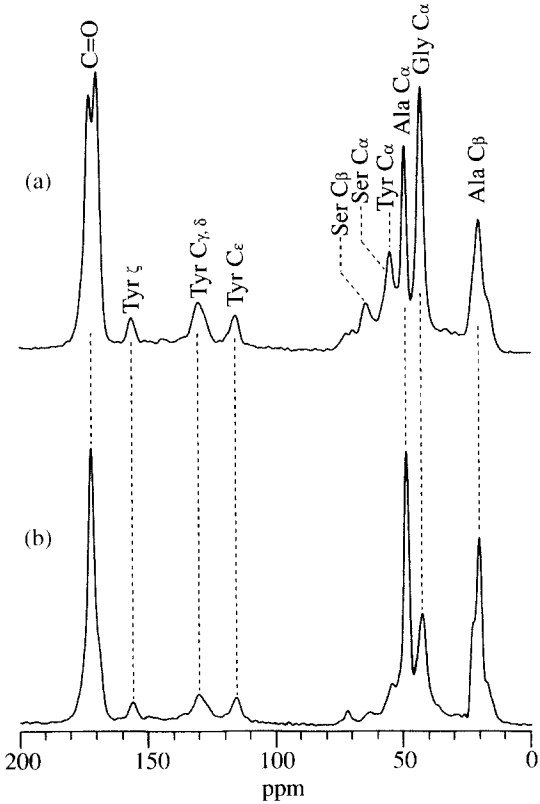

Fig. 5. ^{13}C CP/MAS NMR spectra of *B. mori* (a) and *S.c. ricini* (b) silk fibroin fibers in the solid state.

4. MOTION OF AMINO ACID RESIDUES OF SILK FIBROIN IN AQUEOUS SOLUTION AND IN LIVING SILKWORMS

As shown in Fig. 3, all ^{13}C solution NMR peaks are sharp; i.e., the half-height width is 3.4 Hz on average, indicating very fast segmental motion of the silk fibroin chain, in spite of the very large molecular weight of 391 kDa. In order to study such fast segmental motion more quantitatively, the spin–lattice relaxation times, T_1, for the protonated carbons only, were observed as a function of concentration from 2.1% to 14.5% using the usual inversion-recovery method, i.e. by $(180°-\tau-90°)$ pulse sequences. These spectra were recorded at 50 MHz. The T_1 values were determined by using the peak areas and are plotted against concentration in Fig. 6.[4]

It is likely that T_1 values decrease gradually with increasing concentration except for the Ala C_β, where the data show large scatter. As will be described later, the T_1 values were also determined for silk fibroin stored in silkworm (30%). The NT_1 values obtained for the α-carbons, where N is the number of directly attached hydrogen atoms to the given carbon, were approximately same for the Ala, Gly, and Ser residues (0.26–0.30 s in 2.1% solution and 0.19–0.22 s in liquid silk), indicating isotropic segmental motion of the chain. As for the motion of the side group, the NT_1 values of the C_β carbons were 1.1–1.4 s for the Ala residue 0.22–0.40 s for the Ser residue and 0.14–0.38 s for the Tyr residue. Thus, the rate of internal rotation around the C_α–C_β bond decreases in the order Ala, Ser, Tyr. In particular, the comparable NT_1 value of the Tyr C_β carbon relative to those of the C_α carbons indicates that internal rotation of the C_α–C_β bond is strongly hindered.[29] Similarly, the NT_1 values of the aromatic carbons, C_δ and C_ε, of the Tyr residue are 0.18–0.28 s, indicating that rotation around the C_β–C_γ axis is also strongly hindered.

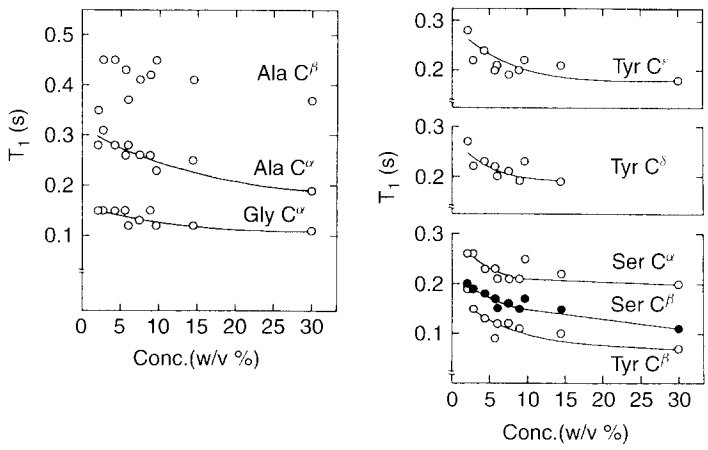

Fig. 6. Concentration dependence of the spin–lattice relaxation times (T_1) of *B. mori* silk fibroin.

In order to determine the correlation time for the backbone segmental motion of *B. mori* silk fibroin quantitatively, NOE as well as T_1 values were measured as a function of concentration.[4] However, it could not be judged from the data whether the NOE values were concentration dependent or not, because of the large scatter. Therefore, the NOE values were averaged over all the concentrations for each carbon. The NT_1 and NOE values averaged over the Ala, Gly, and Ser C_α carbons are used to determine the correlation times of the segmental motion. The NOE value of 2.2 deviates appreciably from the theoretical maximum value 2.988, which indicates that the extreme narrowing condition is no longer applicable in describing the chain motion.[3] Moreover, a correlation time satisfying both T_1 and NOE data was not obtained when a general isotropic rotational diffusion model[3] (single correlation time model) was used. Therefore, the log χ^2 distribution model was applied to determine the correlation time for the segmental motion of silk fibroin as a function of concentration. Interpretation of the model is given in detail elsewhere.[30] The results are shown in Fig. 7.[4]

With increasing concentration, the mean correlation time increased gradually from 0.10 ns (2%) to 0.22 ns (30%). These are within the values typical of a random coil polymer, 0.1–1.0 ns at 30–40°C.[3] Moreover, the width parameter, p, in the log χ^2 distribution model was relatively small: 10–14, indicating broad distribution of the correlation time. This is also typical of a random coil polymer.[3]

Next, in order to discuss the conformation of *S.c. ricini* silk fibroin from the viewpoint of molecular dynamics, ^{13}C NMR T_1 values were also observed. All T_1 values of *S.c. ricini* are somewhat smaller than those of *B. mori* silk fibroin. From both the NT_1 value averaged over the Ala, Gly, and Ser C_α carbons, where N is

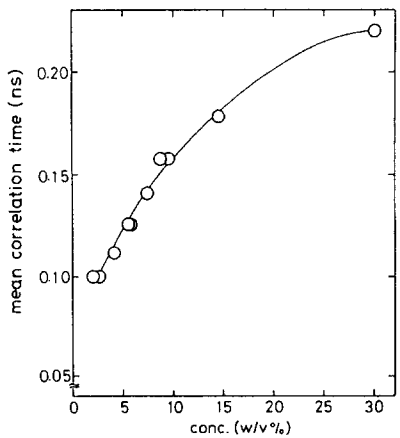

Fig. 7. Concentration dependence of the mean correlation times for the segmental motion of *B. mori* silk fibroin determined from NT_1 and NOE values averaged over Gly C_α, Ala C_α, and Ser C_α assuming the log χ^2 distribution model. The width parameters in the model were 10–14. The NOE value for the liquid silk in the *B. mori* silk gland was assumed to be 2.2.

the number of hydrogen atoms attached to the specified carbon atom directly, and the NOE value of 2.2, assumed by reference to previous data concerning *B. mori* silk fibroin, the average correlation time for the segmental motion of the protein was determined with a log χ^2 distribution model for segmental motion. The value was 3.5×10^{-10} s, compared with 2.2×10^{-10} s for *B. mori* silk fibroin[4] at 25°C. Thus, the segmental motion of the *S.c. ricini* silk fibroin chain is very fast as is also the case for *B. mori* fibroin, which is typical of a random coil polymer.

^{13}C NMR spectra of the silk gland of the mature larva and of the abdomen of the pupa of *S.c. ricini* are shown in Figs 8(a) and (b), together with that of the mature larva of *B. mori* (c).[31]

The concentration of liquid silk in the middle silk gland of *B. mori* mature larva has been reported as ca. 30%.[32] Surprisingly, high resolution ^{13}C NMR spectra are observed and are assigned to triglyceride, trehalose and silk protein in the silkworm. High mobility of these components gives high-resolution NMR, but other components do not give any NMR spectra because of their low mobility. The NMR spectrum of the pupa shows the peaks due to triglyceride and trehalose,

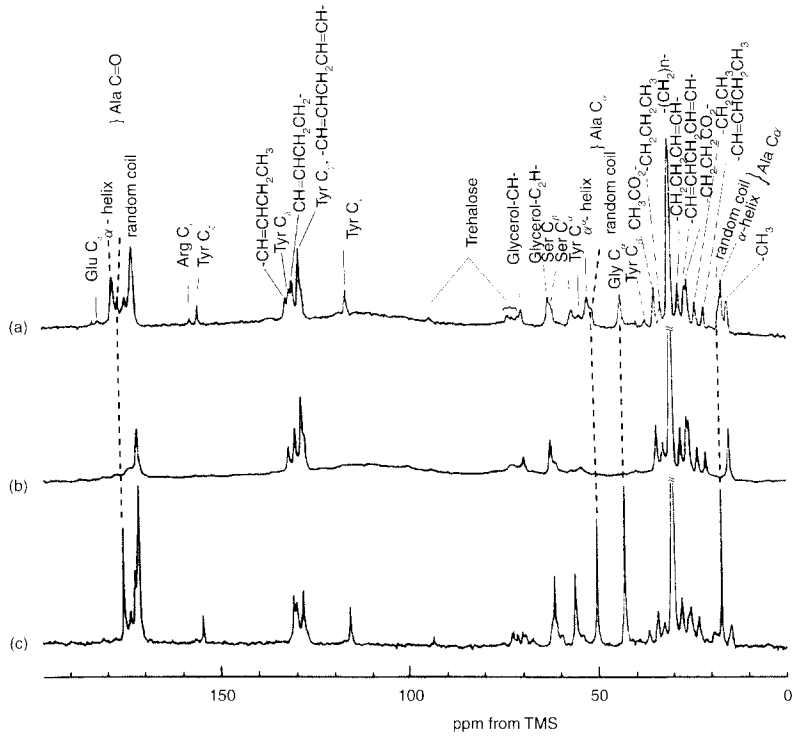

Fig. 8. ^{13}C NMR spectra of the silk gland portion of the mature larva (a) and of the abdomen of the pupa (b) of *S.c. ricini*. The spectrum of the mature larva of *B. mori* is also shown (c).

and therefore, the peaks of the amino acid residues of the silk protein are easily assigned in the spectra of both silkworms. In the NMR spectrum of *B. mori* silkworm, the spectral pattern is different from that of *S.c. ricini* silkworm, mainly in the resonance region of the carbons of the Ala residue. The shapes of the peaks from the Ala residue from *S.c. ricini* silkworm are doublets or asymmetric, indicating the presence of both α-helical and random coil conformations in the silk fibroin, as reported previously.[4,20] However, the corresponding Ala peaks of *B. mori* silk fibroin are all singlets and the peak positions coincide with those of the low-field component of the Ala C_β and of the high-field component of the Ala C_α and C=O of *S.c. ricini* silk fibroin. These data indicate that there is no α-helical portion in the silk fibroin stored in the silk gland of *B. mori* and the conformation is essentially random coil. Thus, it is possible to obtain structural information on silk fibroin from ^{13}C NMR directly, for example, by observing living *S.c. ricini* silkworm while changing the observed temperature. From direct observation of the change in the Ala C=O peak chemical shift in the silkworm when changing the temperature, α-helix-coil transition of Poly(Ala) chain has been observed directly.[33]

Direct ^{13}C NMR observations of living *B. mori* silkworms were applied to the chain dynamics studies of the silk fibroin stored in the silk gland. Figure 9 shows a series of partially relaxed ^{13}C NMR spectra of the middle silk gland portion of intact mature larva of *B. mori*.

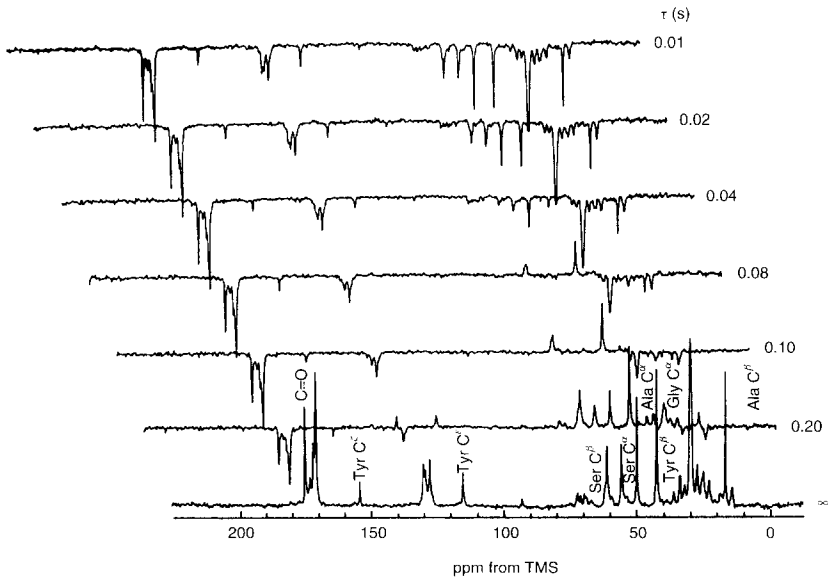

Fig. 9. Partially relaxed ^{13}C NMR spectra of the silk gland portion of intact *B. mori* mature larva. The ^1H nuclei were decoupled only during the sampling time. τ is the delay time between the 180° and 90° pulses and the waiting time was 4 s.

Detailed peak assignments have been reported elsewhere.[4,31] The plots of $M_0 - M_z$ vs τ for the carbons of the Ala, Gly, Ser, and Tyr residues are essentially single exponential. Although the presence of the silk I structure of silk fibroin in *B. mori* silkworm is considered, there is no explicit evidence of the presence of such a structure from the viewpoint of dynamics.

5. MOTION OF Gly AND Ala RESIDUES IN SILK FIBROINS IN THE SOLID STATE

Analysis of the molecular motion of the fibroin in the solid is very important in relation to understanding their physical state. The motion in silk fibroin giving

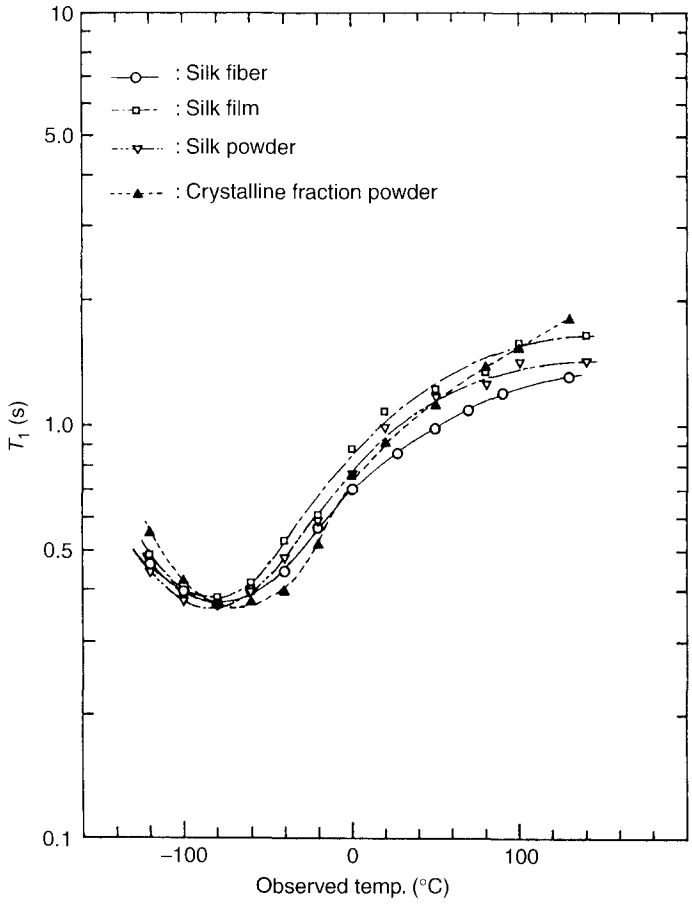

Fig. 10. Temperature dependence of ^{1}H spin–lattice relaxation times, T_1 of *B. mori* silk fibroin fiber, film, powder, and the crystalline fraction powder, in a dry system.

rise to proton relaxation is the reorientation of the methyl groups of the side-chains of Ala residues.[34,35] After a silk sample had been degassed in the NMR tube at 120°C for 12 h under vacuum, the amount of water present was negligible. Figure 10 shows the temperature dependences of the ^1H spin–lattice relaxation times of *B. mori* silk fibroin fiber, film, and powder, and the precipated fraction (Cp fraction) obtained after cleavage of the silk fibroin with chymotrypsin.[36,37]

The minimum relaxation time at 90 MHz occurs at about −70°C to −80°C, independent of the sample. This relaxation comes from the intramolecular motions because silk fibroin is essentially fixed in the solid state. The temperature of −70°C to −80°C is approximately what is expected for a process involving reorientation of the methyl groups of the Ala residues.[34,35,38–40] From the ^{13}C CP/MAS NMR analysis reported previously,[36,41–44] the silk fibroin film not treated with methanol takes predominantly random coil or silk I form while, the silk fibroin fiber and the powders are mainly in the antiparallel β-sheet form. Thus, it was concluded that the curves of T_1 versus observed temperature including the T_1 minimum are independent of the silk fibroin conformation. Figure 11 shows the recovery of magnetization in a typical inversion recovery experiment, indicating a single T_1 value at temperatures of −120°C to −130°C.

The magnetization decay in solid-echo experiments also shows a single Gaussian decay (11 μs) (Fig. 12).

These results indicate that segmental motions of the samples do not occur and therefore, cannot contribute to the relaxation process.[34,35,38–40] As mentioned

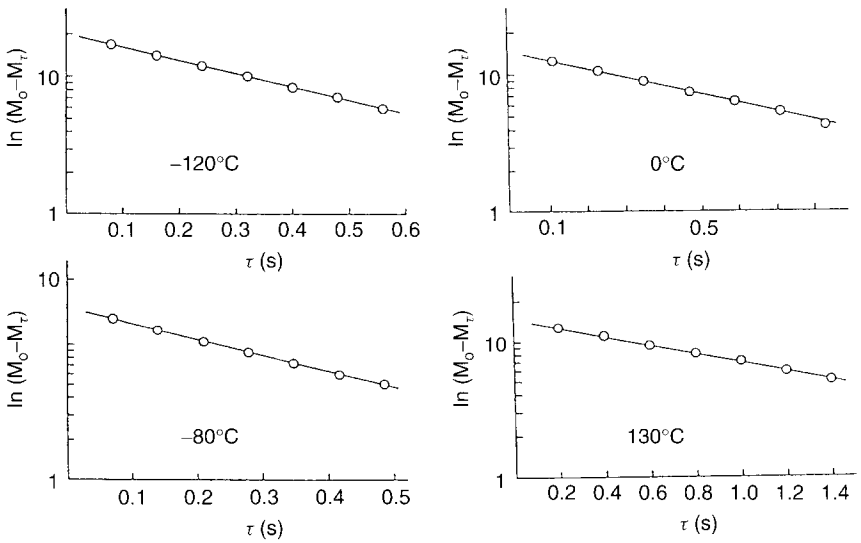

Fig. 11. Plots of $\ln(M_0 - M_t)$ vs. τ of dried *B. mori* silk fibroin powder at −120, −80, 0, and 130°C, where M_0 is the equilibrium amplitude of the fully relaxed spectrum, M_τ is the amplitude of a partially relaxed spectrum, and τ is the delay time between the 180° and 90° pulses.

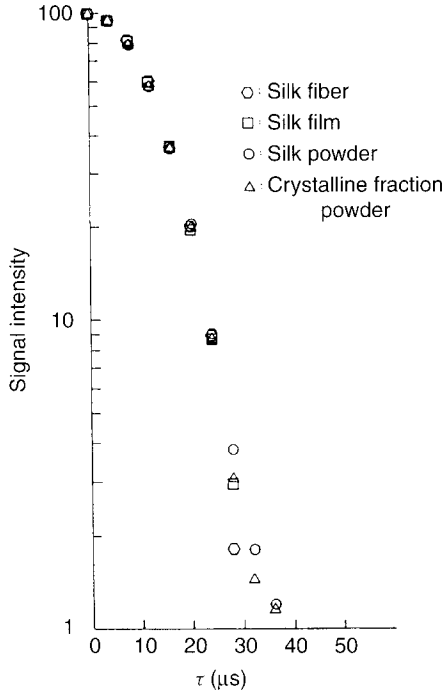

Fig. 12. Solid-echo decays of *B. mori* silk fibroin fiber, film, powder, and the crystalline fraction powder, in dry systems. Observation temperature was 23°C.

above, only the rapid rotation of the methyl groups of the Ala residues is needed to explain these results. This coincides with the results from solid-state ^{13}C CP/MAS[41] and ^{2}H NMR,[44] as will be described in the following sections, although the samples contained around 5–10 w/w% water because the special drying treatment of the silk fibroin samples was not carried out. The ^{1}H T_1 values (<1 s) of Ala C_β in silk fibroin were observed and ascribed to the C_3 rotation of the methyl group. This assignment is also in agreement with the small separation of ^{2}H quadrupole splitting, 39 Hz observed for [Ala-3,3,3-$^{2}H_3$] silk fibroin by ^{2}H NMR. The separations of the splitting were the same for silk fibroins with α-helix, silk I, and silk II conformations. On the other hand, the T_1 values of the α carbons of Ala and Ser residues are very similar (11–18 s) and independent of secondary structure. Further, the T_1^C values of the α carbon of the Gly residue in fibroin are slightly longer (20–25 s) than those of Ala and Ser residues. This was not unexpected because there exists no rapid segmental motion whose correlation time is of the order 10^{-8} s, which is effective as a relaxation pathway. Therefore, it was concluded that T_1 times of backbone carbons in *B. mori* silk fibroin in the solid state are determined mainly by dipolar coupling with protons undergoing rapid intramolecular reorientation, such as C_3 rotation of the methyl group.

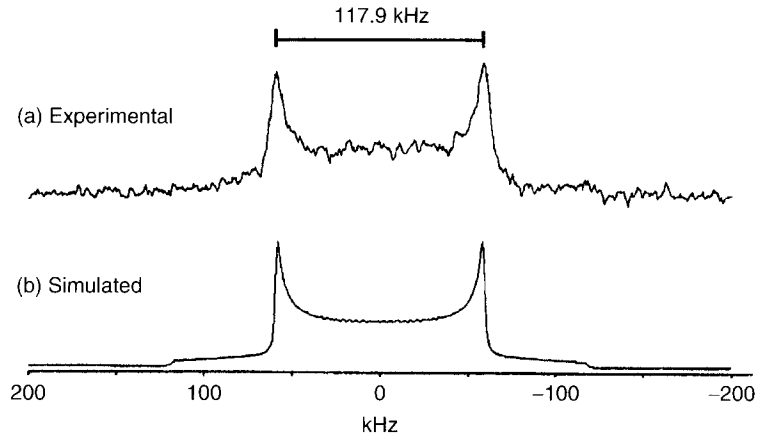

Fig. 13. Observed (a) and simulated (b) ^{2}H NMR powder pattern of [2,2-$^2H_2$]Gly labeled silk fibroin fiber from *B. mori*.

Dynamic of [2,2-$^2H_2$]Gly residue of *B. mori* silk fibroin fiber were analyzed from solid state ^{2}H NMR powder pattern as shown in Fig. 13.

The splitting of $\Delta\nu_Q = 117.9$ kHz is slightly smaller than the expected rigid-lattice value of about 126 kHz. This indicates that the methylene group of the Gly residue is essentially restricted in space and undergoes only some-amplitude vibrational motion at room temperature.[45] Figure 13(b) shows the spectral simulation of [2,2-$^2H_2$]Gly residue by assuming vibrational motion for $C_\alpha - ^2H$ bonds of amplitude 12° with rate 10^3 Hz. This result is in agreement with the prediction from the intermolecular hydrogen bonding network in the silk fibroin backbone with an antiparallel β-sheet conformation.

A ^{2}H NMR study of [3,3,3-$^2H_3$]Ala labeled *B. mori* silk fibroin fiber has been carried out by Asakura *et al.*[45] and Fig. 14 shows the ^{2}H NMR powder pattern of [3,3,3-$^2H_3$]Ala labeled *B. mori* silk fibroin.

This sample gives a splitting of $\Delta\nu_Q = 37.9$ kHz, and this splitting for the [3,3,3-$^2H_3$]-Ala residue is of the same order of magnitude as those seen in the *B. mori* silk fibroin with silk I form, the α-helical sample obtained as dried liquid silk removed from the middle silk gland and the cocoon from *S.c. ricini*.[44] The value of the powder splitting indicates a fast three-fold rotation of the Ala methyl group (10^8 Hz) about its $C_\alpha - C_\beta$ axis with small angle libration (10°) (Fig. 14b).

The determination of such NMR relaxation times as $^H T_{1\rho}$ is a well-established technique to probe the degree of mixing and the presence of phase separation in a sample. Relaxation in the rotating frame is governed by fluctuating local fields in the kHz range. The decrease in signal intensities for Gly C_α and C=O, Ala C_α, C_β and C=O of *B. mori* with silk II form and *S.c. ricini* with α-helix form as a function of spin-lock time (between 0 and 20 ms) in the resonant rf fields of

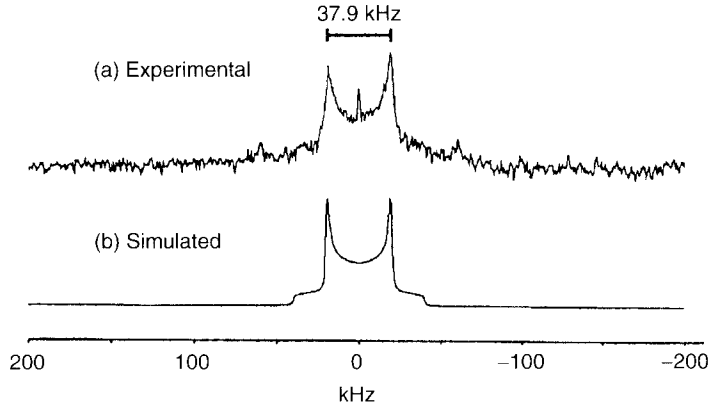

Fig. 14. Observed (a) and simulated (b) ^{2}H NMR powder pattern of [3,3,3-$^2H_3$]Ala labeled silk fibroin from *B. mori*.

Table 2. Observed $T_{1\rho}^{H}$ (ms) values of *B. mori* silk fibroin

	B. mori		*S.c. ricini*	
	$B_1 = 27$ kHz	$B_1 = 50$ kHz	$B_1 = 27$ kHz	$B_1 = 50$ kHz
Ala C_β	4.8	10.8	4.4	7.7
Gly C_α	5.0	10.2	3.7	7.6
Ala C_α	5.4	10.6	4.4	8.2
Gly C=O	6.0	10.8	2.4	5.9
Ala C=O	5.4	10.6	3.5	7.9

27 and 50 kHz were plotted and the data were fitted. The best-fit values for the $^H T_{1\rho}$ attached to different types of carbons are given in Table 2. These values are approximately independent of the species of the carbons. The short relaxation time constant of $^H T_{1\rho}$ suggests that spin diffusion results in the relaxation of all protons by a single efficient relaxation mechanism, probably rotation of the Ala methyl group.

6. MOTION OF Ser RESIDUE IN SILK FIBROINS IN THE SOLID STATE

In both kinds of *B. mori* and *S.c. ricini* silk fibroins, the relatively abundant Ser residue is of particular interest, as it carries a hydroxyl group which may engage in hydrogen bonding and thus contribute to the stability of the fiber. Therefore, it is important to clarify the structure and dynamics of the Ser residue including the side-chain. In *B. mori* fibroin about 75% of all Ser residues occur within the sequence of the repetitive region, which is considered to be the crystalline

domain of fibroin.[46] In contrast, in *S.c. ricini*, all of the Ser residues are found in the Gly-rich region of the sequence which might be expected to have less tendency to assume any defined secondary structure.

T_1^C measurements of ^{13}C NMR peaks of C_α and C_β carbons of Ala and Ser residues in *B. mori* silk fibroin with silk I form were performed[47] using the methods proposed by Torchia.[48] Semilog plots of the peak intensities $M_{cp}(t)$ vs t give rise to single straight lines, except for Ser C_β (Fig. 15).

The plots of Ser C_β signals from silk I are not composed of a single line but a composite of two lines with shorter and longer T_1^C. The shorter T_1^C was obtained by a plot of peaks (closed circles) after contributions of the longer T_1^C were subtracted (closed squares). The remaining peaks however, were found to decay

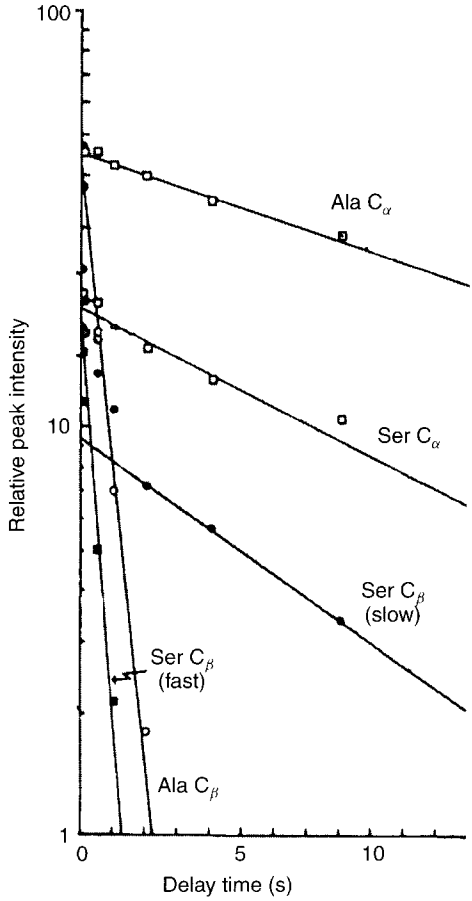

Fig. 15. Plot of relative ^{13}C peak intensities of silk I form *B. mori* silk fibroin vs delay time. Plots of peak intensities for Gly residue are omitted. For separation of Ser C_β into two components.

as approximated by single line. The T_1^C values of Ala, Gly and Ser residues in *B. mori* and *S.c. ricini* fibroins and model oligopeptides of the crystalline fraction of the *B. mori* fibroin are summarized in Table 3.

In all cases, the T_1^C curves of Ser C_β are not approximated by a single line but by a composite of two lines, with shorter and longer T_1^C values. The T_1^C values of Ala and Ser C_α carbons are very similar (10–18 s) among the peptide and fibroins used, irrespective of the difference in the primary and secondary structures. Further, the T_1^C values of Gly C_α in fibroin are slightly longer (20–25 s) than those of Ala and Ser residues. This is not unexpected because no rapid backbone motion exists whose correlation time is on the order of 10^{-8} s, which is effective as a relaxation pathway. Much slower motion, if any, cannot be detected by this sort of relaxation time in the laboratory frame. Therefore, spin–lattice relaxation times of backbone carbons in these polypeptides and proteins are mainly determined by dipolar couplings with proton(s) undergoing rapid intramolecular reorientation, such as the C_3 rotation of the methyl group. The effectiveness of this relaxation pathway varies as a function of r^6 where r is the distance between the carbon and proton in question. Therefore, this effect can be visualized by the observation of a gradual reduction of the T_1^C values from the carbons near the backbone to a site nearer to the methyl or other groups undergoing internal motions.[49] The observation of such a T_1^C gradient is a very useful means for confirming assigned peak.[49] As summarized in Table 3, the T_1^C values of Ser C_β are observed as a composite of two components in all samples of fibroin irrespective of the differences in the conformations. Undoubtedly, the component which gives rise to the longer T_1^C value is ascribed to hydroxymethyl groups

Table 3. Observed T_1^C values (s) of silk fibroins from various sources

	C_α			C_β		C=O		
	Ala	Gly	Ser	Ala	Ser	Ala	Gly	Ser
Silk I								
Cp fraction	15	25	13	0.54	0.50(S) 8.5(L)	48	57	38
Silk II								
Cp fraction	14	20	11	0.53	0.56(S) 31(L)	20(N)	46	20(N)
lyophilized	17	22	18	0.33	0.63(S) 37(L)	32(N)	51	32(N)
Boc-(GSGAGA)$_2$-Obzl	11	15	12	0.38	1.1(S) 25(L)	14(N)	36	14(N)
α-helix (*S.c. ricini*)								
cast film	16	13		0.98				
β-sheet (*S.c. ricini*)						24	33	
cast film	15	17		0.82		19(N)	19(N)	19(N)

(S) Shorter T_1 component, (L) Longer T_1 component, (N) Not resolved.

participating in various types of hydrogen bonds because the spin–lattice relaxation times in the solid are at the low-temperature site. On the basis of the survey of X-ray diffraction data on many globular proteins, Janin *et al.*[50] and Gray and Matthews[51] showed that approximately 70% of the Ser residue have their O_γ atom within hydrogen-bonding distance (3.5 Å) of at least one carbonyl group, with an acceptable angular geometry for the $OH\cdots O{=}C$ bond. The presence of such hydroxymethyl groups in the Ser residue in the *B. mori* fibroin was previously ascribed to a component that gives rise to a static ^2H powder pattern spectra of [Ser-^{2}H]-fibroin with a quadrupole splitting of 125 kHz (~70%).[44,52] On the other hand, the remaining component (~30%) giving rise to reduced quadrupole splittings of less than 35 kHz in ^2H NMR spectra, was ascribed to the Ser hydroxymethyl group which undergoes rapid internal rotation about an axis of the $C_\beta-C_\gamma$ bond and is not involved in any type of hydrogen bonding. Therefore, it is now clear that the above-mentioned rapidly relaxing component of the Ser residue can be undoubtedly ascribed to the Ser group not involved in any type of hydrogen bonding. The relative proportion of this component is roughly estimated as less than 50% on the basis of the relative peak intensity extrapolated at time zero (see Fig. 15), although quantitative evaluation of the relative proportion from this plot is not easy because of several types of uncertainty involved. In any case, it is interesting to note that such an estimated value is roughly in accordance with the data from ^2H NMR powder patterns of [Ser-^{2}H]-fibroin, as described above.

The presence of such a free Ser hydroxymethyl group as a component giving rise to rapidly relaxing species however, seems to be very important as a site for hydration in stabilizing the silk I form. In other words, a solvent-induced conformational change could be associated with the destabilization of the silk I or silk I type form as a result of dehydration.

Recently, Kameda *et al.* characterized and compared the Ser side-chain dynamics of *B. mori* and *S.c. ricini* silk fibroin using solid-state ^2H NMR.[55] A detailed lineshape analysis has provided quantitative data on the rate of motion and on the fractions of two distinct dynamic populations. In addition, the torsion angle of the Ser $C_\alpha-C_\beta$ bond and its orientational distribution was measured in uniformly aligned silk fibers. Figures 16(a) and (b) show the ^2H NMR spectra of [3,3-$^2H_2$]Ser-labeled silk fibroin from *B. mori* and *S.c. ricini*, respectively.

The powder patterns (a) and (b) of the non-oriented silk fibers display no appreciable difference between *B. mori* and *S.c. ricini*. Both proteins give rise to the same set of quadrupole splittings of about 35.5 and 109.3 kHz. The inner component with a splitting of 35.5 kHz stems from Ser side-chains undergoing rapid rotational motion, while the outer splitting represents comparatively immobile residues. A small central peak at zero frequency must be attributed to residual ^2HHO in the sample.[56] The lineshapes of Figs 16(c) and (d) were simulated using the MXQET program developed by Greenfield *et al.*[57] where the exchange rate and libration angle are calculated on the basis of appropriate dynamic models. The experimental spectra could be properly fitted as a sum of three components: namely the two types of notionally distinct Ser side-chains, plus a small

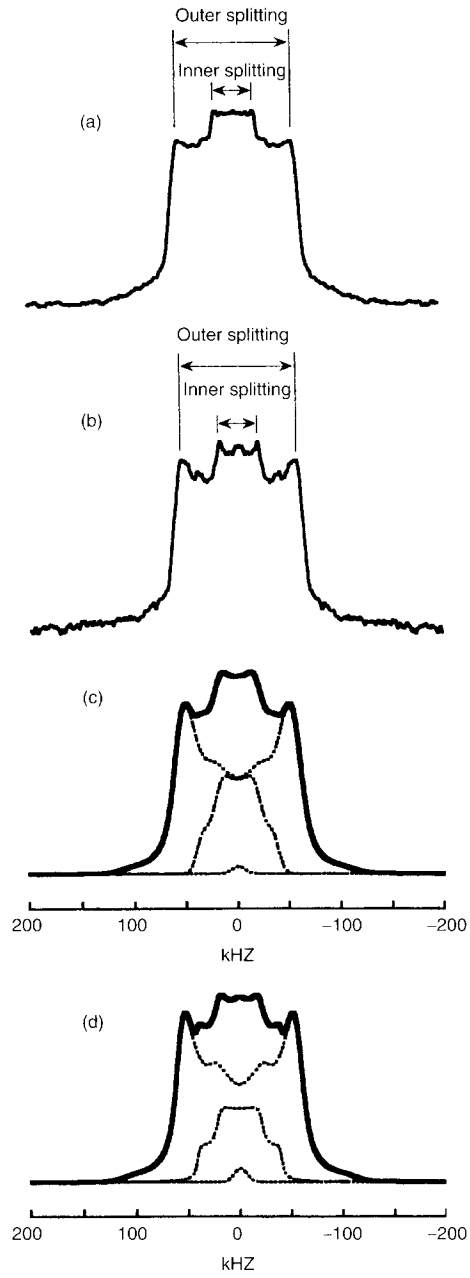

Fig. 16. Experimental ^2H NMR powder spectra obtained from [3,3-$^2H_2$]Ser-labeled *B. mori* (a) and *S.c. ricini* (b) silk fibroin. The respective line shapes (c) and (d) were simulated on the basis of a three-site jump model, showing one fast and one slow motion component each, plus a small contribution of ^2HHO.

Table 4. Powder pattern line shape simulation results of ^2H quadrupole experiments for [3,3-$^2H_2$]Ser-labeled *B. mori* and *S.c. ricini* silk fibroins

Component	Rate (Hz)	Occupancy	Libration (deg)	Fraction(%)
		B. mori		
fast	1×10^6	(33 : 33 : 33)	0	25
slow	5×10^3	(90 : 5 : 5)	15	75
		S.c. ricini		
fast	1×10^6	(33 : 33 : 33)	0	22
slow	5×10^3	(80 : 10 : 10)	15	78

^{2}HHO contribution with a Gaussian lineshape. The best-fit parameters of these simulations are summarized in Table 4.

As shown in Fig. 16(c), the spectrum for *B. mori* could be well simulated assuming that the slow motional component contributes 75% and the rigid component 25% of the total intensity (see Table 4). The slow motional component was simulated assuming a discrete three-site jump of the Ser side-chain, with unequal occupancies (90 : 5 : 5 ratio) and a small librational amplitude. The fast component of *B. mori* satisfies a rapid three-site jump with equal occupancies. Likewise, the spectrum for *S.c. ricini* in Fig. 16(d) could be simulated with 78% corresponding to a slow three-site jump with unequal occupancies (80 : 10 : 10 ratio) and a small librational amplitude, while the remaining 22% arise from a rapid three-site jump. Interestingly, these results indicate that there are no significant differences in the respective dynamic populations of *B. mori* and *S.c. ricini* silk fibroins, despite their unrelated amino acid sequences.

The motional freedom of the Ser side-chain is expected to be severely constrained by hydrogen bonding between the hydroxyl group and adjacent backbone atoms. Therefore, the component with the rapid three-site jump is interpreted to arise from Ser residues that do not form hydrogen bonds. The groups involved in inter- and/or intrachain hydrogen bonding, on the other hand, are attributed to the slow motional component. From the ^2H NMR measurements of uniaxially aligned [3,3-$^2H_2$] Ser-labeled *B. mori* silk fiber, with the fiber axis set parallel and perpendicular to the magnetic field direction, it was found that the dominant conformer of the Ser side-chain of *B. mori* silk fibroin exists in the g^+ conformation.[55] This g^+ conformation is a good candidate for forming intermolecular hydrogen bonds with carbonyl groups on adjacent protein chains. Based on these results, it is apparent that about 3/4 of all Ser side-chains form hydrogen bonds both in *B. mori* and in *S.c. ricini*, this fraction being almost the same despite the difference in molecular structure. They note that intermolecular hydrogen bonding between Ser and carbonyl groups on adjacent protein chains can occur irrespective of the primary and secondary structure because the hydroxyl group is rather flexible. Therefore, the similar ratio of hydrogen-bonded compared to free hydroxyl groups in *B. mori* and *S.c. ricini* is consistent with a

similar interchain environment around serine, despite its different abundance and distribution in the amino acid sequences.

7. MOTION OF Tyr RESIDUE IN SILK FIBROINS IN THE SOLID STATE

The Tyr residue in the *B. mori* silk fibroin present in the repetitive region is about 80% of the total Tyr content. Besides its presumed role in hydrogen bonding, the Tyr residue also plays an important role as an active site for covalently immobilizing enzymes to silk fibers.[58,59] *S.c. ricini* consists of a polyalanine ((Ala)n; $n = 10-14$) which is followed by a Gly-rich sequence containing the bulky residues, as reminiscent of spider dragline silk.[60] The Tyr residue exists mainly in the Gly-rich environment and approximately 60% of all Tyr in the sequence is present as -Tyr-Gly-Gly-Gly- or -Gly-Gly-Gly-Tyr-.[61]

Figures 17(a) and (b) show the experimental ^{2}H-NMR spectra of [3,3-$^2H_2$]Tyr-labeled *B. mori* and *S.c. ricini* silk fibroin, acquired with a recycle delay of 10 s.

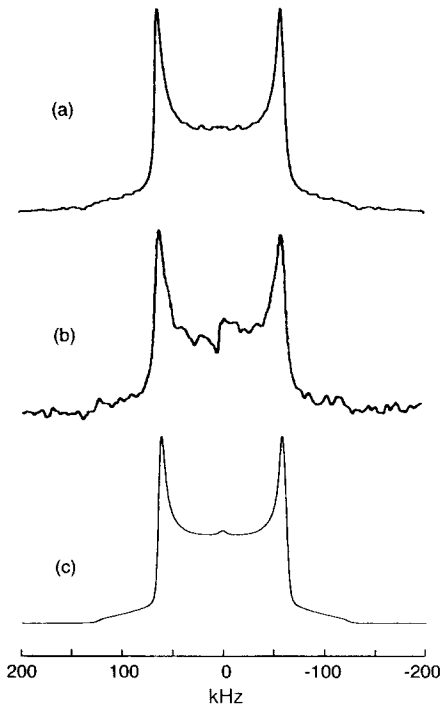

Fig. 17. Experimental (a, b) and simulated (c) solid-state ^{2}H NMR spectra. (a) [3,3-$^2H_2$]Tyr-labeled silk fibroin *B. mori*; (b) [3,3-$^2H_2$]Tyr-labeled silk fibroin *S.c. ricini*; (c) spectral simulations based on a three-site jump model. A 164 kHz quadrupole coupling constant was assumed and a rate constant of 10^3 Hz.

Figure 17(c) illustrates the same powder lineshape, simulated with an asymmetry parameter of 0.00 and a quadrupole coupling constant $Q_{cc} = 164\,kHz$. Based on the model of a three-site jump around the $C_\alpha - C_\beta$ bond, a rate constant of $1.0 \times 10^3\,s^{-1}$ was used. The agreement between the observed (Figs 17(a) and (b)) and simulated (Fig. 17(c)) spectra is good, indicating that rotation about the $C_\alpha - C_\beta$ bond axis can be considered to be essentially static for both *B. mori* and *S.c. ricini* silk fibroins. As will be described below, a large proportion of the Tyr rings undergo fast π-flips with a rate constant of $10^6\,s^{-1}$. Therefore, the predominant side-chain dynamics of Tyr in silk fibroin is restricted to the phenolic ring.

Figures 18(a) and (b) show the experimental (. . . .) and calculated (_____) ^{2}H-NMR spectra for *B. mori* and *S.c. ricini*, respectively, with recycle delays of 10 s.

Because of their two-fold symmetry, the phenolic side-chains of Tyr can execute a π-flip motion about the $C_\beta - C_\gamma$ bond between two orientations of locally equal energy. Generally, the effect of molecular motion reduces the quadrupole coupling to a time-averaged value which is smaller than the rigid lattice constant. Thus, the small inner doublet with a splitting of 30 kHz, which is observed both for *B. mori* and *S.c. ricini* silk fibroin, is attributed to a fast

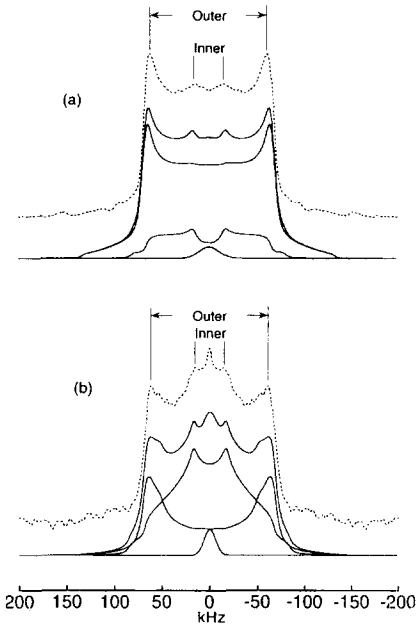

Fig. 18. Experimental (. . . .) and calculated (_____) solid-state ^{2}H NMR spectra of [3′,5′-$^2H_2$]Tyr-labeled *B. mori* (a) and *S.c. ricini* (b) silk fibroin. Spectra were obtained with the quadrupole echo pulse sequence with repetition times of 10 s, and simulation parameters are summarized in Table 5.

π-flip motion of the phenolic ring about its symmetry axis. In contrast, the outer doublet with a splitting of 123 kHz corresponds to a slow motional component. A central peak at zero frequency in Fig. 18 is attributed to residual ^{2}HHO in the silk sample,[56] which can be taken into account in the peak simulation by a Gaussian function. The fraction of the ^{2}HHO component was assumed to be 0.8 and 2.5% of the total spectral intensity, for *B. mori* and *S.c. ricini*, respectively. A comparison of Figs 18(a) and (b) shows that the lineshapes differ significantly from one and other, indicating that the manner of the Tyr π-flip motion must also be different. Hence, a simulation analysis was carried out using the MXQET program from Greenfield *et al.*,[57] assuming a two-site jump model and using the exchange rate and librational angle as variables. The lineshapes of both *B. mori* and *S.c. ricini* fibroins were simulated with a asymmetry parameter $\eta = 0.05$ and a quadrupole coupling constant $Q_{cc} =$ 180.0 kHz. At least two components were required to obtain a good fit, which can be considered as rigid and as mobile on the deuterium NMR time scale. This interpretation is supported by the changes in the spectra as a function of the recycle delay. The rates obtained from the simulated are compiled in Table 5.

The ^{2}H-NMR spectrum of *B. mori* [3′5′-$^2H_2$]Tyr-labeled silk fibroin can be satisfactorily simulated by assuming a fast motional component (1.0×10^6 Hz) that contributes 20% of the intensity, and a slow motional component (1.0×10^3 Hz) that contributes 80%. The respective proportions of the fast and slow populations were estimated by integrating the corresponding spectra.

A rotational jump of the phenolic ring is necessarily influenced by the degree of co-operation with the motions of surrounding groups, because the rotation of a bulky group must displace neighboring side-chains to some extent. Hence, the rate of the Tyr ring flip can provide information about the conformational space around this particular side-chain. Since the repetitive region of a silk has a densely packed structure, the dynamics of the Tyr side-chain are expected to be restricted in this region. Therefore, the Tyr residue in the repetitive and non-repetitive regions can be attributed to the slow and the fast motional components, respectively. Indeed, about 80% of all Tyr residues of *B. mori* silk fibroin exist as a (-Gly-Ala-Gly-Tyr-Gly-Ala-Gly-) sequence in the repetitive region, which quantitatively agrees with the proportion given in Table 5.

Table 5. Powder pattern simulation results of ^{2}H quadrupole-echo line shapes for [3′,5′-$^2H_2$]Tyr-labeled *B. mori* and *S.c. ricini* silk fibroin

	B. mori			*S.c. ricini*		
Component	Rate (Hz)	Libration (deg)	Fraction (%)	Rate (Hz)	Libration (deg)	Fraction (%)
fast	1×10^6	0	20	1×10^7	0	60
slow	1×10^3	10	80	1×10^4	20	40

Also, for *S.c. ricini* silk fibroin there is a slow and fast motional component observed for the Tyr phenolic ring. Table 5 summarizes the parameters obtained by simulating the corresponding ^2H spectrum of Fig. 18 (b). About 60% of the intensity is represented by a fast motional component (1.0×10^7 Hz) and 40% by a slow motional one (1.0×10^4 Hz). Similar to *B. mori* silk fibroin, these populations of phenolic rings with different flip rates are attributed to high and low density packing regions. Therefore, this result provides evidence that also in the Gly-rich sequence of *S.c. ricini*, there are high and low density packing regions. Tyr residues exist in both of these regions and about 60% of the Tyr residues are present in the low density region and the other 40% in the high density region. This dynamic information is useful for the prediction of the secondary structure of the Gly-rich domain in *S.c. ricini* silk fibroin. More recently, we have quantitatively analyzed the orientational distribution of Ala and Gly residues in *B. mori* silk fibroin in the cocoon[62] and in highly-drawn *S.c. ricini* fibers,[63] demonstrating that over 60% of all Gly residues are oriented both in *B. mori* and in *S.c. ricini*. However, the degrees of orientation in *B. mori* and *S.c. ricini* were different, as the Gly-rich region of *S.c. ricini* exhibits a lower degree of orientation than the repetitive region of *B. mori* silk fibroin. This comparatively reduced quality of alignment in the Gly-rich domain of *S.c. ricini* silk fibroin appears to correlate with the increased proportion of the Tyr residues undergoing fast π-flip motions. As described above, the molecular dynamics of phenyl rings in solids have been extensively investigated by solid-state NMR, and indicated that almost all of the rings are either rigid or undergo a π-flip motion at room temperature, depending on the crystalline packing.

Hiraoki *et al.* investigated the phenyl ring dynamics of poly(L-phenylalanine) using ^2H-NMR,[64] showing that it is characterized by a fairly broad distribution of correlation times. The mean correlation time of this distribution was 1.2×10^6 Hz at 25°C, which is close to that of the fast motional component of the *B. mori* and *S.c. ricini* silk fibroins. The Tyr ring flip in the pentapeptide [Leu^5] enkephalin was reported to be 5.6×10^4 Hz at 25°C,[65] which is close to that of the slow motional component observed here for silk fibroin. On the other hand, the ring motion in crystalline N-acetyl-L-Asp-L-Pro-L-Tyr-N′-methylamide was found to be 1.1×10^6 Hz at 27°C,[66] close to that of the fast motional component of the silk fibroins.

In conclusion, solid-state NMR analysis was applied to measure the side-chain dynamics of the tyrosine residues in silk fibroin from *B. mori* and *S.c. ricini*. It was concluded that the Tyr phenolic rings are engaged in fast and in slow π-flip motions, with different proportions. Since 80% of all Tyr residues of *B. mori* are known to exist in the repetitive region of *B. mori* silk fibroin, the observed mobility differences suggest that the reduced mobility correlates with a high packing density in the repetitive regions. Also in *S.c. ricini* silk fibroin there are slow and fast motional components observed for the Tyr phenolic ring. Therefore, it is likely that the Gly-rich domains of *S.c. ricini* also contain regions with high and low packing densities. The Tyr residues exist in both of these regions, with

about 60% present in the low-density region and the remaining 40% is in the high-density region.

8. STRUCTURAL TRANSITION OF *S.c. ricini* SILK FIBROIN

The detailed behavior of the transition is important in understanding the mechanism of producing silk fibroins. The structural transition in the liquid silk of *S.c. ricini* was monitored using solution and solid-state ^{13}C NMR spectroscopy.[24,67] The primary structure of silk fibroin from *S.c. ricini* is composed of polyalanine regions and glycine-rich regions alternately.[20,24,28,63] So far, it has been clarified that up to 70% of the polyalanine regions of the liquid silk of *S.c. ricini* assumes an α-helix structure and the remainder a random coil structure.[24,28]

^{13}C solution NMR spectra of *S.c. ricini* silk fibroin protein were observed between -5 and $+50^{\circ}C$ as a function of temperature.[24] Figure 19 shows the Ala C_α, Gly C_α and Ala C_β resonance regions. Peaks 'c' and 'h' were assigned to random coils and to a fast exchange between helical and random coil states. All peaks become sharp with increasing temperature, indicating an increase in the segmental motion of the protein. In addition, a reduced signal-to-noise ratio between 40 and $50^{\circ}C$ indicates partial formation of aggregates with β-structure (no signal appears for the aggregates).[68] Most striking is the dramatic change observed in the Ala resonance region. The upfield component of the Ala C_β peak, marked 'h', shifts gradually downfield 0.5 ppm and the downfield component 'h' of the Ala C_α peak shifts upfield 1.0 ppm as the temperature is increased from -5 to $+50^{\circ}C$, but other peaks marked c and the Gly C_α peak show almost no temperature dependence. A similar spectral change was also observed in the carbonyl region (Fig. 20).[24]

The peaks marked 'h' and 'h*' were assigned to the Ala carbonyl carbons in the helical states of the internal and terminal residues in the -$(Ala)_n$- sequence, respectively.[20] The peaks marked 'c' were assigned to the Ala carbonyl carbons in the coil state. Peak 'h' shows a gradual upfield shift of 1.8 ppm as the temperature is increased from -5 to $+50^{\circ}C$, but peak 'c', which was assigned to the coil state, shows almost no temperature dependence. This behavior corresponds to that observed for the Ala C_α and C_β resonances. When exchange between the helical and coil states does not occur in peak 'h', the chemical shift differences between the 'h' and 'c' peaks are 2.3 ppm for the carbonyl carbon, 1.9 ppm for the C_α, carbon and 1.1 ppm for the C_β carbon. The individual Gly carbonyl resonances reflecting the sequence show no temperature dependences as also do the Tyr and Ser carbonyl carbon resonances.

In the 'double peaks', the low-field peaks of the C_α and carbonyl carbons shift upfield 1.0 and 1.5 ppm, respectively, while the upfield peak of the C_β carbon shifts downfield 0.5 ppm as the temperature is increased from -5 to $+50^{\circ}C$. However, other peaks show no temperature dependence. In addition, exchanges

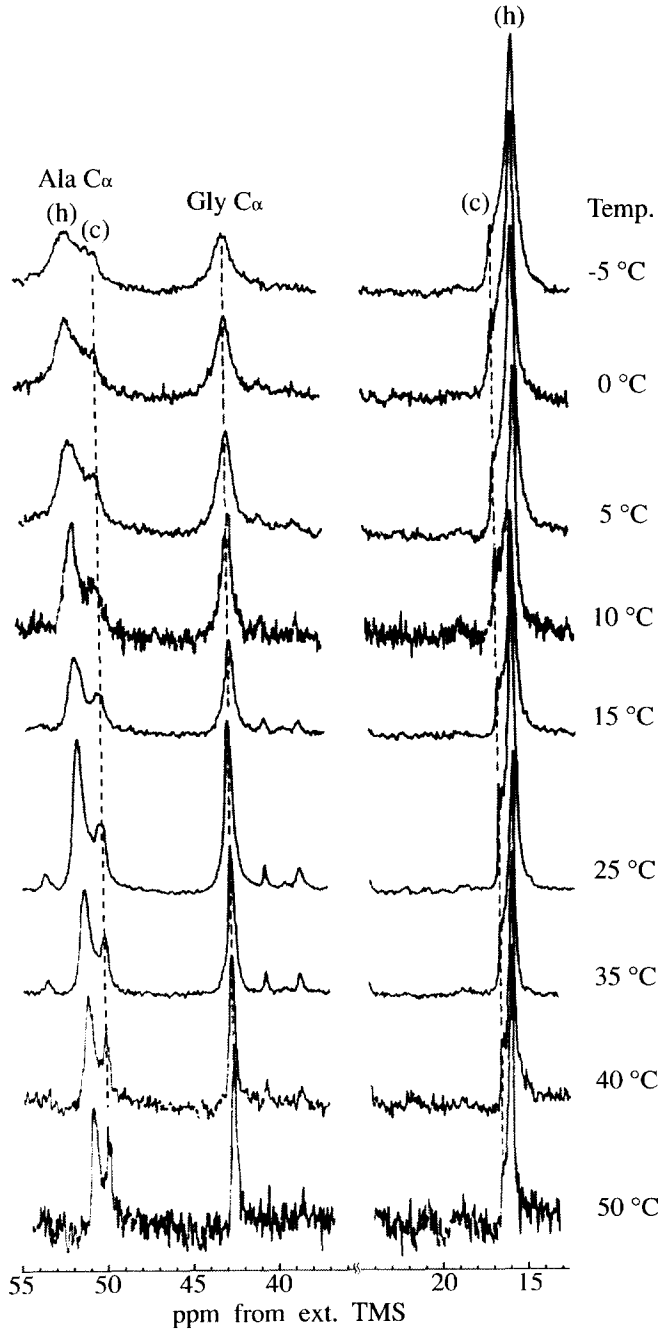

Fig. 19. ^{13}C NMR spectra of *S.c. ricini* liquid silk in the aliphatic region as a of temperature.

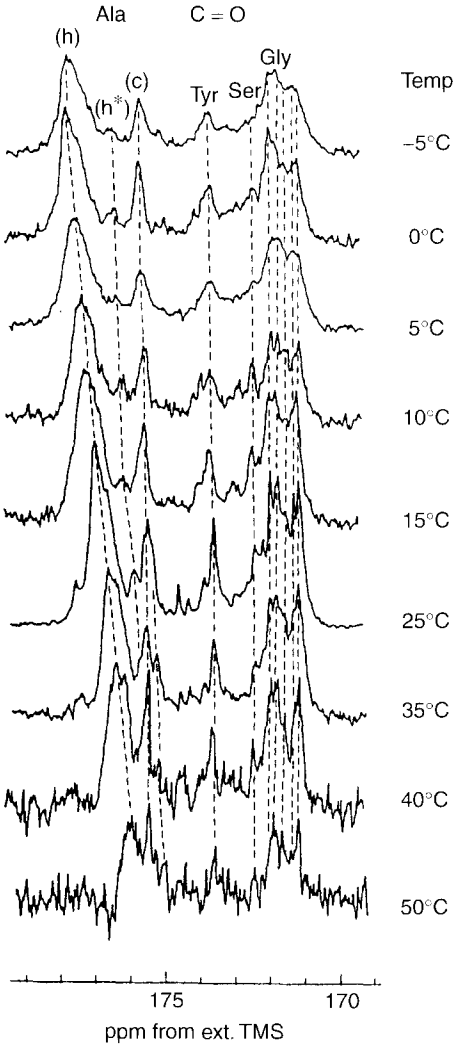

Fig. 20. ^{13}C NMR spectra of *S.c. ricini* liquid silk in the carbonyl region as a function of temperature.

between the individual peaks do not occur. It was concluded that the temperature-dependent peaks are attributable to the -$(Ala)_n$- sequences whose lengths are long enough to form an α-helix and reflect fast exchange with respect to the chemical shift between the helix and coil conformations.[24] On the other hand, the temperature-independent peaks 'c' are attributable to isolated Ala residue. The helix content of *S.c. ricini* silk fibroin determined from the ^{13}C NMR spectra as a function of temperature on the basis of these assignments is in quantitative

agreement with values reported for the CD spectra for *Antheraea pernyi* silk fibroin, whose amino acid composition resembles that of *S.c. ricini* silk fibroin very closely, strongly supporting the assignment of ^{13}C NMR spectra made here. A similar trend was observed for the urea-induced helix–coil transition of the protein. Thus, the conformational change is local and occurs only for the -$(Ala)_n$- sequence, 34% of all residues; other residues remain unaffected by the change. The spin–lattice relaxation data yield fast segmental motion of the backbone chain of 3.5×10^{-10} s at 25°C, which is of the same order as determined for *B. mori* silk fibroin.

The silk fibroins show structural changes from liquid state to solid state.[69] The mechanism of such changes has not been scrutinized because it is difficult to analyze the states of materials of interest using a single instrument simultaneously. In this sense, NMR spectroscopy may be useful to trace both the states in liquid and solid: the liquid part of the material is detected using a ^{13}C single-pulse ^{1}H dipolar-decoupled magic-angle spinning (DD/MAS) method, whereas the solid part is observed using a ^{13}C cross-polarization magic-angle spinning (CP/MAS) method, and these methods are alternately applied with a single solid-state NMR spectrometer.

As described above, the liquid silk is known to accomplish the transition from α-helix to β-sheet (β-transition), the latter structure of which is comparatively rigid and so detected by CP/MAS.[41] In a time series of alternate measurements of DD/MAS and CP/MAS, details of the structural change between these two states were detected. A 50 kHz RF field strength was used for decoupling, with decoupling period of 12.5 ms. A CP contact time of 5 ms was employed. The liquid silk of *S.c. ricini* initially takes a mobile α-helix structure and finally it aggregates to assume a rigid β-sheet structure.[20,24,28,41,63] Hence, NMR lines are first observed in DD/MAS experiments and then the solid components are detected in CP/MAS experiments. Figure 21 shows DD/MAS and CP/MAS spectra of the liquid silk, immediately after it was collected and after around 100 hours.

The former indicates all the expected lines in the DD/MAS spectrum and substantially no peaks in the CP/MAS spectrum, confirming the material to be in a mobile state. On the other hand, the resonance lines observed after 100 hours appear only in the CP/MAS spectrum, characterizing the β-state.

The 100-hour transient state leading to the β-sheet structure requires some clarification in details. For this purpose, we focus on two resonance lines: one is the C_β peak of the Ala side-chain and the other the C_ε peak of the tyrosine residue. By monitoring the peak of the Ala residues contained in the silk fibroin, we can trace changes in its overall molecular motions; among the peaks of Ala, the C_β peak is sensitive to the change of these motions.[24] On the other hand, Tyr has a bulky aromatic side-chain and thereby may be influenced by the change in its circumstances following molecular aggregation to the β-sheet structure.

Figure 22 shows the Ala C_β peak in a time series of DD/MAS and CP/MAS spectra. Within 100 hours from the start, DD/MAS spectra show a C_β peak whose

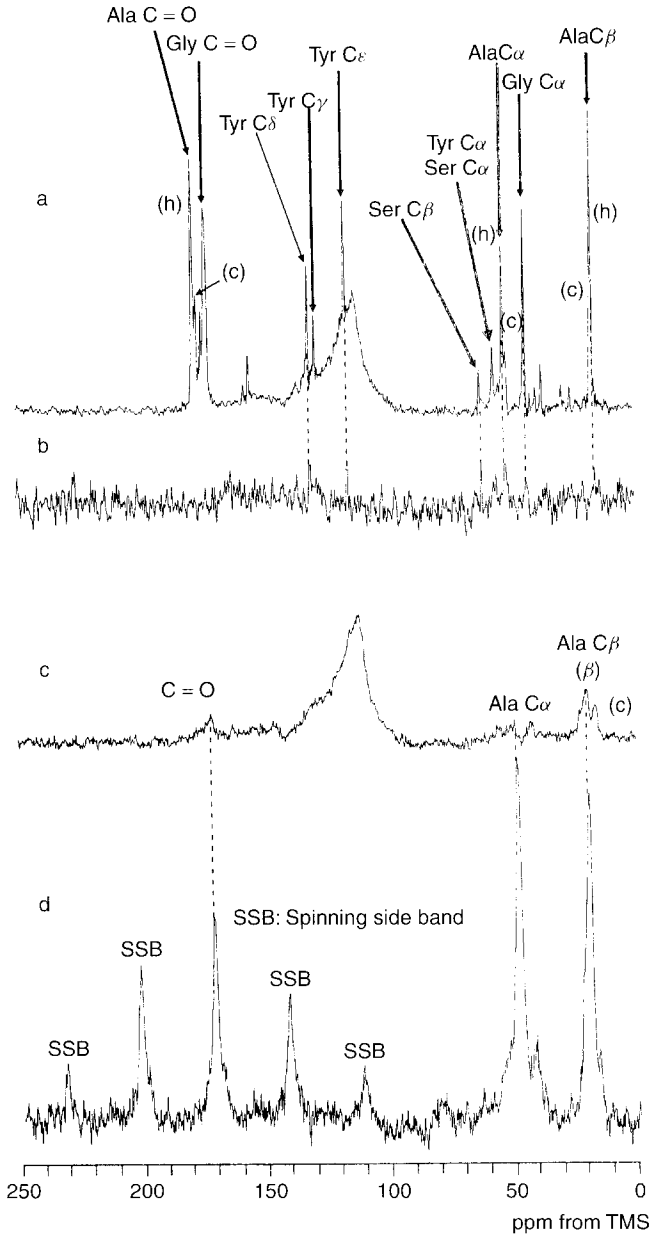

Fig. 21. ^{13}C DD/MAS and CP/MAS NMR spectra of *S.c. ricini* silk fibroin observed immediately after sample preparation (a and b) and after 102 h (c and d), indicating transition to the β-sheet structure. The broad peak at the center of a and c is a background signal coming from the sample tube. (h) denotes the signals arising from the α-helix conformation and (c) the random coil conformation.

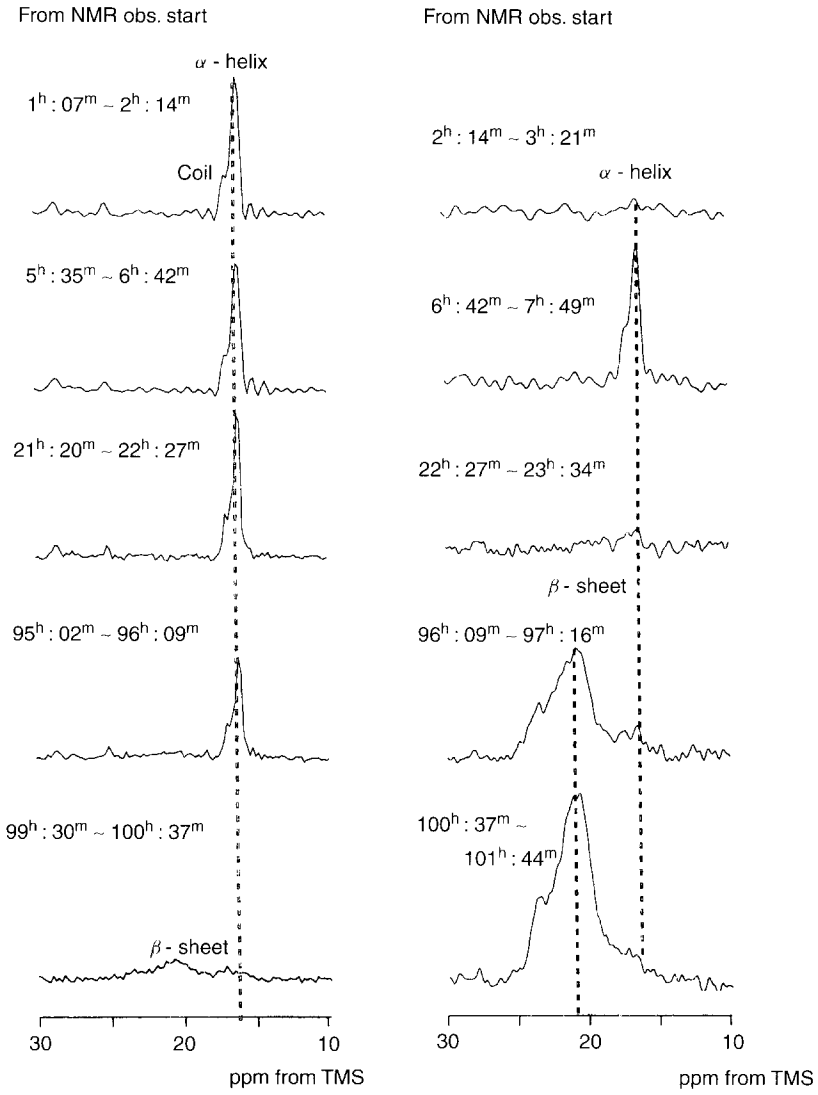

Fig. 22. Expansion of the ^{13}C DD/MAS (left) and CP/MAS (right) NMR spectra of *S.c. ricini* silk fibroin, showing the Ala C_β-region.

chemical shift characterizes the secondary structure as mobile α-helix. At the time point of 100 hours, the peak in the DD/MAS spectrum reduces in intensity, and CP/MAS spectra after this time point show a broad peak at 21 ppm indicating β-sheet structure.[41,63,70,71] Thus, we can confirm the β-transition in a series of NMR spectra. It should be noted that in the CP/MAS spectra we observed a sharp line after 6 hours which decayed over the subsequent 10 hours (Fig. 23).

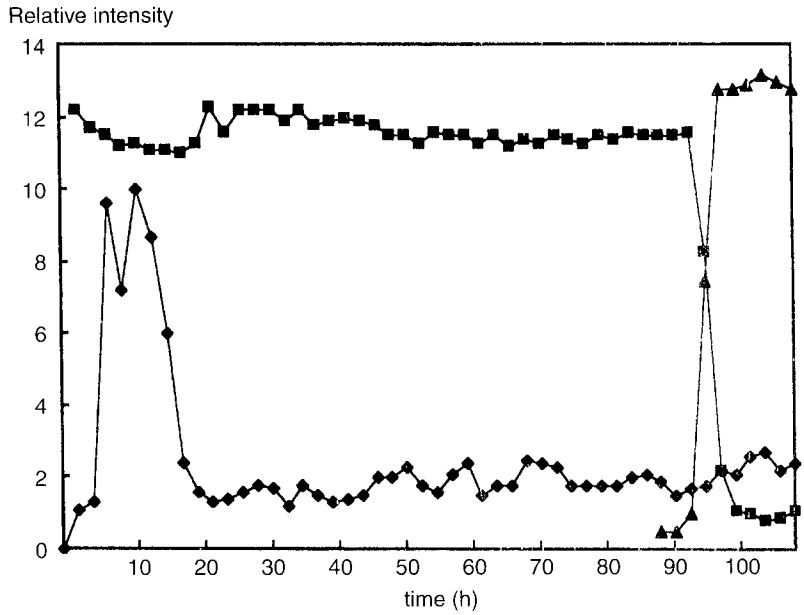

Fig. 23. Relative intensities of the signals, Ala C_β-carbons, assigned to α-helix observed in ^{13}C DD/MAS (■) and ^{13}C CP/MAS (♦) and to β-sheet in the CP/MAS experiments (▲) vs. time.

Thus, there exist comparatively rigid Ala residues for which cross-polarization is effective. This remarkable change of intensity may be attributed to the efficiency of the cross-polarization, which is determined by the cross-relaxation time T_{CH} and the spin–lattice relaxation time in the rotating frame $T_{1\rho}$.[72] During the first stage before 6 hours, the contact time of 5 ms used in the present experiment was too short to yield the CP-enhanced line because of the fast molecular motions. According to the slowdown of the motions, the applied contact time becomes most effective around 6 hours and then less effective because of the very fast $T_{1\rho}$-decay arising from the slow molecular motions. The singular behavior of the Ala peak intensity can thus be explained by the monotonic slowdown of the overall molecular motions.

Nakazawa *et al.*[67] concluded from the above CP-related phenomenon that liquid silk takes the β-transition not directly from a highly mobile state but through the gradual slowdown of molecular motions. Also, it is concluded that just before the β-transition, liquid silk takes the α-helix structure, without assuming the random coil structure.

The CP/MAS spectrum immediately after loading the liquid silk shows the Cε peak on the Tyr residue. Therefore, the motion of the bulky aromatic side-chain is extensively hindered and hence, CP is effective even from the initial state. It is most probable that the mode of the motions of the aromatic ring is 180-degree

flip.[73] This mode is gradually hindered, yielding a more intense CP/MAS peak with time. However, it is surprising that the peak height of the C_ε peak of the Tyr residue abruptly decreases after 17 and 30 h, as depicted in Fig. 24. This peculiar phenomenon may be ascribed to interference between the 180-degree flip motion and ^1H decoupling spin dynamics. That is, when the correlation frequency of the motion or its multiples match the decoupling frequency, the effect of the decoupling is canceled, leading to broad, vanishing resonance lines.[74] In the present case of a decoupling frequency of 50 kHz, it is plausible that the broadening corresponding to 100 kHz occurred at the 17-hour time point and that the correlation frequency matches the decoupling frequency at the 30-hour time point.

As suggested by observation of the Ala C_β peak, the molecular motions gradually slow down, and we can expect overall molecular aggregation which restricts the Tyr 180-degree flip motion. The disappearance, which was observed twice for the C_ε peak of Tyr, can be explained by such a gradual molecular aggregation. On the other hand, once the β-transition takes place at the 100-hour time point, the β-structure prevails over the whole sample within a comparatively short time of 4 hours. In conclusion, using NMR measurements, Nakazawa *et al.* found that most of the liquid silk of *S.c. ricini* takes the form of α-helix structure just before the β-transition and its mobility gradually lowers as molecular aggregation increases.

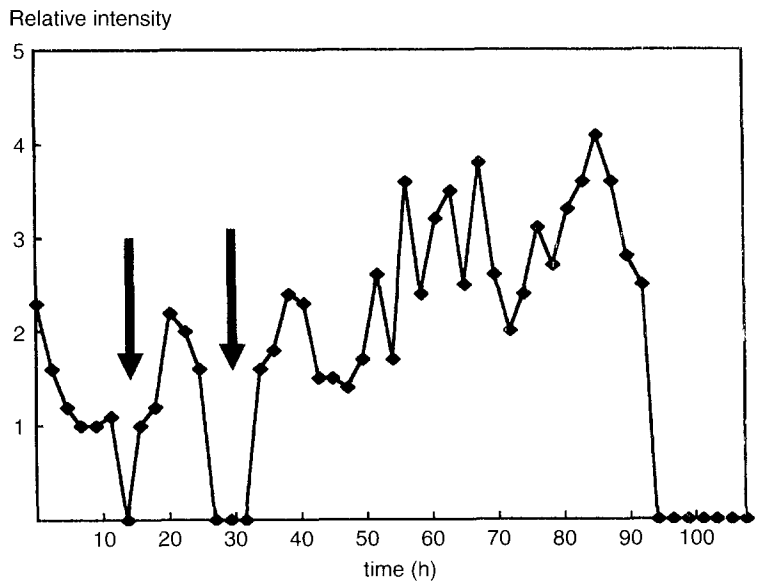

Fig. 24. Relative intensities of signals assigned to Tyr C_ε observed in CP/MAS spectra. The two arrows indicate an abrupt decrease in intensity.

9. DYNAMICS OF WATER MOLECULES IN *B. mori* SILK FIBROIN FILM

We now consider the contribution of water molecules in the protein structure to the relaxation above 250 K. It is interesting to compare our ^1H pulsed NMR data obtained for *B. mori* silk fibroin, dried and undried, with those reported by Andrew *et al.*[38–40] for other proteins. A model[75,76] proposed for silk fibroin films containing water is also examined in light of the present data. Figure 25 shows the temperature dependences of the ^1H spin–lattice relaxation times of *B. mori* silk fibroin films containing 10 w/w% water.[56] For comparison, the data for dried samples also are shown. The curves for the samples containing water are independent of the treatment with methanol during sample preparation, which causes the structural transition from the random-coil form or silk I to silk II.[36,41–44] If there is free water in the films, the curves should change dramatically due to the presence of the ^1H–^1H dipolar relaxation of such free water.[39,40] Above

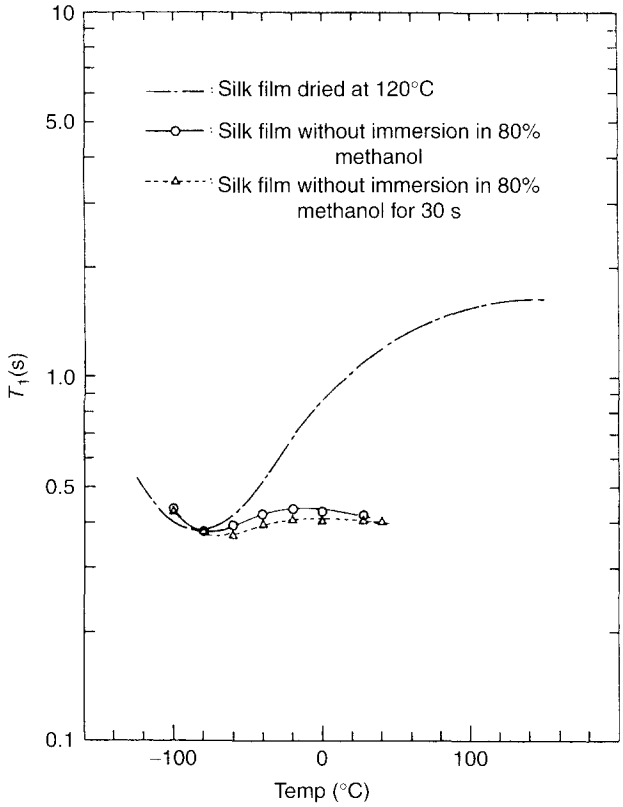

Fig. 25. Temperature dependence of T_1 of undried *B. mori* silk fibroin films. The water content was 10% by weight. For comparison, data for a dried sample are also shown.

$-80°C$, the presence of water molecules causes a decrease of T_1 values due to their reorientation. The change however, is not large, suggesting that all water molecules in these films are bound to silk fibroin molecules with rapid rotation of the methyl groups of the Ala residues. This conclusion was also supported from the temperature dependence of the solid-echo Fourier transform spectra of silk fibroin films without immersion in methanol (Fig. 26). These spectra consist of mobile and immobile components. The fraction of the mobile component was determined as 10% in the peak area; the content of the mobile component is almost the same as the water content determined by the Karl–Fischer method.[56] In contrast, the mobile component can scarcely be observed in film prepared from silk fibroin in D_2O instead of H_2O (data not shown). Therefore, the mobile component is attributable to the water. This peak is still observed at -20 and $-40°C$, indicating bound water.

The decays of the magnetization of undried silk fibroin samples by the solid-echo method show the presence of two components (Fig. 27). The mobile component is attributable to the bound water and the immobile component to silk

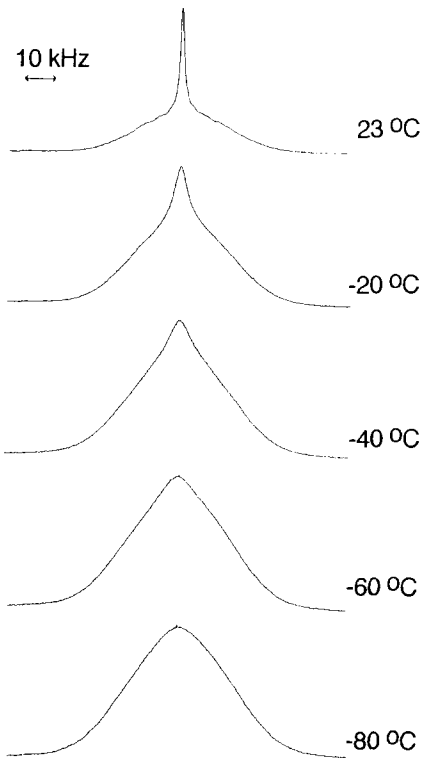

Fig. 26. Solid-echo Fourier transform spectra of *B. mori* silk fibroin films prepared without immersion in methanol at several temperatures.

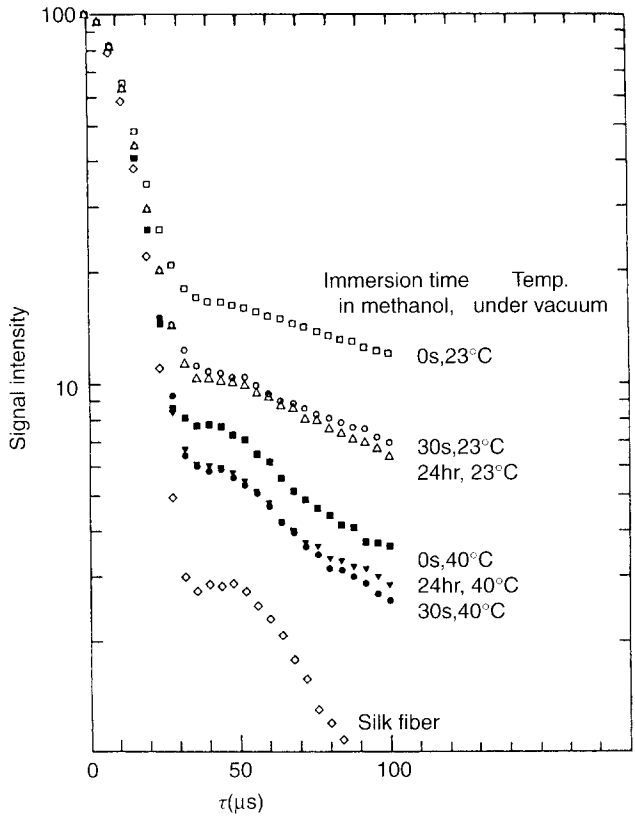

Fig. 27. Solid-echo decays at 23°C of *B. mori* silk fibroin films and fiber without drying. The immersion times of the silk films in 80% methanol and temperature of the silk films under vacuum before NMR measurement are indicated.

fibroin as mentioned above. The decay can be analyzed using the following equation.[77]

$$M(t) = (1 - f)\exp\left[-\frac{1}{2}\left(\frac{t}{T_{2f}}\right)^2\right] + f\exp\left(-\frac{t}{T_{2s}}\right) \quad (1)$$

where $M(t)$ is the intensity of magnetization at time t. The T_2 value determined from fast decay is denoted by T_{2f} and that determined from slow decay by T_{2s}, and f is the fraction of the slow component. In order to change the water content in the sample, the immersion times of the films in 80% methanol and the temperature under vacuum before sealing the NMR tube were changed. Values of T_{2f} were approximately 10 μs, independent of the samples and is same as T_1 values of the dried silk fibroin.[56] However, the values of T_{2s} changed from 50 to 200 μs depending on the samples. These correspond to the T_1 value of bound

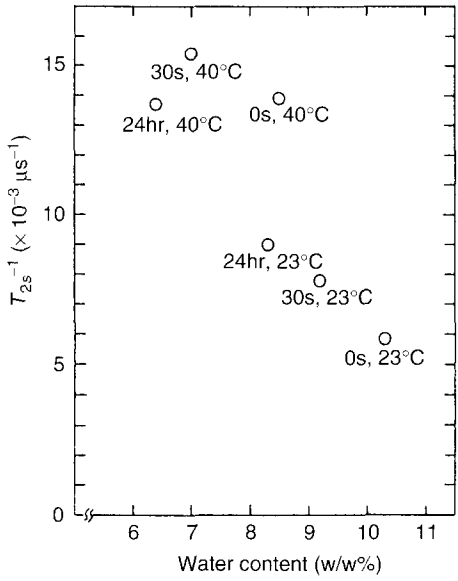

Fig. 28. Plot of T_2^{-1} determined from slow decays shown in Fig. 27, T_{2s}^{-1} vs. water content of *B. mori* silk fibroin films. Notation in the Figure is the same as in Fig. 27. Water content was determined by the Karl–Fishcher method.

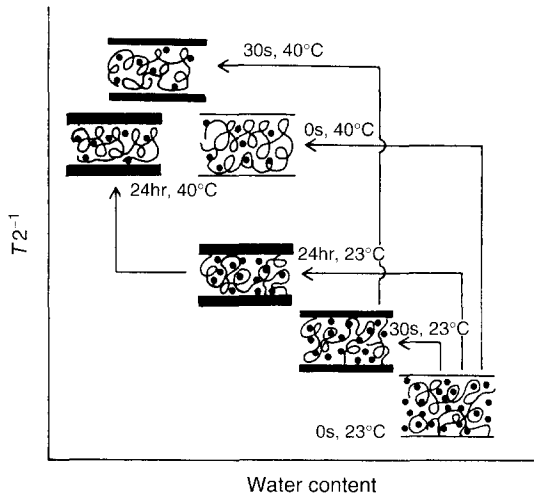

Fig. 29. Model of relationships between the structure of *B. mori* silk fibroin films and distribution of water in the films based on the dependence of T_{2s}^{-1} on water content (Fig. 28). Each sketch indicates the cross-section of the film. Two bands on each film represent the thickness of the layer with silk II structure and the curved lines denote fibroin chains in random-coil conformations. Filled circles denote water molecules. Notation the same as in Fig. 27.

water. Figure 28 shows a plot of T_{2s} of silk fibroin films against water content determined by the Karl–Fischer method. For example, the film denoted (24 h, 23°C) indicates an immersion time in 80% methanol of 24 h and a temperature under vacuum before sealing the NMR tube of 23°C.

The T_{2s} value of water tends to increase with increasing content of water in the film. However, there was a case where T_{2s} values differ even when the water content remains the same. Cross-sections of the silk fibroin films are represented schematically in Fig. 29 on the basis of the plot of T_{2s} of the films versus water content.

Although the film (0 s, 40°C) has the same water content as the film (24 h, 23°C), its T_{2s} is considerably larger than that of the latter film. This means that water molecules trapped exclusively in the interior of the film become more mobile when the surface structure of the film changes from random coil or silk I to silk II. On the other hand, water molecules distributed uniformly over the film are less mobile. This is the case of the film (0 s, 40°C). This finding supports the heterogeneous hydrated structure of the silk fibroin film prepared with the aqueous methanol solution proposed previously.[41,75,76]

10. DYNAMICS OF *B. mori* SILK FIBROIN IN SWOLLEN SILK FIBROIN MEMBRANE

The dynamics of *B. mori* silk fibroin membrane[76] and powder[78] insolubilized with methanol in the swollen state were measured and high-resolution ^{13}C NMR spectra of the silk fibroin membrane treated with methanol in water are shown in Fig. 30 together with the spectrum of the silk fibroin aqueous solution (ca. 2.5 wt%).

The existence of a mobile portion in the inner part of the swollen membrane can be detected from the ^{13}C NMR spectrum of the membrane in water. As described in Section 4, the mean correlation time for the segmental motion of silk fibroin in aqueous solution was determined as 1×10^{-10} s, from NT_1 and NOE values averaged over Gly C_α, Ala C_α and Ser C_α carbons assuming the log χ^2 distribution model. The high-resolution NMR peak of the membrane in water becomes broader than those of the aqueous solution and the mean correlation time of the mobile portion in the swollen membrane was determined to be about 2×10^{-10} s in the same manner. The intensity of the ^{13}C NMR peak of the membrane decreases with increasing methanol treatment time as shown in Fig. 30. When the methanol treatment time is 30 s, the fraction of the portion observed by ^{13}C NMR of the silk fibroin membrane swollen in water and the degree of swelling of the membrane decrease with increasing methanol treatment time. Therefore, high-resolution ^{13}C NMR observation of the membrane swollen in water shows that the random coil portion whose segmental motion is very fast remains in the inner part of the swollen membrane. The fraction of this portion decreases with increasing methanol treatment time during sample preparation.[75]

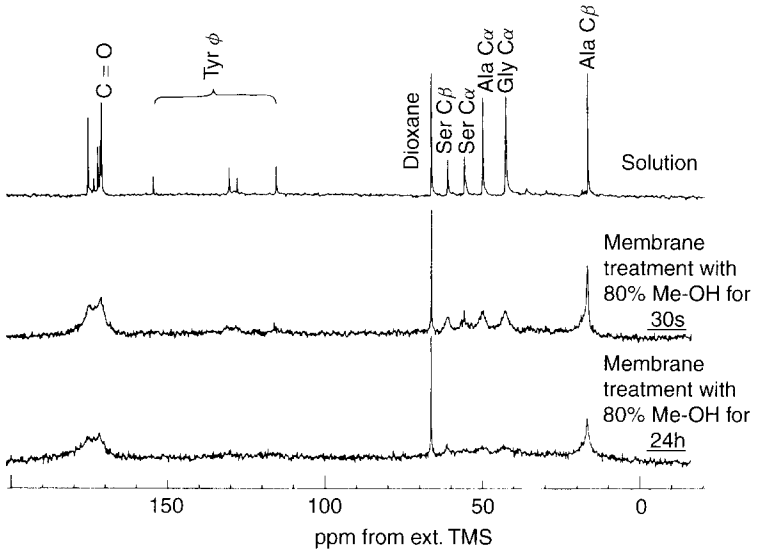

Fig. 30. ^{13}C NMR spectra of silk fibroin solution and silk fibroin membrane treated with methanol in water at 25°C.

The heterogeneous structure of the swollen *B. mori* silk fibroin membrane was clarified from the complicated ESR spectra of the spin-labeled silk fibroin membranes. Spin-label ESR methods are useful for dynamic analysis of silk fibroin because of the inherent high sensitivity of ESR observation and the wide detectable range of the motion of the spin-labeled site, from 10^{-10} to 10^{-4} s. The hydroxy group of the Tyr side-chain is active and thus it can be labeled with nitroxide radical compounds as shown in Fig. 31.[75]

Information about the silk fibroin membrane can be obtained through the mobility of the Tyr side-chain (the spin-labeling site) using ESR spectroscopy. Figure 32 shows ESR spectra of spin-labeled silk fibroin in aqueous solution and several kinds of spin-labeled silk fibroin membranes treated with methanol in both dry and swollen states.

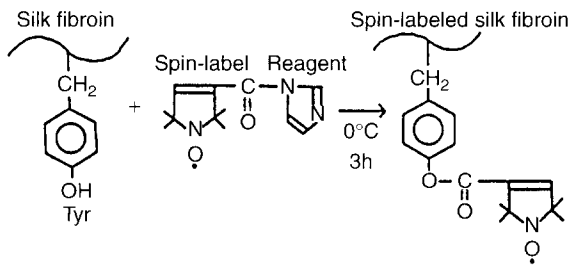

Fig. 31. Scheme of the synthesis of spin-labeled silk fibroin.

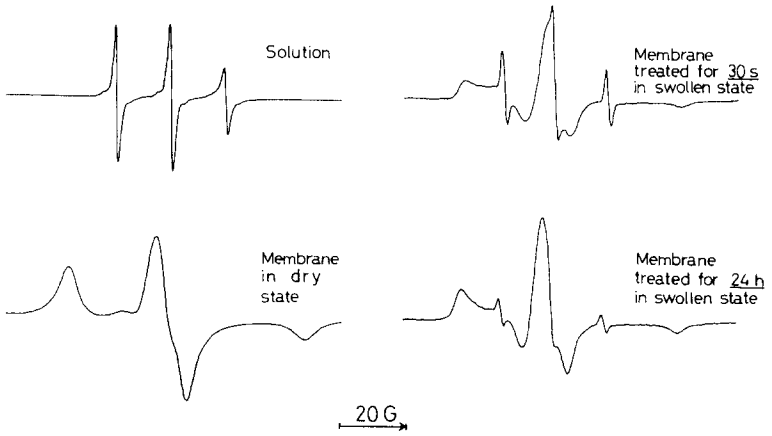

Fig. 32. ESR spectra of spin-labeled silk fibroin in aqueous solution and spin-labeled silk fibroin membrane treated with methanol in dry and swollen states at room temperature.

The ESR spectrum of the aqueous solution is composed of three sharp peaks, which means that the correlation time τ_c for the rotational motion of the nitroxide radical group is 6×10^{-10} s. This is determined from both the peak height and width. On the other hand, the ESR spectrum of the membrane in the dry state is very broad and the τ_c value is determined as 2×10^{-8} s from the maximum separation width. The ESR spectra of the membrane in the swollen state (right side of Fig. 32) are complex, indicating the presence of several components from the viewpoint of the motion of the nitroxide radical group in the membrane. There are several kinds of microenvironment around the Tyr side-chain in membranes swollen by water. The relative intensities of the three sharp ESR peaks of the membrane in the swollen state decrease with increasing methanol treatment time. Thus, by assuming that the ESR spectrum consists of three components from the viewpoint of motion in the ESR time scale, the fraction of each component was determined by the nonlinear least squares method from a computer spectrum simulation (Fig. 33).

The ESR spectra were analyzed quantitatively and the fraction of the fast ($\tau_c = 10^{-10}$), slow ($\tau_c = 10^{-9}$), and very slow ($\tau_c = 10^{-8}$) motions of the spin-label site (Tyr side-chain) were determined. A model is proposed for the heterogeneous structure of the swollen silk fibroin membrane. The ESR spectrum was complex, indicating the heterogeneous structure of the swollen membrane.

On the basis of ^{13}C NMR and ESR data, a model for the heterogeneous structure of the swollen silk fibroin membrane treated with methanol is proposed as shown in Fig. 34.

The square symbols in Fig. 34 indicate the aggregated portion with antiparallel β-sheet form and its dimension is a measure of the degree of growth of such aggregation. The aggregated portion with the antiparallel β-sheet form tends to concentrate at the surface of the membrane.

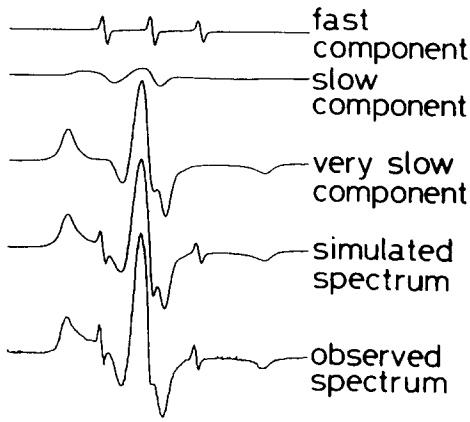

Fig. 33. An example of ESR spectrum simulation. The ESR spectrum of spin-labeled silk fibroin membrane treated with methanol for 24 h was simulated by assuming the spectra of fast, slow, and very slow components corresponding to rotational correlation times of 10^{-10}, 10^{-9}, and 10^{-8} s, respectively. The fraction of fast, slow, and very slow components was determined as 0.01, 0.12, and 0.87, respectively.

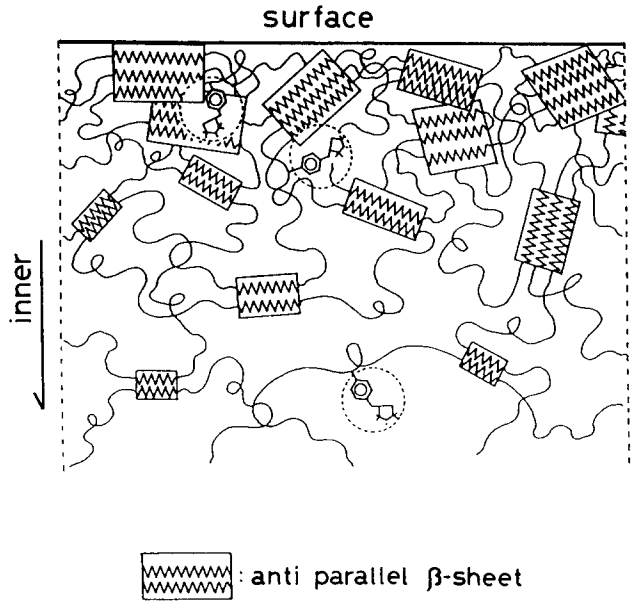

Fig. 34. Model of the heterogeneous structure of silk fibroin membrane treated with methanol in the swollen state. From FT-IR data, the aggregated portion with antiparallel β-sheet form tends to concentrate at the surface of the membrane. From ^{13}C NMR data, the random coil portion whose segmental motion is very fast remains in the inner part of the membrane. From ESR data, the Tyr residues (spin-label sites) of the membrane in the swollen state can be classified into three types.

11. DYNAMICS OF SMALL ORGANIC MOLECULES IN SWOLLEN SILK FIBROIN GEL

NMR imaging has the advantage that it does not disturb the diffusion process, unlike most other techniques, which require stopping the diffusion process and destroying the sample.[12–16] Asakura *et al.*[79] applied this imaging technique to the study of the diffusion process of small organic molecules into a silk fibroin gel swollen in water. The 8 w/v% aqueous solution of *B. mori* silk fibroin was obtained as described in detail elsewhere.[4] The fibroin solution was loaded into a disposable syringe and injected into 80% methanol aqueous solution in order to obtain an insoluble gel of silk fibroin. After this treatment, the cylindrical gel (30 mm length, 6.5 mm diameter) was carefully washed in distilled water and stored in distilled water until MRI measurement. MR imaging observations were performed as follows. After the gel was set in the vessel, 5 ml of 0.5 M 4-hydroxy-2,2,6,6-tetramethylpiperidin-l-oxyl (TEMPOL) aqueous solution was added. The sample was immediately placed in the MRI probe and the data were obtained after one accumulation (5 min). Observation of ^{1}H MR imaging was performed at 25°C with a JEOL GSX270 (WB) NMR spectrometer equipped with a ^{1}H imaging system (NM-GIM270). The imaging was observed using the spin-echo method (spin-echo time, $TE = 29–36$ ms; repetition time between two successive individual pulse series applied, $T_r = 300–2000$ ms). Each MR image was produced using a two-dimensional Fourier transform (data size = 256 × 256). The image resolution was 0.2 mm, and the slice thickness of the observation field was 2 mm.

The T_1 and T_2 values of water trapped in the silk fibroin gel were determined according to the usual inversion-recovery method and the Carr–Purcell–Meiboom–Gill method, respectively, with a JEOL FX-90Q NMR spectrometer at 90 MHz. Figure 35 shows the time dependence of the MR image of the swollen fibroin gel together with the distribution of the signal intensity of water across the sample (one-dimensional profile) after it was immersed in TEMPOL aqueous solution.

The right hand picture (6) in Fig. 35 is also the image of the gel (diameter = 6.5 mm) in the well-swollen state before immersion in the TEMPOL solution. The distribution of water in the fibroin gel was approximately uniform as shown in the profile of Fig. 35 (6) except for the formation of a thin layer of 0.6 mm thickness at the surface. The presence of such a layer is detected by the contrast between the inner and outer parts of the gel, indicating the formation of fine structure with an antiparallel β-sheet form at the surface as a result of the conformational transition from random coil to β-sheet by contact with methanol.[41] As shown in both the images and the one-dimensional profiles of the signal intensity of water across the sample (Fig. 35 (1–5)), the MR imaging pattern changes drastically with time because of diffusion of TEMPOL molecules, which cause paramagnetic relaxation of the water protons in the gel. Since, the gel is in a

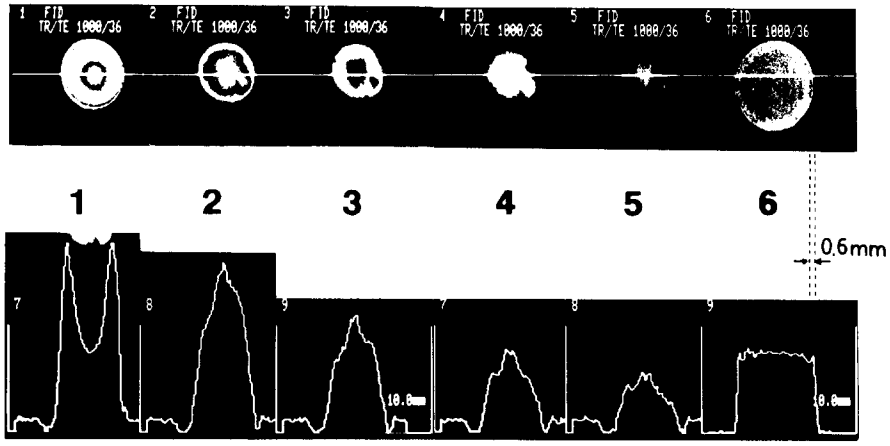

Fig. 35. Time course of MR imaging of silk fibroin gel after contact with TEMPOL aqueous solution. Spin-echo time = 36 ms. Repetition time = 1000 ms. Observation time (min): (1) 5–10, (2) 15–20, (3) 25–30, (4) 35–40, (5) 45–50, and (6) 0, respectively. Each profile corresponds to the center line on the image.

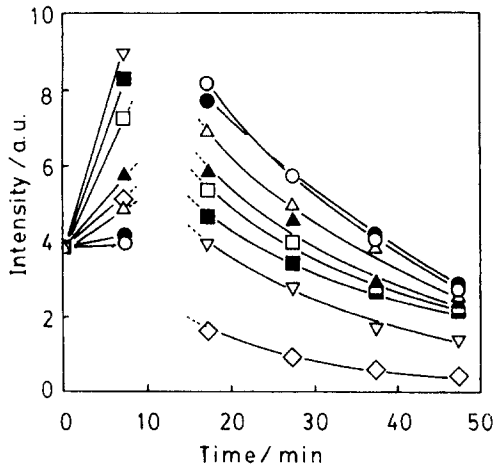

Fig. 36. Change of image intensity as a function of contact time with TEMPOL. These data were calculated from the intensity of the profile at various distances from the surface of the gel. Position from the surface of the gel (centimeters): (○) 0.33, (●) 0.29, (△) 0.26, (▲) 0.23, (□) 0.20, (■) 0.17, (▽) 0.14, (◇) 0.11.

well-swollen state before immersing it in the TEMPOL solution, this remarkable change clearly indicates the decrease in the ^{1}H NMR relaxation times of water because of the presence of TEMPOL. Figure 36 shows the time dependence of the signal intensity at various positions in the gel as determined from the profile.

In the plots, it should be noted that the intensity increases rapidly and then decreases gradually with time. Similar changes were still observed when the experimental conditions were changed, namely: $TE = 29$–36 ms and $T_1 = 300$–2000 ms. This nonuniform change of signal intensity was explained as follows. When MR imaging is measured by the spin-echo method, the signal intensity, I, is (approximately) given by

$$I = k\rho \exp\left(-\frac{TE}{T_2}\right)\left[1 - \exp\left(-\frac{T_\rho}{T_1}\right)\right] \tag{2}$$

where k and ρ denote a constant and the proton spin density of water, respectively. The first exponential term is dependent upon both T_2 and TE ($2 \times$ pulse interval) and the second term upon both T_1 and T_ρ. In this experiment, the values of TE and T_1 were varied between 29 and 36 ms, and 300 and 2000 ms, respectively, ρ was held constant because of the well-swollen state. Therefore, the intensity of the profile strictly includes information on the relaxation times of water molecules rather than the density. In order to evaluate the change of the image profile in accordance with Eq. (3) the values of T_1 and T_2 of water were determined as a function of concentration of TEMPOL from 2 mM to 500 mM (Fig. 37).

The results indicate that the values of relaxation rates, $1/T_1$ and $1/T_2$, agree within experimental error under these experimental conditions. In addition, a plot of these relaxation rates against TEMPOL concentration yields a straight line. From the plots, we obtained the empirical formula

$$\frac{1}{T_1} = \frac{1}{T_2} = 0.312 + 0.1829[TEMPOL] \tag{3}$$

where the units of T_2 and $[TEMPOL]$ are seconds and millimolar, respectively. The correlation coefficient was 0.9997. In addition, the equilibrium values of T_1 and T_2 for water in the silk fibroin gel in the presence of TEMPOL, approximately agree with those in aqueous solution. Thus, we considered that the change of signal intensity observed here could be explained as a function of only one relaxation time, T_1 or T_2, with Eq. (2) by assuming that the frequency dependence of the paramagnetic relaxation is negligible. Figure 38 shows the simulated curves of signal intensity calculated in accordance with Eq. (2) for $T_2 = T_1$ at various values of TE and T_ρ.

As shown in Fig. 38 ($TE = 36$ ms, $T_r = 1000$ ms), the intensities increase rapidly and decrease gradually with increasing $1/T_1$. This tendency agrees with the change in Fig. 36 ($TE = 36$ ms, $T_\rho = 1000$ ms). In addition, other observed profiles of the MR image ($TE = 29$ ms, $T_1 = 300$ or 2000 ms) also changed as shown in Fig. 38. Therefore, it is suggested that the change in intensity of the MR image is explained by the decrease in T_1 and T_2 values of water in the silk fibroin gel as a result of diffusion of TEMPOL. If one-dimensional diffusion of TEMPOL is interpreted in terms of Fick's second law,[80] the average

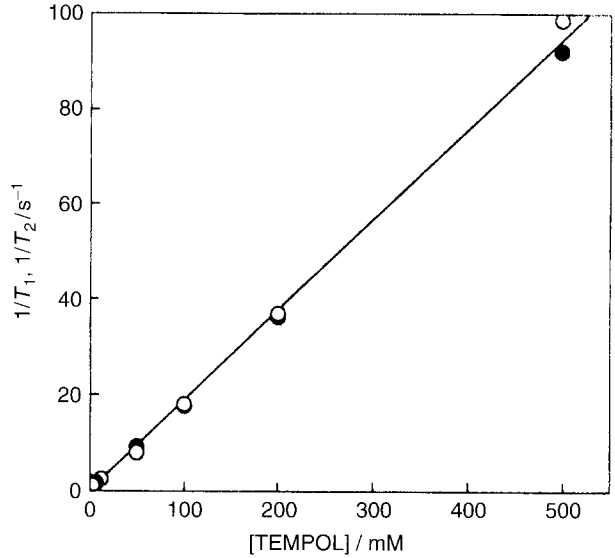

Fig. 37. Plots of relaxation rate, $1/T_1$ (•) and $1/T_2$ (○), as a function of TEMPOL concentration.

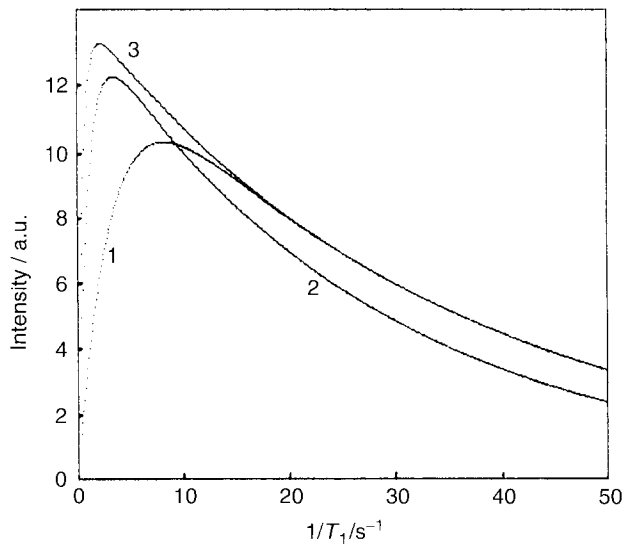

Fig. 38. Simulation of the intensity of the MR image as a function of $1/T_1$. Line 1: $TE = 29$ ms, $T_r = 300$ ms. Line 2: $TE = 36$ ms, $T_r = 1000$ ms. Line 3: $TE = 29$ ms, $T_r = 2000$ ms.

diffusion coefficient, D, is calculated with a reduced absorption curve i.e. a plot of C_τ/C_∞ against $(t/L^2)^{1/2}$, where C_τ and C_∞ represent concentrations of absorbed TEMPOL in the gel at time t and when equilibrium has been reached in the fibroin gel. In accordance with Eqs (2) and (3), the concentration of TEMPOL at various positions L (centimeters) from the surface of the gel was determined.[79] For short times, the average diffusion coefficient, D, is expressed as

$$D = \pi/64/[t/L^2] \tag{4}$$

where $[t/L^2]$ denotes the value of the abscissa when $Ct/C^\infty = 1/2$. From the plots of fraction of diffusion of TEMPOL as a function of $(t/L^2)^{1/2}$, D was calculated as $8.1 \times 10^{-7}\,\mathrm{cm^2\,s^{-1}}$. This value agrees within experimental error with the results calculated from imaging data obtained by using the other measurement parameters. In addition, this order of magnitude is consistent with the diffusivity of glucose in the silk fibroin membrane[81] whose molecular weight is nearly equal to that of TEMPOL.

ACKNOWLEDGEMENT

TA acknowledges support from the Program for Promotion of Basic Research Activities for Innovative Biosciences, Japan.

REFERENCES

1. L. J. Mathias, *Solid State NMR of Polymers*, Plenum Press, 1991.
2. J. Frahm and W. Hanicke, *J. Magn. Reson.*, 1984, **60**, 320.
3. F. Heatley, *Prog. NMR Spectrosc.*, 1979, **13**, 47.
4. T. Asakura, Y. Watanabe, A. Uchida and H. Minagawa, *Macromolecules*, 1984, **17**, 1075.
5. T. C. Farrar and E. D. Becker, In *Pulse and Fourier Transform NMR*, Academic Press, New York, 1971.
6. J. H. Davis, K. R. Jeffrey, M. Bloom, M. I. Valic and T. P. Higgs, *Chem. Phys. Lett.*, 1976, **42**, 390.
7. H. W. Spiess, *Colloid. Polym. Sci.*, 1983, **261**, 193.
8. D. A. Torchia, *Annu. Rev. Biophys. Bioeng.*, 1978, **13**, 125.
9. A. S. Ulrich and S. L. Grage, In *Solid State NMR of Polymers*. I. Ando and T. Asakura (eds), Elsevier, 1998, p. 190.
10. R. Tycko, *Nuclear Magnetic Resonance Probes of Molecular Dynamics*, Kluwer Academic, 1994, p. 27.
11. A. Ganssen, In *NMR in Living Systems*, T. A. Axenrod and G. Ceccarell (eds), Reidel Publishing Co., The Netherlands, 1986, p. 177D.
12. R. J. Gummerson, C. Hall, W. D. Hoff, R. Hawker, G. N. Holland and W. S. Moore, *Nature*, 1979, **281**, 56.
13. S. Blackband and P. Mansfield, *J. Phys. C: Solid State Phys.*, 1986, **19**, 49.
14. L. A. Weisenberger and J. L. Koenig, *J. Polym. Sci., Polym. Lett. Edn*, 1989, **27**, 55.
15. L. A. Weisenberger and J. L. Koenig, *Macromolecules*, 1990, **23**, 2445.
16. L. A. Weisenberger and J. L. Koenig, *Macromolecules*, 1990, **23**, 2454.

17. P. Blumler and B. Blumich, *Magn. Reson. Imaging*, 1992, **10**, 779.
18. S. A. Goldman G. V. Bruno and J. H. Frred, *J. Phys. Chem.*, 1972, **76**, 1858.
19. T. Asakura and D. L. Kaplan, In *Encyclopedia of Agricultural Science*, Vol. 4, Arutzen C. J. (ed.), Academic Press, New York, 1994, p. 1.
20. T. Asakura, H. Kashiba and H. Yoshimizu, *Macromolecules*, 1988, **21**, 644.
21. N. Hojo, *Zoku Kenshi no Kozo* (Structure of Silk Fibers), 1980, Shinshu University, Ueda.
22. C Zhou, F. Cofalonieri, N. Medina, Y. Zivanovic, C. Esnault, T. Yang, M. Jacquet, J Janin, M. Duguet, R. Perasso and Z. Li, *Nucleic Acids Res.*, 2000, **28**, 2413.
23. O. W. Howarth and D. M. Lilley, *Progr. NMR Spectrosc.*, 1978, **12**, 1.
24. T. Asakura and T. Murakami, *Macromolecules*, 1985, **18**, 2614.
25. A. Bundi and K. Wüthrich, *Biopolymers*, 1979, **18**, 285.
26. P. Keim, R. A. Vigna, J. S. Morrow and R. C. Marshall, *J. Biol. Chem.*, 1973, **248**, 7811.
27. P. Keim, R. A. Vigna, R. C. Marshall and R. N. Gurd, *J. Biol. Chem.*, 1973, **248**, 6104.
28. T. Asakura, H. Yoshimizu and F. Yoshizawa, *Macromolecules*, 1988, **21**, 2038.
29. G. Lipari and A. Szabo, *J. Am. Chem. Soc.*, 1982, **104**, 4546.
30. J. Schaefer, *Macromolecules*, 1973, **6**, 882.
31. T. Asakura, M. Demura, A. Uyama, K. Ogawa, K. Komatsu, L. K. Nicholson and T. A. Cross, In *Silk Polymers*, **544**, D. Kaplan, W. W. Adams, B. Farmer and C. Viney (eds), American Chemical Society, Washington DC, 1994, 544, p. 148.
32. K. Komatsu, *Hikaku Kagaku*, 1982, **27**, 193.
33. T. Asakura, H. Suzuki and T. Tanaka, *J. Seric. Sci. Jpn.*, 1985, **54**, 504.
34. E. R. Andrew, T. J. Green and M. J. R. Hoch, *J. Magn. Reson.*, 1978, **29**, 331.
35. E. R. Andrew, R. Gaspar Jr and W. Vennart, *Biopolymers*, 1978, **17**, 1913.
36. H. Saito, R. Tabeta, T. Asakura, Y. Iwanaga, T. Ozaki and I. Ando, *Macromolecules*, 1984, **17**, 1405.
37. T. Asakura, Y. Watanabe and T. Itoh, *Macromolecules*, 1984, **17**, 2421.
38. E. R. Andrew, D. J. Bryant and E. M. Cashell, *Chem. Phys. Lett.*, 1980, **69**, 551.
39. E. R. Andrew, D. J. Bryant and T. Z. Rizui, *Chem. Phy. Lett.*, 1983, **95**, 463.
40. E. R. Andrew, *Polymer*, 1985, **26**, 190.
41. M. Ishida, T. Asakura, T. Yokoi and H. Saito, *Macromolecules*, 1990, **23**, 88.
42. H. Saito, Y. Iwanaga, R. Tabeta, M. Narita and T. Asakura, *Chem. Lett. (Jpn.)*, 1983, 427.
43. T. Asakura, A. Kuzuhara, R. Tabeta and H. Saito, *Macromolecules*, 1985, **18**, 1841.
44. H. Saito, R. Tabeta, A. Kuzuhara and T. Asakura, *Bull. Chem. Soc. Jpn.*, 1986, **59**, 3383.
45. T. Asakura and M. Demura, *Macromol. Symp.*, 1999, **143**, 1.
46. D. J. Strydom, T. Haylett and R. H. Stead, *Biochem. Biophys. Res. Commun.*, 1977, **79**, 932.
47. H. Saito, M. Ishida, M. Yokoi and T. Asakura, *Macromolecules*, 1990, **23**, 83.
48. D. Torchia, *J. Magn. Reson.*, 1978, **30**, 613.
49. T. Shiba and S. Sakakibara, *Protein Research Foundation*. 1988, p 53, Osaka.
50. J. Janin, S. Wodak, M. Levit and B. Maigret, *J. Mol. Biol.*, 1978, **125**, 357.
51. T. Gray and B. W. Matthews, *J. Mol. Biol.*, 1984, **175**, 75.
52. T. Asakura and T. Yamaguchi, *J. Seric. Sci. Jpn.*, 1987, **56**, 300.
53. T. Asakura, R. Sakaguchi, M. Demura, T. Manabe, A. Uyama, K. Ogawa and M. Osanai, *Biotechnol. Bioeng.*, 1993, **41**, 245.
54. L. K. Nicholson, T. Asakura, M. Demura and T. A. Cross, *Biopolymers*, 1993, **33**, 847.
55. T. Kameda, Y. Ohkawa, K. Yoshizawa, E. Nakano, T. Hiraoki, A. S. Ulrich and T. Asakura, *Macromolecules*, 1999, **32**, 8491.
56. T. Asakura, M. Demura, Y. Watanabe and K. Sato, *J. Polym. Sci. Part B, Polym. Phys.*, 1992, **30**, 693.
57. M. S. Greenfield, A. D. Ronemus, R. L. Vold, R. R. Vold, P. D. Ellis and T. E. Raidy, *J. Magn. Reson.*, 1987, **72**, 89.
58. T. Asakura, *Bioindustry*, 1987, **4**, 36.
59. T. Asakura, J. Kanetake and M. Demura, *Polymer-Plastics Technol. Eng.*, 1989, **28**, 453.

60. C. M. Mello, K. Senecal, B. Young, P. Voudros and D. Kaplan, In *Silk Polymers-Materials Science and Biotechnology*, D. Kaplan, W. W. Adams, B. Farmer and C. Viney (eds). ACS, Washington DC, 1994.
61. Y. Yukuhiro, personal communication.
62. T. Asakura, M. Minami, R. Shimada, M. Demura, M. Osanai, T. Fujito, M. Imanari and A. S. Ulrich, *Macromolecules*, 1997, **30**, 2429.
63. T. Asakura, T. Ito, M. Okudaira and T. Kameda, *Macromolecules*, 1999, **32**, 4940.
64. T. Hiraoki, A. Kogame, N. Nishi and A. Tsutsumi, *J. Mol. Struct.*, 1998, **441**, 243.
65. D. M. Rice, R. J. Witterbort, R. G. Griffin, E. Meirovitch, E. R. Stimson, Y. C. Meinwald, J. H. Freed and H. A. Scheraga, *J. Am. Chem. Soc.*, 1981, **103**, 7707.
66. D. M. Rice, Y. C. Meinwald, H. A. Scheraga and R. G. Griffin, *J. Am. Chem. Soc.*, 1987, **109**, 1636.
67. Y. Nakazawa, T. Nakai, T. Kameda and T. Asakura, *Chem. Phys. Lett.*, 1999, **311**, 362.
68. T. Asakura, Y. Watanabe and H. Suzuki, *Macromolecules*, 1983, **16**, 1024.
69. H. Mihara, Y. Takahashi and A. Ueno, *Biopolymers*, 1998, **47**, 83.
70. T. Asakura, M. Demura, T. Date, M. Miyashita, K. Ogawa and M. P. Williamson, *Biopolymers*, 1991, **31**, 1529.
71. T. Asakura, M. Iwadate, M. Demura and M. P. Williamson, *Int. J. Biol. Macromol.*, 1999, **24**, 167.
72. B. C. Gerstein and C. R. Dybowski, *Transient Techniques in NMR of Solids*, Academic Press, 1985.
73. K. Wuthrich, *NMR in Biological Research. Peptide and Proteins*, North-Holland, Amsterdam, 1976.
74. T. Nakai and C. A. McDowell, *Chem. Phys. Lett.*, 1994, **227**, 639.
75. H. Yoshimizu and T. Asakura, *J. Appl. Polym. Sci.*, 1990, **40**, 1745.
76. T. Asakura, H. Yoshimizu and M. Kakizaki, *Biotechnol. Bioeng.*, 1990, **35**, 511.
77. R. Folland and A. Charlesby, *Polymer*, 1979, **20**, 211.
78. H. Yoshimizu and T. Asakura, *J. Appl. Polym. Sci.*, 1990, **40**, 127.
79. T. Asakura, M. Demura, H. Ogawa, K. Matsushita and M. Imanari, *Macromolecules*, 1991, **24**, 620.
80. J. Crank, *The Mathematics of Diffusion*, 2nd edn, Clarendon Press, Oxford, 1975, p. 69.
81. M. Demura and T. Asakura, *Biotechnol. Bioeng.*, 1989, **33**, 589.

Computer Processing Techniques in High-resolution NMR

DAMIEN JEANNERAT

Department of Organic Chemistry, University of Geneva, 30 Quai Ernest Ansermet, CH-1211 Genève 4, Switzerland

1. Introduction 152
Literature 152
2. Standard processing techniques 154
2.1. The Fourier transform 154
2.2. Spectral folding and aliasing 155
2.3. Window functions 156
2.4. Artefact reduction techniques 157
3. Specialized processing techniques 158
3.1. Deconvolution methods 158
3.2. Linear prediction 164
3.3. Filter diagonalization 169
3.4. Wavelets transform 170
3.5. Least-squares fit 172
3.6. Maximum likelihood 174
3.7. Maximum entropy 175
3.8. Bayesian analysis 181
4. Spin networks determination 184
4.1. One-dimensional experiments 184
4.2. $^{13}C-^{13}C$ experiments 185
4.3. COSY and other $^{1}H-^{1}H$ experiments 185
4.4. J-resolved experiments 190
4.5. Heteronuclear experiment 191
4.6. Selective experiments 192
4.7. Neural networks 193
4.8. Scalar coupling constants 194
5. Biological applications 196
5.1. Literature 196
5.2. Historical overview 197
References 197

ANNUAL REPORTS ON NMR SPECTROSCOPY
VOLUME 46 ISBN 0-12-505446-7

1. INTRODUCTION

Being the first paper of the 'annual report' to be devoted to the computer processing of NMR spectra, this review attempts to cover this field from the beginning. In view of the selected historical approach, and given the wealth of literature devoted to the question, this paper will mainly focus on directing the reader towards other literature sources as there is very little scope for further details.

In the mid-1960s, two decisive developments triggered the development of modern NMR. The first was the introduction of pulse techniques by Anderson and Ernst[1] and the second was a key idea leading to the Fast Fourier Transform algorithm proposed by Cooley and Tukey.[2] Computers have been used systematically since then and the history of the processing is rich and varied as the lack of sensitivity of NMR necessitates that data be exploited as efficiently as possible. Despite potential benefits, it must be admitted that the vast majority of users never apply non-standard processing techniques. The fact that specialists themselves often recommend not using processing techniques is another cause for concern. An example of this is the advice given by Hoch and Stern[3] not to use window functions, which is undoubtedly the most widely used processing technique. In any case, the following question is more pertinent then ever in this regard: Why are special processing techniques not used? Firstly, they must demonstrate a very significant advantage over standard methods. Their availability is a second issue which could definitely be improved on, even in a world where no single standard has emerged. Comparative studies are also quite scarce, making it difficult to select between the wide range of alternatives. This being said, this paper will not attempt to propose practical solutions to these problems and only aims to bring together a wide range of references from the literature in the hope that this will provide useful information for readers.

Literature

Two major references should be highlighted. The first is the 1996 monograph by Hoch and Stern *NMR Data Processing*.[3] This is a very good introduction to the subject and provides sufficient background information to enable readers to understand the vocabulary of this review. It covers the basics of spectral processing and devotes chapters to linear prediction and maximum entropy. Some other techniques, such as wavelets and Bayesian methods, are also discussed briefly. The second major reference is a series volume on *Signal Treatment and Signal Analysis in NMR*,[4] published by Routledge. A glance at the list of authors reveals that most of the 24 chapters were written by major players in the fields they cover. This work is very technical and provides a basis, from which the rest of the specialized literature can be accessed. The chapters cover a broad range of theoretical aspects including the Fourier transform, maximum entropy, analysis

of relaxation data, non-linear regression, Padé–Laplace analysis, digital filtering, binomial filters, linear prediction and singular value decomposition. The second half of the volume contains many applications to time, frequency and spatial domains.

Other references of interest are listed below in order of increasing difficulty. At the easy end of the spectrum, there is the short and very elementary introduction in a chapter of the *Encyclopedia of Spectroscopy and Spectrometry* written by Morris.[5] It discusses Fourier transform, zero filling, phasing and also says a few words about linear prediction and maximum entropy. This paper can safely be recommended to undergraduate students. On a more advanced level, a monograph section written by Kalbitzer[6] introduces the problem of peak-picking, symmetry properties, multiplet recognition, spin network reconstruction, sequential assignment and – briefly – special techniques, such as maximum entropy and linear prediction. This gives a good indication of the challenges spectrum analysis poses for students, for example, at graduation level. A little older and also more in-depth discussion is provided by de Beer and van Ormondt[7] who focused on time domain fitting procedures, especially singular value decomposition. In this kind of historical review, it is appropriate to recommend a return to work carried out earlier and in related domains as a possible source of inspiration. This rather more dusty shelf contains the paper on spectrum analysis by Kay and Marple[8] as seen from the mid-1980s.

Obviously the standard monographs on NMR, such as Freeman's *Handbook*[9] and Ernst *et al.*'s *Principles of Nuclear Magnetic Resonance*[10] are of interest in this context as they also discuss some aspects of spectrum processing. In terms of difficulty, Claridge's recent volume on the *Tetrahedron Organic Chemistry Series*,[11] which inherited the title of a contribution compiled twelve years earlier by Derome,[12] lies somewhere between these two monographs. Cavanagh *et al.*'s monograph is a reference of choice[13] for all biological applications.

Finally, two other major sources of information deserve a mention. Firstly, the *Encyclopedia of NMR*,[14] which is an endless source of information. Given that the indexes are completely adequate, it will not be referred to here. Secondly, the *Annual Reports on NMR Spectroscopy* have sections which cover some of the aspects of this review. This is an exhaustive source of information on the most recent literature.

This review is focused on high-resolution applications and covers standard methods and some special techniques. Given the ease with which information can be found on the worldwide web, a review of available processing software turned out to be useless.

The very specialized processing techniques have also been omitted from the discussion. Only a few references are given below, however, these provide an appropriate starting point for more detailed bibliographic searches. These include application to NMR of solids,[15–18] complex hydrocarbon mixtures,[19,20] food analysis[21] and genetic algorithm.[22,23]

2. STANDARD PROCESSING TECHNIQUES

2.1. The Fourier transform

As mentioned above, the introduction of pulsed techniques by Ernst and Anderson[1] revolutionized NMR. Called FT-NMR because of the Fourier transform required to translate time-domain data into the frequency domain, to the despair of researchers developing alternative methods (see Section 3), the name is still legitimate as it is by far the most commonly used transformation technique. At a time when computer resources were quite scarce, the decisive step toward the Fast FT algorithm made by Cooley and Tukey[2] was very welcome. After this start, the field developed in parallel to the increase in computer processing power.

2.1.1. Literature

Two very comprehensive monographs on Fourier transforms dominate. The first is Brigham's classic[24] which covers the Fourier transform (FT), discrete Fourier transform (DFT) and fast Fourier transform (FFT) in detail. The properties are discussed not only mathematically but also visually. As the change in title indicates, the second edition[25] includes applications which mainly feature in the domain of radio frequency. The second classic is Bracewell's *Fourier Transform and its Applications*,[26] of which the third edition[27] is quite recent. It covers the same domain as Brigham but in slightly more detail and includes exercises. Thus it is more a textbook while the other can be considered as a reference manual. The less extended monograph by Marshall and Verdun[28] should also be highlighted for its coverage of NMR applications.

Two other references can be recommended for their brevity. A monograph on wavelets transforms contains a chapter by van den Bogaert[29] which provides a rather elegant and intuitive introduction to FT. In another volume from the same series, Eveleigh[30] also introduces the FT and related transformations in a concise and clear but more classically mathematical way. Finally, the paper by Angelidis[31] is also quite pedagogical but also more in-depth and a little longer.

2.1.2. Historical overview

Computationally important properties of the Fourier analysis were discussed by Ernst[32] at quite an early stage. For example, when combined with Hilbert transforms, the Kramers–Kronig relation between the real and imaginary components of complex data makes it possible to apply post-acquisition phase corrections. Ernst made some proposals for an automatic phase correction algorithm, but this kind of method was only routinely used after the developments made by Levitt and Freeman.[33] Note that compared with phase problems, the use of power

spectra often involved certain inconveniences.[34] Two papers discuss other aspects of Fourier transform data. Weiss *et al.*[35] and Howard[36] treated the question of the precision of signal position as a function of the apodization function for the first and noise for the second. With the development of two-dimensional techniques, quadrature detection in indirect dimensions has been developed. States gave his name to one of them[37] while the TPPI was developed by Marion and Wüthrich.[38] Both of these were further discussed by Keeler and Neuhaus.[39] Other properties of the Hilbert transform are exploited by Zolnai *et al.*[40] They present a method called Zooming, which allows interpolation of the spectral data of any given region of interest. Note that signal truncation gives rise to signal artefacts called sinc wiggles. This problem has found many solutions, mentioned in almost all of the following sections. The solution proposed by Keeler is a recursive method of peak finding applied to one-dimensional[41] or two-dimensional[42] spectra.

2.2. Spectral folding and aliasing

Violation of the Nyquist condition, giving rise to signal folding or aliasing into excessively small spectral windows, enables the saving of acquisition points for any given resolution. In one-dimensional spectroscopy, this is obsolete for two reasons. Firstly, the widely used digital filtering very efficiently eliminates any signal falling outside the chosen spectral window. Secondly, the memory capacity makes any saving in the number of acquisition data points quite futile. For indirectly detected dimensions of multidimensional experiments, on the other hand, reducing the number of acquisition allows one to save experimental time, provided the decrease of S/N ratio is acceptable. These considerations are introduced in the NMR monographs.[9,11,13] Note that Abilgaard[43] discussed some aspects of the problem in the context of least-squares analysis (see Section 3.5). Bax *et al.*[44] discussed them in the context of baseline distortion in indirectly detected dimensions. In order to avoid baseline problems due to phase corrections, they advised that the sampling delay (first increment time) be set to half the dwell time. Hodgkinson and Hore[45] discussed sampling consideration in the context of quantification of NMR data. Non-linear sampling schemes are discussed in detail for systems of increasing complexities. Two-dimensional applications of non-linear sampling are discussed in another paper by Hodgkinson *et al.*[46] It is shown that some non-linear acquisition schemes in which the number of increments is increased for important values of t_1 delays, improves the quantification of spectral parameters such as the active coupling constant. Note that as the FFT is inappropriate for the analysis of such data, most applications use maximum entropy techniques (see Section 3.7) to make the time-to-frequency transformations. For a more detailed discussion, also refer to the papers by Schmieder *et al.*[47–49]

To return to linear sampling, Jeannerat[50] presents a method using reference spectra enabling the resolution of ambiguities in heteronuclear two-dimensional experiments where the spectral window can be reduced up to the point where

the signal linewidth is limited by relaxation. A computer program makes it easy to determine the correct signal chemical shift out of hundreds of possibilities. Similarly relaxation limited high resolution can also be achieved using selective experiments.[51] When compared to the method above, it avoids the problems in chemical shift attribution and the inconveniences of the possible overlap due to folding or aliasing. The work of Morshauser and Zuiderweg[52] in the area of protein studies is just one example of the advantage of applying folding in multi-dimensional experiments. They make their case on four-dimensional experiments where the three indirectly detected dimensions have been folded or aliased. It can be appreciated that, provided the S/N ratio is not the limiting factor, it is possible to reduce the experimental time by a factor equal to the product of the three folding factors. Note that Kumar *et al.*[53] contains an interesting discussion of the underlying problem and the solution of maximum entropy.

2.3. Window functions

Also called apodization functions, window functions consist in giving different weights to different parts of time domain data. They have a history which is almost as long as that of pulse-NMR methods. In the beginning they were used as a way of improving resolution. However, they are routinely used today to diminish truncation artefacts. This rather disappointing evolution is compatible with some recommendations for not using window function.[3] It is nevertheless important to understand them since they have a strong influence on data resolution and S/N ratio. Note a recent review of this matter by Traficante and Rajabzadeh.[54]

2.3.1. Historical overview

A long paper published by Ernst[55] in 1966 discussed the problem of sensitivity in magnetic resonance. It may come as a surprise to see that some methods are considered as being applied at hardware level while nowadays, the immediate reaction is to use computer algorithms. Obviously, this is due to the paradigm change caused by the availability of computers. It is also surprising to see that most of the methods used today were already more or less explicitly presented at that time. An example of this is the Lorentzian-to-Gaussian transformation which was implemented by Ferrige and Lindon[56] in 1978. Before that, Campbell *et al.*[57] showed that good use of apodization methods can be quite efficient when only one-dimensional spectra of small proteins were available. The combination with relaxation agents introduces differences making it possible to obtain interesting information. They proposed a method called the 'convolution difference technique' which consists in multiplication of the FID with an exponential function. De Marco and Wüthrich[58] introduced the sinusoidal window function which was also later discussed by Guéron.[59] This increases resolution at the cost of a slight decrease in S/N ratio. Clin *et al.*[60] later found properties of the sine-bell function, making it possible to process data using the addition of a pair of dispersive

spectra, whereby one of them has been moved by one data point prior to Fourier transform. This opened the possibility of varying the data point shift, an option which has been explored by Lohman[61] as a means of modulating the strength of the windowing. Most functions had been introduced by 1980, thus, despite its age, Lindon and Ferrige's comprehensive review[62] is less obsolete than one might think. All that is missing are the shifted sine bell and the TRAF functions, since most publications in following years consisted in a discussion of the influence of window functions on parameter quantifications. Brereton *et al.*[63] introduced the shifted sine bell in 1981 and demonstrated its advantageous influence on the linewidth. They also show that the knowledge of an approximate T_2^* enables better adjustment of window functions. Traficante[64] introduced yet another function in which T_2^* is a parameter. It is claimed that S/N ratio does not suffer as a result of the application of this resolution enhancement function. The following year, Traficante and Nemeth[65] presented an improved version making it possible to choose to favor S/N ratio or resolution or to obtain an optimum balance between the two. The last contribution is a recent paper in *Concepts in Magnetic Resonance* by Traficante and Rajabzadeh.[54] This paper discusses all window functions with emphasis on the TRAF. Obviously the use of window functions has an influence on the precision and accuracy of the measurement of spectral parameters. Chan and Comisarow[66] discussed this problem of integration of one-dimensional spectra. Weiss *et al.*, who discussed the quality of peak area and NOE factors[67] in 1983, published a second version of the paper with the subtitle 'The effects of Apodization' a few years later.

2.4. Artefact reduction techniques

Baseline correction, t_1 noise[68–70] reductions and related methods are found under this heading. Many concern NOE experiments in which difficulties concerning quantification are the most acute. Note two papers by Weiss and Ferretti[67] and Weiss *et al.*:[71] the first discusses accuracy and precision in the estimation of peak areas and NOE factors, and the second focuses on internuclear distances. Liu *et al.*[72] also discussed the influence of experimental noise and peak integration errors on interproton distances. More recently, Lin *et al.*[70] simulated the influence of experimental imperfections on different kinds of experiments using gradients.

Baseline and baseplane corrections have been the subject of many different developments. A selection of these is described. Barsukov and Arseniev[73] presented a method based on Lagrange polynomials for the efficient reduction of the NOESY ridges. Dietrich *et al.*[74] introduced an automatic processing technique which first identifies peaks, then fits the remainder of the row or column to a fifth degree polynomial and then subtracts it from the original row or column. A few years later, Güntert and Wüthrich[75] introduce the FLATT algorithm about the same idea. For this method the regions of each row which

are devoid of signals are identified, a function that best fits these noisy sections is calculated before being subtracted from the whole row. Chylla and Markley[76] proposed a different approach called FaceLift which first calculates an individual baseline for each row or column and then applies a smoothing technique to avoid irregularities. Also, going to a true two-dimensional baseplane correction, Levy *et al.*[77] introduced a five-step procedure: (i) peaks and ridges are eliminated from the spectrum; (ii) the holes are filled using interpolation; (iii) a refined two-dimensional plane is calculated in the time domain; (iv) its frequency-domain correspondent is subtracted from the raw spectrum; (v) the ridges are corrected. Note that the origin of ridges was discussed by Otting *et al.*[78] who also provided some solutions for their suppression.

3. SPECIALIZED PROCESSING TECHNIQUES

3.1. Deconvolution methods

The definition of the convolution product is quite clear; like the one of the Fourier transforms, it has a given mathematical expression. An important property of convolution is that the product of two functions corresponds to the Fourier transform of the convolution product of their Fourier transforms. In the context of high-resolution FT-NMR, a typical example is the signal of a given spin coupled to a spin one half. In the time domain, the relaxation gives rise to an exponential decay multiplied by a cosine function under the influence of the coupling. In the frequency domain, the first corresponds to a Lorentzian lineshape while the second corresponds to a doublet of delta functions. The spectrum of such a spin has a lineshape which is the result of the convolution product of the Lorentzian with the doublet of delta functions. In contrast, the word 'deconvolution' is not always used with equal clarity. Sometimes it is meant as the strict reverse process of convolution, in which case it corresponds to a division in the reciprocal domain, but it is often used more loosely to mean simplification. This lack of clarity is due to the diversity of solutions offered to the problem of deconvolution, depending on the function to be deconvoluted, the quality one wishes to obtain, and other parameters.

3.1.1. Literature

Deconvolution is briefly treated in books on the Fourier transform,[25,27] however, as the literature devoted to the subject shows, it is a much broader subject. One example is the 1984 monograph by Jansson.[79] The theoretical sections are of general interest but the applications discussed focus on optical spectroscopy and, in a more recent edition,[80] image processing and relaxation. The first chapter is a very pedagogical and intuitive introduction,[81] while the third[82] and fourth[83] chapters provide an introduction to linear and non-linear deconvolution methods

respectively. The conclusion of the third chapter and the introduction of the fourth discuss some important aspects of the difference between the two kinds of processing techniques. Linear methods are seen as the poor man methods and only justified when time is a limiting factor. The others, being able to include constraints, are considered as the serious ones. One should nevertheless note that in NMR, many applications have been developed in the linear domain, especially for coupling constants measurements. In order to moderate Jansson's argument, it should be said that the linear deconvolution is advantageously used to determine these parameters. Other literature sources include the reviews written by Morris and coworkers on reference deconvolution. Concise[84,85] and extended[86] versions of these reviews have been published. The former[84] presents reference deconvolution as a kind of window function tailored to the reference lineshape. The latter[86] is a detailed 60-page discussion. Metz *et al.*[87] published the most recent review of this subject, albeit from a more medical point of view.

3.1.2. Historical overview

In 1977, the foundation for deconvolution was set by Wouters *et al.*[88,89] in the domain of continuous wave techniques called 'reference lineshape adjustment' (RLSA), however it has retained its relevance in FT techniques. The first paper[88] introduces the notion of considering an experimental signal as the convolution product of a function depending on the sample, and a weighting function depending on the experimental conditions. The authors proposed to take the differences in the latter into account in order to obtain similar lineshapes. In the context of difference spectroscopy, the introduction in one of the compared elements of the difference between the experimental condition of the two should result in ideal subtraction. The application of reference lineshape adjustment (RLSA) to gramacidin S can be found in a second paper.[89] In 1980, deconvolution was applied in the time domain by Clark and Lillford[90] for the analysis of NMR relaxation decays. They made no assumption about the decay shape, but the method requires very favorable S/N ratio. The following year, Kauppinen[91] developed the theory of self-deconvolution in the IR domain, allowing the improvement of resolution by a factor of three with S/N ratio of about 1000. More practical approaches reached the domain of NMR in 1983 when Kumar *et al.*[92] proposed a method allowing the distinction of signals overlapping by up to 90% and their quantification at up to 50% overlap. An implementation based on minimization of the sum of squares of the difference between experimental and simulated spectra has become a standard procedure used in many NMR processing software. Belton and Wright[93] introduced constrained deconvolution (CD), a method that considers the spectrum to be the convolution product of a sum of delta functions with a single lineshape plus noise. The positions of the delta functions are determined using a minimization of the smoothness of the convolution product of the reconstituted sum of delta functions minus the experimental spectrum. The lineshape used for minimization has to be introduced. In the mid-1980s, Ni

and Scheraga discussed the application to phase-sensitive spectral analysis[94] and combined self-deconvolution with maximum entropy (see Section 3.7). Bothner-By and Dadok[95] proposed to manipulate the FID of doublets in order to measure the splitting and obtain simplified spectra. The strength of the method over the alternative of the time is the total independence of the lineshape; it requires only that the doublet component have the exact same shape. In order to eliminate the effect of an in-phase doublet corresponding to a cosine function in the time domain, they proposed to divide the FID by a cosine function with a different tentative frequency and to view the amplitude and width of the line and the baseline artifacts as a criterion for a successful simplification.

Deconvolution methods can also be used to suppress residual water signals as demonstrated by Marion *et al.*[96] Assuming that the latter are at the center of the spectral window, water is responsible for the low frequency component of the FID. A convolution of the time domain spectrum with a Gaussian or sine bell makes it possible to filter out the higher frequency and only retains the water component, which can later be subtracted from the original FID. This procedure can be fully automated and is quite appropriate for two- and three-dimensional experiments in the presence of water. The same year, Hoffman and Levy[97] applied a computationally very demanding simulated annealing method to one-dimensional NMR spectra.

In 1988, Morris published his first paper on reference deconvolution[98] using an algorithm they called FIDDLE, i.e. Free Induction Decay Deconvolution for Lineshape Enhancement. Observing that many instrumental imperfections affect equally all the signals in a spectrum, he concluded that one should consider deconvoluting the whole spectrum with the lineshape of an isolated peak to obtain an 'idealized' spectrum. The calculations are similar to that of Bothner-By (see above) in that the experimental FID is divided by the time domain expression of the ideal lineshape, but differs in that it should not contain zeros which cause division problems. An illustration is given in the case of a signal with very high S/N ratio, but one should keep in mind that the success of the process is quite dependent of the S/N ratio of the whole spectrum and especially of the reference signal. The same author[99] presented an application to Nuclear Overhauser Effect Difference (NOED) spectroscopy, in the context of which the problem due to the Block-Siegert shift had been discussed by Mersch and Sanders.[100]

A recursive lineshape deconvolution process enabling the improvement of resolution and contrast in one-dimensional and two-dimensional NMR has been proposed by Ni and Scheraga,[101] while a similar effect is obtained in the field of imaging by Liu *et al.*[102] Still in the domain of medical applications, Jehenson and Syrota[103] proposed a solution tailored to process spectra affected by artefacts due to gradient-induced Eddy currents. In *in vivo* applications, where spectra often show a lineshape which often differs significantly from pure Lorentzian, Gaussian or mixed lineshape, de Graaf *et al.*[104] proposed an alternative to the HOGWASH[41,42] against which some arguments are developed. Called QUALITY, the new method is less demanding with respect to the quality

of the reference line and consists in removing the component that is due to relaxation and isolate from it the component that is due to field inhomogeneities. The latter can then be used to deconvolute the whole spectrum.

In 1991, Gibbs and Morris[105] discussed reference deconvolution as a means of eliminating distortions due to truncation of the reference signal. For many reasons, the reference signal should be as narrow as possible, a requirement that is in conflict with keeping a maximum of signals at both sides. The authors resolved this conflict by giving two solutions to minimize truncation. The first concerns the step whereby the reference signal is inverse-Fourier transformed. Knowing that the dispersive signal decreases far more slowly towards the baseline than absorptive ones, the authors proposed ignoring the imaginary part of the spectrum and taking advantage of the symmetry properties of the FT to reconstruct a reference FID solely based on the real component of the data. The second solution consists in realizing that artefacts due to the ever so slightly truncated absorptive signal artefacts can be eliminated by moving the reference signal to the baseline before the inverse-Fourier transform. In another publication, Gibbs *et al.*[106] are concerned with t_1 noise or, more precisely, the part caused by artefacts in the indirectly detected dimension. They propose the application of a reference deconvolution to each t_1 increment. A more complex alternative is also considered. It consists in using the deconvolution in a two-dimensional fashion taking a rectangular reference signal that covers the whole first frequency domain, in order to include all t_1 noise, and a small region in the second frequency dimension near a single peak. The processing is otherwise similar to the one-dimensional version presented above, except that the signal subtraction, which is usually applied during acquisition by means of phase cycling, is applied here after the reference deconvolution step, making it necessary to acquire two sets of data.

The same year, Huber and Bodenhausen[107] considered the frequency domain deconvolution of the multiplet structure due to scalar coupling of isolated signals in one-dimensional or two-dimensional spectra. Their method makes it possible to measure active and passive couplings in a step-by-step deconvolution of antiphase and in-phase splitting respectively. The method consists in running a pointer from one side of the multiplet and adding or subtracting farther ahead the amplitude measured at the pointer position. The distance to which the amplitudes are changed is a trial coupling constant that successfully simplifies the structure when it matches a coupling constant. It has been applied for the measurement of active coupling in soft-COSY spectra. Another paper[108] shows the advantages of running the above process in both directions.

The coupling constant also interests Jones *et al.*[109] However, they preferred to apply a combination of methods working in the time domain. They proposed to analyze the multiplet structure of COSY cross-peaks by (i) measuring the active coupling using J-doubling (see Section 4.8), (ii) calculating a simplified spectrum using a maximum entropy method, taking into account the knowledge of the coupling J-deconvolution, (iii) estimating the passive coupling, (iv) refining the values found by model fitting to the experimental multiplet. With respect to

the first step, they make some comments about the methods requiring divisions in the time domain, especially the problem posed by division with zero or near zero values, and mention the alternative consisting in making the sum of the squares between experimental and frequency domain data that is under construction.

In 1994, Woodley and Freeman[110] proposed a frequency domain lineshape deconvolution of J-spectra enabling the transformation of signals with broad tails in both orthogonal dimensions into a Gaussian lineshape. In the process, the linewidth is reduced by a factor $\sqrt{3}$. Their method requires a peak picking procedure and gives rise to some artefacts where signals overlap. It is not a deconvolution in the strict sense as it does not exactly revert the effect of the convolution giving rise to the lineshape, but approximates it. The result is nonetheless a projected 'decoupled' one-dimensional spectrum with much better signal separation. In the same vein, del Río Portilla and Freeman[111] introduced an algorithm for doublet deconvolution. Here also, the method simplifies doublets into singlets only in cases devoid of overlap, however, this is fast and may be considered a convenient method for measuring splittings. In the case of complex structures however, it may be difficult to distinguish true couplings from the sum and differences of the latter. In 1995, Maudsley[112] became interested in the processing of *in vivo* applications where linewidths are often severely distorted and proposed the use of self-deconvolution as a means of determining the spectral lineshape which can later be used in a reconstruction method. Broadly speaking it consists in (i) approximating the spectrum lineshape using a Gaussian or Lorentzian functions, (ii) determining the signal's positions in the form of a delta function spectrum using deconvolution, (iii) dividing the experimental FID with the time domain form of the delta function spectrum to obtain, after Fourier transform, a crude spectral lineshape which can be refined later.

In the area of imaging of different chemical species with various concentration ratios and for which the spectral widths are larger than the pixel spatial dimension, deconvolution was shown to be useful by Baldwin *et al.*[113] Barjat *et al.*[114] proceeded in the vein of reference deconvolution in a paper addressing the problem of division by zero and provide a very detailed study of the determination and refinement reference signal. It shows that in the case of favorable S/N ratio, a well-refined reference spectrum permits drastic limitation of artefacts due to division by zero. The following year, the issue of t_1 noise (see above) was revisited by the same group after the introduction of PFG experiments. Horne and Morris,[115] remembering that in two-dimensional and higher-dimensional spectroscopy signal to artefact ratio is often more problematic than signal to noise, show that the threshold of detectability can be reduced by more than an order of magnitude. Firstly, discussing the t_1 noise and S/N ratio in both gradient and phase-cycled COSY, they make it clear that the reputation of gradient experiments as showing no t_1 noise artefacts is ill founded. The reason is simply that the latter methods are no less prone to spectrometer imperfections than the former. Secondly, they remind us (see above) that reference deconvolution can be applied to each t_1 increment of two-dimensional spectra. For some experiments

thus, the modulation of the signal makes some increments show near zero amplitude, which is a complication for the deconvolution. When possible, i.e. when the phase cycle eliminates constant signal, this inconvenience can be avoided by acquiring the spectrum in such a way that deconvolution can be applied before constant signal addition and subtraction.

In the area of solid-state NMR, deconvolution of powder patterns is the subject of a paper by McCabe and Wassall who introduce an FFT version of DePaking[116] and address the problem of identifying superposed signals.[117] The method, first introduced by Bloom *et al.* for axial[118] and non-axial[119] systems, had previously been discussed by Curtis *et al.*[120]

Interested in quantifying signals stemming from spectra of biological media with ^{13}C and deuterium enrichment, for which some prior knowledge is available, Laatikainen *et al.*[121] proposed a linear method that picks up, step-by-step, the identified signals from raw spectra.

To return to the deconvolution of the effect of scalar coupling, Jeannerat and Bodenhausen[122] extended the work carried out by Huber (see above) and proposed a recursive approach to the measurement of coupling constants in cross-peak multiplets of selective experiments. They claimed that the largest splitting can be measured reliably in any multiplet structure devoid of second-order effects. The largest coupling is measured and the value used to eliminate the multiplet structure due to it. The resulting structure is submitted to another measurement-simplification cycle until all the coupling constants have been determined. Application to the measurement of passive couplings in soft-COSY multiplets, requiring the exploration of two independent variables, is also demonstrated in the same paper,[122] while the application to non-selective DQF-COSY spectra is presented elsewhere.[123] A similar method is proposed by Garza-García *et al.*[124] who used a combination of the latter deconvolution scheme with a J-doubling procedure. A detailed discussion of the reliability of the measurement of the coupling constants as a function of the linewidth follows.

In 1998, Hu *et al.*[125] proposed a combination of FDM (see Section 3.3) and reference deconvolution making it possible to obtain a peak list which, according to the authors, is the ultimate goal of most NMR analysis. Reference deconvolution can also be made in the frequency domain as shown by Goez and Heun.[126] They first discussed the problem of the singularity of division by zero, mentioned above, and proposed a computationally more demanding method that requires an iterative algorithm. The idea consists in constructing a frequency domain function that is the inverse of the function giving rise to the signal broadening. A convolution product of such a function with the raw frequency domain spectrum results in a spectrum from which the broadening has been removed. This method is also very sensitive to S/N ratio but it is not obvious how it compares with time domain versions.

Note the special application of lineshape deconvolution by Hou *et al.*[127] to one-dimensional and two-dimensional spectra acquired using special probeheads where more than one detection coil are used in parallel.

3.2. Linear prediction

Linear prediction is a method which takes advantage of a property of linear functions making it possible to extend the data series as a sum of exponential decaying sinusoids. Obviously the range of the extended series depends on the number of known data points, the number of decaying signals and S/N ratio. It enables the filling of the missing parts of a truncated signal at either end or a gap in the middle of free induction decays. The most important use concerns data in indirectly detected dimensions of multidimensional experiments. It is known that in cases in which experiment time restrictions give rise to a severe truncation artefact, sinc wiggles appear after Fourier transformation. Window functions can eliminate these wiggles most of the time at the cost of a decrease in resolution, but linear prediction avoids these inconveniences to the extent that it is successful in extending the FID.

3.2.1. Literature

Two quite comprehensive reviews should be highlighted. First, the recent paper in *Progress in NMR Spectroscopy* by Koehl,[128] and a 1992 paper in *NMR Basic Principles and Progress* by de Beer and van Ormondt.[7] Others are cited in the following paragraphs.

3.2.2. Historical overview

The first discussion of linear prediction (LP) using singular value decomposition (SVD) was presented by Barkhuijsen *et al.*[129] together with a shorter version of the paper.[130] They first highlighted a limitation of FT, for which the smallest observable splitting is the inverse of the duration of the signal. Then, they developed a method inspired by Kumaresan and Tufts[131] whose work was based on the two-hundred-year-old findings of Baron de Prony. It consists in using Singular Value Decomposition (SVD) to analyze raw data and return a table of frequencies, amplitudes, damping factors and phases. The implementation is discussed in detail and applications are shown including simulations of signals with added noise and *in vivo* ^{31}P spectra. The following year they devoted a paper to error theory in LP.[132]

The same year, Tang *et al.*[133] presented an alternative to SVD in order to speed up the determination of LP coefficients. They used the truncated Householder triangularization decomposition, known as QRD, and mention the Cholesky decomposition as less stable. QRD is said to be at least five times faster than SVD. The same paper mentioned the advantage of backward LP over forward LP in making it easy to discriminate between coefficients corresponding to signals and those that correspond to noise, according to their position on a unit circle of the complex plane, at least when the S/N ratio is large enough (20 dB). Still in the context of algorithm improvement, Porat and Friedlander proposed a modification of the Kumaresan–Tufts method.[134]

The following year saw the publication of three papers by Tang and Norris[135–137] using a combination of LP and z-transformation. The first paper presents LPZ-QRD[135] with the claim that it gives better resolution and sensitivity than FT and is computationally more stable than LPQRD and LPSVD, especially with polynomial equations of large order. The second is devoted to a variant using LPZ-QRD, for which it is shown that an increasingly large number of added points allows one to see an increase in resolution.[136] The third is concerned with a combination of LPZ and autoregression called LPZ-AR.[137] It has similarities with maximum entropy methods (MEM), but unlike MEM, implementation of time could be applied to signals with arbitrary phases. A comparison between LPQRD, LPZ-QRD, LPSVD, LPZ-SVD and LPZ-AR using the Burg method was published a few years later.[138] Barkhuijsen *et al.*[139] came back to the field proposing an alternative based on the Hankel matrix called HSVD. It needs less computer calculation but still required the use of the SVD method. The paper concludes with a discussion of the similarities with LPSVD which is developed further by Yan and Gore.[140] De Beer *et al.*[141] review the domain of quantitative analysis of time domain signals. Their paper discusses the principle of linear methods, but also the state space formalism and model fitting methods in a quite pedagogical way before addressing the question of the precision of each method.

Delsuc *et al.*[142] showed that the modification of the Kumaresan–Tufts algorithm introduced by Porat and Friedlander (see above), and later called FB-LP, is able to manage spectra with lower S/N ratio than LPSVD. They proposed combining forward and backward LP in order to avoid cases where the criterion of the unit circle for discriminating signal from noise[133] fails.

Gesmar and Led[143] argued in favor of the Cholesky methods as soon as the number of acquisition points is much larger than the number of signals, for example when working with a broad spectral window line in ^{13}C NMR. They claimed that double precision calculation is stable and such application manageable. The argument of QRD storage requirements and the excessive computer calculation time did not age very well in the context of the increases in computer power and memory capacity. Examples are given for both ^{1}H and ^{13}C spectra of a heptapeptide but the results are disappointing if one expects to isolate each individual signal in crowded regions. Johnson *et al.*[144] propose an application to two-dimensional chemical exchange experiment with the calculation of error estimates using a Monte Carlo method.

In order to avoid some computational limitations, Tang and Norris[145] proposed a modification called LP-ZOOM. The idea consists in focusing on a spectral region of interest and using the z-transform for the analysis.

In 1988, Stephenson published a review on linear prediction and maximum entropy methods.[146]

The next year, Marion and Bax[147] proposed a method to make NOESY spectra more reliable. It consists in using LP in order to correct the first FID points that are otherwise responsible for disturbing baseline artefacts.

Two-dimensional applications are discussed by Gesmar and Led[148] who applied LP to a COSY spectrum just before Zeng *et al.*[149] The latter proposed combining linear prediction in order to prolong the FID and use FT together with window functions which improve resolution. The Total Least Squares (TLS) procedure developed by Tirendi and Martin[150] consists in using DFT in the directly detected dimension and LP in the directly detected dimension only to elongate the data series before being Fourier transformed. They proposed using the computational efficient Levindon–Durbin algorithm to solve the least squares problem. The same year, the same authors[151] discussed the quantification of parameters using their method. For a comparison with LPSVD, see Uike *et al.*[152] who concluded in favor of a modified TLS. Around the same time, Millhauser *et al.*[153] presented the Lanczos-HSVD, also a fast algorithm for spectral decomposition. Olejniczak and Eaton[154] favored the Burg algorithm for the processing of relatively noisy three-dimensional spectra and advised using LP to increase the number of data points by 50%. Interested in the TOCSY-TOCSY three-dimensional experiments, Cieslar *et al.*[155] also exploited linear prediction to improve spectral resolution.

Applications to *in vivo* ^{31}P application, where the S/N ratio is often of concern, have been explored extensively.[156–158]

With application to three-dimensional[159] and four-dimensional[160] experiments in mind, Zhu and Bax[161] introduced a variant of LP taking advantage of the knowledge of the phase in all indirectly detected dimensions. They also argued that it is favorable to start sampling with half a dwell time rather than near zero values.

In 1990, Gesmar *et al.* published a review[162] discussing, among others things, LP methods. This makes it possible to find one's way through the literature following an interesting introduction which explores LSQ methods. The next year, Led and Gesmar published two other reviews[163,164] devoted entirely to LP. The first[163] explains the possibilities of the technique in more detail and proposes referring to Stephenson's review[146] for a deeper theoretical discussion. The second of these reviews[164] is a shorter contribution to a book edited by Hoch.

Application to ^{1}H–^{13}C HSQC and HMBC are presented by Led and Gesmar[165] who show why HSQC experiments should be preferred when attempting to improve resolution using LP. In another paper, they showed the advantage of using LP when working with selective variants of HMBC[166] where important phase problems arise.

The advantage of LP methods for extracting spectroscopic information from spectra is exploited by Haselgrove and Elliott[167] who developed a computer intelligence algorithm which is able to analyze a large quantity of data based on a user-defined pattern of expected components.

In 1992, Diop *et al.*[168] applied LP to *in vivo* ^{31}P NMR, the enhancement procedure used in speech signal processing.[169] In a detailed study including simulations with different S/N ratio, they showed that the enhanced procedure EPLPSVD is able to manage signals with S/N ratio larger then 1.2, while the classical LPSVD only manages data with S/N ratio larger than about 4. In an

extensive study, Zaim-Wadghiri *et al.*[170] applied the methods to thousands of ^{31}P spectra. The same year, Pijnappel *et al.*[171] also discussed additional SVD methods in the context of *in vivo* ^{31}P NMR spectroscopy. A comparison of the results arising from HSVD and LPSVD allowed them to conclude that the first is computationally more efficient.

Zhu and Bax[172] proposed a variant of FB-LP (see above) which, instead of making the new set of roots (after root reflection) based on their position with respect to the unit circle (with the risk of missing small components taken as noise), proposed to take the average of the values found in the two sets of roots. The resulting improvement is claimed to be about 1 dB. The same year, they[173] also introduced a two-dimensional version of LP as an answer to the problems of lineshape distortions and artefacts. They also show that the number of signals found in one-dimensional spectra is at most one quarter of the number of data points. In the three-dimensional version, the requirement for having four times as many points as signals is still valid, however this time, the number of signals is counted in a multidimensional structure and compared to the product of the number of data points in each dimension.

Boudhabhay[174] presented the application of the Padé–Laplace method (PLM) to ^{14}N-NMR while Tellier *et al.*[175] applied it to situations of signal overlap to measure multiexponential proton relaxation with four coefficients.

Kölbel and Schäfer[176] implemented the improvement and automation of the LPSVD algorithm. They addressed the problem of regularization, the step where the singular values are split into those corresponding to noise and signal. They introduced a method called continuous regularization, LPSVD(CR), enabling the determination of the cutting position. The same principle is applied to calculation of the linear equation for calculation of intensities and phases.

Lin *et al.*,[177] interested in the relaxation parameters of NMR decays, developed a variant of LPSVD that reduces noise contamination. It has been applied to cases with a small number of signals and subjected to serious comparison with alternative methods.

One year earlier, De Moor[178] revisited the theoretical aspects of SVD and, in particular, the influence of noise on the success of the decomposition. He introduced the notion of the long and short space of noisy matrices as a way of distinguishing those which make it possible to apply SVD from the others.

Gesmar and Hansen[179] presented another algorithm which produces the same results as QR methods. This is called Fast Linear Prediction (FLP) due to the fact that it is an order of magnitude faster. The paper briefly examines each of the known algorithms and is, thus, a good review of the matter. An extension to the study of this algorithm was proposed a few years later by Ohba.[180] The two latter methods, LPSVD(CR) and ELPSVD, are combined by Diop *et al.*[181] for the automatic quantification of *in vivo* ^{31}P NMR. Yet another method, known as HTLS, is proposed by Van Huffel *et al.*[182] and combines TLS and HSVD. It has been successfully applied to simulated *in vivo* spectra. Note also a new algorithm

introduced by Chen *et al.*[183] which significantly accelerates the computation of Henkel structure.

The ability of LP to resolve pairs of signals as a function of their chemical shift differences and linewidths is discussed by Koehl *et al.*[184] in cases of simulated spectra. The precision and accuracy of LP results is considered. It shows the difficulties LP has in resolving signals separated by a distance smaller than their linewidth at a S/N ratio of 10 dB. The influence of the number of acquired data points seems to favor oversampling when possible. They also published another paper on the limits of LP applied to ^{13}C simulated spectra mimicking a peptide[185] as a function of linewidth and S/N ratio, which may also dampen enthusiasm for these techniques.

Diop *et al.*[186] proposed an improvement of their ELPSVD (see above) and explained how it can be applied, not only to LPSVD but also to HSVD and TLS.

LPSVD is used with success by Lee *et al.*[187] for the processing of VACSY experiments used in solid-state applications where phase twists are unavoidable.

Babcook *et al.*[188] studied the reliability of the measurement of NOESY signals in DNA samples. They claimed that LPSVD is reliable enough to replace the acquisition of between one-half and two-thirds of the data points in the first dimension.

Yet another version of LP has been proposed by Fedrigo *et al.*[189] They introduced a modified autocorrelation function (MAF) based on Cadzow's work (see above) that improves S/N ratio. Examples of low S/N ratio ^{31}P data are given. The same group[190] presented a modified SVD method for application to the processing of selective experiments applied to biopolymers.

Nuzillard[191] demonstrated that application of LP to the first dimension of two-dimensional homonuclear J-resolved experiments usually displayed in magnitude mode can be made sharper and present a higher S/N ratio.

The question of estimating the time origin of signal phases is discussed by Vondra *et al.*[192] The aim is to study signal phases in order to calculate what should be the ideal phase correction parameters.

A fully automatic implementation of LPSVD(CR) for *in vivo* analysis of ^{31}P spectra is presented by Totz *et al.*[193] together with a detailed study of many alternative methods.

Zhu *et al.*[194] proposed the use of LP to remove the solvent signal in non-deuterated solutions and the exclusive use of low power presaturation.

Reynolds *et al.*[195] addressed the question as to why the powerful LP methods remain of so little use years after their potential was first demonstrated. They tried to convince HSQC users to apply linear prediction with their detailed study of natural products. They showed that resolution can be improved by a factor of up to 16 in the first spectral dimension when the S/N ratio is favorable. Similarly, treatment of DQF-COSY spectra makes it possible to obtain a factor of two resolution improvement which means a factor two in acquisition time.

Finally, in the context of signal analysis, the paper by Lin *et al.*,[196] who took an alternative route to determine FID components, deserves to be highlighted.

The method, called ITMPM, is based on information theory and compares quite favorably with LPSVD, especially in cases with low S/N ratio as shown by Monte Carlo simulations.

3.3. Filter diagonalization

Filter diagonalization methods (FDM) consist in considering the problem of the determination of the signal frequencies and amplitudes of an FID as a quantum mechanical problem where eigenvalues are to be calculated. The common element allowing the transposition is the exponential nature of the evolution of both systems. Note that the notation used in the FDM literature has remained that used in quantum mechanics for the Hamiltonian, wave functions, etc., which may be confusing. But since NMR spectroscopists are used to this notation, it makes it easier to keep in mind which signs correspond to which kind of mathematical object, even if it does not designate the particular object they are used to.

3.3.1. Literature

The different implementations of FDM are discussed in a recent paper by Chen and Mandelshtam.[197] The paper mentions DFT/FDM hybrids and multiscale techniques. Theoretical background can also be found in the two papers by Mandelshtam[198] and Hu *et al.*[199]

3.3.2. Historical overview

Neuhauser[200,201] developed filter diagonalization (FD), a method allowing determination of the eigenstates and eigenvalues of an operator, eliminating correlations according to the distance of their states. The distant ones are eliminated through short-time filtering and only the close ones require diagonalization. In 1995, Wall and Neuhauser[202] realized that short time series can be advantageously analyzed using FD, a property that prompted applications to spectroscopy. Mandelshtam and Taylor[203] applied it to vibrational spectroscopy after a simplification which is rigorously applicable to finite discrete time series. Other papers are devoted to a more detailed discussion[204] and application to multidimensional cases.[205] The first application to NMR appeared in 1998. Mandelshtam *et al.*[206] applied FDM to the processing of two-dimensional spectra. The method returns a list of peak frequencies, amplitudes and phases enabling the reconstruction of ersatz spectra which always compare very advantageously with DFT spectra. The authors claimed superiority of FD over linear prediction and showed that experimental time can be saved as FDM can process spectra with a few t_1 increments. Around the same time, Pang *et al.*[207] developed further FDM methods and envisaged a multidimensional application presented in a separate paper by Wall *et al.*[208] presenting the analysis of DQF-COSY spectra. Hu

et al.[125] provided more details on the NMR implementation of FDM. Discussions of the differences with LP-ZOOM (see Section 3.2) and reference deconvolution (see Section 3.1) are also provided. Illustrative examples follow. Applications are discussed in a separate paper by Mandelshtam *et al.*[209] who presented the implementations for one- and two-dimensional spectra together with examples. It has been shown that the passage via the peak list is not obligatory and that FD can also be applied as an improvement method using the averaging of different calculations[210] in an application to 2D *J*-spectra. An application to pulsed EPR is also shown by Jeschke *et al.*[211] Multidimensional FDM methods were reviewed in two parts in 2000, whereby the first[198] considered the theory and implementation while the second[199] discussed application to two-dimensional spectra as well as two-dimensional projections of three- and four-dimensional spectra. Chen and Mandelshtam[197] discussed applications in which the S/N ratio is less favorable. In order to overcome the instability of the calculation and the deterioration of the accuracy of the usual implementation, they introduced a multiscale FD. Instead of searching for narrow and well defined signals, they allow the bandwidth to change, making it possible to reliably locate poorly localized signals. With respect to the problem of calculation averaging to avoid numerical instabilities, two regularizations were proposed by Chen *et al.* The first[212] introduced a new regularized resolvent transform (RRT) while the second[213] presented a new algorithm called FDM2K which avoids the averaging.

3.4. Wavelets transform

While the Fourier transform allows one to alternate between the two orthogonal time and frequency domains, the wavelets transform gives access to both domains at once. It is the mathematical tool of choice for following changes of frequency since it produces results as a function of time and frequency.

3.4.1. Literature

The recent volume of *Data Handling in Science and Technology*, which is devoted to the chemical application of wavelets,[214] deserves to be the top reference on wavelets transform. It includes very clear introductory chapters among which the second[215] will win the favor of NMR spectroscopists for making the bridge between Fourier and wavelets transforms. The rest of the book covers both deeper theoretical aspects[216–221] and some chemical applications, from which NMR is missing. At the level of introduction of the mathematical aspects, the monograph by Kaiser[222] can be recommended for students at the graduation level. Application to NMR reviews are a little scarce, however, both the difficult paper devoted to mathematical aspects of imaging in X-ray and magnetic resonance published by Schempp[223] and a review, *Wavelets Analysis in Analytical Chemistry*, published in 1998,[224] which includes a short section devoted to NMR, are worthy of mention.

The literature discussed below should be consulted for information on more recent developments.

3.4.2. Historical overview

The application of wavelets to the processing of NMR data is quite recent. It started in 1996, when papers were published on very different aspects of NMR. By nature, the wavelets transform (WT) seems quite appropriate for dynamic study, and this is highlighted by Neue[225] who illustrated its strengths in a study of chemical intermediates and slow exchange processes. The paper serves as a good introduction to the technique and demonstrates cases for which it should be of highest interest in NMR. However, other fields have also made good use of WT. With the automatic processing of *in vivo* ^{13}C NMR spectra in mind, Tate *et al.*[226] compared the results of peak amplitude measurements with wavelets transform using a single mother wavelet. The goal was to find the method that distinguishes the best data from different origins. Three statistical methods were used to compare wavelets and peak amplitude measurements: principal components analysis, correlation and discriminant analysis. It is shown that the latter is quite convenient and that wavelets have important advantages over peak amplitude measurements. The same application is considered by Johnson *et al.*[227] who studied multiple-window spectrum estimation (MWSE) methods for processing these noisy data. Note that MWSE does not use wavelets, but has some similarities with them. De Certaines *et al.*[228] use WT for the analysis of lipoprotein, but little is said in the paper about the implementation. Sarty and Kendall[229] applied WT in the field of diffusion imaging techniques. In cases of both good and relatively poor S/N ratio, it is shown that WT give more satisfactory results than FT. Back with imaging spectroscopy, Serrai *et al.*[230] presented a very detailed study of spectroscopic parameters measured using WT. A long and comprehensive discussion of the mathematical aspects is followed by applications to simulated and experimental data in which signal amplitude, frequency, T_2^* and phases are measured. The same year, Barache *et al.*[231] discussed the same type of application, but focused on the elimination of large signals and the correction of phase shifts due to eddy currents. Their treatment differs from others in their choice of continuous instead of discrete WT. They defend their choice and describe its differences in an appendix. Note also that the older method developed by Ordidge and Cresshull[232] enables the correction of phase distortions due to residual Eddy currents triggered by B_0 gradients during acquisition. Back in the context of *in vivo* spectroscopy, Young *et al.*[233] proposed the separation of signals into two kinds. The first are signals whose origin is known and which can be managed using parametric methods. A least-squares fit is used to obtain a first estimate of the spectrum parameters and subtracted from the spectrum. The resulting spectrum, containing the second kind of signal, i.e. noise and artefacts, is analyzed using non-parametric WT. Repeating the two steps causes rapid convergence. In the domain of complex mixtures analysis, Serrai[234] showed how

WT can be applied to the measurement of plasma lipoprotein fractions, an application where quantifications are made difficult by signal overlap and broadening. The same authors[235] published a paper more recently, in which low S/N ratio in ^{23}Na spectra are quantified using WT, and another on ^{1}H-NMR and, more precisely, water suppression, a prerequisite for a quantitative measurement of other signals. This water signal suppression problem has also been studied by Antoine *et al.*[236] who discussed frequency domain approaches and compared wavelets and Gabor transforms to the advantage of the latter. Shao *et al.*[237] examined the ability of WT to enhance spectral resolution. Both simulated and experimental spectra are submitted to WT analysis. It is shown that this technique can be applied with success, but it requires some prior knowledge. Finally, in work in the area of solid-state NMR, Ding and McDowell[238] claimed that DWT-processed SPEDA spectra give better results than CRAMPS techniques. The ideas consist in exploiting the fact that the spectral contents change within the duration of the FID. Wavelets are then on their favorite ground being able to cover the different time frames of the FID.

3.5. Least-squares fit

Fitting experimental data to simulations requires criteria for measuring their success. Least squares (LS) have often used for this task and consist in searching for the minimum of the sum of the squares of the differences between experimental and different simulated data. Note that some methods use a least-squares fit but are named after the way in which the simulations are conducted. For example most implementations of linear prediction conceal a least-squares fit at their core. This section will discuss all of the methods which are not dealt with in other paragraphs.

3.5.1. Literature

The techniques discussed under this heading often have very little in common and this explains the absence of specific literature on this topic. Note the following two papers which discuss the theoretical aspects of linear predictions[239] and a variant used in some linear prediction methods called 'total least square'.[240]

3.5.2. Historical overview

Non-linear-least-squares analysis was first used by Moore[241] in 1975 to determine spectral parameters in cases of exchanging spins described by Gutowsky and Holm.[242] The minimum LS was used as a criterion for the determination of the best parameter for a spectral line obtained using DFT. In 1981, Dietrich and Gerhards[243] discussed a parabolic baseline correction also taking the two phase correction parameters as variables. In the second step, a procedure fits the

peaks that are not overlapping. Other non-linear LS analysis has been used by Abildgaard *et al.*[43] to measure spectral parameters in cases of low numbers of signals with the advantage of providing error estimates in spectra which suffer from strong baseline artefacts.

Working on the problem of NOESY integration (see also Section 2.4), Denk *et al.*[244] proposed a method enabling the evaluation of signal volumes in a way that is similar to one-dimensional spectroscopy, where signals having different relative amplitudes are integrated even in partial overlap situations. Holak *et al.* later proposed[245] the assumption that cross-sections through any signal differ in amplitude but not in lineshape and decided to calculate a signal volume by taking two orthogonal cross-sections that do not necessarily run through the peak maximum. The user selects a cross-section and baseline for each signal. The method had the advantage of allowing for partial overlap without loss of precision. Manassen *et al.*[246] proposed the use of one-dimensional data in order to optimize the number of increments of two-dimensional experiments. The principle involves taking advantage of the parameters extracted from the first in order to help to reconstruct the second.

Kumaresan *et al.*,[247] who are usually active in the field of linear prediction, proposed two approaches which were not too demanding in computational terms and applied to the frequency domain. The first consists in iteratively minimizing the difference between the experimental spectrum and a simulated one that may also require significant computer resource. The second consists in picking one line after the other, a method that should be quite fast.

Taking into account the FT artefacts in spectrum integration studied by McLeod and Comisarow[248] and the work of Holak (see above), Gesmar *et al.*[249] proposed a least-squares analysis of two-dimensional spectra that can accommodate more problematic overlap situations. Led and Gesmar presented a review[250] of the quantification of NMR parameters of biological macromolecules. Finally, and in response to Holak's work, they presented a combination of prediction methods and linear LQ methods to improve NOESY signal integration in a paper by Kristensen *et al.*[251] The first provides the starting values needed by the second and makes it possible to avoid baseline problems (see Section 2.4). Still in the field of NOE quantification, Brown and Huestis[252] applied LS fit to two-dimensional spectra using a modification of Denk's method. It is implemented on the optimization toolbox of the Matlab[253] calculation platform.

Measurement of the active coupling constants from the COSY spectra of polypeptides have been studied by Yang *et al.*[254,255] In the first paper,[254] extensive studies of simulated spectra addressed the quality of their LQ fit implementation, while the second[255] is devoted to the application to experimental data. In 1995, Müller[256] also combined one-dimensional and two-dimensional data. He used least mean squares (LMS) to determine the spectral parameter of a one-dimensional spectrum and exploited them to reconstruct the exchange matrices of two-dimensional exchange experiments. The introduction of prior knowledge into LS calculation is discussed by Stilbs.[257] He focused on applications in

imaging but also addressed problems found in different high-resolution domains. An account of the latest application of LS can be found in the paper by Delagio *et al.*[258] who announced the availability of a computer program measuring active couplings from COSY spectra.

3.6. Maximum likelihood

The principle of maximum likelihood (ML) consists in taking knowledge about the measured signal into account. It makes it possible to filter out components that are not compatible with a chosen model from the experimental data. In NMR the fact of an exponential signal decay function is often taken as prior knowledge, making it easy to eliminate, for example, artefacts due to signals of constant amplitude. Note that ML methods are often found in books on deconvolution because they may be used to obtain simplified spectra. For example the knowledge that one has a doublet or a given lineshape, allows one to determine coupling constants or a peak position and reconstruct spectra where the effect of the coupling on the linewidth has been removed. In such cases, the results of ML or deconvolution is a simplification, however they are obtained quite differently. To make things a little less confusing and illustrate the difficulty in classifying some processing techniques, it should be said that some implementations of maximum entropy use maximum likelihood principles and that most maximum likelihood implementations use least-squares methods to measure fit quality.

3.6.1. Literature

The theory of maximum likelihood (ML) is the subject of a chapter in Janson's book on deconvolution.[83] In another monograph on deconvolution, Frieden[259] also discussed the theory of ML in the context of emission spectra, however the same principles also apply to NMR. The introduction section of the paper makes it clear that the use of prior knowledge makes experimental data more informative. Maximum entropy techniques and others are examples of such integration discussed in the paper.

Also note a review of biological applications in the series *Methods in Enzymology*[260] and a paper originating from the same group by Levy *et al.*[261] in *Computer-enhanced Analytical Spectroscopy*.

3.6.2. Historical overview

The first application of ML in NMR was published in 1989 by Miller and Greene[262] who discussed the potential of the method in detail and for different types of NMR application. After a couple of years of silence, the number of publications on this subject took off in 1993. Jeong *et al.*[263] applied both ML and symmetrized-ML methods to two-dimensional NOE spectra. The possibilities offered by ML methods were taken advantage of to include a

line-narrowing exponential that improves the signal linewidths, making estimates of their volumes more accurate. See details of the methods in the deconvolution sections (Section 3.1[101]). The following year, the same group[264] applied similar methods to three-dimensional spectra. Miller *et al.*[265] later introduced an expectation-maximization (EM) algorithm for the analysis of COSY spectra. An autoregressive method for the analysis of hypercomplex data sets stemming from two-dimensional spectra has been developed by Imanishi *et al.*[266] and tested using both simulated and experimental DQF-COSY spectra of small molecules.

Chylla and Markley[267] discussed the application of maximum likelihood in the case of n-dimensional spectra. An algorithm is proposed and a comparison with DFT, linear prediction and Bayesian methods is made. The authors concluded that ML methods give the same results as the most probable output of Bayesian analysis. Umesh *et al.*[268] introduced a fast ML estimation algorithm. The authors demonstrated the improved computer efficiency of their methods as compared with algorithms for linear prediction or iterative estimation to parameters of individual components. More recently, Zhu *et al.*[269] discussed iterative quadratic maximum likelihood (IQML) methods and claimed their superiority over linear prediction because of better convergence speed and the use of less biased estimators. In their paper, they describe the method and its application to one-dimensional spectra is provided as an illustration along with a comparison with the LPSVD methods (see Section 3.2). In a second paper, the same authors[270] compared IQML with total least squares methods and further explored the comparison with linear prediction methods. The same year, Liu *et al.*[271] presented an algorithm called RELAX which takes care of the measurement of exponentially damped sinusoidal signals. Their claim, based on simulation including white noise, is that it is more efficient than SVD methods used in linear prediction. The same group[272] introduced an algorithm called E-RELAX which enables the inclusion of some prior knowledge into the calculation.

Finally, a recent publication by Warren and Moore[273] proposed the use of ML to measure residual dipolar coupling of partially oriented molecules for which only small data set are available.

3.7. Maximum entropy

Briefly, maximum entropy methods (MEM) consist in constructing synthetic data, and this is the key idea, the minimum number of elements taken from a chosen basis, usually a set of decaying sinusoids. The relationship between this minimum number of elements and entropy is explained in a theoretical paper by Ables.[274]

One of the advantages of MEM is its compatibility with non-linear sampling, a method which enables the avoidance of the Nyquist condition relating resolution and number of acquisition points.[53] It makes it possible to reach both large spectral width and high digital resolution. The additional advantage is that it takes more points in the less noisy part of the spectra, making the S/N ratio

higher than would be possible using conventional techniques. Examples applied to one-dimensional,[275] two-[48,276,277] and three-dimensional[49] spectra illustrate this point. A special application where truncation is necessary for correct analysis was published in German by Schmidt and Ziessow in 1987.[278] In this application reactions take place in the NMR tube with rate constants that are in the order of the acquisition time. Since the content of the tube changes during a single acquisition, the FID must be chopped to follow the relative quantity of reactants and products. In cases where NMR spectra are not simple decaying sinusoids but functions of other parameters, such as dipolar tensor values, or the distribution of the latter, as in liquid crystals, MEM can still be used efficiently. In every case where the unknowns are uniquely determined for any experimental data, they can be derived by including the model functions in the ME calculation. Examples are given by Catalano *et al.*,[279] or in a different field, by Hore and Daniell[280] in an application of MEM to zeugmatography,[281] where the knowledge of phases and off-resonance effects enables the construction of a spin densities map much more easily than using conventional methods.

3.7.1. Literature

The chapter in the monograph by Hoch and Stern[3] is certainly a good introduction. The paper by Mazzeo and Levy[282] also provides an account of the topic at a moderate level of difficulty. At a more detailed level, one can find the 1988 review by Stephenson[146] *Linear Prediction and Maximum Entropy Methods* or the paper by Hoch[283] in *Methods in Enzymology*. In 1991, Jones and Hore publish two papers devoted to a comparison of MEM with FT. The first focused on truncation and the resolution/sensitivity pair.[284] Having stated that some superiority claims are cosmetic, they provide convincing arguments in favor of MEM. The second paper compared different implementations of ME, DFT window functions and least squares fitting with respect to the accuracy and precision of heights and signal integrals.[285] Finally the annual series *Maximum Entropy and Bayesian Methods*[286] is definitely a major source of information.

3.7.2. Historical overview

In the late 1970s, maximum entropy methods (MEM) started to be applied to the processing of images normally obtained after FT[287] and examples were taken in the field of radio astronomy. The advantages included the reduction of sidelobes, smoother maps (less noise), and independence from phase, etc. NMR spectroscopists also wanted to benefit from these advantages. The first NMR applications to the analysis of one-dimensional spectra were published in the 1980s in two papers by Sibisi *et al.*[288,289] The first[288] discussed the reconstruction of a two-dimensional map where resonance frequencies and decay rates are put on two different axes. Simulation of one-dimensional spectra with artificial noise showed that spectra could be reconstructed based on the maximum entropy principle. The

second paper[289] describes the first practical application of the technique. Using the Cambridge MEM algorithm, they obtained spectra with slightly better resolution and clear noise reduction compared with FT.

The method really took off in 1985. Laue *et al.*[290] explained MEM in more detail and discussed the application of data published earlier.[289] During the same year they also presented an application to spectra having both positive and negative peaks.[291] The following year, they presented the first application to two-dimensional spectra.[292] Part of the MEM interest in two-dimensional spectra resides in the inconvenience that the indirectly detected dimensions are prone to show sinc wiggles due to truncation, a kind of problem that ME may be better able to resolve than FT or the use of window functions. The difficulty of the presence of negative signals is simply overcome by allowing oscillators with negative magnitudes. The idea has been tested in one-dimensional spectra obtained using the INEPT sequence having positive and negative peaks as compared with normal ^{13}C spectra. The fact is that negative peaks are allowed results in the MEM spectrum with more noise than when the search is restricted to positive peaks, however the results are still better than those obtained using FT. The first example is an application to a DQF-COSY spectrum having positive and negative peaks but all in pure absorption signals. The second example falls in the category of spectra having signals of all four phases and that could even manage mixed phases. The COSY spectrum shown is of the second kind with pure dispersive signals along the diagonal. It is processed after doubling the number of oscillators in order to take two possible orthogonal phases into account. This separation comes with a positive surprise: it is easy to reconstruct spectra devoid of diagonals, which has long been a goal in itself. Note the short paper by Barna *et al.*[293] which makes a list of most of these points. To return to 1985, two new players joined the field. Hore *et al.* published an application of MEM to *J*-spectra together with a short and clear explanation of the MEM principle and the different steps paving the way to the MEM spectra.[294] The second, Hoch,[295] pointed out the advantage offered by MEM in enabling avoidance of the FT-generated artefacts in case of truncation. The same paper clearly explains that MEM, unlike DFT, is able to discriminate signals according to their envelope forms. An application to the processing of data obtained with a COSY sequence is shown. It should be noted that the example given relies on DFT for the processing in the indirectly detected dimension. Comparing MEM and DFT for the processing of the other dimension leads to the observation that the first results in better S/N ratio and resolution than DFT, even when only half of the data are used. Since the dimension in play is indirect, it means that MEM allows one to reduce the total acquisition time, in this case by a factor of two. But Hoch also shows that the disadvantage of MEM lies in its non-linearity.[295] For this he compared the results of the processing of the simulation of two signals with a factor ten difference in width and a relative amplitude of factor five where synthetic noise has been added. It is pointed out that the ME results have very different absolute or relative amplitudes while DFT is quite reliable with this respect. He advised caution in all applications relying

on quantitative information. Martin[296] highlighted the ability of MEM to avoid signals due to constant weak perturbation but their main objective is to dampen the impression that MEM results in spectra having better S/N ratio than DFT. Their examples show that the baseline level may be deceptive, especially when it is shifted up or when comparisons are made, for example, with spectra presented in power mode.

Ni *et al.* presented a combination of maximum entropy and Fourier self-deconvolution (later called Fourier spectral deconvolution) applied for the first time to Raman spectroscopy[297] and the field of NMR.[298] It is claimed that the advantage of this combination (MEFSD) lies in the fact that it does not require the lineshape to be Lorentzian (i.e. the decay to be purely exponential) but it can be of any shape. It allows the combination with window functions to achieve optimum resolution. The better resolution as compared to Sibisi's implementation of MEM[288] is due to the absence of freedom given by the latter in the linewidth of signals. Ni, assuming the same linewidth in each signal, obtained responses as narrow as delta functions. In this respect, the comparison of MEFSD with MEM is not general since the MEM implementations developed after Sibisi do not all give freedom to the coefficient of the decay rate and do not show the corresponding line broadening.

Viti *et al.*[299] noted that some of the papers in the MEM field use spectra with S/N ratio that are so good that DFT is also able to display all the information present. They demonstrated that MEM can perform better in applications to ^{31}P signals in human cells where S/N ratio is much lower. The paper compares the Yule–Walker and the Burg algorithms for the autoregressive step. Working with spectra with only positive peaks, the choice of power spectra density (PSD) is logical and avoids the problem of phase. The criteria for the best PSD are also discussed: Akaike's Final Prediction Criterion (FPC), Akaide's Information Criterion (AIC), the Bayesian Information Criterion (BIC) and empirical ones are compared. In the example discussed, BIC emerges as inferior to the FPC and AIC and the Burg algorithm seems to give slightly better resolution. In a second paper, Viti *et al.* extended the discussion of the Burg algorithm and discussed the idea of filtering the spectral regions known to have no signal when FPC fails to give good result due to low S/N ratio.[300] The application to ^{31}P spectra of living systems is presented in a paper by Barone *et al.*[301] Working on the same problem but using MEFSD techniques, Mazzeo *et al.*[302] concluded that spectral segments can be efficiently analyzed by MEM. In the same area, practical applications[303] to ^{1}H and ^{13}C confirmed the relevance of MEM for resolution enhancement in cases of overlap or signal broadening, but remember that S/N ratio should be appropriately high. This requirement can be understood as the concession that signals found by MEM are also visible using DFT, but that the latter gives better resolution. The paper, unlike many others, gives extensive numerical spectral characteristics (S/N ratio, delta chemical shifts, etc.) making arguments stronger than a few impressive spectral regions processed using different methods. A paper devoted to *in vivo* ^{31}P spectroscopy[304] showed

that MEM is efficient at managing spectra where a major component, in this case phospholipids, tend to hide signals of interest, but reminds us of the problem of quantification of signals in a study using simulated spectra in diverse S/N ratio conditions.

Distortions due to the ring down effects of low frequency isotopes can be compensated by cutting the beginning of the spectrum and reconstructing the missing points using MEM as shown by Laue.[305]

Wright and Belton[306] introduced a new way of calculating the entropy. The requirements they fulfill are based on considerations that the entropy measures should be the same in both frequency and time domains, that the phase should not need to be known, that any phase should be equally manageable, that the criteria should be symmetrical with respect to the two domains, and that they should be general for any field of NMR spectroscopy. Some of these requirements were not always included in previous implementations of entropy criteria, the Shannon being one of them. Newman also discussed the different MEM implementations, in particular with respect to the problem of separating signals into the four possible phases.[307] He claimed that the Burg algorithm and the method introduced by Wright and Belton[306] are of no use in the resolution of this problem. He proposes the minimum area algorithm (MARS),[307] a variant of Laue's[290] which differs in the absence of renormalization, the rescaling of the Lagrange multipliers at each step of the calculation, and the use of a constant tolerance instead of χ^2. It has better discrimination against out-of-phase signals and requires less computer time. Daniell and Hore also took a stance[308] which opposes that of Wright and Belton[306] and proposed a new way of calculating the maximum entropy function based on quantum mechanics considerations and working with complex data. A comparison of this with other methods follows.

Another comparison of MEM and HOGWASH[41,42] methods was undertaken by Davies *et al.*[309] and reveals that both have similar difficulties, but that the second has smaller computer requirements when it comes to enhanced resolution.

When Delsuc and Levy[310] made the first attempt to deconvolute doublets due to scalar couplings, they used the Skilling and Bryan methods using real data sets instead of the power data as proposed by Wright and Belton.[306] Application to one-dimensional INADEQUATE[311] showed that antiphase doublets can be simplified and the center of each signal can give rise to clear signal. However, the authors used a single average value of the splitting as an illustration of this. The method works in the identification of all doublets only because the linewidths are in the range of the variance of the splitting. In order to manage situations where the later condition is not fulfilled, Delsuc introduced two-dimensional J-deconvolution. The idea consists in repeating J-deconvolution using a range of J-values that constitute a set of reconstructed spectra. Where the trial splitting corresponds to actual splittings, the MEM response signal should be the strongest. When applied to multiplets containing more than one coupling, such a two-dimensional map shows complex patterns where the spin multiplicity can be identified. The authors also proposed to apply their MEM technique, which

they called *J*-deconvolution, to two-dimensional INADEQUATE after DFT in the indirectly detected dimension and *J*-deconvolution to the second dimension. Unlike applications aimed at avoiding signal truncation, MEM is applied here to what is directly detected, i.e. where the splittings have to be found in order to identify resonances.

MEM reached the domain of imaging in 1987–88[312] and solid-state[313] applications. In the first case, ME proved useful, in particular, in reconstructing missing parts of spectra, but in both domains the non-linearity of the method is said to cause problems.[313,314] De Simone *et al.* devoted a paper[314] to the latter problem in a study of the influence of noise on the deviation of the linear response of NMR images. They concluded that ME is a useful technique for qualitative measurements but not quantitative measurements. During the same period, Barna *et al.*[275,276] demonstrated the powerful advantage of MEM in being able to manage non-equally distant data points in applications using exponential sampling.

In the early 1990s, Hoch *et al.* pointed out the diversity of the denotation of the word entropy in the context of ME of complex data.[315] They proposed to set aside Shannon's theoretical equation of entropy and pragmatically favor the forms that result in the best spectral reconstruction. The paper[315] presents a comparison of five ways of calculating entropy and concluded that the best one is that which combines the phase indifference (using absolute magnitude data points) with convexity (separation into four orthogonal phases). The same year, Hore *et al.*[316] introduced a method making it possible to eliminate from NOESY spectra the signals that are due to zero-quantum coherences in series taken at different T_2. In 1991, Kauppinen *et al.*[317] discussed their LOMEP method, which is a combination of MEM, linear prediction, and window functions. After a quick tour of the methods available at that time, Uchiyama and Minamitani[318] applied the Burg methods for the analysis of *in vivo* ^{39}K spectra.

Multidimensional applications are discussed by Delsuc *et al.*[319] who presented applications to protein NMR and their GIFA processing software.

Robin *et al.* proposed a processing scheme using ME for the processing of three-dimensional spectra[320] where ME is applied to the two indirectly detected dimensions prone to truncation, while DFT is used in the last one. They claim to make a gain in acquisition time of a factor of about five.

Back to more theoretical aspects, Stern and Hoch introduced the 'Rowland algorithm'[321] for the computation of ME in 1992. For an equivalent calculation time, it requires less computer memory than Skilling and Bryan's 'Cambridge algorithm',[322] however it is unable to determine the decay rates of signals. The following year, Hodgkinson *et al.* processed three-dimensional experiments using ME in all three dimensions in about one day of computer time.[323] More recent studies have applied ME to three-dimensional spectra proposed to process spectra regions after regions[324] and discussed the use of parallel processing.[325]

The measure of coupling constants using MEM first discussed by Delsuc *et al.*[310] has been further developed by Seddon *et al.*[326] They introduced a

method enabling the simplification and measurement of coupling constants in complex multiplet structures. Applied to simulated EPR spectra and experimental ^{19}F spectra, the method is able to simplify structures where S/N ratio is near unity. Note that in the examples given, it was applied to signals which all have the same phase. The following year, Stoven *et al.*[327] introduced an 'N-Channel' MEM applicable, in principle, to both one-dimensional and two-dimensional spectra, however it would appear to be difficult to implement it routinely. Schmieder *et al.*[47] addressed the problem of quantification with two ideas. The first enables avoidance of the linearity problems in row-by-row approaches without having to satisfy the very demanding memory requirements of whole spectra analysis, while the second, called '*in situ* calibration' makes it possible to avoid the inconvenience of individual calculations.

There has been little development in the theory of MEM in recent years, however the diversity of applications has increased greatly. Examples include the measurement of rotameric distribution in carbohydrates,[328] peptides,[329] or more generally[330] in isotropic environments. Other applications include studies of the internal order in liquid crystals,[331–333] a new attempt at the *in vivo* application of ^{31}P phase-modulated rotating-frame imaging (PMRFI),[334] and a study of amphiphilic molecules in ternary systems.[335]

3.8. Bayesian analysis

Bayesian methods can be seen as a way of obtaining answers, expressed in terms of probability, to questions asked concerning experimental data and prior knowledge. They are based on logic and, more specifically, the induction principle. The ability of inductive logic, which, according to Cox,[336] is equivalent to probability theory, to resolve scientific problems is highlighted by Garrett.[337] A strong point in favor of Bayesian methods is that, by nature, they provide a degree of confidence in their results. Note that the relationships between Bayesian and maximum entropy methods is quite strong as argued by many and discussed by Jaynes.[338]

3.8.1. Literature

In order to get used to the terminology and notation, it may be helpful to read Jaynes's paper[339] on Laplace's probability theory, or Polya's paper[340] discussing the calculus of probability and the logic of plausible reasoning. The spectroscopic aspects can be found in the extended version[341] of Bretthorst's PhD dissertation. The proceeding series devoted to maximum entropy and Bayesian published since the mid-1980s is another reference work in this area. The volume corresponding to the 1988 '*8th MaxEnt Workshop*' in Cambridge, England[342] is given in the reference section as an example.

3.8.2. Historical overview

After a first paper in 1988,[343] Bretthorst paved the way for the application of Bayesian probability theory (BPT) in a series of three papers.[344–346] The first[344] presents the connection between the theory and the case of NMR phenomena and discusses parameter estimation and detection of quadrature signals. The second[345] shows the ability of Bayesian methods to measure the quality of a model. The third[346] provides examples of applications to experimental data where decaying sinusoids are assumed. A fourth paper, produced during the following two years, discusses computer time requirements and noise, and it is shown to be important to include knowledge in the analysis,[347] while a fifth publication is devoted to amplitude estimations for multiplets of well-separated resonances.[348]

A comparison between Bayesian and Fourier analysis is provided by Kotyk *et al.*[349] and Evilia *et al.*[350] They both show that the Bayesian methods provide more precise frequency estimates and far more precise amplitude estimates than DFT and explain the difference. However, it should be said that the methods are so different in nature that comparison is more difficult than for other methods discussed in this paper. For example, by 'known T_2', the Kotyk *et al.*[349] mean that T_2 has been included in the calculation as a matched exponential apodization. Vines *et al.*[351] demonstrated the ability to measure scalar couplings that are much smaller than linewidth in the case of spectra with favorable S/N ratio. The same authors took advantage of the ability of BPT to accurately measure linewidth to improve exchange parameters and gain in the precision and accuracy of thermodynamic properties.[352]

Application to two-dimensional spectra started in 1993 when Chylla and Markley[353] applied BPT to constant time experiments. The results of both simulations and experimental data are quite impressive. The fact that BPT is not only compared to DFT, but also to linear prediction makes the demonstration even more sound. Independently, Routh *et al.*[354] also tackled the processing of two-dimensional spectra following a discussion of noise statistics.

Whittenburg[355] showed that BPT can also be used as a preprocessing technique. Instead of directly using BPT for signal parameter determination, they first used it to correct the first data point which, when affected by experimental imperfections, gives rise to baseline roll. This in turn makes it possible to improve spectral parameters determination using BPT – as the authors did – or standard techniques. Kotyk *et al.*[356] presented the second part of their comparison between DFT and BPT in the case of truncated FIDs. The conclusions are similar in that the second shows superiority in terms of precision and accuracy of the measurement of both frequencies and amplitudes.

Imaging is another domain in which BPT was successfully applied by Neil and Bretthorst.[357]

Interested in the processing of spectra of macromolecules, Antz *et al.*[358] introduced Bayesian methods with the aim of classifying peaks by classes. Working

in the frequency domain, they took advantage of some known properties of the different classes of signals such as peakshape, amplitude, and broadness to discriminate true signal from artefacts due to thermal noise, t_1 noise, and water suppression imperfections. The characteristics of each type of signal are identified by selecting regions for which signals are dominantly members of a certain class. For example, regions of NOESY spectra for which the diagonal gives no signals are known to be due to thermal noise, etc. For other classes, signals are not of a unique kind but statistics can nevertheless be generated on them. Classification is made according to absolute intensity, ratio of peak volume to peak intensity, relative volume of the tail, and relative volume of the top of the peak. Even if the different types of signal seem similar at first sight, the determination of the signal class is surprisingly efficient using Bayesian analysis. The authors introduced such analysis into their NMR data processing software package AURELIA[359] (see paragraph software). A couple of years later, Schulte *et al.*[360] discussed the beneficial influence of taking into account the symmetry of signal with respect to spectral diagonal.

The same year, Le *et al.*[361] discussed the principle of z-surfaces for structural information determination based on experimental parameters. It consists in a statistical treatment which, given an experimental parameter, returns a probability for any given structural feature. The quality of the information is a function of the correlation between the experimental and structural parameters. The paper shows, among other things, that chemical shifts are structurally informative.

In 1996, Whittenburg[362] presented a solvent suppression method using Bayesian analysis methods but which assumes the solvent peak to have Lorentzian lineshape.

In 1997, a review paper by Gottvald[363] surveyed inverse methodologies for *in vivo* spectroscopy. There is extensive coverage of Bayesian methods as well as a discussion of other methods.

In 1998, Andrec and Prestegard[364] measured the coupling constants in antiphase patterns. They introduced a variant using a Metropolis–Hasting Monte Carlo method. Application to the measurement of coupling constants smaller than linewidth is shown to be applicable to simulations and experimental data stemming from INADEQUATE experiments.

More recently, Ochs *et al.*[365] applied Bayesian methods to the processing of chemical shift images where a large number of spectra have to be analyzed automatically.

Back to high-resolution NMR, Andrec *et al.*[366] used Bayesian techniques to attribute probabilities to dynamic parameters using relaxation data in a Lipari–Szabo model-free approach. The following year, the same group[367] discussed the contributions of rotational diffusion anisotropy and estimated them using Bayesian methods. The importance of such measurement is highlighted in order to avoid misinterpretation of relaxation data contributing to bias molecular motion parameters.

McMahon and Oldfield[368] compared Bayesian, Monte Carlo and simple graphical methods in the determination of order parameters and demonstrated the advantages of the first.

Finally, it should be noted that Bayesian methods are also used in NQR spectroscopy for the detection of landmines.[369]

4. SPIN NETWORKS DETERMINATION

This section discusses diverse processing techniques aimed more or less directly at the extraction of topological information.

4.1. One-dimensional experiments

Heuristic pattern recognition methods developed by Jurs *et al.*[370] were first applied to proton-decoupled ^{13}C data by Wilkins *et al.* In a first paper,[371] they proposed, broadly speaking, to consider each spectrum of a ^{13}C spectra database as a 200-dimensions vector in a pattern space corresponding to a one ppm resolution. The set of vectors is separated into classes according to the presence or absence of functional groups in the molecule. The learning stage consists in computing decision functions, vectors having the same dimension as the spectra, by applying a simple algebra that increases the weight of certain vector elements when it finds correspondence in the class of vectors containing the functional group and decreases when correspondence is found in the class of spectra that does not. After running the learning process with the whole database and a refinement stage, the decision functions are ready to be applied to ^{13}C spectra of unknown molecules where they work like caches. When applied to test molecules, it is claimed that the presence of functional groups is detected with a similar success rate to similar methods applied to IR and MS spectra. Six papers by the same authors aim at the same goal of improving pattern recognition using different variants. The first[372] shows that working with data using the Hadamard transform of frequency domain data is potentially interesting even though it is not as efficient here as in the frequency domain. The second[373] compares the results of the aforementioned paper[372] with learning based on the Hadamar transform of time domain and frequency domain data.[371] It is also shown that signal amplitude should be taken into account and the paper also contains a discussion of simulated FID. The third[374] takes advantage of the synergy between the different methods of improving predicting power. Another paper[375] shows the potential of SIMPLEX methods to compensate for the weakness of the approaches discussed above. The final paper considers the introduction of Bayesian methods[376] which had demonstrated their superiority over all others. This field has gained from the availability NMR databases and the methods to exploit them, but they are not discussed here.

4.2. $^{13}C-^{13}C$ experiments

The INADEQUATE experiment, developed by Bax *et al.*[311,377,378] will not be presented: due to its lack of sensitivity, it is seldom used and this is why little will be said about its processing. A computer program called COSMIC developed by Richardz *et al.*[379] which analyses spectra and produces carbon connectivity lists as an output is, however, worthy of mention. The introduction of pulse field gradients made it possible to design much more sensitive proton detection sequences that are quite suitable for the construction of spin networks and structure determination,[380,381] even if they work only with those carbons that are directly bound to protons.

4.3. COSY and other $^{1}H-^{1}H$ experiments

The improvement of NOESY and COSY spectra was made possible by Baumann *et al.*[382] who proposed the elimination of spurious peaks of two-dimensional spectral, exploiting the fact that real peaks are symmetrical with respect to the diagonal of the spectrum. Their symmetrization process consists in assigning the value of the mathematical average of their amplitudes to each pair of symmetry-related data points. In addition to the diminution of the spurious signals by a factor 2, it has the additional advantage of increasing the S/N ratio by a factor $\sqrt{2}$. An alternative by Baumann *et al.*[383] suggests taking the smaller of the two symmetry-related data points instead of the mathematical average. This turns out to be an extremely efficient way to eliminate the tails of strong diagonal signals running mostly along the first dimensions of two-dimensional spectra. These are discussed by Bolton[384] who proposed displaying spectra with different contents at the two sides of the diagonal. He argued in favor of presenting the symmetrical part of the spectrum on one side and a measurement of the difference on the second. With the application of NMR to the processing of small proteins in mind, Neidig *et al.*[385] proposed the use of computers to simplify the work with complex COSY and NOESY spectra. They discussed the difficulty of automatic peak picking and explained how computers should assist the users in spectra attribution. Kleywegt *et al.*[386] introduced a NOESY peak integration computer-processing tool called STELLA which assists users with peak picking and integration. It includes a learning stage allowing the computer to categorize peaks as real or spurious using some of its properties as a criterion.

Analysis of COSY spectra started with the paper by Bax and Freeman[387] who discussed the potential of the 'Jeener's experiment'. A modification, later called COSY-45, is introduced for the observation of the relative sign of coupling constants in triangularly coupled spin systems. This kind of multiplet structure prompted the development of specific sequences in order to extract a certain kind of coupling constant information and coupling network. Another modification involves the use of selective pulses giving rise to spectra that are simplified in

their first spectral dimension. Two special window functions have also been introduced. The first is appropriate to the kind of data produced by COSY experiments and favors the cross-peak signal over diagonal peaks, the latter being a source of trouble due to the large extent of their dispersive tails. The second function has the same advantage but differs in that it produces spectra with circular peaks while the normal spectrum has four-point-star lineshape. Another advantage it offers is that it enables favoring the later components of the decay, emphasizing cross-peaks due to very small couplings. It does this without requiring long acquisition times, which was very problematic due to the limited computer resources. The following year, the double quantum version of the COSY experiment[388] transformed the troublesome dispersive diagonal into a purely absorptive one as described by Nishida *et al.*[389] A few years later another variant called P.COSY, a modification of Mueller's P.E.COSY,[390] was proposed by Marion and Bax.[391] It was claimed to have the quality of DQF-COSY and twice its sensitivity. Note that Pelczer[392] proposed a processing scheme called S.COSY making it possible to suppress the diagonal of the COSY spectra using differences in phase properties for the elimination of unwanted signals.

COSY and DQF-COSY spectra were the first to be used for the construction of ^{1}H spin networks. In that context, Eich *et al.*[393] solved a particular problem which may be encountered in such analysis. When a linear three spin system A-M-X is to be identified, accidental overlap in the M regions may make it difficult to eliminate the possibility that the system is not a pair of subsystems A-M and a M′-X. In this respect, the relayed COSY,[393] giving rise to cross-peaks for both directly coupled pairs of spin and also for pairs of spin sharing a common coupling partner, provides a reliable way of distinguishing the two situations. The same distinction can be made using triple-quantum spectroscopy as proposed by Braunschweiler *et al.*[394] It has the advantage that – unlike relayed-COSY spectra – it only shows signal stemming from three (and more) spin systems. This is only one of the conceivable recipes using multiple quantum.[395] Many other questions on spin network can be resolved in multiple-quantum experiments[396] provided some time can be spent on the analysis of the multiple-quantum dimension where chemical shifts are somewhat mixed up. In a similar context, Müller[397] proposed the use of zero-quantum experiments for the mapping of spin–spin couplings. One advantage is the independence of such terms from field inhomogeneity and, possibly, the absence of difficulty in finding signals in the indirectly detected dimension.

Levitt and Ernst[398] introduced another network assembly tool by proposing experiments that filter specific spin patterns. They made it possible to simplify spectra and keep only those signals stemming from AX_n spin systems. The same authors later carried out a more detailed study[399] of spin topology filtration. The theory was further developed, practical aspects considered, and an application to an AX_3 filtered COSY spectrum of a small protein given as an illustration. A few years later, Radloff and Ernst[400] presented a general theory of spin topology. The detection of specific spin systems was also discussed by Gray and Brown[401] in

the context of experiments with three time evolutions. Filters for geminal protons are proposed by Domke *et al.*[402] as a means of simplifying COSY spectra. Still in the domain of spin network selective experiments, but much more recently, Dötsch[403] developed amino-acid-type-selective experiments. In the same vein, Schubert *et al.*[404,405] developed the MUSIC excitation scheme making it possible to selectively excite given amino acids. It is based on the replacement of the first INEPT of a pulse sequence with a magnetization transfer scheme which is XH_2 or XH_3 selective and for which delays are set to correspond to a given individual or family of amino acids.

Back to 1984, Meier *et al.*[406] discussed the potential of pattern recognition, a subject which has since been widely explored. In 1985, Pfändler *et al.*[407] proposed the analysis of the COSY spectra of weakly coupled spin system using a five-step procedure. The first consists in the acquisition of a correlation spectrum. In the second, a computer algorithm searches for square patterns of the antiphase splittings using a grid-like mask with a spacing that corresponds to a trial value of the active coupling constant. This allows the creation of a table giving the pattern's positions and the distance between the antiphase splittings. A spectrum from which the active coupling has been removed can then be reconstructed later. The third step consists in the determination of the center of cross-peaks using the method developed by Shaka *et al.*[42] to group together the different square patterns of each cross-peak. This reduction of pattern enables the creation of a table of cross-peaks. The next step consists in assembling the different cross-peaks of each spin and displaying the results. The method has been successfully applied to a mixture of molecules where partial overlap occurred and where the S/N ratio was not very high. Bolton[408] also proposed a simplification procedure for DQF-COSY spectra after which, two-spin systems displayed one single peak instead of sixteen. It is, however, difficult to see how such a scheme can be applied to more complex cases. In the same vein as Pfändler, Hoch *et al.*[409] and, independently, Glaser and Kalbitzer[410] proposed searching the spectra for symmetrical features instead of square patterns as seen above. In some respects, this is more efficient since only two variables are required for such a search and there is no need to rely on a guess for the splitting. The paper[410] highlights the fact that symmetry is present at three levels: individual signals, individual cross-peaks, and with respect to the spectrum diagonal. Each is exploited in their pattern recognition procedure.

Independently, the problem of cross-peak recognition was being further studied by Mádi *et al.*[411] who proposed processing them in two steps, and also addressed the problem of missing signals in situations where standard methods risk missing signals. The first step involves the detection of coarse features. A computer program searches for data points above a given threshold and defines a square region around each of them. All the regions that partially overlap are considered to be parts of the same cluster. The method should be able to assemble all of the signals of an isolated cross-peak, or possibly a group of overlapping cross-peaks, under the same cluster. The clusters containing less than a minimum

number of signals and those near the spectrum diagonal are rejected. The second step consists in a detailed analysis of each cluster. A measurement of the local symmetry is applied in order to find the position of the cross-peak, or, in cases of overlap the centers of each peak.

A second method for the measurement of local symmetry is presented in another paper by Meier *et al.*[412] Both methods are used not only to determine the cross-peak center in E.COSY spectra but also to exploit the local symmetry within the signal to measure coupling constants. Widmer and Wüthrich[413] took a different approach when publishing a catalogue of the cross-peak structure of correlation spectroscopy. They first showed how the fine structure of multiplets evolves as a function of the linewidth, the number of acquisition points, truncation, etc. They also highlighted how both relaxation properties and processing parameters influence multiplet structure. Increasingly large second-order effects are introduced in simulations of some spin topologies that are pertinent to the study of biological macromolecules.

In 1988, considering the goal of correlation spectroscopy to lie in the determination of the coupling networks, Pfändler and Bodenhausen[414] proposed a method allowing the construction of such networks using the fragments that can be constituted by analyzing cross-peak multiplet structures. Their goal is then to extract all the topological information present in any given cross-peak, which, in the topology language, translates into two nodes connected by an edge due to the active coupling, and additional open-ended edges for each passive coupling. They used z-filtered COSY[415] and anti-z-COSY spectra. E.COSY[416,417] and complementary E.COSY spectra would also be appropriate, however the former have the advantage of providing pure absorptive lineshape even in situations of strong coupling.[418] The use of pairs of experiments, which had previously been investigated by the same authors[419] makes cross-peak center determination easier and avoids some of the problems arising from signal overlap. But the main reason is that the difference between the complementary cross-peaks can be exploited to gain information on the passive spins. To put it briefly, the method[414] first simplifies the multiplet structure with respect to the active coupling and codes the information present in the multiplet in such a way that makes search of a cross-peak library as useful as possible. It should be noted that most of the time experimental cross-peaks can be assigned to more than one element in the library of fragments of coupling networks. This is problematic since it makes it difficult to assemble the whole network. Application to a small peptide containing a very dense coupling network of a tri-proline peptide is given as an illustration[414] while the analysis of a larger, but more classical peptide, is presented in a separate paper.[420]

The problem of the assembly of coupling networks is the subject of two separate publications.[421,422] Novič and Bodenhausen[423] used a different method to identify the fragment of the coupling network within cross-peak structures. The first difference is the fact that they require a single spectrum such as z-filtered COSY[415] or E.COSY and use a symmetry mapping technique to determine each

coupling. The first step consists in a search for cross-peak multiplets using symmetry properties. Then, for each cross-peak, all of the extrema above a threshold which is some fraction of the highest point of the cross-peak are located and copied into a synthetic multiplet. The active coupling is determined as the most frequent distance between the positive and negative peaks. When the center of the multiplets have been identified, the cross-peaks are ready to enter a recursive structure analysis (see above[412]) in which the coupling to passive spins can be measured using a property of the multiplet's symmetry mapping and the multiplet structure simplified with respect to the corresponding splitting. When no more couplings are found, the fragment of the coupling network is clearly determined. The construction of the complete network is straightforward and moderate second-order effects do not impede the working of the procedure.

In another paper, considering the difference between self-convolution and the symmetry mapping discussed above,[423] the same group[424] highlighted the fact that the somewhat idealized multiplet constructed solely on the basis of extrema is more robust as material for symmetry mapping analysis, and results in less artefacts than when using raw data. Independently Meier and Ernst[425] proposed a similar recursive multiplet contraction procedure. However, unlike Novič *et al.* (see above), who use a reconstructed multiplet based solely on signal extrema, they used natural data. Their variant demonstrated the ability to process partially overlapping cross-peaks.

Mádi and Ernst[426] proposed yet another tool for E.COSY spectra analysis using a least-squares method where the signals of individual, or possibly overlapping, cross-peaks are simulated and fitted. The convergence criteria are quite sophisticated and show their efficiency through fast convergence.

Another modification of the COSY experiment was proposed by Schulte-Herbrüggen *et al.*[427] This increased the range of possible multiplet structures through the use of special mixing processes.

Back to the standard correlation spectra, and in the context of the search for methods to obtain one-dimensional spectra devoid of coupling structures, Woodley and Freeman[428] considered scanning DQF-COSY spectra and searching for cross-peaks only at the chemical shift where protons are known to be located according to the results of processing a J-spectrum. Application to low S/N ratio (e.g. >3) is given in a separate paper.[429]

TOCSY spectra are also quite interesting in the context of the construction of coupling networks allowing the immediate identification of all members of an isolated coupling network. They can also be rendered quantitative as shown by Fogolari *et al.*[430] One-dimensional selective modifications and combinations with DEPT and INEPT were developed and reviewed in the introduction to a paper by Doss.[431]

Situations where overlap and relaxation makes it difficult to do more than detect the presence of cross-peaks require less ambitious analysis schemes. Craig and Kuntz[432] proposed the construction of a matrix representation of COSY or TOCSY spectral data. Like block action, matrix manipulation highlights structural

features of the coupling network. Heuristic approaches are explored by Xu *et al.*[433] starting with a paper on the prediction of NMR spectra as a function of quantum orders. Xu and Sanctuary[434] later explored the problem of the assembly of large coupling networks where overlap causes difficulties in the reliable drawing of edges. They considered the analysis of data from COSY experiments and introduced a computer algorithm exploiting the fact that the nodes of a network can be reached using different pathways, making it possible to manage ambiguous and missing information. They applied similar methods to the processing of protein[435] and peptide.[436] COSY and TOCSY spectra using 'fuzzy' logic.

Back to cases of more general interest, they considered the construction of spin networks and three-dimensional structures using data from different kind of spectra including $^{13}C-^{13}C$, $^{1}H-^{13}C$, $^{1}H-^{1}H$ connectivity through scalar coupling, and $^{1}H-^{1}H$ through space information.[437] Van Geerestein-Ujah *et al.*[438] also applied graph theory to secondary structure recognition and sequential assignment of ^{13}C and ^{15}N enriched protein in an implementation called SERENDIPITY. A 1997 review of the application of fuzzy logic and graph theory in chemistry is given by Xu.[439] Peng *et al.*[440–442] also developed a computer-assisted structure elucidation procedure called CISOC-SES. Their target is the determination of the molecular structure of unknown molecules using a set of data, including one-dimensional, COSY, NOESY, short- and long-range heteronuclear spectra as inputs.

Back to more classical methods applied to the analysis of DQF-COSY spectra. Schmidt[443] proposed a least-squares method for complete spectrum simulation. It works using spectral simulation, taking into account some second-order effects, but avoids density-matrix calculation which would be too demanding in computational terms. Jeannerat[123] applied a computer-assisted deconvolution method allowing extraction of the coupling constants of manually selected cross-peaks, within the limits of a weak coupling regime. Once the cross-peaks have been analyzed, a software module assembles the coupling network on the basis of correspondences in chemical shifts and coupling constants.

4.4. J-resolved experiments

Proton spectra with invisible homonuclear coupling have long been the subject of research. The simplicity of such spectra makes it easy for chemists to assign resonances because of the simplification achieved through the absence of signal multiplicity. Today, chemistry students still learn how homonuclear scalar couplings influence resonance lineshapes, showing that ideal solutions have not been found despite ongoing efforts.[444] Spectra obtained using the two-dimensional J-resolved experiment proposed by Aue *et al.*[445] should be close to this ideal, provided they can be correctly processed. The abundance of the literature sampled below shows the difficulties presented by fulfillment of the latter condition.

Experiments similar to the ^{1}H J-resolved experiment were applied to ^{13}C spectra and the difficulties arising in the processing, and the advantages of the method were later addressed by Bodenhausen *et al.*[446] and independently

by Nagayama *et al.*[447] The possibility of obtaining signal shapes that are not affected by field inhomogeneity have been highlighted in particular,[446,448] and the possibility of using different decoupling schemes is examined.[446,449] As soon as phase correction became accessible,[33] the absolute value mode has been replaced by phase-sensitive methods[450] and the difficulty of phasing J-resolved spectra emerged.

Other phase problems have been discussed by Bax *et al.*[451] who proposed the use of pseudo-echo to improve phase problems when the consequential decrease in S/N is tolerable. Blümich and Ziessow[452] proposed using a projection method called 'skyline' to make the phase imperfections less disturbing. Two years later, Shaka *et al.*[42] proposed resolution of the phase-twist problem by making a peak-picking list where the largest peak is located in frequency, amplitude, and phase and subtracted from the raw spectrum. The procedure is repeated until no signals are left. The second step consists in subtracting the equivalent of the dispersive component of each peak of the list from the unprocessed spectrum. Vuister and Boelens[453] introduced a three-dimensional version of the proton J-resolved experiment resulting in better separation in the case of partial signal overlap. Yet another version of the experiment is proposed by Xu *et al.*[454] and developed in a second paper.[455] First they introduced a spin-lock scheme to the pulse sequence in order to obtain pure absorption lineshape. Another consequence of the modification is the changes in the multiplet structure of the peaks. The C_4 symmetry element introduced is exploited using a symmetry filter, making it possible to identify separate resonances very satisfactorily as long as second-order effects are not too important. Woodley and Freeman[456] used a similar symmetry filter technique but avoid the use of the purging pulse, applying a processing trick to obtain signals with phase distortion but having symmetry properties compatible with filter analysis. A similar scheme was developed by Simova *et al.*[457] but instead of a cross-like structure, each proton gives rise to a square array when using a z-filter. The presence of more peaks, which may be seen as a complication, is compensated by the presence of more testable features in their structures.

A comparison with the methods discussed above is proposed after the addition of slight modification in order to take some second-order effects into account. Note that in cases of severe overlap, signals can be efficiently separated before center localization. More recently, the multiple-quantum variant was developed by Liu and Zhuang[458] in order to study the relaxation properties of protons coupled to ^{13}C methyl groups. Finally Furihata and Seto[459] introduced a J-resolved HMQC combination facilitating easy measurement of non-geminal $^1H-^1H$ coupling in cases where proton pairs are strongly coupled in the absence of ^{13}C.

4.5. Heteronuclear experiment

Some researchers went one step farther towards molecular structure elucidation by including ^{13}C into the coupling network. Szalma and Pelczer[460] proposed the

schematic separation of the signals of a $^{1}H-^{1}H$ correlation spectrum with respect to the chemical shift of the ^{13}C to which they are attached using a ^{1}H $^{1}H-^{13}C$ correlation spectrum. They described the creation of a sort of three-dimensional spectrum where the COSY cross-peaks appear at each level that a signal is found in the corresponding position of the $^{1}H-^{13}C$ spectrum. Note that when compared with a three-dimensional spectrum where the proton signal occurs only at the position of the directly bound carbon to one of the protons, such reconstruction introduces signals at two positions of the directly bound carbon of both active protons when the coupling is not geminal, and to even more positions as soon as overlap occurs in the proton dimension.

In consideration of the fact that direct $^{1}H-^{13}C$ connectivity does not significantly increase the information content, Eggenberger and Bodenhausen[461] proposed the use of a modified pseudo multiple-quantum experiment proposed by Sørensen and Ernst.[462] It is a ^{13}C-detected experiment that is special in that a $^{1}H-^{1}H$ transfer is produced in the middle of the first evolution time. The resulting spectra show two type of signals. The first are the signatures of normal directly-bound $^{1}H-^{13}C$, while the second are similar to a double-quantum experiment in that they appear at the average chemical shift of pairs of coupled protons and the chemical shift of their directly connected carbon in the first and second dimensions respectively. Such a spectrum allows easy connection of pairs of directly bound $^{1}H-^{13}C$.

4.6. Selective experiments

Selective experiments enabling one to focus on a region of interest within a molecule are extremely useful because of the potential for the exploitation of information present in their fine structures.[463] Many could also be applied in a systematic manner to different spectral regions of given molecules, provided they can be acquired quickly and are suitable for automatic computer processing. Many different experimental schemes have been proposed. The DAISY experiment proposed by Friedrich *et al.*[464] enables one to determine whether there are two remote spins in the same coupling network. The same authors[465,466] proposed the use of soft pulses in order to simplify three-dimensional experiments.

The band-selective modification of the COSY sequence presented by Brüschweiler *et al.*[467] consists in the replacement of the first hard pulse by a soft pulse, making it possible to obtain spectra having high resolution in both dimensions. The same paper presents other variants having the effect of eliminating some couplings. The soft-COSY experiments[468,469] make it possible to obtain information about the coupling partners of the spin giving rise to the cross-peak by zooming into a chosen cross-peak. The structure allows a pair-wise attribution of passive spins and the determination of the relative signs of the coupling constants. The measurement of all coupling constants allowing the determination of coupling network fragments can be carried out using two-dimensional deconvolution techniques.[122,470]

Variants of the soft-COSY, like the SIS-COSY[471] experiment, increase the information content when compared to soft-COSY spectra, making it possible to affect the multiplet structure. In one of the variants, it acts as though the relative signs of the coupling to a chosen coupling partner of the active spins has been inverted. The flexibility of the SIS-COSY experiment is welcomed when a spectral region of interest is important for the coupling network assembly, as highlighted by Emsley and Bodenhausen.[471] SIS-COSY has other applications as proposed in a publication on a DNA fragment[472] and is quite appropriate to the automatic measurement of coupling constants using convolution methods.[473] Another application of the SIS-COSY experiment is the separation of cross-peaks,[474] however, the application of such a method requires knowledge about the coupling partners of the active spins. An alternative based on 'spin pinging' has been proposed by Xu *et al.*[475]

Separation of cross-peaks is also possible using purely computational methods. McIntyre and Freeman[476] proposed a method enabling the recursive unraveling of COSY and DQF-COSY spectra cross-peak signals. The method relies on the presence of regions where orthogonal cross-sections are not affected by overlap at the corners of the overlapping regions. The cross-sections make it possible to reconstruct the entire cross-peak and subtract it from the overlapping regions. Woodley and Freeman[429] propose another method which exploits the two anti-symmetry planes of DQF-COSY cross-peaks for determination and then subtracts from overlapping multiplets a complete cross-peak using one quarter of the signal without overlap. The alternative, published by Jeannerat and Bodenhausen,[477] is more general, being able to separate signals solely on the basis of the presence of a symmetry axis, giving access to signals stemming from E.COSY and soft-COSY experiments. However, it has only been discussed in cases of pairs of overlapping signals. Selective experiments are also interesting for fine relaxation studies. These include Müller *et al.*[478] and Zwahlen *et al.*[479] with their QUIETE-NOESY.

4.7. Neural networks

The first application of a neural network in NMR was proposed by Thomsen and Meyer[480] who analyzed one-dimensional spectra of simple molecules before application to complex oligosaccharides.[481] Kjær and Poulsen[482] showed that the center of COSY cross-peaks can be found using neural networks. Their implementation consists of a feed-forward three-layer with 256 inputs programmed using a back-propagation error algorithm. As shown by Corne *et al.*,[483] NOESY spectra signals can be classified as genuine or spurious using similar networks. The following year, the same group[484] applied a two-layer feed-forward network with Widrow–Hoff supervised training to the same NOESY data. Two-level networks emerge as preferable in a comparison with three-level networks. In 1994, Hare and Prestegard[485] used neural networks for amino acid recognition

from TOCSY spectra. A review devoted to neural network pattern recognition was published by Corne[486] in 1996. The following year, Huang *et al.*[487] demonstrated the relevance of neural networks in protein studies showing that after proper training, they were able to predict from TOCSY-HSQC and HNHA spectra the secondary structure at a rate of 96%, while amino-acid prediction was 60% of spin systems, and correct amino acid class was among the top two choices.

4.8. Scalar coupling constants

Although the literature about coupling constants is very extensive, this section will be quite short. A large number of reviews are constantly being published and the *NMR Special Report* devotes a chapter to the subject every year. Another reason for the brevity of the discussion is that many of the techniques have been discussed in earlier sections of this paper.

4.8.1. Literature

The annual NMR Specialist Report is certainly an important source of up-to-date information. Other reviews of scalar coupling constants are devoted to particular aspects. In 1995, Jones[488] focused on deconvolution techniques, J-doubling, etc. while Biamonti *et al.*[489] covered discussions on proteins and nucleic acids. The following year, Eberstadt *et al.*[490] covered a large range of pulse sequences and applications concerning a broad domain between chemistry and biology. In 1997, Thomas[491] presented a review focusing on the relations between coupling constants and molecular structure, this being the most relevant application to chemistry.

4.8.2. Historical overview

As mentioned above, only a few techniques will be discussed here as many rely on specific methods discussed in other sections of this review. A common point of most of the methods discussed below is the attempt to simplify multiplet structures by different means and to extract useful information by quantifying the induced changes.

It is well known that the direct measurement of splitting differs more and more from the true coupling as the linewidth becomes broader. When signals are in-phase, as in one-dimensional spectra, the distance between the extrema tends to be smaller than the true coupling, and finally disappear when both lines fuse into one, only broadened by the unresolved coupling. When the coupling appears in antiphase, as in COSY, the distance between the positive and negative peaks increase as the linewidth increases because of the partial cancellation occurring between the true positions of the lines.[492] This problem is addressed by Oschkinat and Freeman[493] in the case of COSY spectra. The principle of the method, called

DISCO, consists in processing two data matrices of the same experimental data. The first has the cross-peaks in absorption mode, the second, orthogonal in phase, has the diagonal peaks in pure absorption. Taking the sums and the differences of absorptive traces through cross-peaks and the diagonal cancels peaks that would otherwise perturb direct measurements, allowing the separation of both types of signal. In the case of a simple doublet, the addition and subtraction give rise to two isolated peaks with positions differing by the true coupling constant. Kessler *et al.*[494] further developed the method considering also addition and subtraction of traces through the different cross-peaks of a given spin. Application to the measurement of coupling constants in proline residues of a peptide demonstrates the efficiency of the method.

Over the following years many experiments were developed whereby the signal structure contains a lot of information on the coupling constants, cf. E-COSY[495,496] and P.E.COSY.[390] Others stem from heteronuclear experiments, such as the method of Bermel *et al.*[497] which is a good illustration of the way problems were approached at the time, and, more recently, the heteronuclear XLOC experiments[498,499] which show structures similar to E.COSY spectra.

Back to a more fundamental level, Kim and Prestegard[500] showed that simple lineshape analysis makes it possible to take the linewidth into account when measuring coupling constants in broad signals. The paper discussed both doublets that are displayed in absorption mode and the very neglected case where they are dispersive.

Many interesting contributions were made a few years later. In 1993, del Río Portilla and Freeman[501,502] proposed the use of complementary spectra for the determination of coupling constants. The method consists in a pair of experiments in which one is acquired by selectively decoupling one spin. The multiplet structure of all coupling partners of the decoupled spin are simplified. This facilitates the use of a simplified structure as a starting material for simulation of the effect of the missing coupling using convolution. In the same vein, long-range heteronuclear couplings have been measured by Uhrín *et al.*[503] using a pair of HMQC experiments which differ on the basis of the presence of a refocusing pulse in one of them. The measurement of long-range coupling in heteronuclear experiments proposed by Bazzo *et al.*[504] is also relevant in this context. In 1990, Titman and Keeler[505] proposed a convolution method allowing measurement of the active couplings from COSY and TOCSY spectra. The principle exploits the fact that the only difference between the two multiplet structures is that the active coupling gives rise to antiphase structure in the COSY and in-phase in the TOCSY. The idea is to add an in-phase doublet to a COSY multiplet and an antiphase doublet to the corresponding trace in a TOCSY structure. When the added structures are separated by the same distance as the active coupling, both convoluted multiplets are identical. The measurement of the similarity then provides the value of the coupling constants. A variant, in the form of a pulse sequence called SIAM providing both kinds of structure, has been proposed by Prasch *et al.*[506] Processing techniques for the processing of selective experiments have also been

developed for the measurement of active[470,507,508] and passive[473] splittings. *J*-doubling is another well-known method used to separate signal components and measure coupling constants, introduced by McIntyre and Freeman,[509] del Río Portilla *et al.*[510] and for applications to COSY cross-peaks by Le Parco *et al.*[511] These *J*-doubling applications are still in general use.[512] Stonehouse and Keeler[492] introduced another way of measuring coupling which allows the measurement of unresolved in-phase splittings. It is based on a time-domain analysis of signals that must be extracted from a spectrum, centered, and back-Fourier transformed to obtain a pseudo-FID. Then an integral similar to the FT is calculated over the pseudo-FID, except that only values that are smaller than zero are summed. The resulting function has the property of reaching a minimum for the correct value of the coupling. A similar scheme is applicable to antiphase splittings, making it possible to analyze COSY cross-peaks. The paper discussed many sources of potential problems including the behavior as a function of the S/N ratio.

5. BIOLOGICAL APPLICATIONS

There is extensive coverage of biological applications in the literature, making a comprehensive review of the domain redundant. The next section will first briefly present the many reviews and series articles and then discuss some selected papers of particular interest.

5.1. Literature

Following the seminal work of Wüthrich,[513] there are many papers on general protein studies using NMR.[514–521] In the more specific domain of computer processing, one of the main and up-to-date reviews is that by Pelczer and Carter[522] which was published in 1997 and covers a very broad range of literature.

Two series of particular interest include volumes devoted to NMR. The first is the *NATO Advanced Science Institute Series* which in 1991 devoted a volume to *Computational Aspects of Biological Applications*.[523] Some selected chapters are listed in the references.[164,319,422,524–534] The second is *Methods in Enzymology*, which devoted a number of volumes to the biological application of NMR. Some may be outdated, having being published in the early[535,536] and mid-1990s,[537,538] but the later issues are quite recent.[539,540] A selection of the content concerning computational aspects can be found in the references,[250,260,541–547] with the exception of issues which were not available when this chapter was being compiled.

5.2. Historical overview

In 1982, Wagner and Wüthrich[548] discussed the potential of the sequential assignment of proteins using NOE signals. The next decisive step involved the introduction of ^{13}C enrichment in the mid-1980s. One example of development is given by Bax and Weiss[549] who acquired the first ^{13}C edited NOESY spectrum. From the following year, different groups worked on computer-assisted spectral attribution. The paper by Billeter *et al.*[550] about the ASSIGN program is just a recent example.

Dealing with the ambiguities of NOE signals, a process requiring human intervention, is a major difficulty. The ability of computer software to provide the user with all of the information required to lift them was, and still is, the key quality of an assignment program. Cieslar, Clore, and Gronenborn[551] also proposed a method which they implemented in a computer program. The following year, a combination of methods were put forward by Eads and Kuntz.[552] The introduction of the ^{15}N label on top of ^{13}C closed the spin network but this did not solve all the problems. Stockman *et al.*[553] discussed two-dimensional approaches to double labeling protein structure studies. In 1991, three-dimensional spectra of uniformly enriched proteins were acquired by Bax and Ikura.[554]

With the availability of all these tools, developments have been very fruitful, each exploiting specific advantages of more-than-two dimensions and enrichments. Here again, one should consult the specific literature listed above or the selection of journal articles given in the references.[555–567] Note a proposal for the analysis of spectra of biological samples without assignment[568] and consideration by Hoch[521] of the fitting of protein structure to experimental data.

REFERENCES

1. R. R. Ernst and W. A. Anderson, *Rev. Sci. Instr.*, 1966, **37**, 93.
2. J. W. Cooley and J. W. Tukey, *Math. Computation*, 1965, **19**, 297.
3. J. C. Hoch and A. S. Stern, *NMR Data Processing*, Wiley-Liss, New York, 1996.
4. D. N. Rutledge, *Signal Treatment and Signal Analysis in NMR*, Vol. 18 (eds. B. G. M. Vandeginste and S. C. Rutan), Elsevier, Amsterdam, 1996.
5. G. A. Morris, in *Encyclopedia of Spectroscopy and Spectrometry*, Vol. 2 (eds G. E. Tranter and J. L. Holmes), pp. 1514–1521, Academic Press, San Diego, 2000.
6. H. R. Kalbitzer, in *Two-dimensional NMR Spectroscopy. Application for Chemists and Biochemists: Methods in Stereochemical Analysis* (eds W. R. Croasmun and R. M. K. Carlson), VCH, Cambridge, UK, 1994.
7. R. de Beer and D. v. Ormondt, in *NMR Basic Principles and Progress*, Vol. 26 (eds P. Diehl, E. Fluck, H. Günther, R. Kosfeld and J. Seelig), pp. 201–248, Springer-Verlag, Berlin, Heidelberg, 1992.
8. S. M. Kay and S. L. Marple Jr, *Proc. IEEE*, 1981, **69**, 1380.
9. R. Freeman, *A Handbook of NMR*, Longman, New York, 1987.
10. R. R. Ernst, G. Bodenhausen and A. Wokaun, *Principles of Nuclear Magnetic Resonance in One and Two Dimensions*, Clarendon Press, Oxford, 1987.
11. T. D. W. Claridge, *High Resolution NMR Techniques in Organic Chemistry*, Vol. 19 (ed. J. E. Baldwin), Pergamon Press, Oxford, 1999.

12. A. E. Derome, *Modern NMR Techniques for Chemistry Research*, Vol. 6 (ed. J. E. Baldwin), Pergamon Press, Oxford, 1987.
13. J. Cavanagh, W. Fairbrother, A. G. Palmer III and N. J. Skelton, *Protein NMR Spectroscopy. Principles and Practice*, Academic Press, San Diego, 1996.
14. D. M. Grant and R. K. Harris (eds) *Encyclopedia of Nuclear Magnetic Resonance*, John Wiley & Sons, Chichester, 1996.
15. H. Barkhuijsen, R. de Beer, M. J. Duijvestijn, C. van der Lugt, D. van Ormondt and R. A. Wind, *J. Magn. Reson.*, 1985, **62**, 153.
16. R. Tycko and A. E. Berger, *J. Magn. Reson.*, 1999, **141**, 141.
17. M. J. Duer, *Chem. Phys. Lett.*, 1997, **277**, 167.
18. H.-G. Bartel and M. Nofz, *Chemom. Intell. Lab. Syst.*, 1997, **36**, 53.
19. M. Matlengiewicz, N. Henzel, J.-C. Lauer, T. Laurens, D. Nicole and P. Rubini, *Analyst (London)*, 1992, **117**, 387.
20. O. Ivanciuc, J.-P. Rabine and D. Cabrol-Bass, *Comput. Chem. (Oxford)*, 1997, **21**, 437.
21. D. N. Rutledge and A. S. Barros, *Analyst (Cambridge, UK)*, 1998, **123**, 551.
22. W. Y. Choy and B. C. Sanctuary, *J. Chem. Inf. Comput. Sci.*, 1998, **38**, 685.
23. G. J. Metzger, M. Patel and Y. Hu, *J. Magn. Reson., Ser. B*, 1996, **110**, 316.
24. E. O. Brigham, *The Fast Fourier Transform*, Prentice-Hall, Englewood Cliffs, 1974.
25. E. O. Brigham, *The Fast Fourier Transform and Its Applications*, Prentice-Hall, Englewood Cliffs, 1988.
26. R. N. Bracewell, *The Fourier Transform and its Application*, McGraw-Hill, New York, 1978.
27. R. N. Bracewell, *The Fourier Transform and its Application*, McGraw-Hill, New York, 2000.
28. A. G. Marshall and F. R. Verdun, *Fourier Transform in NMR, Optical and Mass Spectrometry*, Elsevier, Amsterdam, 1990.
29. B. van den Bogaert, in *Wavelets in Chemistry: Data Handling in Science and Technology*, Vol. 22 (ed. B. Walczak), pp. 3–31, Elsevier, Amsterdam, 2000.
30. L. J. Eveleigh, in *Signal Treatment and Signal Analysis in NMR: Data Handling in Science and Technology*, Vol. 18 (ed. B. N. Rutledge), pp. 1–24, Elsevier, Amsterdam, 1996.
31. P. A. Angelidis, *Concepts in Magn. Reson.*, 1996, **8**, 339.
32. R. R. Ernst, *J. Magn. Reson.*, 1969, **1**, 7.
33. M. H. Levitt and R. Freeman, *J. Magn. Reson.*, 1979, 675.
34. A. Ejchart and K. Wróblewski, *J. Magn. Reson.*, 1980, **40**, 469.
35. G. H. Weiss, J. A. Ferretti and R. A. Byrd, *J. Magn. Reson.*, 1987, **71**, 97.
36. S. J. Howard, in *Deconvolution* (ed. P. A. Jansson), pp. 261–287, Academic Press, Orlando, 1984.
37. D. J. States, R. A. Haberkorn and D. J. Ruben, *J. Magn. Reson.*, 1982, **48**, 286.
38. D. Marion and K. Wüthrich, *Biochem. Biophys. Res. Commun.*, 1983, **113**, 967.
39. J. Keeler and D. Neuhaus, *J. Magn. Reson.*, 1985, **63**, 454.
40. Z. Zolnai, N. Juranic', J. L. Markley and S. Macura, *J. Magn. Reson., Ser. A*, 1996, **119**, 53.
41. J. Keeler, *J. Magn. Reson.*, 1984, **56**, 463.
42. A. J. Shaka, J. Keeler and R. Freeman, *J. Magn. Reson.*, 1984, **56**, 294.
43. F. Abildgaard, H. Gesmar and J. J. Led, *J. Magn. Reson.*, 1988, **79**, 78.
44. A. Bax, M. Ikura, L. E. Kay and G. Zhu, *J. Magn. Reson.*, 1991, **91**, 174.
45. P. Hodgkinson and P. J. Hore, *Adv. Magn. Reson.*, 1997, **20**, 187.
46. P. Hodgkinson, K. J. Holmes and P. J. Hore, *J. Magn. Reson., Ser. A*, 1996, **120**, 18.
47. P. Schmieder, A. S. Stern, G. Wagner and J. C. Hoch, *J. Magn. Reson.*, 1997, **125**, 332.
48. P. Schmieder, A. S. Stern, G. Wagner and J. C. Hoch, *J. Biomol. NMR*, 1993, **3**, 569.
49. P. Schmieder, A. S. Stern, G. Wagner and J. C. Hoch, *J. Biomol. NMR*, 1994, **4**, 483.
50. D. Jeannerat, *Magn. Reson. Chem.*, 2000, **38**, 415.
51. J.-M. Bernassau and J.-M. Nuzillard, *J. Magn. Reson., Ser. A*, 1994, **108**, 248.
52. R. C. Morshauser and E. R. P. Zuiderweg, *J. Magn. Reson.*, 1999, **139**, 232.
53. A. Kumar, S. C. Brown, M. E. Donlan, B. U. Meier and P. W. Jeffs, *J. Magn. Reson.*, 1991, **95**, 1.

54. D. D. Traficante and M. Rajabzadeh, *Concepts in Magnetic Resonance*, 2000, **12**, 83.
55. R. R. Ernst, *Adv. Nucl. Magn.*, 1966, **2**, 1.
56. A. G. Ferrige and J. C. Lindon, *J. Magn. Reson.*, 1978, **31**, 337.
57. I. D. Campbell, C. M. Dobson, R. J. P. Williams and A. V. Xavier, *J. Magn. Reson.*, 1973, **11**, 172.
58. A. De Marco and K. Wüthrich, *J. Magn. Reson.*, 1976, **24**, 201.
59. M. Guéron, *J. Magn. Reson.*, 1978, **30**, 515.
60. B. Clin, J. d. Bony, P. Lalanne, J. Biais and B. Lemanceau, *J. Magn. Reson.*, 1979, **33**, 457.
61. J. A. B. Lohman, *J. Magn. Reson.*, 1980, **38**, 163.
62. J. C. Lindon and A. G. Ferrige, *Prog NMR Spectrosc*, 1980, **14**, 27.
63. R. G. Brereton, M. J. Garson and J. Staunton, *J. Magn. Reson.*, 1981, **43**, 224.
64. D. D. Traficante, *J. Magn. Reson.*, 1986, **66**, 182.
65. D. D. Traficante and G. A. Nemeth, *J. Magn. Reson.*, 1987, **71**, 237.
66. S. O. Chan and M. B. Comisarow, *J. Magn. Reson.*, 1983, **54**, 201.
67. G. H. Weiss and J. A. Ferretti, *J. Magn. Reson.*, 1983, **55**, 397.
68. A. F. Mehlkopf, D. Korbee and T. A. Tiggelman, *J. Magn. Reson.*, 1984, **58**, 315.
69. M. H. Levitt, G. Bodenhausen and R. R. Ernst, *J. Magn. Reson.*, 1984, **58**, 462.
70. G. Lin, X. Liao, D. Lin, S. Zheng, Z. Chen and Q. Wu, *J. Magn. Reson.*, 2000, **144**, 6.
71. G. H. Weiss, J. E. Kiefer and J. A. Ferretti, *J. Magn. Reson.*, 1992, **97**, 227.
72. H. Liu, P. Spielmann, N. B. Ulyanov, D. E. Wemmer and T. L. James, *J. Biomol. NMR*, 1995, **6**, 390.
73. I. L. Barsukov and A. S. Arseniev, *J. Magn. Reson.*, 1987, **73**, 148.
74. W. Dietrich, C. H. Rüdel and M. Neumann, *J. Magn. Reson.*, 1991, **91**, 1.
75. P. Güntert and K. Wüthrich, *J. Magn. Reson.*, 1992, **96**, 403.
76. R. A. Chylla and J. L. Markley, *J. Magn. Reson., Ser. B*, 1993, **102**, 148.
77. G. C. Levy, G.-W. Jeong, J. Yu and K. Wang, *J. Magn. Reson., Ser. A*, 1994, **111**, 179.
78. G. Otting, H. Widmer, G. Wagner and K. Wüthrich, *J. Magn. Reson.*, 1986, **66**, 187.
79. P. A. Jansson, *Deconvolution*, Academic Press, Orlando, 1984.
80. P. A. Jansson, *Deconvolution of Images and Spectra*, Academic Press, San Diego, 1997.
81. P. A. Jansson, in *Deconvolution* (ed. P. A. Jansson), pp. 1–34, Academic Press, Orlando, 1984.
82. P. A. Jansson, in *Deconvolution* (ed. P. A. Jansson), pp. 67–92, Academic Press, Orlando, 1984.
83. P. A. Jansson, in *Deconvolution* (ed. P. A. Jansson), pp. 93–134, Academic Press, Orlando, 1984.
84. G. A. Morris and H. Barjat, in *Methods for Structure Elucidation by High-Resolution NMR: Anal. Spectrosc. Libr.*, Vol. 8 (eds G. Batta, K. E. Kövér and C. Szántay), pp. 303–316, Elsevier, Amsterdam, 1997.
85. G. A. Morris, in *Signal Treatment and Signal Analysis in NMR: Data Handl. Sci. Technol.*, Vol. 18 (ed. D. N. Rutledge), pp. 346–361, Elsevier, Amsterdam, 1996.
86. G. A. Morris, H. Barjat and T. J. Horne, *Prog. Nucl. Magn. Reson. Spectrosc.*, 1997, **31**, 197.
87. K. R. Metz, M. M. Lam and A. G. Webb, *Concepts Magn. Reson.*, 2000, **12**, 21.
88. J. M. Wouters and G. A. Petersson, *J. Magn. Reson.*, 1977, **28**, 81.
89. J. M. Wouters, G. A. Petersson, W. C. Agosta, F. H. Field, W. A. Gibbons, H. Wyssbrod and D. Cowburn, *J. Magn. Reson.*, 1977, **29**, 93.
90. A. H. Clark and P. J. Lillford, *J. Magn. Reson.*, 1980, **41**, 42.
91. J. K. Kauppinen, D. J. Moffatt, H. H. Mantsch and D. G. Cameron, *Appl. Spectrosc.*, 1981, **35**, 271.
92. A. Kumar, C. H. Sotak, C. L. Dumoulin and G. C. Levy, *Comput. Enhanced Spectrosc.*, 1983, **1**, 107.
93. P. S. Belton and K. M. Wright, *J. Magn. Reson.*, 1986, **68**, 564.
94. F. Ni and H. A. Scheraga, *J. Magn. Reson.*, 1986, **70**, 506.
95. A. A. Bothner-By and J. Dadok, *J. Magn. Reson.*, 1987, **72**, 540.
96. D. Marion, M. Ikura and A. Bax, *J. Magn. Reson.*, 1989, **84**, 425.

97. R. E. Hoffman and G. C. Levy, *J. Magn. Reson.*, 1989, **83**, 411.
98. G. A. Morris, *J. Magn. Reson.*, 1988, **80**, 547.
99. G. A. Morris and D. Cowburn, *Magn. Reson. Chem.*, 1989, **27**, 1085.
100. J. D. Mersch and J. K. M. Sanders, *J. Magn. Reson.*, 1982, **50**, 289.
101. F. Ni and H. A. Scheraga, *J. Magn. Reson.*, 1989, **82**, 413.
102. J. Liu, A. O. K. Nieminen and J. L. Koenig, *Appl. Spectrosc.*, 1989, **43**, 1260.
103. P. Jehenson and A. Syrota, *Magn. Reson. Med.*, 1989, **12**, 253.
104. A. A. de Graaf, J. E. van Dijk and W. M. M. J. Bovée, *Magn. Reson. Med.*, 1990, **13**, 343.
105. A. Gibbs and G. A. Morris, *J. Magn. Reson.*, 1991, **91**, 77.
106. A. Gibbs, G. A. Morris, A. G. Swanson and D. Cowburn, *J. Magn. Reson., Ser. A*, 1993, **101**, 351.
107. P. Huber and G. Bodenhausen, *J. Magn. Reson., Ser. A*, 1993, **102**, 81.
108. P. Huber and G. Bodenhausen, *J. Magn. Reson., Ser. A*, 1993, **104**, 96.
109. J. A. Jones, D. S. Grainger, P. J. Hore and G. J. Daniell, *J. Magn. Reson., Ser. A*, 1993, **101**, 162.
110. M. Woodley and R. Freeman, *J. Magn. Reson., Ser. A*, 1994, **111**, 225.
111. F. del Río Portilla and R. Freeman, *J. Magn. Reson., Ser. A*, 1994, **108**, 124.
112. A. A. Maudsley, *J. Magn. Reson., Ser. B*, 1995, **106**, 47.
113. C. A. Baldwin, P. Alexander and L. F. Gladden, *J. Magn. Reson., Ser. A*, 1995, **112**, 169.
114. H. Barjat, G. A. Morris, A. G. Swanson, S. Smart and S. C. R. Williams, *J. Magn. Reson., Ser. A*, 1995, **116**, 206.
115. T. J. Horne and G. A. Morris, *J. Magn. Reson., Ser. A*, 1996, **123**, 246.
116. M. A. McCabe and S. R. Wassall, *J. Magn. Reson., Ser. B*, 1995, **106**, 80.
117. M. A. McCabe and S. R. Wassall, *Solid State Nucl. Magn. Reson.*, 1997, **10**, 53.
118. M. Bloom, J. H. Davis and A. L. Mackay, *Chem. Phys. Lett.*, 1981, **80**, 198.
119. E. Sternin, M. Bloom and A. L. MacKay, *J. Magn. Reson.*, 1983, **55**, 274.
120. R. D. Curtis, P. J. Tonge, I. C. P. Smith and H. C. Jarrell, *J. Magn. Reson., Ser. A*, 1993, **102**, 110.
121. R. Laatikainen, M. Niemitz, W. J. Malaisse, M. Biesemans and R. Willem, *Magn. Reson. Med.*, 1996, **36**, 359.
122. D. Jeannerat and G. Bodenhausen, *J. Magn. Reson.*, 1999, **141**, 133.
123. D. Jeannerat, *Magn. Reson. Chem.*, 2000, **38**, 156.
124. A. Garza-García, G. Ponzanelli-Velázquez and F. del Río-Portilla, *J. Magn. Reson.*, 2001, **148**, 214.
125. H. Hu, Q. N. Van, V. A. Mandelshtam and A. J. Shaka, *J. Magn. Reson.*, 1998, **134**, 76.
126. M. Goez and R. Heun, *J. Magn. Reson.*, 1999, **136**, 69.
127. T. Hou, E. MacNamara and D. Reftery, *Analytica Chemica Acta*, 1999, **400**, 297.
128. P. Koehl, *Prog. Nucl. Magn. Reson. Spectrosc.*, 1999, **34**, 257.
129. H. Barkhuijsen, R. de Beer, W. M. M. J. Bovée and D. van Ormondt, *J. Magn. Reson.*, 1985, **61**, 465.
130. H. Barkhuijsen, R. de Beer, W. M. M. J. Bovée, J. H. N. Creyghton and D. van Ormondt, *Magn. Reson. Med.*, 1985, **2**, 86.
131. R. Kumaresan and D. W. Tufts, *IEEE Trans. Acoust. Speech Signal Process.*, 1982, **30**, 833.
132. H. Barkhuijsen, R. de Beer and D. van Ormondt, *J. Magn. Reson.*, 1986, **67**, 371.
133. J. Tang, C. P. Lin, M. K. Bowman and J. R. Norris, *J. Magn. Reson.*, 1985, **62**, 167.
134. B. Porat and B. Friedlander, *IEEE Trans. Acoust. Speech Signal Process.*, 1986, **34**, 1336.
135. J. Tang and J. R. Norris, *J. Chem. Phys.*, 1986, **84**, 5210.
136. J. Tang and J. R. Norris, *J. Magn. Reson.*, 1986, **69**, 180.
137. J. Tang and J. R. Norris, *Chem. Phys. Lett.*, 1986, **131**, 252.
138. J. Tang and J. R. Norris, *J. Magn. Reson.*, 1988, **78**, 23.
139. H. Barkhuijsen, R. de Beer and D. van Ormondt, *J. Magn. Reson.*, 1987, **73**, 553.
140. H. Yan and J. C. Gore, *J. Magn. Reson.*, 1988, **80**, 324.

141. R. de Beer, D. Van Ormondt, W. W. F. Pijnappel and J. W. C. van der Veen, *Isr. J. Chem.*, 1988, **28**, 249.
142. M. A. Delsuc, F. Ni and G. C. Levy, *J. Magn. Reson.*, 1987, **73**, 548.
143. H. Gesmar and J. J. Led, *J. Magn. Reson.*, 1988, **76**, 183.
144. B. A. Johnson, J. A. Malikayil and I. M. Armitage, *J. Magn. Reson.*, 1988, **76**, 352.
145. J. Tang and J. R. Norris, *J. Magn. Reson.*, 1988, **79**, 190.
146. D. S. Stephenson, *Prog. Nucl. Magn. Reson. Spectrosc.*, 1988, **20**, 515.
147. D. Marion and A. Bax, *J. Magn. Reson.*, 1989, **83**, 205.
148. H. Gesmar and J. J. Led, *J. Magn. Reson.*, 1989, **83**, 53.
149. Y. Zeng, J. Tang, C. A. Bush and J. R. Norris, *J. Magn. Reson.*, 1989, **83**, 473.
150. C. F. Tirendi and J. F. Martin, *J. Magn. Reson.*, 1989, **81**, 577.
151. C. F. Tirendi and J. F. Martin, *J. Magn. Reson.*, 1989, **85**, 162.
152. M. Uike, T. Uchiyama and H. Minamitani, *J. Magn. Reson.*, 1992, **99**, 363.
153. G. L. Millhauser, A. A. Carter, D. J. Schneider, J. H. Freed and R. E. Oswald, *J. Magn. Reson.*, 1989, **82**, 150.
154. E. T. Olejniczak and H. L. Eaton, *J. Magn. Reson.*, 1990, **87**, 628.
155. C. Cieslar, T. A. Holak and H. Oschkinat, *J. Magn. Reson.*, 1990, **89**, 184.
156. J. L. Galazzo and J. E. Bailey, *Biotechnol. Tech.*, 1989, **3**, 13.
157. F. Luthon, R. Blanpain, M. Decorps and J. P. Albrand, *J. Magn. Reson.*, 1989, **81**, 538.
158. T. Uchiyama, H. Minamitani, K. Ichimori, H. Nakazawa and H. Oki, *J. Tokai Exp. Clin. Med.*, 1991, **16**, 231.
159. L. E. Kay, D. Marion and A. Bax, *J. Magn. Reson.*, 1989, **84**, 72.
160. L. E. Kay, M. Ikura, G. Zhu and A. Bax, *J. Magn. Reson.*, 1991, **91**, 422.
161. G. Zhu and A. Bax, *J. Magn. Reson.*, 1990, **90**, 405.
162. H. Gesmar, J. J. Led and F. Abildgaard, *Prog. Nucl. Magn. Reson. Spectrosc.*, 1990, **22**, 255.
163. J. J. Led and H. Gesmar, *Chem. Rev.*, 1991, **91**, 1413.
164. H. Gesmar and J. J. Led, in *Computational Aspects of the Study of Biological Macromolecules by Nuclear Magnetic Resonance Spectroscopy: NATO ASI Ser., Ser. A*, Vol. 225 (eds J. C. Hoch, F. M. Poulsen and C. Redfield), pp. 67–85, Plenum Press, New York, 1991.
165. J. J. Led and H. Gesmar, *J. Biomol. NMR*, 1991, **1**, 237.
166. J. J. Led, F. Abildgaard and H. Gesmar, *J. Magn. Reson.*, 1991, **93**, 659.
167. J. Haselgrove and M. Elliott, *Magn. Reson. Med.*, 1991, **17**, 496.
168. A. Diop, A. Briguet and D. Graveron-Demilly, *Magn. Reson. Med.*, 1992, **27**, 318.
169. J. A. Cadzow, *IEEE Trans. Acoust. Speech Signal Process.*, 1988, **36**, 49.
170. Y. Zaim-Wadghiri, A. Diop, D. Graveron-Demilly and A. Briguet, *Biochimie*, 1992, **74**, 769.
171. W. W. F. Pijnappel, A. van den Boogaart, R. de Beer and D. van Ormondt, *J. Magn. Reson.*, 1992, **97**, 122.
172. G. Zhu and A. Bax, *J. Magn. Reson.*, 1992, **100**, 202.
173. G. Zhu and A. Bax, *J. Magn. Reson.*, 1992, **98**, 192.
174. S. Boudhabhay, B. Ancian, P. Levoir, R. Dubest and J. Aubard, *Comput. Chem. (Oxford)*, 1992, **16**, 271.
175. C. Tellier, M. Guillou-Charpin, D. Le Botlan and F. Pelissolo, *Magn. Reson. Chem.*, 1991, **29**, 164.
176. W. Kölbel and H. Schäfer, *J. Magn. Reson.*, 1992, **100**, 598.
177. Y.-Y. Lin, N.-H. Ge and L.-P. Hwang, *J. Magn. Reson., Ser. A*, 1993, **105**, 65.
178. B. De Moor, *IEEE Trans. Signal Process.*, 1993, **41**, 2826.
179. H. Gesmar and P. C. Hansen, *J. Magn. Reson., Ser. A*, 1994, **106**, 236.
180. Y. Ohba, *Spectrochim. Acta, Part A*, 2000, **56**, 235.
181. A. Diop, W. Kölbel, D. Michel, A. Briguet and D. Graveron-Demilly, *J. Magn. Reson., Ser. B*, 1994, **103**, 217.
182. S. Van Huffel, H. Chen, C. Decanniere and P. Van Hecke, *J. Magn. Reson., Ser. A*, 1994, **110**, 228.

183. H. Chen, S. Van Huffel, C. Decanniere and P. Van Hecke, *J. Magn. Reson., Ser. A*, 1994, **109**, 46.
184. P. Koehl, C. Ling and J. F. Lefèvre, *J. Chim. Phys. Phys.-Chim. Biol.*, 1994, **91**, 595.
185. P. Koehl, C. Ling and J. F. Lefèvre, *J. Magn. Reson., Ser. A*, 1994, **109**, 32.
186. A. Diop, Y. Zaim-Wadghiri, A. Briguet and D. Graveron-Demilly, *J. Magn. Reson., Ser. B*, 1994, **105**, 17.
187. Y. K. Lee, R. L. Vold, G. L. Hoatson, Y. Y. Lin and A. Pines, *J. Magn. Reson., Ser. A*, 1995, **112**, 112.
188. D. M. Babcook, P. V. Sahasrabudhe and W. H. Gmeiner, *Magn. Reson. Chem.*, 1996, **34**, 851.
189. M. Fedrigo, G. Esposito, S. Cattarinussi, P. Viglino and F. Fogolari, *J. Magn. Reson., Ser. A*, 1996, **121**, 97.
190. M. Fedrigo, F. Fogolari, P. Viglino and G. Esposito, *J. Magn. Reson., Ser. B*, 1996, **113**, 160.
191. J.-M. Nuzillard, *J. Magn. Reson., Ser. A*, 1996, **118**, 132.
192. V. Vondra, A. van den Boogaart, D. Graveron-Demilly and D. van Ormondt, *J. Magn. Reson., Ser. A*, 1996, **119**, 271.
193. J. Totz, A. van den Boogaart, S. Van Huffel, D. Graveron-Demilly, I. Dologlou, R. Heidler and D. Michel, *J. Magn. Reson.*, 1997, **124**, 400.
194. G. Zhu, D. Smith and Y. Hua, *J. Magn. Reson.*, 1997, **124**, 286.
195. W. F. Reynolds, M. Yu, R. G. Enriquez and I. Leon, *Magn. Reson. Chem.*, 1997, **35**, 505.
196. Y.-Y. Lin, P. Hodgkinson, M. Ernst and A. Pines, *J. Magn. Reson.*, 1997, **128**, 30.
197. J. Chen and V. A. Mandelshtam, *J. Chem. Phys.*, 2000, **112**, 4429.
198. V. A. Mandelshtam, *J. Magn. Reson.*, 2000, **144**, 343.
199. H. Hu, A. A. De Angelis, V. A. Mandelshtam and A. J. Shaka, *J. Magn. Reson.*, 2000, **144**, 357.
200. D. Neuhauser, *J. Chem. Phys.*, 1990, **93**, 2611.
201. D. Neuhauser, *J. Chem. Phys.*, 1994, **100**, 5076.
202. M. R. Wall and D. Neuhauser, *J. Chem. Phys.*, 1995, **102**, 8011.
203. V. A. Mandelshtam and H. S. Taylor, *Phys. Rev. Lett.*, 1997, **78**, 3274.
204. V. A. Mandelshtam and H. S. Taylor, *J. Chem. Phys.*, 1997, **107**, 6756.
205. V. A. Mandelshtam and H. S. Taylor, *J. Chem. Phys.*, 1998, **108**, 9970.
206. V. A. Mandelshtam, H. Hu and A. J. Shaka, *Magn. Reson. Chem.*, 1998, **36**, S17.
207. J. W. Pang, T. Dieckmann, J. Feigon and D. Neuhauser, *J. Chem. Phys.*, 1998, **108**, 8360.
208. M. R. Wall, T. Dieckmann, J. Feigon and D. Neuhauser, *Chem. Phys. Lett.*, 1998, **291**, 465.
209. V. A. Mandelshtam, H. S. Taylor and A. J. Shaka, *J. Magn. Reson.*, 1998, **133**, 304.
210. V. A. Mandelshtam, N. D. Taylor, H. Hu, M. Smith and A. J. Shaka, *Chem. Phys. Lett.*, 1999, **305**, 209.
211. G. Jeschke, V. A. Mandelshtam and A. J. Shaka, *J. Magn. Reson.*, 1999, **137**, 221.
212. J. Chen, V. A. Mandelshtam and A. J. Shaka, *J. Magn. Reson.*, 2000, **146**, 363.
213. J. Chen, A. J. Shaka and V. A. Mandelshtam, *J. Magn. Reson.*, 2000, **147**, 129.
214. B. Walczak, *Wavelets in Chemistry*, Vol. 22 (eds B. G. M. Vandeginste and S. C. Rutan), Elsevier, Amsterdam, 2000.
215. B. van den Bogaert, in *Wavelets in Chemistry: Data Handling in Science and Technology*, Vol. 22 (ed. B. Walczak), pp. 33–55, Elsevier, Amsterdam, 2000.
216. Y. Mallet, D. Coomans and O. de Vel, in *Wavelets in Chemistry: Data Handling in Science and Technology*, Vol. 22 (ed. B. Walczak), pp. 177–200, Elsevier, Amsterdam, 2000.
217. Y. Mallet, O. de Vel and D. Coomans, in *Wavelets in Chemistry: Data Handling in Science and Technology*, Vol. 22 (ed. B. Walczak), pp. 57–84, Elsevier, Amsterdam, 2000.
218. O. de Vel, Y. Mallet and D. Coomans, in *Wavelets in Chemistry: Data Handling in Science and Technology*, Vol. 22 (ed. B. Walczak), pp. 85–118, Elsevier, Amsterdam, 2000.
219. M. N. Nounou and B. R. Bakshi, in *Wavelets in Chemistry: Data Handling in Science and Technology*, Vol. 22 (ed. B. Walczak), pp. 119–150, Elsevier, Amsterdam, 2000.

220. Y. Mallet, D. Coomans and O. de Vel, in *Wavelets in Chemistry: Data Handling in Science and Technology*, Vol. 22 (ed. B. Walczak), pp. 151–164, Elsevier, Amsterdam, 2000.
221. B. Walczak and D. L. Massart, in *Wavelets in Chemistry: Data Handling in Science and Technology*, Vol. 22 (ed. B. Walczak), pp. 165–176, Elsevier, Amsterdam, 2000.
222. G. Kaiser, *A Friendly Guide to Wavelets*, Birkhäuser, Boston, 1994.
223. W. Schempp, *Acta Applicandae Mathematicae*, 1997, **48**, 185.
224. X. Shao and W. Cai, *Rev. Anal. Chem.*, 1998, **17**, 235.
225. G. Neue, *Solid State Nucl. Magn. Reson.*, 1996, **5**, 305.
226. A. R. Tate, D. Watson, S. Eglen, T. N. Arvanitis, E. L. Thomas and J. D. Bell, *Magn. Reson. Med.*, 1996, **35**, 834.
227. G. Johnson, D. J. Thomson, E. X. Wu and S. C. R. Williams, *J. Magn. Reson., Ser. B*, 1996, **110**, 138.
228. J. D. de Certaines, L. Nadal, G. Leray, H. Serrai and C. J. Lewa, *Anticancer Res.*, 1996, **16**, 1451.
229. G. Sarty and E. Kendall, *J. Magn. Reson., Ser. B*, 1996, **111**, 50.
230. H. Serrai, L. Senhadji, J. D. De Certaines and J. L. Coatrieux, *J. Magn. Reson.*, 1997, **124**, 20.
231. D. Barache, J. P. Antoine and J.-M. Dereppe, *J. Magn. Reson.*, 1997, **128**, 1.
232. R. J. Ordidge and I. D. Cresshull, *J. Magn. Reson.*, 1986, **69**, 151.
233. K. Young, B. J. Soher and A. A. Maudsley, *Magn. Reson. Med.*, 1998, **40**, 816.
234. H. Serrai, L. Nadal, G. Leray, B. Leroy, B. Delplanque and J. D. De Certaines, *NMR Biomed.*, 1998, **11**, 273.
235. H. Serrai, A. Borthakur, L. Senhadji, R. Reddy and N. Bansal, *J. Magn. Reson.*, 2000, **142**, 341.
236. J.-P. Antoine, A. Coron and J.-M. Dereppe, *J. Magn. Reson.*, 2000, **144**, 189.
237. X. Shao, H. Gu, J. Wu and Y. Shi, *Appl. Spectrosc.*, 2000, **54**, 731.
238. S. Ding and C. A. McDowell, *Chem. Phys. Lett.*, 2000, **322**, 341.
239. A. G. Evans and R. Fischl, *IEEE Trans. Audio Electroacoustics*, 1973, **21**, 61.
240. G. H. Golub and C. F. van Loan, *Siam J. Numer. Anal.*, 1980, **17**, 883.
241. P. Moore, *J. Chem. Soc., Faraday Trans. I*, 1975, **72**, 826.
242. H. S. Gutowsky and C. H. Holm, *J. Chem. Phys.*, 1956, **25**, 1228.
243. W. Dietrich and R. Gerhards, *J. Magn. Reson.*, 1981, **44**, 229.
244. W. Denk, R. Baumann and G. Wagner, *J. Magn. Reson.*, 1986, **67**, 386.
245. T. A. Holak, J. N. Scarsdale and J. H. Prestegard, *J. Magn. Reson.*, 1987, **74**, 546.
246. Y. Manassen, G. Navon and C. T. W. Moonen, *J. Magn. Reson.*, 1987, **72**, 551.
247. R. Kumaresan, C. S. Ramalingam and D. van Ormondt, *J. Magn. Reson.*, 1990, **89**, 562.
248. K. McLeod and M. B. Comisarow, *J. Magn. Reson.*, 1989, **84**, 490.
249. H. Gesmar, P. F. Nielsen and J. J. Led, *J. Magn. Reson., Ser B*, 1994, **103**, 10.
250. J. J. Led and H. Gesmar, in *Nuclear Magnetic Resonance, Part C: Methods in Enzymology*, Vol. 239 (eds T. L. James and N. J. Oppenheimer), pp. 318–345, Academic Press, 1994.
251. S. M. Kristensen, M. D. Sørensen, H. Gesmar and J. J. Led, *J. Magn. Reson., Ser. B*, 1996, **112**, 193.
252. J. W. Brown and W. H. Huestis, *J. Biomol. NMR*, 1994, **4**, 645.
253. MATLAB, (c) Copyright 1984.
254. J.-X. Yang and T. F. Havel, *J. Biomol. NMR*, 1994, **4**, 807.
255. J.-X. Yang, A. Krezel, P. Schmieder, G. Wagner and T. F. Havel, *J. Biomol. NMR*, 1994, **4**, 827.
256. A. Müller, *J. Magn. Reson., Ser. A*, 1995, **114**, 238.
257. P. Stilbs, *J. Magn. Reson.*, 1998, **135**, 236.
258. F. Delaglio, Z. Wu and A. Bax, *J. Magn. Reson.*, 2001, **149**, 276.
259. B. R. Frieden, in *Deconvolution* (ed. P. A. Jansson), pp. 227–259, Academic Press, Orlando, 1984.
260. P. N. Borer and G. C. Levy, in *Nuclear Magnetic Resonance, Part C: Methods in Enzymology*, Vol. 239 (eds T. L. James and N. J. Oppenheimer), pp. 257–288, Academic Press, 1994.

261. G. C. Levy, P. N. Borer and G.-W. Jeong, in *Computer-Enhanced Analytical Spectroscopy*, Vol. 4 (ed. C. L. Wilkins), pp. 73–96, Plenum Press, New York, 1993.
262. M. I. Miller and A. S. Greene, *J. Magn. Reson.*, 1989, **83**, 525.
263. G. W. Jeong, P. N. Borer, S. S. Wang and G. C. Levy, *J. Magn. Reson., Ser. A*, 1993, **103**, 123.
264. S. Wang, I. Pelczer, P. N. Borer and G. C. Levy, *J. Magn. Reson., Ser. A*, 1994, **108**, 171.
265. M. I. Miller, S. C. Chen, D. A. Kuefler and D. A. d'Avignon, *J. Magn. Reson., Ser. A*, 1993, 104.
266. Y. Imanishi, T. Matsuura, C. Yamasaki, T. Yamazaki, K. Ogura and M. Imanari, *J. Magn. Reson., Ser. A*, 1994, **110**, 175.
267. R. A. Chylla and J. L. Markley, *J. Biomol. NMR*, 1995, **5**, 245.
268. S. Umesh and D. W. Tufts, *IEEE Trans Signal Process.*, 1996, **44**, 2245.
269. G. Zhu and Y. Hua, *Chem. Phys. Lett.*, 1997, **264**, 424.
270. G. Zhu, W. Y. Choy and B. C. Sanctuary, *J. Magn. Reson.*, 1998, **135**, 37.
271. Z.-S. Liu, J. Li and P. Stoica, *Signal Processing*, 1997, **62**, 311.
272. Z. Bi, A. P. Bruner, J. Li, K. N. Scott, Z.-S. Liu, C. B. Stopka, H.-W. Kim and D. C. Wilson, *J. Magn. Reson.*, 1999, **140**, 108.
273. J. J. Warren and P. B. Moore, *J. Magn. Reson.*, 2001, **149**, 271.
274. J. G. Ables, *Astron. Astrophys. Suppl.*, 1974, **15**, 383.
275. J. C. J. Barna, E. D. Laue, M. R. Mayger, J. Skilling and S. J. P. Worrall, *J. Magn. Reson.*, 1987, **73**, 69.
276. J. C. J. Barna and E. D. Laue, *J. Magn. Reson.*, 1987, **75**, 384.
277. E. D. Laue, in *Maximum Entropy and Bayesian Methods*, Cambridge, England, 1988 (ed. J. Skilling), pp. 275–284, Kluwer Academic Publishers, Dordrecht, 1989.
278. M. Schmidt and D. Ziessow, *Ber. Bunsen-Ges. Phys. Chem.*, 1987, **91**, 1110.
279. D. Catalano, L. Di Bari, C. A. Veracini, G. N. Shilstone and C. Zannoni, *J. Chem. Phys.*, 1991, **94**, 3928.
280. P. J. Hore and G. J. Daniell, *J. Magn. Reson.*, 1986, **69**, 386.
281. D. I. Hoult, *J. Magn. Reson.*, 1979, **33**, 183.
282. A. R. Mazzeo and G. C. Levy, *Comput. Enhanced Spectrosc.*, 1986, **3**, 165.
283. J. C. Hoch, in *Nuclear Magnetic Resonance, Part A: Special Techniques and Dynamics: Methods in Enzymology*, Vol. 176 (eds N. J. Oppenheimer and T. L. James), pp. 216–241, Academic Press, 1989.
284. J. A. Jones and P. J. Hore, *J. Magn. Reson.*, 1991, **92**, 276.
285. J. A. Jones and P. J. Hore, *J. Magn. Reson.*, 1991, **92**, 363.
286. J. Skilling and S. Sibisi, *Maximum Entropy and Bayesian Methods*, Cambridge, England, 1994 (ed. A. van der Merwe), Kluwer Academic Publishers, Dordrecht, 1996.
287. S. F. Gull and G. J. Daniell, *Nature*, 1978, **272**, 686.
288. S. Sibisi, *Nature*, 1983, **301**, 134.
289. S. Sibisi, J. Skilling, R. G. Brereton, E. D. Laue and J. Staunton, *Nature*, 1984, **311**, 446.
290. E. D. Laue, J. Skilling, J. Staunton, S. Sibisi and R. G. Brereton, *J. Magn. Reson.*, 1985, **62**, 437.
291. E. D. Laue, J. Skilling and J. Staunton, *J. Magn. Reson.*, 1985, **63**, 418.
292. E. D. Laue, M. R. Mayger, J. Skilling and J. Staunton, *J. Magn. Reson.*, 1986, **68**, 14.
293. J. C. J. Barna, E. D. Laue, M. R. Mayger, J. Skilling and S. J. P. Worrall, *Biochem. Soc. Trans.*, 1986, **14**, 1262.
294. P. J. Hore, *J. Magn. Reson.*, 1985, **62**, 561.
295. J. C. Hoch, *J. Magn. Reson.*, 1985, **64**, 436.
296. J. F. Martín, *J. Magn. Reson.*, 1985, **65**, 291.
297. F. Ni and H. A. Scheraga, *J. Raman Spectrosc.*, 1985, **16**, 337.
298. F. Ni, G. C. Levy and H. A. Scheraga, *J. Magn. Reson.*, 1986, **66**, 385.
299. V. Viti, P. Barone, L. Guidoni and E. Massaro, *J. Magn. Reson.*, 1986, **67**, 91.
300. V. Viti, E. Massaro, L. Guidoni and P. Barone, *J. Magn. Reson.*, 1986, **70**, 379.

301. P. Barone, E. Massaro, V. Viti and L. Guidoni, *Physiol. Chem. Phys. Med. NMR*, 1987, **19**, 29.
302. A. R. Mazzeo, M. A. Delsuc, A. Kumar and G. C. Levy, *J. Magn. Reson.*, 1989, **81**, 512.
303. T. N. Huckerby, I. A. Nieduszynski, G. H. Cockin, J. M. Dickenson, H. Morris, P. N. Sanderson and D. J. Thornton, *Eur. Polym. J.*, 1989, **25**, 861.
304. M. L. Waller and P. S. Tofts, *Magn. Reson. Med.*, 1987, **4**, 385.
305. E. D. Laue, K. O. B. Pollard, J. Skilling, J. Staunton and A. C. Sutkowski, *J. Magn. Reson.*, 1987, **72**, 493.
306. K. M. Wright and P. S. Belton, *Mol. Phys.*, 1986, **58**, 485.
307. R. H. Newman, *J. Magn. Reson.*, 1988, **79**, 448.
308. G. J. Daniell and P. J. Hore, *J. Magn. Reson.*, 1989, **84**, 515.
309. S. J. Davies, C. Bauer, P. J. Hore and R. Freeman, *J. Magn. Reson.*, 1988, **76**, 476.
310. M. A. Delsuc and G. C. Levy, *J. Magn. Reson.*, 1988, **76**, 306.
311. A. Bax, R. Freeman and S. P. Kempsell, *J. Am. Chem. Soc.*, 1980, **102**, 4849.
312. B. C. De Simone, F. De Luca and B. Maraviglia, *Magn. Reson. Med.*, 1987, **4**, 78.
313. J. M. Dereppe and N. Jakus, *J. Magn. Reson.*, 1988, **79**, 307.
314. B. C. De Simone, F. De Luca and B. Maraviglia, *Magn. Reson. Med.*, 1988, **8**, 332.
315. J. C. Hoch, A. S. Stern, D. L. Donoho and I. M. Johnstone, *J. Magn. Reson.*, 1990, **86**, 236.
316. P. J. Hore, D. S. Grainger, S. Wimperis and G. J. Daniell, *J. Magn. Reson.*, 1990, **89**, 415.
317. J. K. Kauppinen, D. J. Moffatt, M. R. Hollberg and H. H. Mantsch, *Appl. Spectrosc.*, 1991, **45**, 1516.
318. T. Uchiyama and H. Minamitani, *J. Magn. Reson.*, 1991, **94**, 449.
319. M. A. Delsuc, M. Robin, C. Van Heijenoort, C. B. Reisdorf, E. Guittet and J. Y. Lallemand, in *Computational Aspects of the Study of Biological Macromolecules by Nuclear Magnetic Resonance Spectroscopy: NATO ASI Ser.*, Ser. A, Vol. 225 (eds J. C. Hoch, F. M. Poulsen and C. Redfield), pp. 163–174, Plenum Press, New York, 1991.
320. M. Robin, M.-A. Delsuc, E. Guittet and J.-Y. Lallemand, *J. Magn. Reson.*, 1991, **92**, 645.
321. A. S. Stern and J. C. Hoch, *J. Magn. Reson.*, 1992, **97**, 255.
322. J. Skilling and R. K. Bryan, *Mon. Not. R. Astr. Soc*, 1984, **211**, 111.
323. P. Hodgkinson, H. R. Mott, P. C. Driscoll, J. A. Jones and P. J. Hore, *J. Magn. Reson., Ser. B*, 1993, **101**, 218.
324. G. Zhu, *J. Magn. Reson., Ser. B*, 1996, **113**, 248.
325. K.-B. Li, A. S. Stern and J. C. Hoch, *J. Magn. Reson.*, 1998, **134**, 161.
326. M. J. Seddon, A. G. Ferrige, P. N. Sanderson and J. C. Lindon, *J. Magn. Reson., Ser. A*, 1996, **119**, 191.
327. V. Stoven, J. P. Annereau, M. A. Delsuc and J. Y. Lallemand, *J. Chem. Inf. Comput. Sci.*, 1997, **37**, 265.
328. L. Poppe, *J. Am. Chem. Soc.*, 1993, **115**, 8421.
329. M. Groth, J. Malicka, C. Czaplewski, S. Oldziej, L. Lankiewicz, W. Wiczk and A. Liwo, *J. Biomol. NMR*, 1999, **15**, 315.
330. R. Berardi, F. Spinozzi and C. Zannoni, *J. Chem. Phys.*, 1998, **109**, 3742.
331. R. Berardi, F. Spinozzi and C. Zannoni, *J. Chem. Soc., Faraday Trans.*, 1992, **88**, 1863.
332. J. W. Emsley, I. D. Wallington, D. Catalano, C. A. Veracini, G. Celebre and M. Longeri, *J. Phys. Chem.*, 1993, **97**, 6518.
333. S. Caldarelli, D. Catalano, L. Di Bari, M. Lumetti, M. Ciofalo and C. A. Veracini, *J. Mol. Struct.*, 1994, **323**, 181.
334. J. A. Jones, P. J. Hore, C. P. Relf, R. Ouwerkerk and P. Styles, *J. Magn. Reson.*, 1992, **98**, 73.
335. A. Suzuki, N. Miura and Y. Sasanuma, *Langmuir*, 2000, **16**, 6317.
336. R. T. Cox, *Am. J. Physics*, 1946, **14**, 1.
337. A. J. M. Garrett, in *Maximum Entropy and Bayesian Methods*, Cambridge, England, 1988: *Fundamental Theories of Physics* (ed. J. Skilling), pp. 107–116, Kluwer Academics Publishers, Dordrecht, 1989.
338. E. T. Jaynes, in *Maximum Entropy and Bayesian Methods in Science and Engineering*, Vol. 1 (eds G. L. Erickson and C. R. Smith), pp. 25–29, Kluwer Academic Publishers, Dordrecht, 1988.

339. E. T. Jaynes, in *Maximum-Entropy and Bayesian Methods in Science and Engineering*, Vol. 1 (eds G. L. Erickson and C. R. Smith), pp. 1–24, Kluwer Academics Publishers, Dordrecht, 1988.
340. G. Polya, in *Pattern of Plausible Inference: Mathematics and Plausible Reasoning*, Vol. 2 (ed. G. Polya), pp. 109–141, Princeton University Press, Princeton, 1954.
341. G. L. Bretthorst, *Bayesian Spectrum Analysis and Parameter Estimation*, Vol. 48 (eds J. Berger, S. Fienberg, J. Gani, K. Krickeberg and B. Singer), Springer-Verlag, New York, 1988.
342. J. Skilling, *Maximum Entropy and Bayesian Methods*, Cambridge, England, 1988 (ed. A. van der Merwe), Kluwer Academic Publishers, Dordrecht, 1989.
343. G. L. Bretthorst, C.-C. Hung, D. A. d'Avignon and J. J. H. Ackerman, *J. Magn. Reson.*, 1988, **79**, 369.
344. G. L. Bretthorst, *J. Magn. Reson.*, 1990, **88**, 533.
345. G. L. Bretthorst, *J. Magn. Reson.*, 1990, **88**, 552.
346. G. L. Bretthorst, *J. Magn. Reson.*, 1990, **88**, 571.
347. G. L. Bretthorst, *J. Magn. Reson.*, 1991, **93**, 369.
348. G. L. Bretthorst, *J. Magn. Reson.*, 1992, **98**, 501.
349. J. J. Kotyk, N. G. Hoffman, W. C. Hutton, G. L. Bretthorst and J. J. H. Ackerman, *J. Magn. Reson.*, 1992, **98**, 483.
350. R. F. Evilia, R. Effiong and S. L. Whittenburg, *Spectrosc. Lett.*, 1993, **26**, 1559.
351. K. S. Vines, R. F. Evilia and S. L. Whittenburg, *J. Magn. Reson.*, 1992, **100**, 195.
352. K. S. Vines, R. F. Evilia and S. L. Whittenburg, *J. Phys. Chem.*, 1993, **97**, 4941.
353. R. A. Chylla and J. L. Markley, *J. Biomol. NMR*, 1993, **3**, 515.
354. A. Rouh, A. Louis-Joseph and J. Y. Lallemand, *J. Biomol. NMR*, 1994, **4**, 505.
355. S. L. Whittenburg, *Spectrosc. Lett.*, 1995, **28**, 1275.
356. J. J. Kotyk, N. G. Hoffman, W. C. Hutton, G. L. Bretthorst and J. J. H. Ackerman, *J. Magn. Reson., Ser. A*, 1995, **116**, 1.
357. J. J. Neil and G. L. Bretthorst, *Magn. Reson. Med.*, 1993, **29**, 642.
358. C. Antz, K.-P. Neidig and H. R. Kalbitzer, *J. Biomol. NMR*, 1995, **5**, 287.
359. K.-P. Neidig, M. Geyer, A. Goerler, C. Antz, R. Saffrich, W. Beneicke and H. R. Kalbitzer, *J. Biomol. NMR*, 1995, **6**, 255.
360. A.-C. Schulte, A. Görler, C. Antz, K.-P. Neidig and H. R. Kalbitzer, *J. Magn. Reson.*, 1997, **129**, 165.
361. H.-B. Le, J. G. Pearson, A. C. de Dios and E. Oldfield, *J. Am. Chem. Soc.*, 1995, **117**, 3800.
362. S. L. Whittenburg, *Spectrosc. Lett.*, 1996, **29**, 393.
363. A. Gottvald, *Int. J. Appl. Electromagn. Mechanics*, 1997, **8**, 17.
364. M. Andrec and J. H. Prestegard, *J. Magn. Reson.*, 1998, **130**, 217.
365. M. F. Ochs, R. S. Stoyanova, F. Arias-Mendoza and T. R. Brown, *J. Magn. Reson.*, 1999, **137**, 161.
366. M. Andrec, G. T. Montelione and R. M. Levy, *J. Magn. Reson.*, 1999, **139**, 408.
367. M. Andrec, K. G. Inman, D. J. Weber, R. M. Levy and G. T. Montelione, *J. Magn. Reson.*, 2000, **146**, 66.
368. M. T. McMahon and E. Oldfield, *J. Biomol. NMR*, 1999, **13**, 133.
369. S. L. Tantum, L. M. Collins, L. Carin, I. Gorodnitsky, A. D. Hibbs, D. O. Walsh, G. A. Barrall, D. Gregory, R. Matthews and S. Vierkötter, in *Proc. SPIE-Int. Soc. Opt. Eng.* pp. 474–482, 1999.
370. P. C. Jurs, B. R. Kowalski, T. L. Isenhour and C. N. Reilley, *Anal. Chem.*, 1969, **41**, 1949.
371. C. L. Wilkins, R. C. Williams, T. R. Brunner and P. J. McCombie, *J. Am. Chem. Soc.*, 1974, **93**, 4182.
372. T. R. Brunner, R. C. Williams, C. L. Wilkins and P. J. McCombie, *Anal. Chem.*, 1974, **46**, 1798.
373. T. R. Brunner, C. L. Wilkins, R. C. Williams and P. J. McCombie, *Anal. Chem.*, 1975, **47**, 662.
374. C. L. Wilkins and T. L. Isenhour, *Anal. Chem.*, 1975, **47**, 1849.
375. T. R. Brunner, C. L. Wilkins, T. F. Lam, L. J. Soltzberg and S. L. Kaberline, *Anal. Chem.*, 1976, **48**, 1146.

376. C. L. Wilkins and T. R. Brunner, *Anal. Chem.*, 1977, **49**, 2136.
377. A. Bax, R. Freeman and S. P. Kempsell, *J. Magn. Reson.*, 1980, **41**, 349.
378. A. Bax, R. Freeman, T. A. Frenkiel and M. H. Levitt, *J. Magn. Reson.*, 1981, **43**, 478.
379. R. Richardz, W. Ammann and T. Wirthlin, *J. Magn. Reson.*, 1981, **45**, 270.
380. T. K. Pratum, *J. Magn. Reson., Ser. A*, 1995, **117**, 132.
381. J. Kawabata and E. Fukushi, *J. Magn. Reson., Ser. A*, 1995, **117**, 88.
382. R. Baumann, A. Kumar, R. R. Ernst and K. Wüthrich, *J. Magn. Reson.*, 1981, **44**, 76.
383. R. Baumann, G. Wider, R. R. Ernst and K. Wüthrich, *J. Magn. Reson.*, 1981, **44**, 402.
384. P. H. Bolton, *J. Magn. Reson.*, 1986, **67**, 391.
385. K. P. Neidig, H. Bodenmueller and H. R. Kalbitzer, *Biochem. Biophys. Res. Commun.*, 1984, **125**, 1143.
386. G. J. Kleywegt, R. Boelens and R. Kaptein, *J. Magn. Reson.*, 1990, **88**, 601.
387. A. Bax and R. Freeman, *J. Magn. Reson.*, 1981, **44**, 542.
388. U. Piantini, O. W. Sørensen and R. R. Ernst, *J. Am. Chem. Soc.*, 1982, **104**, 6800.
389. T. Nishida, I. Schulz, X.-L. Wu, P. Xu, J. Keeler and R. Freeman, *J. Magn. Reson.*, 1990, **88**, 636.
390. L. Mueller, *J. Magn. Reson.*, 1987, **72**, 191.
391. D. Marion and A. Bax, *J. Magn. Reson.*, 1988, **80**, 528.
392. I. Pelczer, *J. Am. Chem. Soc.*, 1991, **113**.
393. G. Eich, G. Bodenhausen and R. R. Ernst, *J. Am. Chem. Soc.*, 1982, **104**, 3731.
394. L. Braunschweiler, G. Bodenhausen and R. R. Ernst, *Mol. Phys.*, 1983, **48**, 535.
395. D. P. Weitekamp, *Adv. Magn. Reson.*, 1983, **11**, 111.
396. M. A. Thomas and A. Kumar, *J. Magn. Reson.*, 1983, **54**, 319.
397. L. Müller, *J. Magn. Reson.*, 1984, **59**, 326.
398. M. H. Levitt and R. R. Ernst, *Chem. Phys. Lett.*, 1983, **100**, 119.
399. M. H. Levitt and R. R. Ernst, *J. Chem. Phys.*, 1985, **83**, 3297.
400. C. Radloff and R. R. Ernst, *Mol. Phys.*, 1989, **66**, 161.
401. B. N. Gray and L. R. Brown, *J. Magn. Reson.*, 1991, **92**, 320.
402. T. Domke, P. Xu and R. Freeman, *J. Magn. Reson.*, 1991, **92**, 218.
403. V. Dötsch, R. E. Oswald and G. Wagner, *J. Magn. Reson., Ser. B*, 1996, **110**, 107.
404. M. Schubert, M. Smalla, P. Schmieder and H. Oschkinat, *J. Magn. Reson.*, 1999, **141**, 34.
405. M. Schubert, H. Oschkinat and P. Schmieder, *J. Magn. Reson.*, 2001, **148**, 61.
406. B. U. Meier, G. Bodenhausen and R. R. Ernst, *J. Magn. Reson.*, 1984, **60**, 161.
407. P. Pfändler, G. Bodenhausen, B. U. Meier and R. R. Ernst, *Anal. Chem.*, 1985, **57**, 2510.
408. P. H. Bolton, *J. Magn. Reson.*, 1986, **70**, 344.
409. J. C. Hoch, S. Hengyi, M. Kjær, S. Ludvigsen and F. M. Poulsen, *Carlsberg Res. Commun.*, 1987, **52**, 111.
410. S. Glaser and H. R. Kalbitzer, *J. Magn. Reson.*, 1987, **74**, 450.
411. Z. L. Mádi, B. U. Meier and R. R. Ernst, *J. Magn. Reson.*, 1987, **72**, 584.
412. B. U. Meier, Z. L. Mádi and R. R. Ernst, *J. Magn. Reson.*, 1987, **74**, 565.
413. H. Widmer and K. Wüthrich, *J. Magn. Reson.*, 1987, **74**, 316.
414. P. Pfändler and G. Bodenhausen, *J. Magn. Reson.*, 1988, **79**, 99.
415. H. Oschkinat, A. Pastore, P. Pfändler and G. Bodenhausen, *J. Magn. Reson.*, 1986, **69**, 559.
416. C. Griesinger, O. W. Sørensen and R. R. Ernst, *J. Am. Chem. Soc.*, 1985, **107**, 6394.
417. C. Griesinger, O. W. Sørensen and R. R. Ernst, *J. Chem. Phys.*, 1986, **85**, 6837.
418. P. Pfändler and G. Bodenhausen, *J. Magn. Reson.*, 1987, **72**, 475.
419. P. Pfändler and G. Bodenhausen, *J. Magn. Reson.*, 1986, **70**, 71.
420. P. Pfändler and G. Bodenhausen, *Magn. Reson. Chem.*, 1988, **26**, 888.
421. P. Pfändler and G. Bodenhausen, *J. Magn. Reson.*, 1990, **87**, 26.
422. L. Emsley and G. Bodenhausen, *in Computational Aspects of the Study of Biological Macromolecules by Nuclear Magnetic Resonance Spectroscopy: NATO ASI Ser., Ser. A*, Vol. 225 (eds J. C. Hoch, F. M. Poulsen and C. Redfield), pp. 151–162, Plenum Press, New York, 1991.
423. M. Novič and G. Bodenhausen, *Anal. Chem.*, 1988, **60**, 582.

424. M. Novič, U. Eggenberger and G. Bodenhausen, *J. Magn. Reson.*, 1988, **77**, 394.
425. B. U. Meier and R. R. Ernst, *J. Magn. Reson.*, 1988, **79**, 540.
426. Z. L. Mádi and R. R. Ernst, *J. Magn. Reson.*, 1988, **79**, 513.
427. T. Schulte-Herbrüggen, Z. L. Mádi, O. W. Sørensen and R. R. Ernst, *Mol. Phys.*, 1991, **72**, 847.
428. M. Woodley and R. Freeman, *J. Am. Chem. Soc.*, 1995, **117**, 6150.
429. M. Woodley and R. Freeman, *J. Magn. Reson., Ser. A*, 1996, **118**, 39.
430. F. Fogolari, G. Esposito, S. Cattarinussi and P. Viglino, *Concepts Magn. Reson.*, 1996, **8**, 229.
431. G. A. Doss, *J. Magn. Reson.*, 1992, **99**, 178.
432. E. C. Craig and I. D. Kuntz, *J. Magn. Reson., Ser. B*, 1993, **102**, 265.
433. J. Xu, B. N. Gray and L. R. Brown, *Tetrahedron Computer Methodology*, 1990, **3**, 479.
434. J. Xu and B. C. Sanctuary, *J. Chem. Inf. Comput. Sci.*, 1993, **33**, 490.
435. J. Xu, S. K. Straus, B. C. Sanctuary and L. Trimble, *J. Chem. Inf. Comput. Sci.*, 1993, **33**, 668.
436. J. Xu, P. L. Weber and P. N. Borer, *J. Biomol. NMR*, 1995, **5**, 183.
437. J. Xu and P. N. Borer, *J. Chem. Inf. Comput. Sci.*, 1994, **34**, 349.
438. E. C. van Geerestein-Ujah, M. Mariani, H. Vis, R. Boelens and R. Kaptein, *Biopolymers*, 1996, **39**, 691.
439. J. Xu, in *Fuzzy Logic in Chemistry* (ed. D. H. Rouvray), pp. 249–282, Academic Press, San Diego, 1997.
440. C. Peng, S. Yuan, C. Zheng and Y. Hui, *J. Chem. Inf. Comput. Sci.*, 1994, **34**, 805.
441. C. Peng, S. Yuan and C. Zheng, *J. Chem. Inf. Comput. Sci.*, 1995, **35**, 539.
442. C. Peng, G. Bodenhausen, S. Qiu, H. H. S. Fong, N. R. Farnsworth, S. Yuan and C. Zheng, *Magn. Reson. Chem.*, 1998, **36**, 267.
443. J. M. Schmidt, *Mol. Phys.*, 1998, **95**, 809.
444. V. A. Mandelshtam, Q. N. Van and A. J. Shaka, *J. Am. Chem. Soc.*, 1998, **120**, 12161.
445. W. P. Aue, J. Karhan and R. R. Ernst, *J. Chem. Phys.*, 1976, **64**, 4226.
446. G. Bodenhausen, R. Freeman, R. Niedermeyer and D. L. Turner, *J. Magn. Reson.*, 1977, **26**, 133.
447. K. Nagayama, P. Bachmann, K. Wüthrich and R. R. Ernst, *J. Magn. Reson.*, 1978, **31**, 133.
448. A. Bax, A. F. Mehlkopf and J. Smidt, *J. Magn. Reson.*, 1979, **35**, 167.
449. K. Nagayama, *J. Chem. Phys.*, 1979, **71**, 4404.
450. L. D. Hall and S. Sukumar, *J. Magn. Reson.*, 1980, **38**, 555.
451. A. Bax, R. Freeman and G. A. Morris, *J. Magn. Reson.*, 1981, **43**, 333.
452. B. Blümich and D. Ziessow, *J. Magn. Reson.*, 1982, **49**, 151.
453. G. W. Vuister and R. Boelens, *J. Magn. Reson.*, 1987, **73**, 328.
454. P. Xu, X.-L. Wu and R. Freeman, *J. Am. Chem. Soc.*, 1991, **113**, 3596.
455. P. Xu, X.-L. Wu and R. Freeman, *J. Magn. Reson.*, 1991, **95**, 132.
456. M. Woodley and R. Freeman, *J. Magn. Reson., Ser. A*, 1994, **109**, 103.
457. S. Simova, H. Sengstschmid and R. Freeman, *J. Magn. Reson.*, 1997, **124**, 104.
458. M. Liu and X. Zhang, *J. Magn. Reson.*, 2000, 146.
459. K. Furihata and H. Seto, *Tetrahedron Lett.*, 2001, **42**, 899.
460. S. Szalma and I. Pelczer, *J. Magn. Reson.*, 1988, **76**, 416.
461. U. Eggenberger and G. Bodenhausen, *Anal. Chem.*, 1989, **61**, 2298.
462. O. W. Sørensen and R. R. Ernst, *J. Magn. Reson.*, 1983, **55**, 338.
463. R. Freeman and L. McIntyre, *Israeli J. Chem.*, 1992, **32**, 231.
464. J. Friedrich, S. Davies and R. Freeman, *J. Magn. Reson.*, 1988, **80**, 168.
465. J. Friedrich, S. Davies and R. Freeman, *Mol. Phys.*, 1988, **64**, 691.
466. S. Davies, J. Friedrich and R. Freeman, *Magn. Reson. Chem.*, 1988, **26**, 903.
467. R. Brüschweiler, C. Griesinger, O. W. Sørensen and R. R. Ernst, *J. Magn. Reson.*, 1988, **78**, 178.
468. R. Brüschweiler, J. C. Madsen, C. Griesinger, O. W. Sørensen and R. R. Ernst, *J. Magn. Reson.*, 1987, **73**, 380.
469. J. Cavanagh, J. P. Waltho and J. Keeler, *J. Magn. Reson.*, 1987, **74**, 386.

470. C. Peng, D. Jeannerat and G. Bodenhausen, *Magn. Reson. Chem.*, 1997, **35**, 91.
471. L. Emsley and G. Bodenhausen, *J. Am. Chem. Soc.*, 1991, **113**, 3309.
472. L. Emsley, T. J. Dwyer, H. P. Spielmann and D. E. Wemmer, *J. Am. Chem. Soc.*, 1993, **115**, 7765.
473. D. Jeannerat and G. Bodenhausen, *J. Magn. Reson., Ser. A*, 1996, **118**, 126.
474. L. Emsley, P. Huber and G. Bodenhausen, *Angew. Chem. Int. Ed. Engl.*, 1990, **29**, 517.
475. P. Xu, X.-L. Wu and R. Freeman, *J. Magn. Reson.*, 1990, **89**, 198.
476. L. McIntyre and R. Freeman, *J. Magn. Reson.*, 1990, **89**, 632.
477. D. Jeannerat and G. Bodenhausen, *J. Magn. Reson., Ser. A*, 1996, **119**, 139.
478. N. Müller, L. Di Bari and G. Bodenhausen, *J. Magn. Reson.*, 1991, **94**, 73.
479. C. Zwahlen, S. J. F. Vincent, L. Di Bari, M. H. Levitt and G. Bodenhausen, *J. Am. Chem. Soc.*, 1994, **116**, 362.
480. J. U. Thomsen and B. Meyer, *J. Magn. Reson.*, 1989, 84.
481. B. Meyer, T. Hansen, D. Nute, P. Albersheim, A. Darvill, W. York and J. Sellers, *Science*, 1991, **251**, 542.
482. M. Kjær and F. M. Poulsen, *J. Magn. Reson.*, 1991, **94**, 659.
483. S. A. Corne, A. P. Johnson and J. Fisher, *J. Magn. Reson.*, 1992, **100**, 256.
484. S. A. Corne, J. Fisher, A. P. Johnson and W. R. Newell, *Anal. Chim. Acta*, 1993, **278**, 149.
485. B. J. Hare and J. H. Prestegard, *J. Biomol. NMR*, 1994, **4**, 35.
486. S. A. Corne, *Conc. Magn. Reson.*, 1996, **8**, 303.
487. K. Huang, M. Andrec, S. Heald, P. Blake and J. H. Prestegard, *J. Biomol. NMR*, 1997, **10**, 45.
488. J. A. Jones, *Concepts Magn. Reson.*, 1996, **8**, 175.
489. C. Biamonti, C. B. Rios, B. A. Lyons and G. T. Montelione, *Adv. Biophys. Chem.*, 1994, **4**, 51.
490. M. Eberstadt, G. Gemmecker, D. F. Mierke and H. Kessler, *Angew. Chem. Int. Ed. Engl.*, 1995, **34**, 1671.
491. W. A. Thomas, *Progr. in NMR Spectrosc.*, 1997, **30**, 183.
492. J. Stonehouse and J. Keeler, *J. Magn. Reson., Ser. A*, 1995, **112**, 43.
493. H. Oschkinat and R. Freeman, *J. Magn. Reson.*, 1984, **60**, 164.
494. H. Kessler, A. Müller and H. Oschkinat, *Magn. Reson. Chem.*, 1985, **23**, 844.
495. C. Griesinger, O. W. Sørensen and R. R. Ernst, *J. Am. Chem. Soc.*, 1985, **107**, 6394.
496. C. Griesinger, O. W. Sørensen and R. R. Ernst, *J. Magn. Reson.*, 1987, **75**, 474.
497. W. Bermel, K. Wagner and C. Griesinger, *J. Magn. Reson.*, 1989, **73**, 223.
498. M. D. Sørensen, S. M. Kristensen, J. J. Led and O. W. Sørensen, *J. Magn. Reson., Ser. A*, 1993, **103**, 364.
499. H. Thøgersen and O. W. Sørensen, *J. Magn. Reson., Ser. A*, 1994, **119**, 118.
500. Y. Kim and J. H. Prestegard, *J. Magn. Reson.*, 1989, **84**, 9.
501. F. del Río Portilla and R. Freeman, *J. Magn. Reson., Ser. A*, 1993, **104**, 358.
502. F. del Río Portilla and R. Freeman, *J. Chem. Soc., Faraday Trans.*, 1993, **89**, 4275.
503. D. Uhrín, V. Varma and J.-R. Brisson, *J. Magn. Reson., Ser. A*, 1996, **119**, 120.
504. R. Bazzo, G. Barbato and D. O. Cicero, *J. Magn. Reson., Ser. A*, 1995, **117**, 267.
505. J. J. Titman and J. Keeler, *J. Magn. Reson.*, 1990, **89**, 640.
506. T. Prasch, P. Gröschke and S. J. Glaser, *Angew. Chem. Int. Ed. Engl.*, 1998, **37**, 802.
507. S. J. F. Vincent, C. Zwahlen and G. Bodenhausen, *J. Magn. Reson., Ser. A*, 1994, **110**, 266.
508. D. Jeannerat and G. Bodenhausen, *J. Magn. Reson., Ser. A*, 1995, **117**, 123.
509. L. McIntyre and R. Freeman, *J. Magn. Reson.*, 1992, **96**, 425.
510. F. del Río Portilla, V. Blechta and R. Freeman, *J. Magn. Reson., Ser. A*, 1994, **111**, 132.
511. J.-M. Le Parco, L. McIntyre and R. Freeman, *J. Magn. Reson.*, 1992, **97**, 553.
512. J. Yang, K. McAteer, L. A. P. Silks, R. Wu, N. G. Isern, C. J. Unkefer and M. A. Kennedy, *J. Magn. Reson.*, 2000, **146**, 260.
513. K. Wüthrich, *NMR of Proteins and Nucleic Acids*, Wiley, New York, 1986.
514. G. M. Clore and A. M. Gronenborn, *Annu. Rev. Biophys. Biophys. Chem.*, 1991, **20**, 29.
515. A. Bax and S. Grzesiek, *Acc. Chem. Res.*, 1993, **26**, 131.

516. H. A. Havel, *Spectroscopic Methods for Determining Protein Structure in Solution*, VCH Publishers, Cambridge, UK, 1996.
517. A. M. Gronenborn and G. M. Clore, in *Spectroscopic Methods for Determining Protein Structure in Solution* (ed. H. A. Havel) VCH Publishers, Cambridge, UK, 1996.
518. P. Güntert, in *Protein NMR Techniques: Methods in Molecular Biology*, Vol. 60 (ed. G. D. Reid), pp. 157–194, Humana, Totowa, NJ, 1997.
519. M. G. Hinds and R. S. Norton, *Mol. Biotechnol.*, 1997, **7**, 315.
520. D. L. Turner, L. Brennan, S. G. Chamberlin, R. O. Louro and A. V. Xavier, *Eur. Biophys. J.*, 1998, **27**, 367.
521. J. C. Hoch, A. S. Stern and P. J. Connolly, in *Protein Dynamics, Function, and Design: NATO ASI Ser., Ser. A*, Vol. 301 (ed. O. Jardetzky), pp. 15–26, Plenum, New York, 1998.
522. I. Pelczer and B. G. Carter, in *Methods in Molecular Biology*, Vol. 60 (ed. D. G. Reid), pp. 71–155, Humana, Totowa, NJ, 1997.
523. J. C. Hoch, F. M. Poulsen and C. Redfiled, *Computational Aspects of the Study of Biological Macromolecules by Nuclear Magnetic Resonance Spectroscopy*, Vol. 225, Plenum Press, New York, 1991.
524. J. M. Withka, S. Swaminathan and P. H. Bolton, in *Computational Aspects of the Study of Biological Macromolecules by Nuclear Magnetic Resonance Spectroscopy: NATO ASI Ser., Ser A*, Vol. 225 (ed. J. C. Hoch, F. M. Poulsen and C. Redfield), pp. 409–420, Plenum Press, New York, 1991.
525. W. Boucher, A. R. C. Raine and E. D. Laue, in *Computational Aspects of the Study of Biological Macromolecules by Nuclear Magnetic Resonance Spectroscopy: NATO ASI Ser., Ser. A*, Vol. 225 (eds J. C. Hoch, F. M. Poulsen and C. Redfield), pp. 87–103, Plenum Press, New York, 1991.
526. R. R. Ernst, in *Computational Aspects of the Study of Biological Macromolecules by Nuclear Magnetic Resonance Spectroscopy: NATO ASI Ser., Ser. A*, Vol. 225 (eds J. C. Hoch, F. M. Poulsen and C. Redfield), pp. 1–25, Plenum Press, New York, 1991.
527. J. C. Hoch, in *Computational Aspects of the Study of Biological Macromolecules by Nuclear Magnetic Resonance Spectroscopy: NATO ASI Ser., Ser. Ac.*, Vol. 225 (eds J. C. Hoch, F. M. Poulsen and C. Redfield), pp. 253–267, Plenum Press, New York, 1991.
528. M. Kjær, K. V. Andersen, S. Ludvigsen, H. Shen, D. Windekilde, B. Sørensen and F. M. Poulsen, in *Computational Aspects of the Study of Biological Macromolecules Nuclear Magnetic Resonance Spectroscopy: NATO ASI Ser., Ser. A*, Vol. 225 (eds J. C. Hoch, F. M. Poulsen and C. Redfield), pp. 291–302, Plenum Press, 1991.
529. G. J. Kleywegt, R. Boelens and R. Kaptein, in *Computational Aspects of the Study of Biological Macromolecules by Nuclear Magnetic Resonance Spectroscopy: NATO ASI Ser., Ser. A*, Vol. 225 (eds J. C. Hoch, F. M. Poulsen and C. Redfield), pp. 427–437, Plenum Press, New York, 1991.
530. P. J. Kraulis, in *Computational Aspects of the Study of Biological Macromolecules by Nuclear Magnetic Resonance Spectroscopy: NATO ASI Ser., Ser. A*, Vol. 225 (eds J. C. Hoch, F. M. Poulsen and C. Redfield), pp. 361–362, Plenum Press, 1991.
531. S. Kumazawa, S. Endo, T. Yamazaki, K. Fujita and K. Nagayama, in *Computational Aspects of the Study of Biological Macromolecules by Nuclear Magnetic Resonance Spectroscopy: NATO ASI Ser., Ser. A*, Vol. 225 (eds J. C. Hoch, F. M. Poulsen and C. Redfield), pp. 439–443, Plenum Press, 1991.
532. G. C. Levy, S. Wang, P. Kumar, G.-W. Jeong and P. N. Borer, in *Computational Aspects of the Study of Biological Macromolecules by Nuclear Magnetic Resonance Spectroscopy: NATO ASI Ser., Ser. A*, Vol. 225 (eds J. C. Hoch, F. M. Poulsen and C. Redfield), pp. 105–126, Plenum Press, 1991.
533. J. L. Markley, P. Darba, J. Fejzo, A. M. Krezel, S. Macura, C. W. McNemar, E. S. Mooberry, B. R. Seavey, W. M. Westler and Z. Zolnai, in *Computational Aspects of the Study of Biological Macromolecules by Nuclear Magnetic Resonance Spectroscopy: NATO ASI Ser., Ser. A*, Vol. 225 (eds J. C. Hoch, F. M. Poulsen and C. Redfield), pp. 39–50, Plenum Press, 1991.

534. E. T. Olejniczak, H. L. Eaton, E. R. P. Zuiderweg and S. W. Fesik, in *Computational Aspects of the Study of Biological Macromolecules by Nuclear Magnetic Resonance Spectroscopy: NATO ASI Ser., Ser. A*, Vol. 225 (eds J. C. Hoch, F. M. Poulsen and C. Redfield), pp. 191–198, Plenum Press, 1991.
535. N. J. Oppenheimer and T. L. James (eds) *Nuclear Magnetic Resonance, Part A: Special Techniques and Dynamics: Methods in Enzymology*, Vol. 176, Academic Press, 1989.
536. N. J. Oppenheimer and T. L. James (eds) *Nuclear Magnetic Resonance, Part B: Structure and Mechanism: Methods in Enzymology*, Vol. 177, Academic Press, 1989.
537. T. L. James and N. J. Oppenheimer (eds) *Nuclear Magnetic Resonance, Part C: Methods in Enzymology*, Vol. 239, Academic Press, 1994.
538. T. L. James, V. Dötsch and U. Schmitz (eds) *NMR and Nucleic Acids: Methods in Enzymology*, Vol. 261, Academic Press, 1995.
539. T. L. James, V. Dötsch and U. Schmitz (eds) *Nuclear Magnetic Resonance of Biological Macromolecules, Part A: Methods in Enzymology*, Vol. 338, Academic Press, 2001.
540. T. L. James, V. Dötsch and U. Schmitz (eds) *Nuclear Magnetic Resonance of Biological Macromolecules, Part B: Methods in Enzymology*, Vol. 339, Academic Press, 2001.
541. A. G. Redfield, in *Nuclear Magnetic Resonance, Part A: Special Techniques and Dynamics: Methods in Enzymology*, Vol. 176 (eds N. J. Oppenheimer and T. L. James), pp. 253–270, Academic Press, 1989.
542. A. Bax, in *Nuclear Magnetic Resonance, Part A: Special Techniques and Dynamics: Methods in Enzymology*, Vol. 176 (eds N. J. Oppenheimer and T. L. James), pp. 151–168, 1989.
543. A. Bax, S. W. Sparks and D. A. Torchia, in *Nuclear Magnetic Resonance, Part A: Special Techniques and Dynamics: Methods in Enzymology*, Vol. 176 (eds N. J. Oppenheimer and T. L. James), pp. 134–150, Academic Press, 1989.
544. P. N. Borer and G. C. Levy, in *Nuclear Magnetic Resonance, Part C: Methods in Enzymology*, Vol. 239 (eds T. L. James and N. J. Oppenheimer), pp. 257–288, Academic Press, 1994.
545. A. Bax, G. W. Vuister, S. Grzesiek, F. Delaglio, A. C. Wang, R. Tschudin and G. Zhu, in *Nuclear Magnetic Resonance, Part C: Methods in Enzymology*, Vol. 239 (eds T. L. James and N. J. Oppenheimer), pp. 79–105, Academic Press, 1994.
546. H. Oschkinat and D. Croft, in *Nuclear Magnetic Resonance, Part C: Methods in Enzymology*, Vol. 239 (eds T. L. James and N. J. Oppenheimer), pp. 308–318, Academic Press, 1994.
547. M. Kjær, K. V. Andersen and F. M. Poulsen, in *Nuclear Magnetic Resonance, Part C: Methods in Enzymology*, Vol. 239 (eds T. L. James and N. J. Oppenheimer), pp. 288–307, Academic Press, 1994.
548. G. Wagner and K. Wüthrich, *J. Mol. Biol.*, 1982, **155**, 347.
549. A. Bax and M. A. Weiss, *J. Magn. Reson.*, 1987, **71**, 571.
550. M. Billeter, V. J. Basus and I. D. Kuntz, *J. Magn. Reson.*, 1988, **76**, 400.
551. C. Cieslar, G. M. Clore and A. M. Gronenborn, *J. Magn. Reson.*, 1988, **80**, 119.
552. C. D. Eads and I. D. Kuntz, *J. Magn. Reson.*, 1989, **82**, 467.
553. B. J. Stockman, M. D. Reily, W. M. Westler, E. L. Ulrich and J. L. Markley, *Biochem.*, 1989, **28**, 230.
554. A. Bax and M. Ikura, *J. Biomol. NMR*, 1991, **1**, 99.
555. M. S. Friedrichs, L. Mueller and M. Witteking, *J. Biomol. NMR*, 1994, **4**, 703.
556. J. B. Olson Jr. and J. L. Markley, *J. Biomol. NMR*, 1994, **4**, 385.
557. D. Zimmerman, C. Kulikowski, L. Wang, B. Lyons and G. T. Montelione, *J. Biomol. NMR*, 1994, **4**, 241.
558. R. P. Meadows, E. T. Olejniczak and S. W. Fesik, *J. Biomol. NMR*, 1994, **4**, 79.
559. J.-P. Simorre, B. Brutscher, M. S. Caffrey and D. Marion, *J. Biomol. NMR*, 1994, **4**, 325.
560. Q. Zhang, J. Chen, E. K. Gozansky, F. Zhu, P. L. Jackson and D. G. Gorenstein, *J. Magn. Reson., Ser. B*, 1995, **106**, 164.
561. N. Morelle, B. Brutscher, J.-P. Simorre and D. Marion, *J. Biomol. NMR*, 1995, **5**, 154.
562. C. G. Hoogstraten and J. L. Markley, *J. Mol. Biol.*, 1996, **258**, 334.
563. M. Nilges, *Curr. Opin. Struct. Biol.*, 1996, **6**, 617.

564. D. A. Pearlman, *J. Biomol. NMR*, 1996, **8**, 49.
565. D. A. Pearlman, *J. Biomol. NMR*, 1999, **13**, 325.
566. P. M. Bowers, C. E. M. Strauss and D. Baker, *J. Biomol. NMR*, 2000, **18**, 311.
567. A. Ross, G. Schlotterbeck, W. Klaus and H. Senn, *J. Biomol. NMR*, 2000, **16**, 139.
568. R. A. Atkinson and V. Saudek, in *Dynamics and the Problem of Recognition in Biological Macromolecules: NATO ASI Ser., Ser. A*, Vol. 288 (eds O. Jardetzky and C. Lefèvre), pp. 49–55, Plenum, New York, 1996.

Index

Note – Page numbers in *italic* type refer to figures and tables.

ACCORD-HMBC experiment, 63–8, *64*, *67*, *68*, 70, *71*, *72*, 80
ACCORD-HMQC experiment, *see* Accordion HMQC
Accordion delay, definition of, 61–3
Accordion Direct Single Quantum Correlation, *see* ADSQC
Accordion HMQC, 44–5, *45*, 68
ADSQC, 40–4, *41*, *42*, 43, 45
Akaide's Information Criterion (AIC), 178
Ala C_α resonance, 127, *128*
Ala C_β resonance, 127, *128*, 130–2, *131*, *132*
Ala carbonyl carbon resonances, 127
Ala residues, 106, 109, 112, 126
  motion of, 113–17
Aliasing, 155–6
Alkenylcarbyne-tungsten complexes, 54
Alkenylvinylidene-tungsten complexes, 54
Amino acid residues
  motion of 109–12
  see also Ala residues; Gly residues; Ser residues; Tyr residues
Amino acids, 187, 193–4
Amphidinol 3, 89
Antheraea pernyi silk fibroin, 130
Apodization functions, 156
Apratoxin A, 96
Armepavine, 59–60
Artefact reduction techniques, 157–8
ASSIGN program, 197
AURELIA, 183

Baseline corrections, 157, 172
Baseplane corrections, 157, 158
Bayesian analysis, 175, 181–4
Bayesian Information Criterion (BIC), 178
Bayesian Probability Theory (BPT), 182
β-sheet form, antiparallel, 141, *142*, 143
β-transition, 130, 132–3
BIRD pulse, 46, 74, *76–7*, 77
BIRD-HMBC experiment, 79–81
Broadband HMBC, 81–3, *82*
Broadline NMR, 8–9
B. mori silkworm, 103
  silk fibroin
  amino-acid composition of, 105–6
    ^{13}C NMR spectra of, 106–8, *107*, *108*, 139, *140*
    ESR spectra of, 140–1, *141*, *142*
    films, 135–9, *135*, *136*, *137*, *138*
    gel of, 143–7, *144*
    ^{2}H NMR powder pattern of, 116, *116*, *117*, 120, *121*, 123–6, *123*, *124*, 125
    in cocoon, 126
    in swollen silk fibroin membrane, 139–41, *140*, *141*
    motion of amino acid residues of, 109–12
    NMR relaxation times, 116–17
    solid-echo decays of, 114, *115*
    spin-labeled, 140, *140*, *141*, *142*
    structure of, 123
    T_1^C measurements of 118–19
    water molecules in, 135–9
  silk glands, 104, *104*
    ^{13}C NMR spectra of, 111–13, *111*, *112*
Bombyx mori, *see B. mori* silkworm
Burg algorithm, 178, 179
Butyl rubber, 16

^{13}C enrichment, 197
^{13}C MAS NMR, 21–6
^{13}C NMR, 12–21, 28–9, 184
  in vivo, 171
Cambridge algorithm, 180

Carbohydrates, conformational analysis of, 87–96
^{13}C–^{13}C experiments, 185
Cedarin, 53
Ceftiofur, 41
Chelilutine free base, 60
Chelirubine free base, 60
CIGAR-HMBC experiment, 63, 70–4, *73*
CISOC-SES, 190
Computer processing of NMR spectra, 152–97
  biological applications of, 196–7
  literature on, 152–3, 154, 158–9, 164, 169, 170–1, 172, 174, 176, 181, 194, 196
Conformational analysis, 87–96
Constant time variable delay, 68–9, *69*
Convolution product, 158
Correlation time, rotating, 103
COSMIC, 185
COSY experiments, 185–91
COSY-45, 185
COSY-type response artefacts, 78
Coupling constants, 37, 180–1, 183, 193
  one-bond, ranges of, 40
  scalar, 194–6
Couplings, heteronuclear, 38
  long-range
    applications of, 87–96
    measurement of, 85–7
Couplings, homonuclear, 190–1
CP(/)MAS spectra, 22, 26, 130–4, *131*, *132*, *133*
Cross-linking, 2, 4, 6, 30, 31
  applications of, 3
  H-type cross-links, 6, 12, *13*, 14, 16, 23, 26
  solution-state NMR studies of, 12–14
  Y-type cross-links, 6, 12, *13*, 13–14, 16, 23, 26
Cross-peak determination, 187–9
Cross-polarization (CP), 21
CT-HMBC, 60–1, *62–3*, 72
Cyclopentafurnanones, 78

DAISY experiment, 192
DD/MAS spectra, 130–4, *131*, *132*, *133*
Decay of magnetization, 10
Deconvolution methods, 158–63, 174, 194
  constrained (CD), 159
  doublet, 162
  J-deconvolution, 179–80
  linear, 158, 159
  non-linear, 158, 159
  of multiplets due to scalar coupling, 161, 163
  of powder patterns, 163
  reference, 159–63, 170
  self-deconvolution, 159, 160, 162
Decoupling, broadband heteronuclear, 49, 57
DEPT, 189
DFT, 154, 172, 177, 178, 180, 182
D-HMBC, 49–57, 96
  long-range ^{1}H–^{13}C applications of, 49–55
  long-range ^{1}H–^{15}N applications of, 55–7
  3D-HMBC, 57–8
Diffusion anisotropy, rotational, 183
Diffusion imaging, 171
Diffusion of organic molecules in gel, 143–7
DISCO, 195
DQF-COSY spectra, 163, 168, 169, 175, 177, 186, 190, 193
Dysiherbaine, 89
Dytesinin A, 93
Dytesinin B, 93

E.COSY, 188, 189, 193, 195
Electron spin resonance (ESR) spectroscopy, 5, 102, 103, 140
ELPSVD, 167
Enkephalin, 126
Entropy, 180
EPLPSVD, 166, 168
E-RELAX algorithm, 175
Erythromycin A, 92
Espicufolin, 51
Ethylene propylene rubber (EPR), 14, 20, 22
Evolution time, constant, 46
Expectation-maximization algorithm (EM), 175
EXSIDE experiment, 66, 87, 92

^{19}F NMR, 8–9, 27–8, 181
Facelift approach, 158
Fast Linear Prediction (FLP), 167
FB-LP, 165, 167
FDM methods, 169–70
FDM2K algorithm, 170
FFT, 152, 154
FIDDLE algorithm, 160
Filter diagonalization, 169–70
Final Prediction Criterion (FPC), 178
FLATT algorithm, 157
Fluorinated ethylene-propylene copolymers (FEP), 28
Fluoropolymers, 27
^{19}F–^{15}N correlation methods, 45
Folding, spectral, 155–6
Fourier transform (FT), 154–5, 176, 177
  Discrete Fourier Transform, *see* DFT
  Fast Fourier Transform, *see* FFT
FTIR, 5–6
FT-NMR, 154

G-BIRD$_R$-HSQMBC, 87
Gel dose, 13
GHMBC, 48, 70, 96
GHSQC, 41–3, *42*
GIFA processing software, 180
Gly C_α resonance, 127, *128*
Gly carbonyl carbon resonances, 127
Gly residues, 109, 126
  motion of, 115–17
Griseusin-B, 50–1
GSQMBC experiment, 58–60, 86, 92–3
G-value, 8

^{1}H NMR, 9, 12, 15, 16, 18, 135
^{2}H NMR, 102–3
Halishigamides A-D, 52
Harman, 91
^{1}H–^{13}C correlation methods, 39, 45, *47*, 49, 58, 60, 192
HECADE experiment, 86
HETLOC experiment, 85, 87–9, 96
^{1}H–^{1}H experiments, 185–91
High-density poly(ethylene)s (HDPE), 13–14
HMBC, 47–8, 86, 96, 166
  broadband HMBC, 81–3, *82*
  constant time HMBC, *see* CT-HMBC
  decoupled-HMBC, *see* D-HMBC
  J-HMBC, 86, 87, *90*, 90–1
  psHMBC, 86
HMQC, 39, 195
  Accordion HMQC, 44–5, *45*, 68
  J-multiplied HMQC, 87
HMSC experiment, 84–5
^{1}H–^{15}N correlation methods, 39, 45, *47*, 60, 70
HOGWASH method, 160, 179
^{1}H–^{31}P correlation methods, 60
HSQC, 39, 40, 89, 166, 168
  gradient-enhanced, 58–60
HSQC-HECADE pulse sequence, 86
HSQC-TOCSY experiment, 86
HSQMBC experiment, 86, 93–6
HSVD, 165, 167
HTLS, 167
^{1}H–^{183}W inverse detection methods, 54

Imaging, 180, 182
IMPEACH-MBC experiment, 57, 68–70, *69*, *71*, *72*
In situ calibration, 181
INADEQUATE experiment, 179, 180, 183, 185
INEPT sequence, 177, 187, 189
Iterative quadratic maximum likelihood (IQML) methods, 175
ITMPM, 169

J-based conformation analysis method, 87, 89
$^1J_{CH}$ couplings, 74
$^2J_{CH}$ couplings, 74, 77, 78, 88
$^3J_{CH}$ couplings, 74, 77, 78
$^nJ_{CH}$ couplings, 87, 88, 92
$^3J_{HH}$ couplings, 75, 77, 85, 87, 88
$^nJ_{XH}$ couplings, 92–3
J_{scale} parameter, 72–4, 76, 78
J-deconvolution, 179–80
J-doubling, 161, 163, 194, 196
J-filters, low-pass, 55, 57, 79, 80
J-HMBC experiment, 86, 87, *90*, 90–1
J-IMPEACH-MBC pulse sequence, 87
^{2}J,^{3}J-HMBC experiment, 63, 74–8, *75*, *76–7*, *78*, *79*

J-resolved experiments, 92–3, 168, 190–1
J-resolved HMBC pulse sequences, 86
J-scaling, 93

^{39}K spectra, *in vivo*, 180
Kalkitoxin, 95
Kauradienoic acid, 74

Lanczos-HSVD, 166
Least-squares methods, 172–4, 176, 190
Linear prediction (LP), 164–9, 182
Lipoprotein, 171, 172
LOMEP method, 180
LPQRD, 165
LPSVD, 165, 167, 168, 175
LPSVD(CR), 167, 168
LPZ-AR, 165
LP-ZOOM, 165, 170
LPZ-QRD, 165
LPZ-SVD, 165

Magic-angle spinning (MAS), 21
Maitotoxin, 88–9
Malyngamides, 94
Maximum entropy methods (MEM), 175–81
  N-Channel, 181
Maximum likelihood (ML), 174–5
MBOB experiment, 83–4
MEFSD, 178
Mescengricin, 52, 56–7
Metallothioneins, 44
Methylenes, diastereotopic, 88
Minimum area algorithm (MARS), 179
MJ-HMQC experiment, 87
Modified autocorrection function (MAF), 168
Molecular weights, measurements of, 6
Monazomycin, 55, 57
Monensin sodium, 90–1
Monte Carlo methods, 183, 184
Multiple quantum experiments, 186
Multiple-window spectrum estimation (MWSE) methods, 171
MUSIC excitation scheme, 187
MXQET program, 120, 125

^{15}N NMR, 60
Nakadomarin A, 54
Naphthomycinol, 51
N^6-[(dimethylamino)methylene]adenine, 60
Neural networks, 193–4
NMR, broadline, 8–9
NMR, pulsed, 9–12
NMR imaging, 30, 103
NMR methods, 8, 30–1
  two-dimensional, 38
NOE values, 102, 110
NOED spectroscopy, 160
NOESY spectra, 157, 165, 173, 180, 185, 193, 197
Nothramycin, 54
NQR spectroscopy, 184
Nuclear Overhauser enhancement, *see* NOE values

^{17}O NMR, *29*, 29–30
Octasaccharides, 55
Okadaic acid, 88
Oligopeptides, 119
Oligosaccharides, 92, 193
Organic molecules, diffusion of, 143–7

^{31}P NMR, *in vivo*, 164, 166–8, 178
Padé–Laplace method (PLM), 167
Pandamarilactonine, 90
Pattern recognition, 187
P.COSY, 186
P.E.COSY, 186, 195
2-Pentanone, 78
Phase-modulated rotating-frame imaging (PMRFI), 181
Phormidolide, 94, 95
Poly(butadiene) (PBD), 23–4, *24*
Poly(diene)s, 23–5
Poly(dimethyl siloxane) (PDMS), 10, *11*, 26
Poly(ethylene) (PE), 11–12, 14, *15*, 22, 30
Poly(isobutylene) (PIB), 16, *17*
Poly(isoprene), *29*, 30
Poly(L-phenylalanine), 126
Polymerization of monomers, 2
Polymers, 1–35
  applications of irradiation of, 2–4
  crystalline structure in, 25–6

mechanical properties of, 7
oxidative degradation of, 28–30
radiation chemistry of, 4–8
Poly(methacrylate)s, 2, 14–16
Poly(methyl methacrylate) (PMMA), 16, 18–19
Poly(olefin)s, 2, 12, *13*, 13–14, 22–3
Polypeptides, 173
Poly(propylene) (PP), 5, 19
Poly(styrene) (PSTY), 5
Poly(sulfone)s, 2, 5
Poly(tetrafluoroethylene) (PTFE), 8–9, 27, *28*
Power spectra density (PSD), 178
Promothiocin B, 55
Protein structure studies, 196, 197
psHMBC, 86
Pulsed NMR, 9–12
introduction of, 152, 154
$^{31}P-^{183}W$ inverse detection methods, 54
Pyralomycin 1a, 55–6
Pyridines, 91

QRD, 164
QUALITY method, 160–1
QUIETE-NOESY, 193

Racemization, 16–19
Radiation chemistry reviews, 7
Radiation dose, unit of, 8
Radiation grafting, 2
Radiation sterilization, 3
Radiation yield, unit of, 8
RDSQC, 43–4, *44*
Reference landscape adjustment (RLSA), 159
Regularized Resolvent Transform (RRT), 170
RELAX algorithm, 175
Relaxation rates, 145, *146*
Rotating correlation time, 103
Rowland algorithm, 180
Rubbers, cross-linked, 25

Samia cynthia ricini, *see S.c. ricini* silkworm
Sanguilutine, 60
Sanguinarine pseudobase, 60
Scission, chain, 2, 4, 6, *18*, 26
solution-state NMR studies of, 14–16
S.COSY, 186
S.c. ricini silkworm, 103
silk fibroin
amino-acid composition of, 105–6
^{13}C NMR spectra of, 107–8, *108*, 127–30, *128*, *129*
^{2}H NMR powder pattern of, 120, *121*, 123–6, *123*, *124*, 125
motion of amino acid residues of, 110–12
NMR relaxation times, 116–17
structural transition of, 127–34
T_1^C measurements of 119
silk glands, ^{13}C NMR spectra of, 111–12, *111*
Ser carbonyl carbon resonances, 127
Ser residues, 109, 117
hydroxymethyl groups in, 119–20
motion of, 117–23
side-chains, 120–3
SERENDIPITY, 190
Sericin, 104
Shift correlation, heteronuclear
direct, 38, 39–45
accordion-optimized, 40–5
heteronucleus-detected, 39
inverse-detected, 38, 39
proton-detected, 38, 39
long-range, 38, 45–85, 96
accordion-optimized, 48, 61–78
heteronucleus-detected, 39, 46
inverse-detected, 48
proton-detected, 38, 49
simultaneous direct and long-range, 83–5
^{29}Si MAS NMR, 26
SIAM pulse sequence, 195
Silk fibers, 103
Silkworm silks, properties of, 103
SIMPLEX methods, 184
Sinc wiggles, 155, 164, 177
Sine bell function, shifted, 157
Singular Value Decomposition (SVD), 164
SIS-COSY experiment, 193
Skyline projection method, 191
Soft-COSY experiments, 192, 193

Solid-state NMR, 21–6
Soluble fractions, measurement of, 7
Solution-state NMR, 12–21
  limits to, 20–1
Solvent suppression methods, 183
SPEDA spectra, 172
Spider dragline silks, 103, 106, 123
Spin networks determination, 184–96
  heteronuclear experiments, 191–2
  selective experiments, 192–3
Spin pinging, 193
Spin topology, 186
Spin–echo method, 145
Spin–lattice relaxation times, *see* T_1 relaxation times
Spin–spin relaxation times, *see* T_2 relaxation times
STAR operator, 74, *75*, 76–8, *76–7*
STELLA tool, 185
Strictosidine, 89
Strychnine, 64–6, *65*, 68, 78, *79*, 85, 94
Sucrose, 94
Sulfomycin-I, 57

T_1 relaxation times, 22, 102, 109, *109*, 114, 115
T_2 relaxation times, 11, 12, 21, 102
Taurospongin A, 53
Taxezopidine A, 53
TEMPOL solution, 143–7
Total Least Squares (TLS) procedure, 166
TOCSY spectra, 189–90, 194, 195
TRAF functions, 157
Tyr C_ε resonance, 130, *131*, 133–4, *134*
Tyr carbonyl carbon resonances, 127
Tyr residues, 109
  motion of, 123–7
  phenolic rings, 124–6
  side-chains, 124–6, 140–1

Volatile products analysis, 6

Water signal suppression, 160, 172
Wavelets transform (WT), 154, 170–2
Window functions, 156–7, 164, 176–8

XCORFE experiment, 46, 74, 77, 78
XLOC experiments, 87, 195

Yule–Walker algorithm, 178

Zeugmatography, 176
z-filtered COSY, 188
Zooming, 155
z-surfaces, 183